Copyright

by

Mehmet Zeki Erincik

2017

The Thesis Committee for Mehmet Zeki Erincik
Certifies that this is the approved version of the following thesis:

New Discovery to Reduce Residual Oil Saturation by Polymer Flooding

APPROVED BY
SUPERVISING COMMITTEE:

Supervisor:

Gary A. Pope

Co-Supervisor:

Matthew T. Balhoff

New Discovery to Reduce Residual Oil Saturation by Polymer Flooding

by

Mehmet Zeki Erincik, BS

Thesis

Presented to the Faculty of the Graduate School of

The University of Texas at Austin

in Partial Fulfillment

of the Requirements

for the Degree of

Master of Science in Engineering

The University of Texas at Austin

May 2017

Dedication

To my dear mother Aygül who passed away from cancer on July 13th 2015.

Acknowledgements

My master's study at UT, and my life in Austin/TX was very fruitful and successful thanks to many wonderful diverse individuals who are from different countries, races, colors, religions, and genders. I owe appreciation to all of them. First, I would like to express my deepest appreciation to my supervisors Dr. Gary Pope and Dr. Matthew Balhoff for their precious guidance, supervision, support, and tremendous patience. They challenged me to improve my skills and knowledge, guided me in the right direction of researching, and encouraged me through all phases of my research. Their project management skills, work discipline, and passion to chemical EOR inspired me a lot. I admired the supervision style of both. They challenged me to improve my skills and knowledge, guided me in the right direction of researching, and encouraged me through all phases of my research. I would like to thank both for their insightful comments and helpful advice at the stage of writing thesis. Their supervision helped me to become a good researcher, and a better engineer. I am honored for being under their supervision.

I owe thanks to Turkish Petroleum Corporation, Turkish Consulate General in Houston, and Office of the Educational Attaché for their support during my graduate study at UT Austin. I look forward to going back to my home country and contributing to make my country and the world a better place.

I would like to thank my colleague Pengpeng Qi for his cooperation and contribution in this research, for teaching me how to do coreflood experiments, for his smile and positive attitude. I really enjoyed working with him. I would like to thank my laboratory manager Mr. Jith Liyanage who provided a safe and an efficient laboratory environment for conducting my experiments and for his guidance and safety instructions during all experiments. I would like to thank Vincent Lee who trained me when I first started working in the laboratory. I would like to thank Mathieu Maubert for teaching and helping me to conduct my first oil flooding. I would like to thank undergraduate research assistants, Zach Quintanilla, Yifan Li, and Adam Verma for their help during different

steps of the coreflood experiments. I would like to specially thank to my colleague Leonard Chang for his friendship and willingness to help.

I would like to thank all researchers I have met during my study including my office and laboratory colleagues Nabi Nizamiddin, Denning Wang, Jun Lu, Jonathan Driver Austin Lim, Arnob Bhuyan, Sung Hyun Jang, Mohsen Tagahviar, Erin Shook, Maryam Shafiekhani, Nadeeka Upamali, Jose Parra, Alex Cui, Paul Jordan, Miguel Mejia, Sean Li, Jenny Ryu, Patrick Lim, Lauren Churchwell, Dharmika Lansakara, Rafael Longoria, Travis Pitcher, Luis Hernandez, Omid Peimani, Brien Allen, Pinaki Ghosh, Tanya Xu, Sajjad Neshat, and Himanshu Sharma for their friendship, support, and making me feel like I am home.

I would like to thank to the research and departmental staff including Esther Barrientes, Amy Stewart, Frankie Hart, Joanna Castillo, Glen Baum, and Gary Miscoe for their support.

I would like to thank Dr. Mustafa Onur, Dr. Omer Inanc Tureyen, Dr. Abdurrahman Satman, Mr. Jim Hanson for recommending me during my application to UT Austin, and for all of their support and communication through my petroleum engineering career.

I would like to thank to Morgan Hoke, Grace Howley, Juan Abreu, Samantha Philipp, Tosa Nehikhuere, Nathan Bussel, Alan Lam, Gene Hsu, Crystal Huang, Dayeed Khan, Michael Liu, Shannon Rouhana, Alex Gigliotti, Nancy Zhou, who were my officer colleagues at SPE Student Chapter at UT Austin between 2015-2017, and who made my UT Austin journey more enjoyable and memorable.

I am also thankful to my friends and colleagues Cagdas Eritici, Javid Shiriyev, Elif Ozdingis, Hayrettin Aygol, Emre Ozen, Kahraman Barut, and Erdi Aydin for their friendship and support.

There are no words to show my appreciation to my dear parents, sisters, and brothers who always shared their positive energies and love. I will always remember my dear mother Aygül who raised me with love and compassion. Z4Z.

Abstract

A New Discovery to Reduce Residual Oil Saturation by Polymer Flooding

Mehmet Zeki Erincik, MSE

The University of Texas at Austin, 2017

Supervisor: Gary A. Pope

Co-Supervisor: Matthew T. Balhoff

Eight coreflood experiments were conducted to investigate the effect of aqueous hydrolyzed polyacrylamide (HPAM) polymer solutions on residual oil saturation in sandstone cores. Seven of the experiments were conducted in high-permeability (~1500 mD) Bentheimer sandstones, six of the cores were saturated with a viscous oil (~120 cp), and one core was saturated with a light (10 cp) oil. The eighth experiment was performed in a Berea sandstone core using the light oil. Experiments #6 to 8 were done by Pengpeng Qi. These experiments are included in this thesis to provide more complete and convincing results.

All experiments were first saturated with brine, flooded with oil to reach initial oil saturation, and then waterflooded with brine to zero oil cut. For experiments with viscous oil, a viscous glycerin solution was injected after the waterflood until the oil cut was zero. FP 3630S polymer was used in the seven Bentheimer coreflood experiments and FP 3330S polymer was used in the Berea coreflood experiment. The polymer solutions in low salinity

brine had a high relaxation time. Additional hydrolysis of the polymers was done to further increase the relaxation time. The coreflood experiments were designed to maximize the effect of viscoelasticity on the residual oil saturation by flooding the cores at a high Deborah number, N_{De}, which ranged from 30-300.

The low-salinity polymer floods were followed by a second polymer flood with a similar viscosity, but higher salinity (viscosity was controlled by increasing polymer concentration). The higher salinity resulted in a much lower polymer relaxation time than the first polymer in low salinity brine, and therefore a lower N_{De} for the coreflood. Two of the experiments included additional polymer floods by alternating between the low and high salinity polymer solutions.

The original objective of this work was to investigate the effect of polymer elasticity (measured by the dimensionless Deborah number, N_{De}) on residual oil saturation. The polymer flooding experiments were designed to keep the capillary number less than the capillary number of the preceding glycerin floods as well as less than the critical capillary number to avoid a reduction in the residual oil saturation caused by a high capillary number. Early in this experimental study, a surprising and remarkable discovery was made that completely changed the direction of the research. The residual oil saturation following the high-salinity polymer floods was reduced to remarkably low values.

All eight experiments showed that the low-salinity polymer floods with high Deborah numbers resulted in additional oil recovery. The average reduction in oil saturation was ~10% for the seven Bentheimer corefloods, including the one with light oil (4%). There was a (weak) correlation indicating lower residual oil saturations with increasing N_{De} consistent with the observations by Qi et al. (2017).

The most surprising observation and discovery was that the residual oil saturation decreased between 4 and 21% with an average reduction of 11% when high-salinity

polymer solution was injected following the low-salinity polymer flood with the same viscosity and at the same or similar flow rates. The total reduction in residual oil saturation from both polymer floods was 21% below the residual oil saturation of the glycerin floods with the same viscosity. The lowest residual oil saturation in these experiments was only 7%. This is a truly remarkable result considering the interfacial tension between the polymer solution and oil is about the same as between water and oil.

Additional measurements are needed to understand the mechanisms e.g. wettability measurements before and after the polymer floods in low and high salinity brines.

Table of Contents

List of Tables xv

List of Figures xvi

Chapter 1: Introduction 1

1.1 BACKGROUND 1

1.2 OBJECTIVE 2

Chapter 2: Literature Review 3

2.1 ENHANCED OIL RECOVERY (EOR) 3

2.1.1 Thermal EOR 4

2.1.2 Solvent EOR 5

2.1.3 Chemical EOR 5

2.2 RESIDUAL OIL SATURATION 5

2.3 MOBILITY RATIO AND CAPILLARY NUMBER 7

2.3.1 Mobility Ratio 7

2.3.2 Capillary Number 8

2.4 POLYMER FLOODING 13

2.5 HPAM POLYMER PROPERTIES 13

2.5.1 Chemical Structure 13

2.5.2 Degree of Hydrolysis and Molecular Weight 15

2.5.3 Polymer Concentration and Brine Salinity 15

2.5.6 Temperature 17

2.5.8 Viscoelasticity and Deborah Number 18

Chapter 3: Experimental Approach 21

3.1 CORE PREPARATION AND COREFLOOD SETUP 21

3.1.1 Core Preparation 21

3.1.2 Coreflood Apparatus 24

3.2 SATURATING THE CORE 27

3.3 SALINITY TRACER TEST 28

3.4 DETERMINING THE BRINE PERMEABILITY OF THE CORE 30

3.5 REDUCING THE CORE 31
3.6 OIL FLOOD.....34
3.8 WATERFLOOD 37
3.9 GLYCERIN FLOOD 39
3.10 LOW-SALINITY, HIGH-VISCOELASTICITY POLYMER FLOOD42
3.11 HIGH-SALINITY, LOW-VISCOELASTICITY POLYMER FLOOD46
3.12 FLUID PREPARATION EQUIPMENT 48
3.12.1 Mixing Equipment 48
3.12.2 Filtration Equipment 48
3.12.3 Degassing Equipment 49
3.12.4 Equipment Used for Transferring the Fluid.....50
3.13 FLUID MEASUREMENT EQUIPMENT 51
3.13.1 Mass Measurement 51
3.13.2 Rheology 51
3.13.3 Oxidation Reduction Potential (ORP) Measurement.....58
3.13.4 pH Measurement 58
3.13.5 Salinity Measurement 59
3.14 FLUID FLOODING EQUIPMENT 60
3.14.1 Stainless Steel Cylinders.....60
3.14.2 Glass columns 60
3.14.3 Pump 61
3.14.4 Pressure transducers and data acquisition recorder 62
3.14.5 Fraction collector 62
Chapter 4: Results and Analysis 64
4.1 EXPERIMENT #1 64
4.1.1 Core Preparation, Saturating the Core, Salinity Tracer Test 64
4.1.2 Core Reduction and Conditioning 66
4.1.3 Oil Flood 67
4.1.4 Waterflood 69
4.1.5 Glycerin Flood 70

4.1.6 Low-Salinity Polymer Flood....71
4.1.7 High-Salinity Polymer Flood....77
4.1.8 Oil Saturation, Oil Cut, and Pressure Drop....81
4.2 EXPERIMENT #2....84
4.2.1 Core Preparation, Saturating the Core, and Salinity Tracer Test85
4.2.2 Core Reduction and Conditioning....86
4.2.3 Oil Flood....88
4.2.4 Waterflood....90
4.2.5 Glycerin Flood....92
4.2.6 Low-salinity Polymer Flood....93
4.2.7 High-Salinity Polymer Flood....97
4.2.8 Oil Saturation, Oil Cut, and Pressure Drop....102
4.3 EXPERIMENT #3....104
4.3.1 Core Preparation, Saturating the Core, Salinity Tracer Test 104
4.3.2 Core Reduction and Conditioning....106
4.3.3 Oil Flood....108
4.3.4 Waterflood....110
4.3.5 Glycerin Flood....112
4.3.6 Low-salinity Polymer Flood....113
4.3.7 High-Salinity Polymer Flood....116
4.3.8 Oil Saturation, Cumulative Oil Recovered, and Oil Cut 120
4.4 EXPERIMENT #4....122
4.4.1 Core Preparation, Saturating the Core, Salinity Tracer Test 123
4.4.2 Core Reduction and Conditioning....125
4.4.3 Oil Flood....127
4.4.4 Waterflood....128
4.4.5 Glycerin Flood....130
4.4.6 Low-salinity Polymer Properties....131
4.4.7 High-Salinity Polymer Properties....132
4.4.8 Alternating Polymer Floods....135

4.4.9 Oil Saturation, Oil Cut, and Cumulative Oil Recovered 140
4.5 EXPERIMENT #5 141
4.5.1 Core Preparation and Saturating the Core 141
4.5.2 Core Reduction and Conditioning, Salinity Tracer Test.....143
4.5.3 Oil Flood 146
4.5.4 Waterflood 148
4.5.5 Glycerin Flood 150
4.5.6 Low-salinity Polymer Properties 151
4.5.7 High-salinity Polymer Properties.....152
4.5.8 Alternating Polymer Floods.....154
4.5.9 Oil Saturation, Oil Cut, and Pressure Drop.....160
4.6 EXPERIMENT #6 162
4.6.1 Core Preparation, Saturating the Core, Salinity Tracer Test 163
4.6.2 Core Reduction and Conditioning 164
4.6.3 Oil Flood 164
4.6.4 Waterflood 165
4.6.5 Glycerin Flood 166
4.6.6 Low-salinity Polymer Flood 167
4.6.7 High-Salinity, Low Elasticity Polymer Flood 169
4.6.8 Oil Saturation, Oil Cut, and Pressure Drop.....169
4.7 EXPERIMENT #7 172
4.7.1 Core Preparation, Saturating the Core, Salinity Tracer Test 172
4.7.2 Core Reduction and Conditioning 174
4.7.3 Oil Flood 174
4.7.4 Waterflood 175
4.7.6 Low-Salinity, High Elasticity Polymer Flood 175
4.7.7 High-salinity Polymer Flood.....176
4.7.8 Oil Saturation, Cumulative Oil Recovered, and Oil Cut 176
4.8 EXPERIMENT #8 178
4.9 ANALYSIS OF THE EXPERIMENTS 181

Chapter 5: Conclusions and Future Work.....186
5.1 CONCLUSIONS.....186
5.2 FUTURE WORK.....189
References.....191

List of Tables

Table 4.1: Core and fluid properties of experiment #1. 65

Table 4.2: Steady-state pressure drop data, effective oil permeability, and end-point oil permeability from oil flood of experiment #1. 68

Table 4.3: Core and fluid properties of experiment #2. 84

Table 4.4: Steady-state pressure drop data, effective oil permeability, and end-point oil permeability from oil flooding for experiment #2. 88

Table 4.5: Core and fluid properties of experiment #3. 105

Table 4.6: Steady-state pressure drop data, effective oil permeability, and end-point oil permeability from oil flooding for experiment #3. 108

Table 4.7: Core and fluid properties of experiment #4. 123

Table 4.8: Steady-state pressure drop data, effective oil permeability, and end-point oil permeability from oil flooding for experiment #4. 127

Table 4.9: Oil saturation reduction for alternating polymer injection intervals.135

Table 4.10: Core and fluid properties of experiment #5. 142

Table 4.11: Steady-state pressure drop data, effective oil permeability, and end-point oil permeability from oil flooding for experiment #5. 146

Table 4.12: Core and fluid properties of experiment #6. 162

Table 4.13: Core and fluid properties of experiment #7. 172

Table 4.14: Core and fluid properties of experiment #8. 178

Table 4.15: Summary of the residual oil saturation results of all eight coreflood experiments in this thesis 182

List of Figures

Figure 2.1: Oil Recovery Classifications (Lake et al., 2014). 3

Figure 2.2: Oil production illustration (Lindey, 2001).....4

Figure 2.3: Comparison of experimental and fractional flow results for cumulative oil recovery of waterflood and polymer flood for an experiment of Koh et al. (2016) 7

Figure 2.4: Capillary desaturation curve (Lake et al., 2014).....10

Figure 2.5: Capillary Desaturation Curve for Berea Sandstone 11

Figure 2.6: Capillary desaturation curve (Qi et al., 2017).....12

Figure 2.7: Chemical Structure of Partially hydrolyzed polyacrylamide (HPAM)14

Figure 2.9: Salinity and polymer concentration effect on the viscosity at 10 s^{-1} equivalent shear rate for Flopaam^{TM} 3630S at 25°C in log-log scale (Koh, 2015) 16

Figure 2.10 Salinity effect on the polymer viscosity (at 11 s^{-1} equivalent shear rate) for five different 1500 ppm high molecular weight polymers at 23 ℃ (Levitt and Pope, 2008).....17

Figure 2.11: Effect of temperature on viscosity for 3000 ppm FlopaamTM 3630S in 1400 ppm TDS aqueous solution.....18

Figure 2.12: Dynamic frequency sweep test result for 2000 ppm Flopaam 3630S in 1000 ppm NaCl and 400 ppm NaHCO3 at 25 ℃ 20

Figure 3.1: Two Bentheimer sandstone cores filled with slow-setting epoxy. ...23

Figure 3.2: Leaking observation from middle tap of an epoxied Bentheimer sandstone core which is tested inside a container filled with water. 24

Figure 3.3: Coreflood apparatus showing a core with four sections connected to four 0-35 psi differential pressure transducers; and with inlet & outlet connected to two 0-150 psi absolute pressure transducers, and a 0-300 psi differential pressure transducer. 26
Figure 3.4: Typical tracer test result showing normalized effluent salinity during 2% KCl brine injection (displacing 6% KCl brine), from an initial salinity index of 46 parts per thousand (ppt) to a final salinity index of 15 ppt. 30
Figure 3.5: An example of pressure drop data during tracer test and permeability measurement 31
Figure 3.6: Typical ORP (R.mV) and iron concentration (ppm) data.....33
Figure 3.7: Typical pH and iron concentration (ppm) data 33
Figure 3.9: Typical plot of the pressure drop, and the interstitial velocity data during 137 cP crude oil flooding conducted at 85 psi constant pressure and 23 °C. 36
Figure 3.10: Typical pressure drop, and the interstitial velocity data during waterflooding at 23°C 37
Figure 3.11: Typical pressure drop during a glycerin (60 cp) flood at 2 ft/D 40
Figure 3.12: Viscosity of aqueous glycerin solutions, Glycerin wt% versus Viscosity (adapted from Segur and Oberstar (1951)) 41
Figure 3.13: Typical viscosity measurement of 82 wt% glycerin in 12 wt% brine41
Figure 3.14: Typical pressure drop during 2000 ppm FP 3630S HPAM Polymer in 1000 ppm NaCl, 400 ppm NaHCO3 aqueous solution at 1 ft/D and 23 ℃ 44

Figure 3.15: Typical pressure drop during 3548 ppm FP-3630S HPAM Polymer in 24030 ppm NaCl, 280 ppm NaHCO3 aqueous solution at 1 ft/D and 23 ℃.....46
Figure 3.16: The apparatus used for polymer degassing (Koh, 2015), and an example picture of degassing 49
Figure 3.17: A typical setup of transferring polymer solution to an injection column 50
Figure 3.18: Digital balance scales.....51
Figure 3.19: Dynamic strain sweep test (DSST) set-up screen 52
Figure 3.20: An example of dynamic strain sweep test (DSST) result for 2000 ppm FP-3630S HPAM Polymer in 1000 ppm NaCl + 400 ppm NaHCO3 aqueous solution at 23 ℃.....53
Figure 3.21: Dynamic frequency sweep test (DFST) set-up screen.....54
Figure 3.22: DFST result for 2000 ppm FP-3630S HPAM Polymer in 1000 ppm NaCl + 400 ppm NaHCO3 aqueous solution at 23 ℃.....55
Figure 3.23: DFST result for 3548 ppm FP-3630S HPAM Polymer in 24030 ppm NaCl + 280 ppm NaHCO3 aqueous solution at 23 ℃.....55
Figure 3.24: Steady rate sweep test (SRST) set-up screen.....56
Figure 3.25: Steady rate sweep test (SRST) result for 2000 ppm FP-3630S HPAM Polymer in 1000 ppm NaCl + 400 ppm NaHCO3 aqueous solution at 23 ℃.....57
Figure 3.26: Example of curve fit function after steady rate sweep test (SRST) for 2000 ppm FP-3630S HPAM Polymer in 1000 ppm NaCl + 400 ppm NaHCO3 aqueous solution at 23 ℃.....57
Figure 3.27: Oakton Waterproof ORPTestr® 10.....58

Figure 3.28: Thermo Scientific Orion 3 STAR Benchtop pH Meter.....59
Figure 3.29: Portable refractometer and dual scale 59
Figure 3.30: Stainless steel double ended cylinder.....60
Figure 3.31: Kontes Chromaflex® glass columns.....61
Figure 3.32: Teledyne ISCO 5000 syringe pump and LabView™ software.....62
Figure 3.33: Fraction collector.....63
Figure 4.1: Normalized effluent salinity during 2% KCl brine injection for experiment #1, from a salinity index of 46 ppt to 15 ppt.....66
Figure 4.2: Flow rate during 124 cP crude oil flooding conducted at 50 psi constant pressure and 23 °C for experiment #1.....68
Figure 4.3: Pressure drop, and the interstitial velocity data during 124 cP crude oil flooding conducted at 50 psi constant pressure and 23 °C for experiment #1.....69
Figure 4.4: Pressure drop, and the interstitial velocity data during waterflooding at 23°C for experiment #1.....70
Figure 4.5: Pressure drop data and the interstitial velocity during glycerin flooding at 23 °C for experiment #1.....71
Figure 4.6: DFST result for 2000 ppm FP-3630S HPAM polymer in 1000 ppm NaCl + 400 ppm NaHCO3 aqueous solution at 23 °C for experiment #1. 72
Figure 4.7: SRST result for 2000 ppm FP-3630S HPAM polymer in 1000 ppm NaCl and 400 ppm NaHCO3 aqueous solution at 23 °C for experiment #1.73
Figure 4.8: Pressure drop data, and the interstitial velocity during 2000 ppm FP-3630S HPAM Polymer in 1000 ppm NaCl + 400 ppm $NaHCO_3$ aqueous solution flood at 23 °C for experiment #1. 75

Figure 4.9: Injection and apparent viscosity comparison by using C=4 for Bentheimer sandstone core for experiment #1 at 23 °C. 75
Figure 4.10: Effluent pH and normalized effluent viscosity at 23 °C for experiment #1.....76
Figure 4.11: Viscosity comparison of the injected polymer solution and the effluents at 23 °C for experiment #1.....76
Figure 4.12: DFST result for 3800 ppm FP-3630S HPAM polymer in 26400 ppm NaCl, 300 ppm $NaHCO_3$ aqueous solution at 23 °C for experiment #1. 79
Figure 4.13: SRST result for 3800 ppm FP-3630S HPAM polymer in 26400 ppm NaCl, 300 ppm $NaHCO_3$ aqueous solution at 23 °C for experiment #1. 79
Figure 4.14: Pressure drop data and the interstitial velocity during high-salinity polymer flood at 23 °C for experiment #1.....80
Figure 4.15: Normalized effluent salinity during high-salinity polymer flood for experiment #1.....80
Figure 4.16: Normalized effluent salinity, oil cut and oil saturation during the high-salinity polymer flood for experiment #1 81
Figure 4.17: Oil saturation for experiment #1. 82
Figure 4.18: Oil cut versus pore volumes injected for both the low-salinity and high-salinity polymer floods for experiment #1.....82
Figure 4.19: Pressure drop for both low-salinity and high-salinity polymer floods for experiment #1.....83
Figure 4.20: Normalized effluent salinity during 2% KCl brine injection for experiment #2, from a salinity index of 46 ppt to 15 ppt.....86

Figure 4.21: ORP (R.mV) and Iron Concentration (ppm) of the effluents. 87
Figure 4.22: pH and Iron concentration (ppm) of the effluents. 87
Figure 4.23: Flow rate during 126 cP crude oil flooding conducted at 85 psi constant pressure and 23 ℃ temperature for experiment #2. 89
Figure 4.24: Pressure drop and the interstitial velocity data during 126 cP crude oil flooding conducted at 85 psi constant pressure and 23 °C for experiment #2.....89
Figure 4.25: Pressure drop and the interstitial velocity data during waterflooding at 23°C for experiment #2.....90
Figure 4.26: Normalized effluent salinity during 2nd salinity tracer test for experiment #2, from a salinity index of 2 ppt to 30 ppt.....92
Figure 4.27: Pressure drop data, and the interstitial velocity during glycerin flooding at 23 °C for experiment #2.....93
Figure 4.28: DFST result for 2000 ppm FP-3630S HPAM polymer in 1000 ppm NaCl + 400 ppm NaHCO3 aqueous solution at 23 °C for experiment #2. 94
Figure 4.29: SRST result for 2000 ppm FP-3630S HPAM polymer in 1000 ppm NaCl + 400 ppm NaHCO3 aqueous solution at 23 °C for experiment #2. 95
Figure 4.30: Pressure drop data, and the interstitial velocity during 2000 ppm FP-3630S HPAM polymer in 1000 ppm NaCl + 400 ppm NaHCO3 aqueous solution flood at 23 °C for experiment #2. 96
Figure 4.31: Viscosity comparison of the injected polymer solution and the effluents at 23 °C for experiment #2.....97

Figure 4.32a: DFST result for 3400 ppm FP-3630S HPAM polymer in 26400 ppm NaCl, 300 ppm $NaHCO_3$ aqueous solution at 23 °C for experiment #2. 99

Figure 4.32b: SRST result for high-salinity polymer solution compared to the low-salinity polymer solution at 23 °C for experiment #2.....99

Figure 4.33: Pressure drop data, and the interstitial velocity during high-salinity polymer flood at 23 °C for experiment #2. 100

Figure 4.34: Normalized effluent salinity during high-salinity polymer flood for experiment #2, from a salinity index of 5 ppt to 30 ppt.....101

Figure 4.35: Normalized effluent salinity, oil cut, and oil saturation during high-salinity polymer flood for experiment #2. 101

Figure 4.36: Oil saturation versus pore volumes for experiment #2. 102

Figure 4.37: Oil cut versus pore volumes for both low-salinity and high-salinity polymer floods for experiment #2.....103

Figure 4.38: Pressure drop for both low-salinity and high-salinity polymer floods for experiment #2.....103

Figure 4.39: Normalized effluent salinity during 2% KCl brine injection for experiment #3, from a salinity index of 47 ppt to 16 ppt.....106

Figure 4.40: ORP (R.mV) and Iron Concentration (ppm) of the effluents. 107

Figure 4.41: pH and Iron Concentration (ppm) of the effluents.....107

Figure 4.42: Flow rate during 114 cP crude oil flooding conducted at 85 psi constant pressure and 23 °C temperature for experiment #3. 109

Figure 4.43: Pressure drop, and the interstitial velocity data during 114 cP crude oil flooding conducted at 85 psi constant pressure and 23 °C for experiment #3.....109

Figure 4.44: Pressure drop, and the interstitial velocity data during waterflooding at 23°C for experiment #3. 110
Figure 4.45: Normalized effluent salinity of 2nd salinity tracer test, from a salinity index of 2 ppt to 30 ppt. 111
Figure 4.46: Pressure drop data, and the interstitial velocity during glycerin flooding at 23 °C for experiment #3. 112
Figure 4.47: DFST result for 2000 ppm FP-3630S HPAM polymer in 1000 ppm NaCl + 400 ppm NaHCO3 aqueous solution at 23 °C for experiment #3. 114
Figure 4.48: Pressure drop data, and the interstitial velocity during low-salinity polymer flood at 23 °C for experiment #3. 115
Figure 4.49: Viscosity comparison of the injected low-salinity polymer solution and the effluents at 23 °C for experiment #3. 115
Figure 4.50: DFST result for 3548 ppm FP-3630S HPAM polymer in 24000 ppm NaCl, 300 ppm $NaHCO_3$ aqueous solution at 23 °C for experiment #3. 117
Figure 4.51: SRST result for high-salinity polymer compared to the low-salinity polymer solution at 23 °C for experiment #3. 117
Figure 4.52: Pressure drop data and the interstitial velocity during high-salinity polymer flood at 23 °C for experiment #3. 119
Figure 4.53: Normalized effluent salinity during high-salinity polymer flood for experiment #3, from a salinity index of 5 ppt to 28.5 ppt. 119
Figure 4.54: Normalized effluent salinity, oil cut, and oil saturation during high-salinity polymer flood for experiment #3. 120
Figure 4.55: Oil saturation versus pore volumes for experiment #3. 121

Figure 4.56: Oil cut versus pore volumes for both low-salinity and high-salinity polymer floods for experiment #3.....121
Figure 4.57: Pressure drop for both low-salinity and high-salinity polymer floods for experiment #3.....122
Figure 4.58: Normalized effluent salinity during 2% KCl brine injection for experiment #4, from a salinity index of 46.5 ppt to 16 ppt.....125
Figure 4.59: ORP (R.mV) and iron concentration (ppm) of the effluents. 126
Figure 4.60: pH and iron concentration (ppm) of the effluents.....126
Figure 4.61: Pressure drop and the interstitial velocity data during 129 cP crude oil flood conducted at 85 psi constant pressure and 23 °C for experiment #4. 128
Figure 4.62: Pressure drop and the interstitial velocity data during waterflooding at 23°C for experiment #4.....129
Figure 4.63: Normalized effluent salinity during 2nd salinity tracer test for experiment #4, from a salinity index of 2 ppt to 31.5 ppt.....130
Figure 4.64: Pressure drop data, and the interstitial velocity during glycerin flooding at 23 °C for experiment #4.....131
Figure 4.65: DFST result for 2000 ppm FP-3630S HPAM polymer in 1000 ppm NaCl + 400 ppm $NaHCO_3$ aqueous solution at 23 °C for experiment #4. 132
Figure 4.66: (DFST) result of the high-salinity polymer (# JBA 2114/4-6) in 24000 ppm NaCl, 300 ppm $NaHCO_3$ aqueous solution at 23 °C for experiment #4.....134
Figure 4.67: SRST result for high-salinity polymer compared to the low-salinity polymer solution at 23 °C for experiment #4. 134

Figure 4.68: Pressure drop for both low-salinity and high-salinity polymer floods for experiment #4.....137
Figure 4.69: Capillary number for both low-salinity and high-salinity polymer floods for experiment #4.....138
Figure 4.70: Normalized effluent salinity during high-salinity polymer injection between 9.1 and 10.3 PV for experiment #4, from a salinity index of 4 ppt to 28 ppt. 139
Figure 4.71: Normalized effluent salinity, oil cut, and oil saturation during alternating polymer floods for experiment #4.....139
Figure 4.72: Oil saturation versus pore volumes for experiment #4. 140
Figure 4.73: Oil saturation, cumulative oil recovered, and oil cut for experiment #4. 141
Figure 4.74: ORP (R.mV) and iron concentration (ppm) of the effluents. 144
Figure 4.75: pH and iron concentration (ppm) of the effluents.....144
Figure 4.76: Normalized effluent salinity during 0.1% NaCl brine injection for experiment #5, from a salinity index of 40 ppt to a 2 ppt.....145
Figure 4.77: Flow rate during 137 cP crude oil flooding conducted at 85 psi constant pressure and 23 °C temperature for experiment #5. 147
Figure 4.78: Pressure drop, and the interstitial velocity data during 137 cP crude oil flooding conducted at 85 psi constant pressure and 23 °C for experiment #5.....147
Figure 4.79: Pressure drop and the interstitial velocity data during waterflooding at 23°C for experiment #5.....148
Figure 4.80: Normalized effluent salinity during 2nd salinity tracer test for experiment #5, from a salinity index of 3l.5 ppt to 3 ppt.....150

Figure 4.81: Pressure drop data, and the interstitial velocity during glycerin flooding at 23 °C for experiment #5.....151
Figure 4.82: DFST result for 2000 ppm FP-3630S HPAM polymer in 1000 ppm NaCl + 400 ppm $NaHCO_3$ aqueous solution at 23 °C for experiment #5. 152
Figure 4.83: DFST result of the 3547 ppm FP-3630S HPAM polymer (# JBA 2114/4-6) in 24000 ppm NaCl, 300 ppm $NaHCO_3$ aqueous solution at 23 °C for experiment #5.....153
Figure 4.84: SRST result for 3547 ppm FP-3630S HPAM polymer in 24000 ppm NaCl, 300 ppm NaHCO3 aqueous solution compared with 2000 ppm FP-3630S HPAM polymer in 1000 ppm NaCl + 400 ppm $NaHCO_3$ aqueous solution at 23 °C for experiment #5.....154
Figure 4.85: Pressure drop data during alternating polymer floods for experiment #5. 158
Figure 4.86: Capillary number data during alternating polymer floods for experiment #5.....158
Figure 4.87: Normalized salinity versus effluent volume of the polymer salinity tracer test, from a salinity index of 2 ppt to 28 ppt. 159
Figure 4.88: Normalized salinity versus effluent volume of the polymer salinity tracer test, from a salinity index of 28 ppt to 2.7 ppt. 160
Figure 4.89: Oil saturation versus pore volumes for experiment #5. 161
Figure 4.90: Oil saturation, cumulative oil recovered, and oil cut for experiment #5. 161
Figure 4.91: Normalized effluent salinity during the 2% KCl brine injection for experiment #6, from a salinity index of 47 ppt to15 ppt.....164

Figure 4.92: Pressure drop data and the interstitial velocity during glycerin flooding at 23 °C for experiment #6. 167
Figure 4.93: Oil saturation versus pore volumes for experiment #6. 170
Figure 4.94: Oil cut data for the glycerin flood, low-salinity, and high-salinity polymer floods for experiment #6.....170
Figure 4.95: Pressure data for glycerin flood, low-salinity, and high-salinity polymer floods for experiment #6. 171
Figure 4.96: Normalized effluent salinity during 2% KCl brine injection for experiment #7, from a salinity index of 54 ppt to 5 ppt.....173
Figure 4.97: Oil saturation versus pore volumes for experiment #7. 176
Figure 4.98: Oil cut data for low-salinity, and high-salinity polymer floods for experiment #7.....177
Figure 4.99: Pressure data for glycerin flood, low-salinity, and high-salinity polymer floods for experiment #7. 177
Figure 4.100: Oil saturation versus pore volumes for experiment #8. 180
Figure 4.101: Oil cut data for low-salinity, and high-salinity polymer floods for experiment #8.....181

Chapter 1: Introduction

1.1 BACKGROUND

Production from hydrocarbon reservoirs generally occurs in up to three phases. During primary recovery, hydrocarbons are produced without injection of water, gas or other fluids into the reservoir so the production decreases as the reservoir pressure decreases. Subsequently, water (or sometimes gas) is injected as a secondary recovery method to increase the pressure and displace the oil towards the production wells. Although often successful, more than 50% of the "original oil in place" (OOIP) generally remains unrecovered at the economic limit of secondary recovery. Part of the oil is not contacted by the injected water (bypassed oil due to incomplete volumetric sweep of the reservoir) and part of the oil is contacted by the water but not completely displaced by the water. Part of the remaining oil in the swept zone is caused by the trapping of oil in pores by capillary forces (residual oil) and part of the remaining oil in the swept zone is caused by incomplete displacement of the mobile oil in the pores (displacement sweep efficiency).

Enhanced oil recovery (EOR) can be used to increase oil recovery following either primary or secondary recovery. Common EOR methods include thermal, gas, and chemical methods. Chemical EOR includes the use of polymer flooding, surfactant-polymer flooding and alkaline-surfactant-polymer flooding among others. Polymers are added to the water to increase its viscosity and thus lower the mobility ratio, which improves both the volumetric and displacement sweep efficiencies. Unlike surfactants, polymers do not lower the interfacial tension (IFT) between the water and oil. Therefore, polymer flooding does not reduce the residual oil saturation by reducing the capillary forces (Lake et al., 2014; Sorbie, 1991; Green and Willhite, 1998).

However, many studies have shown that under some conditions the residual oil saturation can be significantly reduced using polymers (Wreath, 1989; Wang *et al*., 2000; Wang *et al*., 2001; Xia *et al*., 2004**,** Yin *et al*., 2006; Wu *et al.,* 2007; Xia *et al.,* 2008; Jiang *et al.,* 2008; Huh and Pope, 2008; Urbissinova *et al.,* 2010; Sheng, 2010; Afsharpoor and Balhoff, 2013; Ehrenfried, 2013; Vermolen *et al.,* 2014; Koh *et al*., 2016; Qi *et al.,* 2017;). Qi et al. (2017) conducted a series of coreflood experiments in nearly homogenous Bentheimer cores (~ 1500 mD) saturated with viscous oil (~ 150 cp) at residual water saturation and then waterflooded with brine and a viscous glycerin solution to ensure all unswept oil was produced and the core was at residual saturation. Injection of viscoelastic polymer solution following the glycerin flood resulted in a significant reduction in the residual oil saturation. Qi et al. (2017) showed a decreasing trend in residual oil saturation as the Deborah number increased.

1.2 OBJECTIVE

The initial objective of this research was to further understand and quantify the impact of polymer viscoelasticity on residual oil saturation by conducting coreflood experiments using viscoelastic polymers at higher Deborah numbers than done in previous experiments. However, after recovering significant, additional oil from a salinity tracer test when a "high salinity, low viscoelasticity polymer" was injected after a "low salinity, high viscoelasticity polymer", the objective was changed. Therefore, the primary objective of this research became to conduct coreflood experiments to measure the reduction in the residual oil saturation when a high-salinity, low elasticity polymer solution was injected following injection of a low-salinity, high elasticity polymer solution.

Chapter 2: Literature Review

2.1 ENHANCED OIL RECOVERY (EOR)

Enhanced oil recovery (EOR) is the recovery of additional oil by injecting fluids into the oil reservoir as displacing fluid. Most definitions of EOR exclude the injection of water (waterflooding or secondary recovery). EOR aims to increase the amount of crude oil produced and extend the economic life of the production wells (Lake et al., 2014; Sorbie, 1991). Oil recovery classifications are illustrated in Figure 2.1 (Lake et al., 2014).

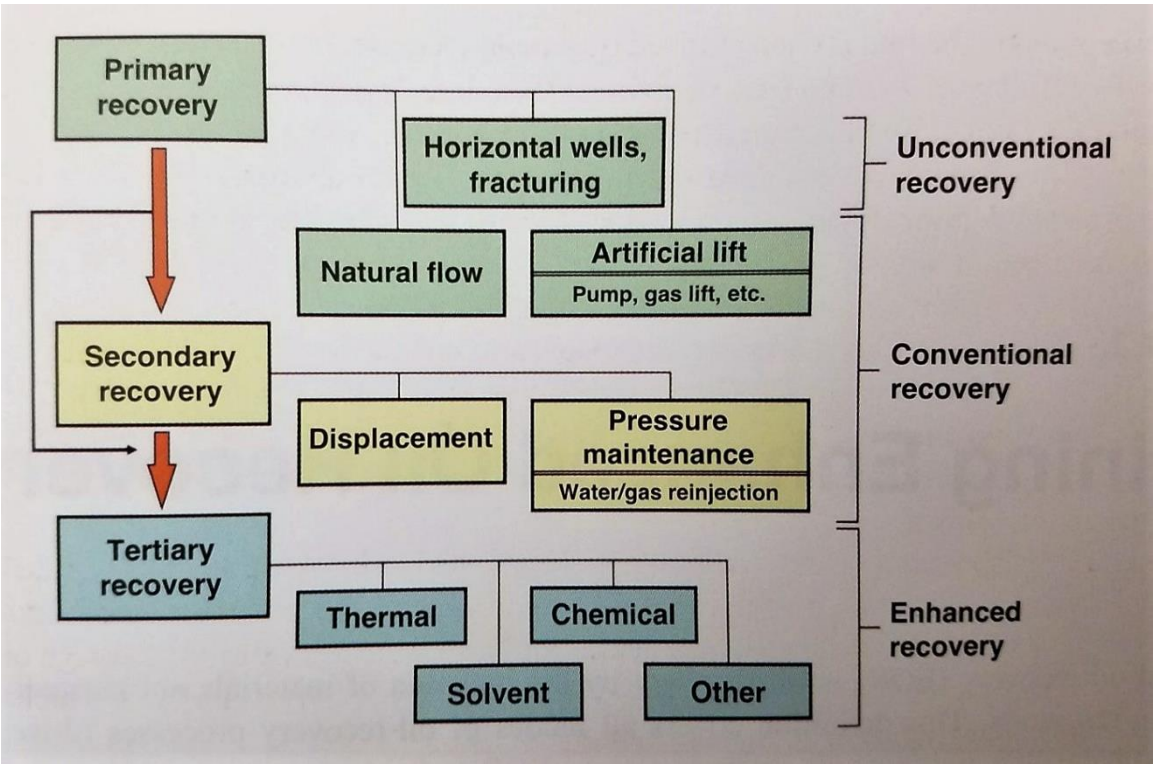

Figure 2.1: Oil Recovery Classifications (Lake et al., 2014).

Figure 2.2 is an illustration of oil production showing the primary recovery, secondary recovery, and enhanced oil recovery. Since the illustration was originally drawn

in 1980's, it shows an additional 4-11% of the original oil in place for the enhanced oil recovery method. However, with today's technology, additional recovery should be higher.

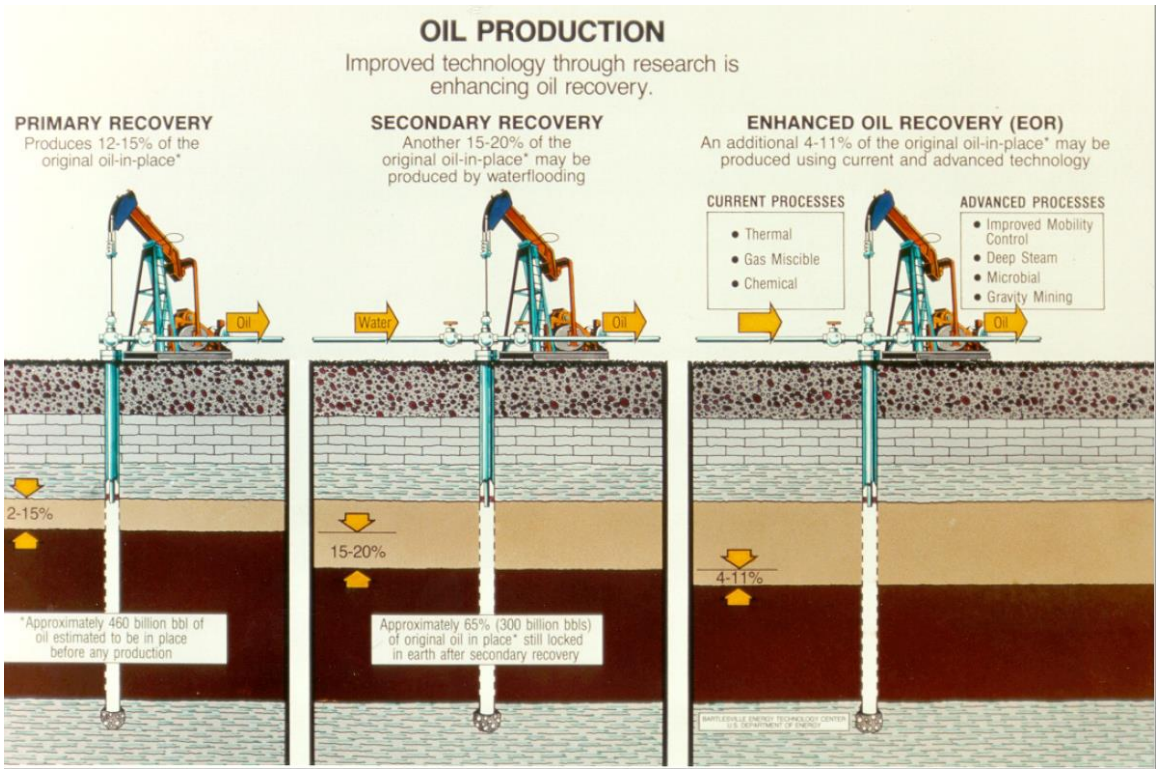

Figure 2.2: Oil production illustration (Lindey, 2001)

2.1.1 Thermal EOR

Thermal enhanced oil recovery includes injecting steam and injecting air for in-situ combustion (Lake et al., 2014) to recover heavy and viscous oil by reducing the oil viscosity and by distillation of the oil.

2.1.2 Solvent EOR

Solvent enhanced oil recovery is the oil recovery method being applied by injecting immiscible or miscible solvents into the oil reservoir (Lake et al., 2014). Commonly used solvents include natural gas, nitrogen gas, and carbon dioxide gas.

2.1.3 Chemical EOR

Chemical enhanced oil recovery (CEOR) methods include polymer flooding (the injection of water-soluble polymers), surfactant-polymer (SP) flooding, and alkaline-surfactant-polymer (ASP) flooding. Polymer flooding improves both displacement and volumetric sweep efficiencies. Surfactants (or detergents) are used to recover residual oil by reduction of interfacial tension (IFT) and to enhance imbibition in naturally fractured reservoirs by both wettability alteration and reduction of IFT.

2.2 RESIDUAL OIL SATURATION

Residual oil is the oil ganglia trapped in pore throats by capillary forces. Residual oil saturation depends on wettability, pore size distribution and interfacial tension among other factors. Residual oil saturations following displacement by water are typically in the range of 0.20 to 0.40. The residual oil saturation following polymer floods with different properties is the main focus of this study.

Mobile oil is the oil saturation minus the residual oil saturation. Only a fraction of the mobile oil is displaced at any given time by any given displacing fluid such as water or polymer solution. The displacement sweep efficiency is the fraction of the mobile oil that has been displaced at a given time. The displacement sweep efficiency depends on the heterogeneity of the rock and the mobility ratio (defined below) among other factors (Qi et. al., 2017). High mobility ratios can lead to unstable displacements (fingering) that result

in poor volumetric sweep efficiency even in nearly homogeneous cores, but this is not the focus of this study.

Morrow and Buckley (2011) found from their laboratory studies that injecting low-salinity brine after injecting high-salinity brine increases the oil recovery. Many mechanisms have been proposed to explain this phenomenon. One mechanism is a wettability alteration resulting in the reduction in residual oil saturation.

Koh et al. (2016) used fractional flow theory to analyze their polymer coreflood experiments. Displacement sweep efficiency can be calculated from fractional flow theory (Lake et al., 2014). They found that displacement sweep efficiency was the main mechanism for the reduction in the oil saturation under the conditions of their experiments. According an extrapolation made by them, to reach the true residual oil saturation for an oil reservoir containing a viscous oil would require injecting on the order of 1000 pore volumes of water (Figure 2.3). For that reason, they used residual oil saturation after polymer flooding at 100% water cut in their fractional flow calculations for both polymer floods and water floods.

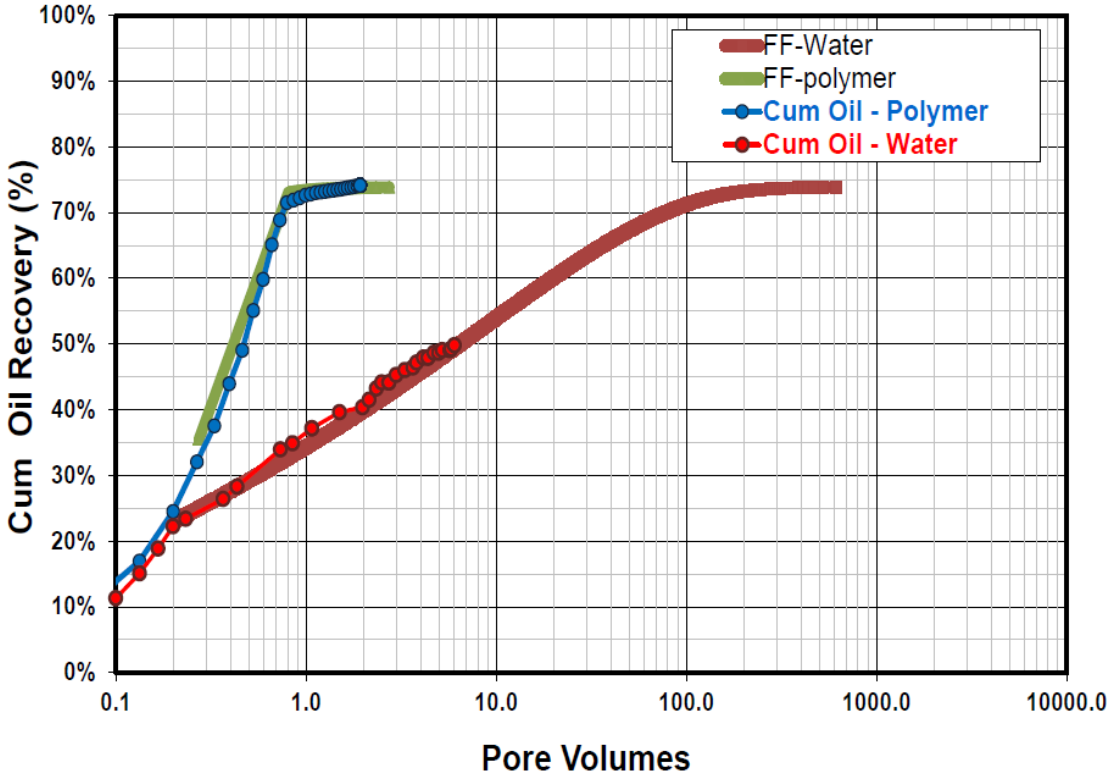

Figure 2.3: Comparison of experimental and fractional flow results for cumulative oil recovery of waterflood and polymer flood for an experiment of Koh et al. (2016)

2.3 MOBILITY RATIO AND CAPILLARY NUMBER

Mobility ratio and the capillary number which are important parameters to determine the oil saturations following waterflood and polymer flood, will be presented in the following subsections.

2.3.1 Mobility Ratio

Mobility ratio (M) is defined as the mobility of the displacing fluid divided by the mobility of the displaced fluid. In this research, displacing fluids are water, glycerin, or polymer solution, and the displaced fluid is oil.

The end-point mobility ratio (M°) is defined in the following equation:

$$M^{\circ} = \frac{\lambda_i}{\lambda_o} = \frac{\frac{k_{ri}}{\mu_i}}{\frac{k_{ro}}{\mu_o}} = \frac{k_{ri}\mu_o}{k_{ro}\mu_i} \tag{2.1}$$

where, λ_i is the mobility of displacing fluid at residual oil saturation and λ_o is the mobility of the oil at residual water saturation; k_{ri} is displacing fluid end-point relative permeability, and k_{ro} is end-point oil relative permeability; μ_i is displacing fluid viscosity and μ_o is oil viscosity. In this equation, the notation "i" was used to show the displacing fluid. For waterflood "i" can be replaced by "w", for glycerin flood it can be replaced by "gly", and for polymer flood it can be replaced by "p". When the displacing fluid generates an oil bank, then the mobility of the displaced fluid in the mobility ratio is the oil mobility plus the water mobility flowing in the oil bank. Other useful definitions include the mobility ratio across a shock front. The appropriate definition depends on the application.

2.3.2 Capillary Number

Capillary number (N_c) is the dimensionless ratio of viscous forces to capillary forces (Lake et al., 2014) and is a special case of the trapping number (Pope et al., 2000). The capillary number was defined by Brownell and Katz (1947), Stegemeier (1977) and Chatzis and Morrow (1983) among others as follows:

$$N_c = \frac{k\nabla\Phi}{\sigma} \tag{2.2}$$

where, k is the brine permeability when S_w=1, σ is the interfacial tension between the oil and the displacing fluid and $\nabla\Phi$ is the magnitude of the local potential gradient. In

the absence of gravitational forces, the potential gradient reduces to the pressure gradient. For a steady state displacement in a linear core of length L, the pressure gradient is the pressure drop (ΔP) divided by L. By adding units and conversion factors capillary number can be defined as follows:

$$N_c = \frac{k(\frac{\Delta P}{L})}{\sigma} = \frac{k(Darcy)*0.99*10^{-8}(\frac{cm^2}{Darcy})*\frac{\Delta P(psi)}{L(cm)}*\frac{6.89*10^4(\frac{dynes}{cm^2})}{(psi)}}{\sigma(dynes/cm)} \quad (2.3)$$

Darcy's law can be used with Eq. (2.2) to derive another commonly used form of the capillary number. If relative permeability is neglected, the capillary number can be expressed as follows:

$$N_c = \frac{u\mu}{\sigma} \quad (2.4)$$

where, u is the Darcy velocity (q/A), μ is the viscosity of the displacing fluid, and σ is the interfacial tension between the oil and the displacing fluid. This form is convenient to use when both the Darcy velocity and the viscosity are constant (Newtonian fluid). Equation 2.3 is the more fundamental form of the capillary number and was used in this study.

The relationship between residual oil saturation and the capillary number (N_c) is shown schematically for uniform sandstones in Figure 2.4. This relationship is called the capillary desaturation curve (CDC). An example of a measured residual oil saturation in a water-wet Berea sandstone is shown in Figure 2.5 (Delshad, 1990). The critical N_c (when the oil saturation starts to decrease) is on the order of 10^{-5} for the non-wetting phase in a typical sandstone using Equation (2.2) for the definition of capillary number, but it is very different in most carbonates (Kamath et al., 2001). Residual oil saturation decreases when

the N_c is above the critical N_c. Typical N_c values for waterfloods are less than 10^{-7}. Generally when the heterogeneity of the rock increases the critical capillary number decreases and the reduction in the residual oil saturation is more gradual.

To reduce residual oil saturation below the waterflood residual oil saturation in sandstones, it is required to increase the N_c significantly. This can be achieved in laboratory conditions by increasing the magnitude of the pressure gradient, when other variables (i.e. permeability and interfacial tension) are constant. However, the pressure gradient in the oil reservoirs is generally not high enough to surpass the critical N_c.

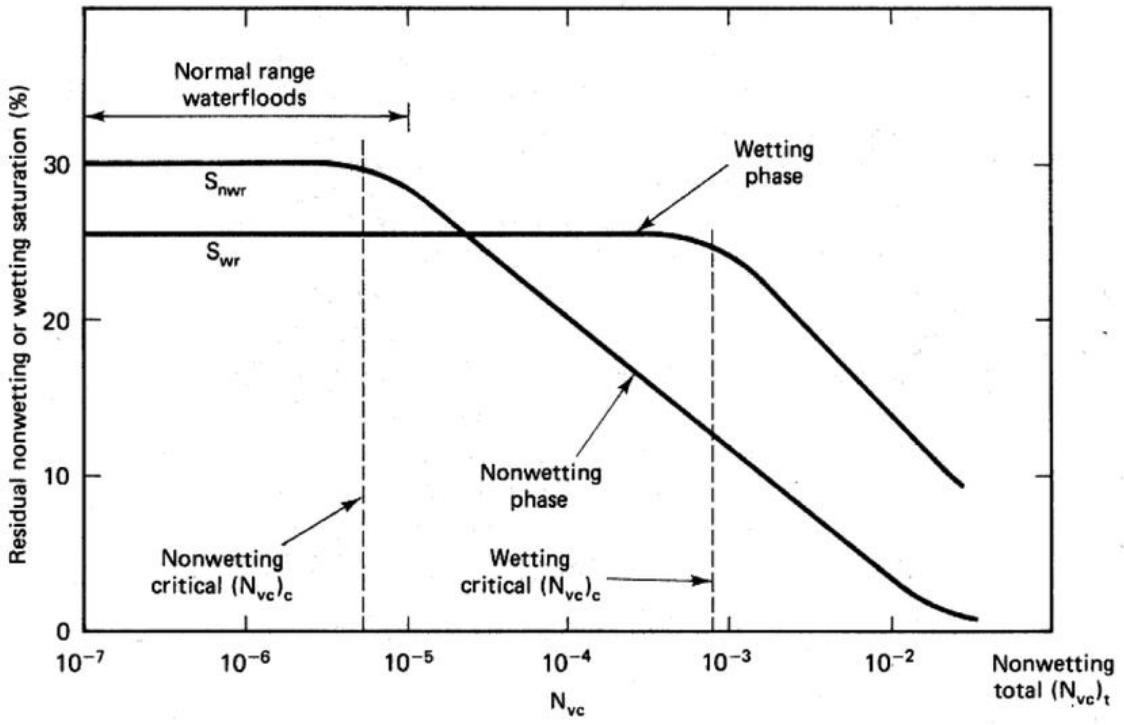

Figure 2.4: Capillary desaturation curve (Lake et al., 2014)

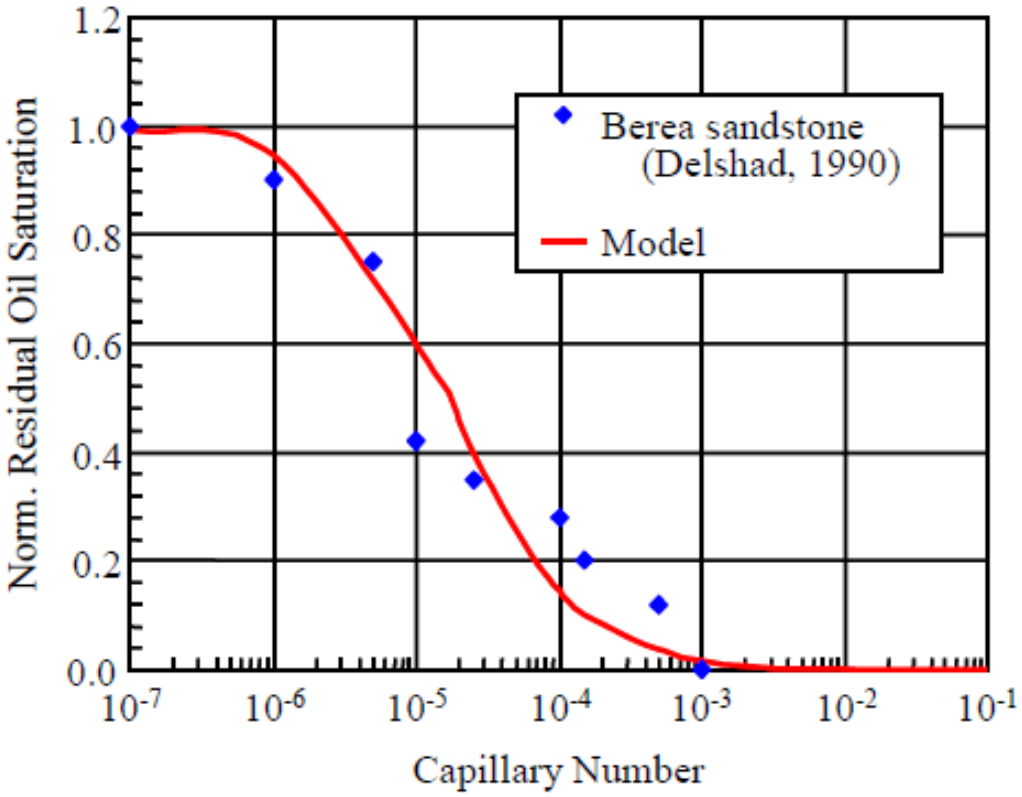

Figure 2.5: Capillary Desaturation Curve for Berea Sandstone

Qi et al. (2017) measured the interfacial tension between oil and brine as 15.6 dynes/cm, between oil and glycerin as 21.3 dynes/cm, and between oil and HPAM polymer as 17.3 dynes/cm. The capillary desaturation curve (CDC) for HPAM polymer solution in Bentheimer sandstone measured by Qi et al. (2017) is shown in Figure 2.6. Measurement of the CDC of HPAM polymer displacement, the polymer had been flooded at different constant pressure gradients, obtained oil saturation and effluent flow rates at given steady state pressure gradients, and finally calculated capillary numbers. The CDC of HPAM polymer through Bentheimer sandstone shows a critical N_c of approximately 10^{-4} (~30psi/ft) which is higher than the critical N_c of Berea sandstone. This is because Berea sandstone has a much wider pore size distribution than Bentheimer sandstone. In this

research, coreflood experiments were conducted at low pressure gradients where the N_c is less than the critical N_c so any reduction in oil saturation could be attributed to effects besides an increase in capillary number.

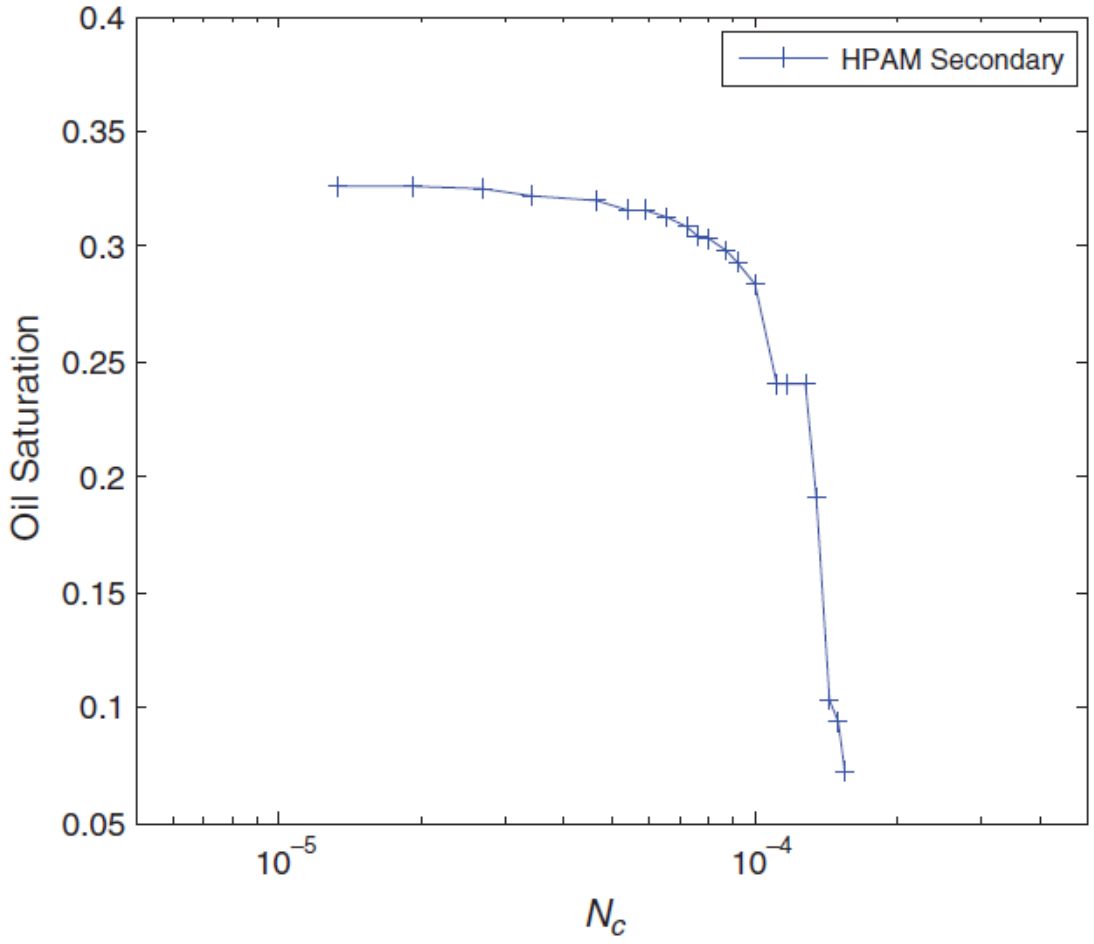

Figure 2.6: Capillary desaturation curve (Qi et al., 2017)

2.4 POLYMER FLOODING

Polymer flooding has been practiced in the field since the 1960s (Pye, 1964; Sorbie, 1991). To conduct a successful polymer flood, an excellent quality polymer solution is needed. Quality of the polymer solution depends on the polymer manufacturing, water quality, polymer mixing and polymer filtration (Pope, 2015).

Although several polymers have been proposed for use in enhanced oil recovery applications, hydrolyzed polyacrylamide (HPAM) is by far the most widely used in industry practice. HPAM has been used for mobility control since 1960s and is the polymer studied here. In the following section, the properties of HPAM such as chemical structure, degree of hydrolysis, molecular weight, polymer concentration, brine salinity, temperature, and viscoelasticity is presented.

2.5 HPAM POLYMER PROPERTIES

HPAM is a synthetic polymer which has been used for viscosifying aqueous solutions to be injected into oil reservoirs for enhancing the oil recovery. HPAM was available and accessible in the market as it was being used in other industries. HPAM's degree of hydrolysis and molecular weight are important properties in terms of its performance (Sorbie, 1991). The polymer solution viscosity is a function of brine salinity and hardness, polymer concentration, polymer molecular weight, temperature, and shear rate.

2.5.1 Chemical Structure

HPAM is a synthetic straight-chain polymer of acrylamide monomers, some of which have been hydrolyzed. Some commercial products are made as co-polymers of acrylamide and acrylic acid and may also be called HPAM for convenience. The molecule

is a flexible chain structure known as a random coil in polymer chemistry. HPAM shows elastic behavior because of this structure (Sorbie, 1991). The chemical structure of HPAM is shown in Figure 2.7.

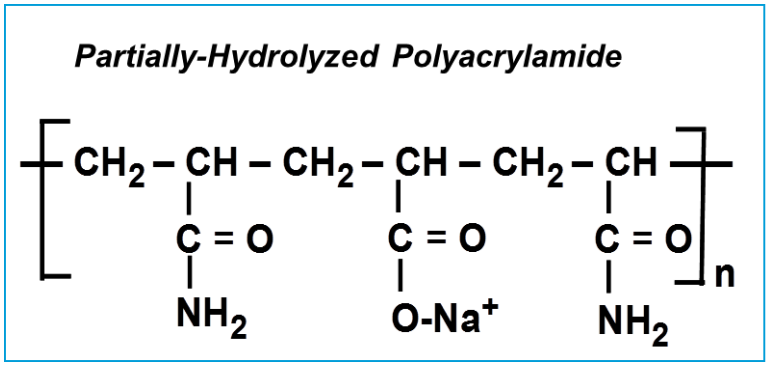

Figure 2.7: Chemical Structure of Partially hydrolyzed polyacrylamide (HPAM)

Since the molecule is a polyelectrolyte, it interacts actively with ions in solution. Since the polyacrylamide chain is flexible, it may respond much more to the ionic strength of the aqueous solvent, and its solution properties are sensitive to salt/hardness. This is illustrated schematically in Figure 2.8, in which the effect of ionic strength on the hydrodynamic size of the molecule is shown schematically.

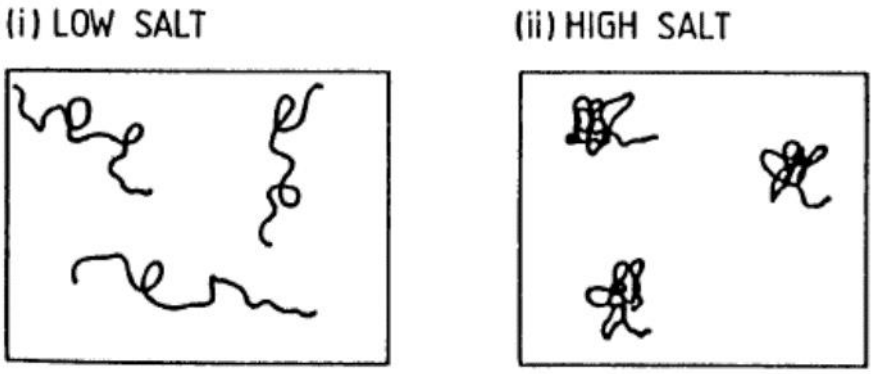

Figure 2.8: Schematic of the effect of solution ionic strength on the conformation of flexible coil polyelectrolytes such as HPAM.

2.5.2 Degree of Hydrolysis and Molecular Weight

HPAM's performance depends on its degree of hydrolysis and molecular weight. HPAM polymers hydrolyze at high temperature and/or high pH. The molecular weight of the polymer is mostly unaffected during hydrolysis. The viscosity of the polymer solution is higher in soft brine than hard brine. Polyacrylamides undergo hydrolysis under both acidic and basic conditions and introduce negative charges into the polymer chain. In hard brines, the interaction between the divalent cations and the negatively charged polymer may result in precipitation of polymer molecules at sufficiently high hardness, and a corresponding decrease the solution viscosity. The degree of hydrolysis is typically between 15% and 40% for commercial HPAM polymers used for enhanced oil recovery. During its residence in the reservoir at elevated temperature and/or pH, the degree of hydrolysis of polyacrylamide polymers increases (Ryles, 1988; Moradi-Araghi and Doe, 1987; Levitt and Pope, 2008).

The thickening potential of a polymer is determined in part by the molecular weight of the polymer. Molecular weight of the polymer is related to its molecular size and has a direct effect on its transport in porous media. A polymer with higher molecular weight gives a solution with a higher viscosity. There are various molecular weights (low to very high) for the HPAM polymers manufactured in today's market. The typical molecular weight of HPAM used in polymer floods is in the range of 2 to 20 $\times$ 10^6 g/mole. Flopaam 3630S is a commercial co-polymer manufactured by SNF with a high molecular weight of about 20 $\times$ 10^6 g/mole. FP 3630S was used in this study.

2.5.3 Polymer Concentration and Brine Salinity

The effect of FP 3630S polymer concentration and salinity on polymer viscosity at 10 s^{-1} shear rate are shown in Figure 2.9 (Koh, 2015). At 3000 ppm, when salinity increases from 0.1wt% NaCl to 4 wt% NaCl in water, polymer viscosity at 10 s^{-1} decreases from 225

cp to 55 cp. For the same salinity, for instance 1 wt% NaCl, when the polymer concentration increases from 500 ppm to 3000 ppm, polymer viscosity at 10 s^{-1} increases from 5 cp to 84 cp.

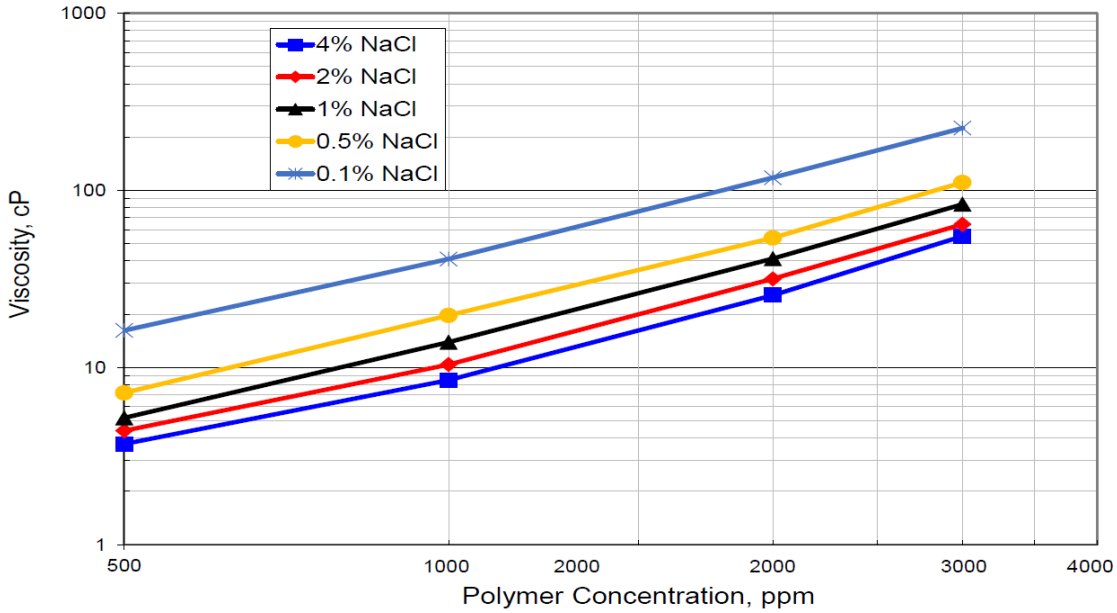

Figure 2.9: Salinity and polymer concentration effect on the viscosity at 10 s^{-1} equivalent shear rate for Flopaam™ 3630S at 25°C in log-log scale (Koh, 2015)

Polymer viscosity data for five high molecular weight polymers at 1500 ppm, 11 s^{-1} and 23 C are shown in Figure 2.10 as a function of salinity. There is slight decrease in the viscosity for salinities greater than about 3 wt% NaCl. This shows high molecular weight HPAM polymer solutions can be used even at high salinities (Levitt and Pope, 2008).

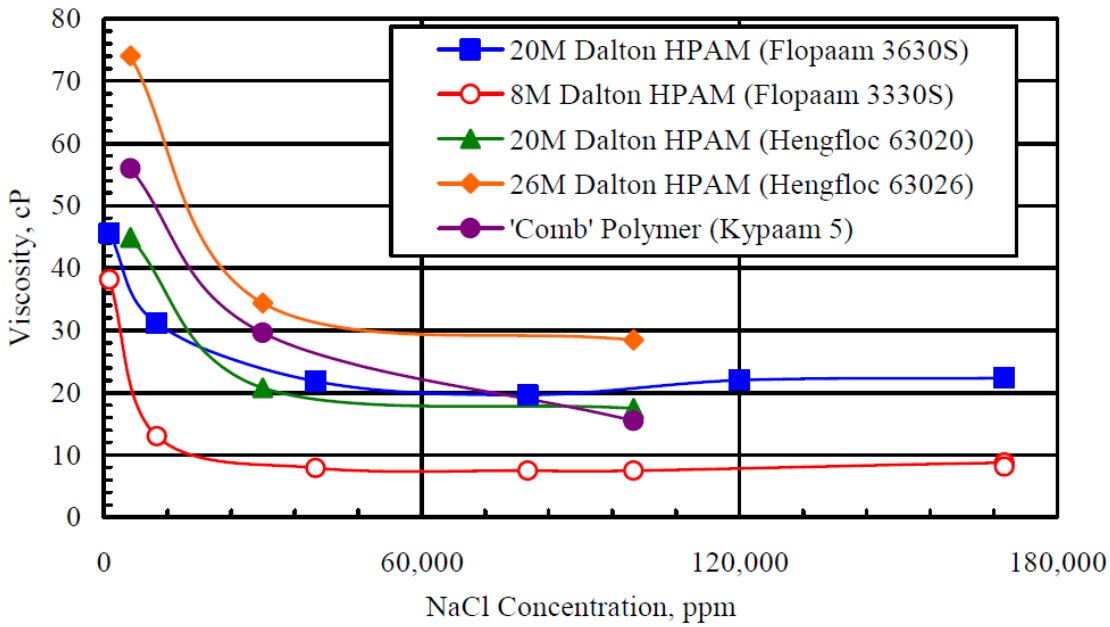

Figure 2.10 Salinity effect on the polymer viscosity (at 11 s^{-1} equivalent shear rate) for five different 1500 ppm high molecular weight polymers at 23 °C (Levitt and Pope, 2008)

2.5.6 Temperature

HPAM polymer viscosity decreases with increasing temperature in the same way as water. Example data are shown in Figure 2.11

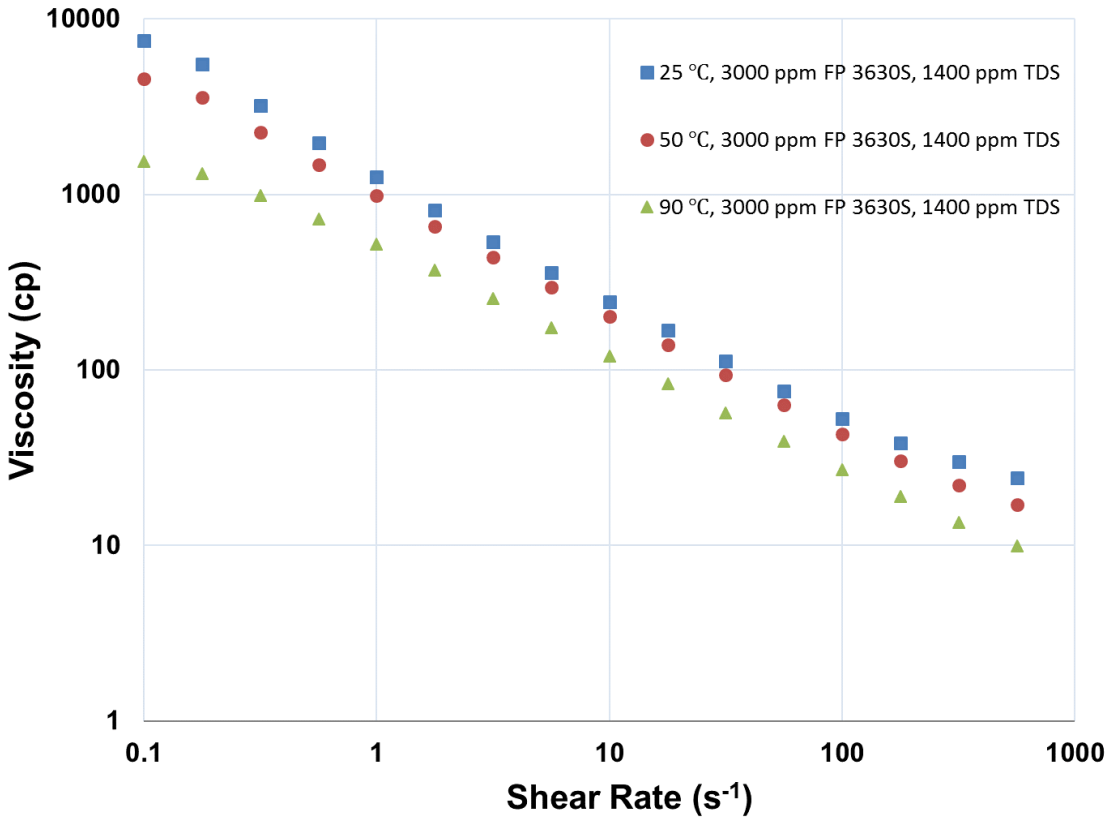

Figure 2.11: Effect of temperature on viscosity for 3000 ppm FlopaamTM 3630S in 1400 ppm TDS aqueous solution

2.5.8 Viscoelasticity and Deborah Number

The effect of the elasticity of a polymer is observed when its relaxation time is greater than the transit time in a pore (Sorbie, 1991). The Deborah number (N_{De}) is a dimensionless number defined as the ratio of the relaxation time to the average transit time of the polymer in the pores of the rock. The definition of Deborah number used in this work is as follows:

$$N_{De} = \tau_r \dot{\gamma}_{eq} \tag{2.5}$$

where τ_r is the relaxation time and $\dot{\gamma}_{eq}$ is the equivalent shear rate defined as follows:

$$\dot{\gamma}_{\text{eq}} = C\left(\frac{3n+1}{4n}\right)^{\frac{n}{n-1}} \frac{4u}{\sqrt{8kk_{rw}\phi S_w}} \tag{2.6}$$

where C is the shear correction factor, n is the power law exponent, u is the Darcy velocity, k is the brine permeability, k_{rw} is the water relative permeability, ϕ is the porosity, and S_w is the aqueous phase saturation. Similar equations have been used by Wreath, Cannella, Green and Willhite, Delshad and others. The effect of viscoelasticity on flow of the polymer solution in a porous medium becomes significant when the Deborah number exceeds values on the order of 1 (Hirasaki and Pope, 1974; Durst et al., 1981; Haas and Durst, 1982; Jones et al., 1987; Masuda et al., 1992; Delshad et al., 2008; Koh, 2015; Qi et al., 2017).

The relaxation time (τ_{r}) for a polymer solution is defined as the time required for the polymer solution to be displaced from equilibrium to decay back to its original value. There are different models to predict the relaxation time, such as G' and G" cross-over point model (Volpert, et al., 1998) which is for linear viscoelastic fluids and very practical; Rouse model (Rouse, 1953), and Generalized Maxwell Model (GMM) (Schiessel et al., 1995; Kim et al. 2010) which are very complex models for non-linear viscoelastic models. Rouse (1953) concluded that GMM can define the viscoelastic properties of polymer solution. Both Rouse model and GMM have many relaxation time values.

Kim et al. (2010) created an empirical model for relaxation time prediction. They used the cross-over point as the initial estimation, and then used non-linear fitting of the GMM model. They concluded that the highest relaxation time they obtained with this method is the best fitting relaxation time for the polymers FP 3630S, FP 3330S, and AN-125. Qi et al. (2017) compared their cross-over point relaxation time data to the Rouse model and GMM by using nonlinear regression and found out good fits within experimental error. Therefore, they decided to use cross-over point model in their study.

According to the G' and G" cross-over point model (Volpert, et al., 1998; Delshad et al., 2008; Ehrenfried, 2013; Koh, 2015; Qi et al., 2017), relaxation time of the fluid is the inverse of the frequency (ω) at which G' and G" cross. G' is the elastic component of the viscoelasticity, while G" is the viscous component of viscoelasticity. Relaxation time can be determined by conducting dynamic frequency sweep test (DFST) in the rheometer. An example of DFST is given in Figure 2.12. As it can be seen from the figure, 0.09788 rad/s is the frequency (ω) at which G' and G" cross, and the inverse of that frequency is 10.2 s. The average residence time in pores is defined as the ratio of the interstitial velocity to the average grain diameter of a porous medium. It is also defined as the inverse of the effective (equivalent) shear rate.

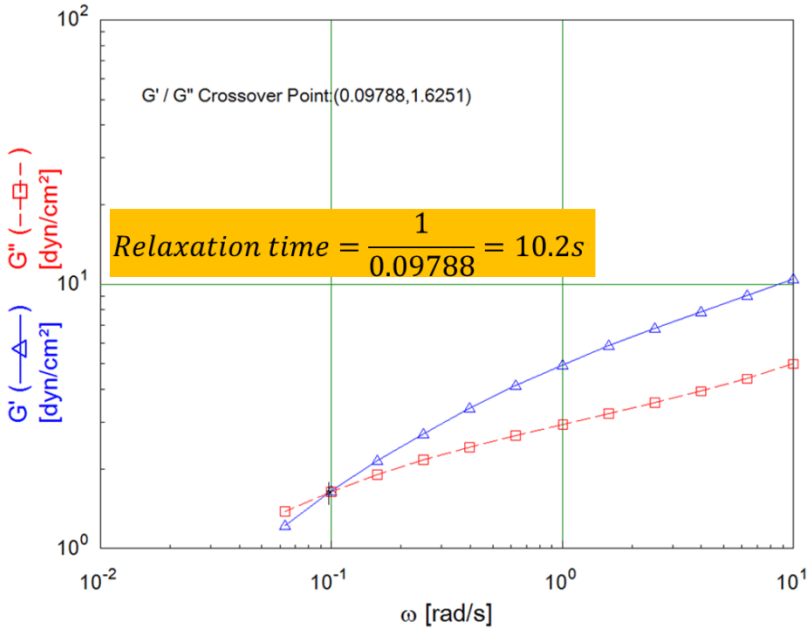

Figure 2.12: Dynamic frequency sweep test result for 2000 ppm Flopaam 3630S in 1000 ppm NaCl and 400 ppm NaHCO3 at 25 °C

Chapter 3: Experimental Approach

The experimental approach including experimental materials, equipment, procedures, measurements, and calculations to conduct the core flooding experiments performed in this work is presented in this chapter. The experimental approach is presented step by step from core preparation to polymer flooding. The experimental approach is similar to that used by Fortenberry (2013), Unomah (2013), Koh (2015), Lee (2015) and Qi et al. (2017).

3.1 CORE PREPARATION AND COREFLOOD SETUP

All cores used in this research were Bentheimer sandstone and had a diameter of 2 inches and length of 12 inches (1 ft). The cores which were provided by Kocurek Industies, pre-cored in these dimensions. The cores were ready to be potted in epoxy. The length of the cores (1 ft) was chosen because it is suitable for accurate measurement of pressure gradients, and maintains acceptably low dispersion and capillary end effects (Lee, 2015).

3.1.1 Core Preparation

Materials used for core preparation include a core, a 2.5" diameter and 14" length transparent polycarbonate cylinder tube, two 2” diameter polycarbonate endcaps, epoxy resin (EPON Resin 828), hardener (Versamid 140), silicon glue, aluminum foil, pressure taps, nylon fitting connectors, thread seal tape, 5-min epoxy, and five three-way valves were used. The equipment used for epoxied core preparation are drill, drill bits, air system, and a tub used for leaking test.

The core preparation procedure is described as follows:

1. Measure the dimensions of the core (diameter and length) from three different spots. The bulk volume (V_b) is calculated using equation 3.1 and the average of the three measurements:

$$V_b = hA = h\pi(D^2 / 4) \quad (3.1)$$

Where h is the core length in cm, A is the cross-sectional area of the core, and D is the diameter of the core in cm. The relative error between using only one measurement and the average of three dimensions is about 0.6%.

2. Weigh the core and calculate the bulk density of the core as follows:

$$\rho_{bulk} = \frac{M}{V_b} \quad (3.2)$$

Where ρ_{bulk} is the bulk density in g/cm^3, M is the mass of the core in grams, and V_b is the bulk volume of the core in cm^3.

3. Use 5-min epoxy to seal the edges between the core and 2" polycarbonate endcaps, and to seal the core face. 5-min epoxy prevents the imbibition of the slow-setting epoxy into the rock which has high permeability. Block the hole of the bottom endcap, and place the core on an aluminum foil with silicon glue to prevent leaking of slow-setting epoxy.
4. Slide a 2.5" diameter and 14" length clear-polycarbonate tube around the core by keeping the core in the center.
5. Prepare a slow-setting epoxy by mixing the epoxy resin (EPON Resin 828) and hardener (Versamid 125) with a weight ratio of 2:1 until it is mixed homogeneously. The required volume of the slow-setting epoxy is volume of the annulus between the tube and core, plus an excess of 10% in case the epoxy is leaked.
6. Fill the annulus with the slow-setting epoxy by pouring it slowly from only one point, and let it rise from bottom to top to prevent having air bubbles. Leave the core over-night to let the slow-setting epoxy to be set-up. Figure 3.1 shows two Bentheimer cores filled with slow-setting epoxy.

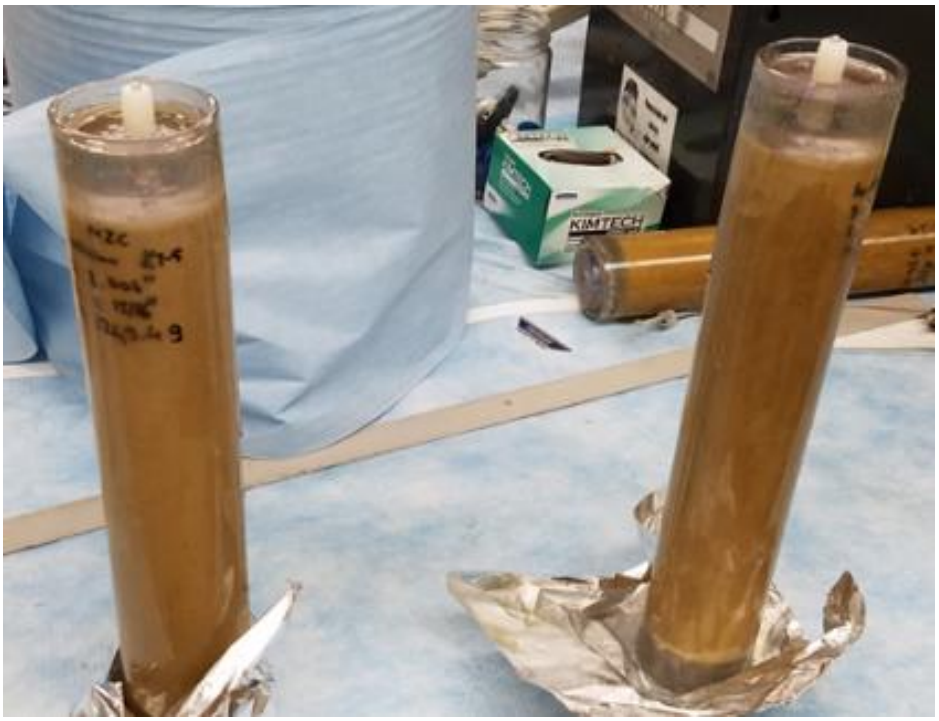

Figure 3.1: Two Bentheimer sandstone cores filled with slow-setting epoxy.

7. Drill the core at three locations along the core face to make holes for pressure tap fittings. The location of those three holes are 3”, 6”, and 9” from bottom of the core (not the tube) on a same vertical line to divide the core into four equal sections. Insert three pressure tap fittings inside those holes after filling with 5-min epoxy. Screw two pressure tap fittings to the endcaps of the core, and connect 3-way valve to those fittings.
8. After approximately 5 minutes of set-up time, drill those 3 pressure tap fittings (one at a time) while injecting air from one of the end-taps. Connect Swagelok® three-way valves to those three pressure tap fittings after the holes are drilled properly.

9. Conduct the water leak test of the core at 95 psi by injecting air from inlet while all other valves are closed, and the core is placed inside a container filled with water. Increase the air pressure to 95 psi gradually while wearing the safety mask. The leak test is recommended to be conducted for 10 minutes, and the core inside the water container should be monitored for any leaks (confirmed from the observation of bubbles). If bubbles observed, identify the cause of the leaks, stop leak test, fix the problem, and re-test until it passes the leaking test. Figure 3.2 shows an image of leaking observation from middle tap of an epoxied Bentheimer sandstone core which is tested inside a container filled with water.

Figure 3.2: Leaking observation from middle tap of an epoxied Bentheimer sandstone core which is tested inside a container filled with water.

3.1.2 Coreflood Apparatus

A diagram of the coreflood apparatus used in this research is shown in Figure 3.3. The core is divided into four sections. The pressure tap on each section is linked to a 0-35 psi differential pressure transducer; the inlet and outlet of the core is linked to a 0-300 psi

differential pressure transducer. Additionally, the inlet and outlet of the core are linked to two 0-150 psi absolute pressure transducers. The linkage/connection between the pressure taps and the pressure transducers are the Swagelok® three-way valves and the tubing filled with water. Using this hydraulic connection and a National Instruments LabView™ data acquisition system software, the pressure drops for each section and the entire core are measured, recorded and displayed instantly on a computer. The core has an inlet where the fluid is injected into the core, and an outlet where the displaced fluid is produced (effluent) and goes to Teledyne Isco Retriever™ 500 fraction collector. If air gets in the core accidentally, then a back-pressure regulator (BPR) is connected to the outlet line to remove the air from core by setting the BPR at 50 psi and injecting the brine at 50 psi.

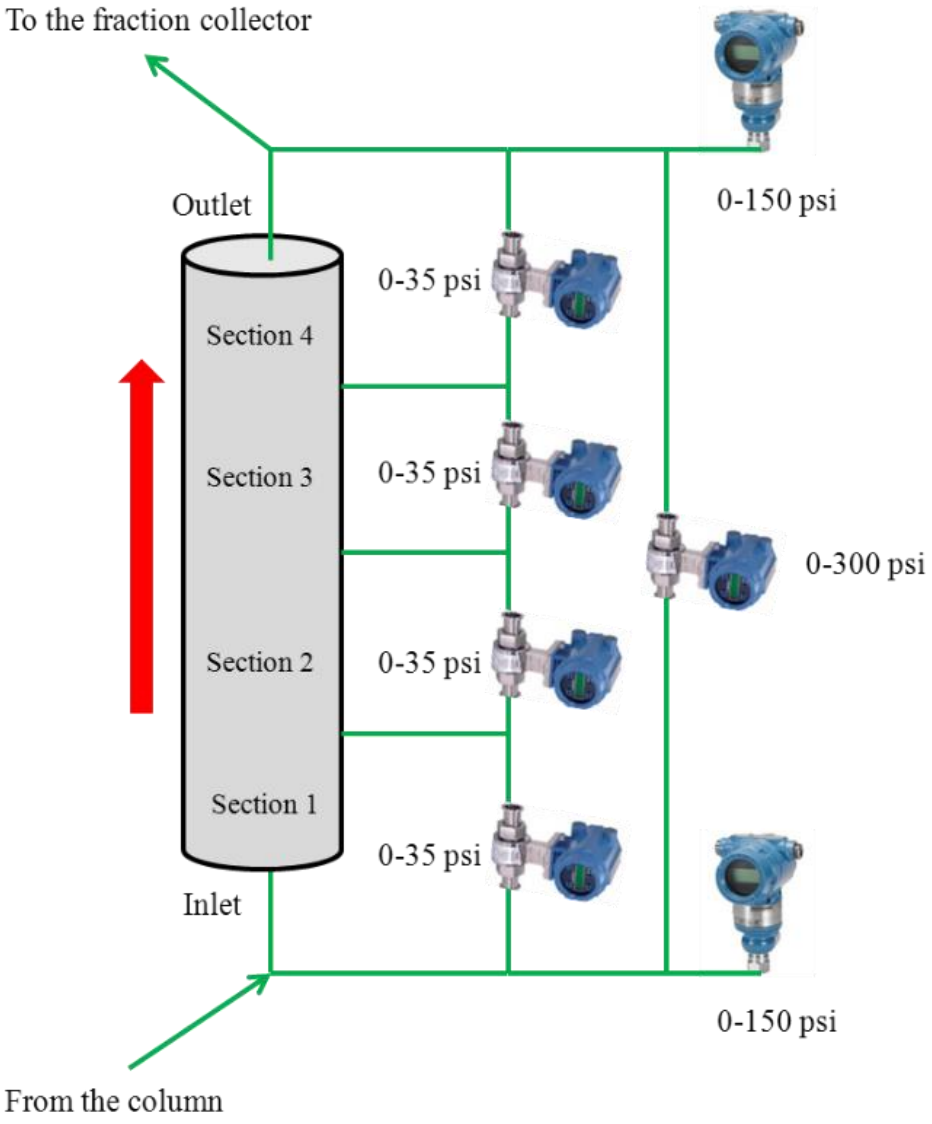

Figure 3.3: Coreflood apparatus showing a core with four sections connected to four 0-35 psi differential pressure transducers; and with inlet & outlet connected to two 0-150 psi absolute pressure transducers, and a 0-300 psi differential pressure transducer.

3.2 SATURATING THE CORE

After the core is potted in epoxy and passes the leak test, it is ready to determine its pore volume (*PV*) by both the mass method and the volume method. *PV* is defined as the total volume of the pores in a rock or, equivalently, the aqueous volume when the core is 100% saturated with brine (Lee, 2015). The core is vacuumed for 2 hrs by using a vacuum pump, and then it is weighed and recorded to obtain its initial mass. A graduated cylinder is filled with a high salinity brine (e. g. 6% KCl). Then, one end of the tubing was placed inside the graduated cylinder to the bottom, and the other end is connected to the inlet valve of the core. The tubing is secured with tape and filled with brine by using a syringe. This is done to prevent the air from entering the core. The brine volume in the graduated cylinder is recorded as the initial volume. Finally, the core is vacuum saturated with the brine until no change in the volume of graduated cylinder is observed. This volume is recorded as the final volume, and the core is weighed to record the final mass.

PV calculation based on mass is defined by equation 3.3:

$$PV = \frac{M_{\text{final}} - M_{\text{initial}}}{\rho_{\text{brine}}} - V_{\text{dead}} \tag{3.3}$$

Where *PV* is pore volume of the core in ml; M_{final}, and M_{initial} are final mass and initial mass in grams respectively; ρ_{brine} is brine density in grams/cm^3, and V_{dead} is the dead volume in ml, and assumed to be 2 ml. V_{dead} is total volume (~2 ml) of the fluid inside the nylon tubings (~1 ml; capacity ~0.03 ml/in) which connect the valves with the end-taps on inlet, outlet, and the core face; and inside the end-taps (~1 ml; capacity ~0.85 ml/in) of the inlet and outlet.

PV is calculated by the volume method using equation 3.4:

$$PV = V_{\text{initial}} - V_{\text{final}} - V_{\text{dead}} \tag{3.4}$$

Where $V_{\text{initial and}}$ V_{final} are initial volume and final volume (ml), respectively. PV determination with the mass method and volume method are used to estimate porosity. Porosity is defined as the ratio of the pore volume to the bulk volume of the rock.

$$\phi = \frac{PV}{V_b} \tag{3.5}$$

Where ϕ is the porosity.

PV obtained from mass method and volume method should be confirmed by conducting salinity tracer test which will be discussed in the following section.

Preliminary brine permeability determination

After saturating the core with high salinity (6% KCl) brine, the same brine solution is vacuum transferred to an injection column, and then injected into the core at five different flow rates to determine the initial brine permeability. In this work, flow rates were varied between 1 ml/min (~9.5 ft/D) to 12 ml/min (~114 ft/D). By using the pressures recorded for each flow rate, the permeability is calculated by using Darcy's law for single phase and steady state flow. Permeability calculation will be discussed in Section 3.4 in detail.

3.3 SALINITY TRACER TEST

After saturating the core with brine and then injecting a few PVs of that high salinity brine, a salinity tracer test is performed to determine the heterogeneity of the core, and to measure the aqueous pore volume. The salinity tracer test is conducted by injecting a lower salinity fluid (e.g. 2% KCl aqueous solution) at 2 ml/min (~19 ft/D) to displace the higher salinity fluid (6% KCl aqueous solution) until the effluent concentration is observed to have the same salinity as the injected brine. In this work, effluent samples were collected in volumes of 4 ml/tube. By using a refractometer, the refractive index (salinity index) of each effluent was read and then normalized by using the initial and final salinity index. Initial salinity index is the salinity index at the beginning of the tracer test, while final

salinity index is the salinity index at the end of the tracer test. Normalized salinity index ($Sal_{\text{normalized}}$) is calculated as follows:

$$Sal_{\text{normalized}} = \frac{Sal_{\text{effluent}} - Sal_{\text{initial}}}{Sal_{\text{final}} - Sal_{\text{initial}}} \tag{3.6}$$

For example, if the effluent salinity index shows 40 ppt, initial salinity index shows 47 ppt, and final salinity index shows 16 ppt, then the normalized salinity is 0.23.

The normalized salinity was plotted against the effluent volume. A typical salinity tracer test plot is shown in Figure 3.4. Aqueous volume is the summation of the area above the curve which is a determination based on the mass balance. Since the horizontal axis (x) is in ml, and the vertical axis (y) is normalized dimensionless value, the product of the x and y gives a volume. The area above the curve for n effluent samples is defined in equation 3.7 as follows:

$$PV = \sum_{\text{i}=1}^{\text{i}=n} V_{\text{i}} (1 - Sal_{\text{normalized}})_{\text{i}} \tag{3.7}$$

Where i is the i$^{\text{th}}$ effluent sample, and V_{i} is the volume of the i$^{\text{th}}$ sample.

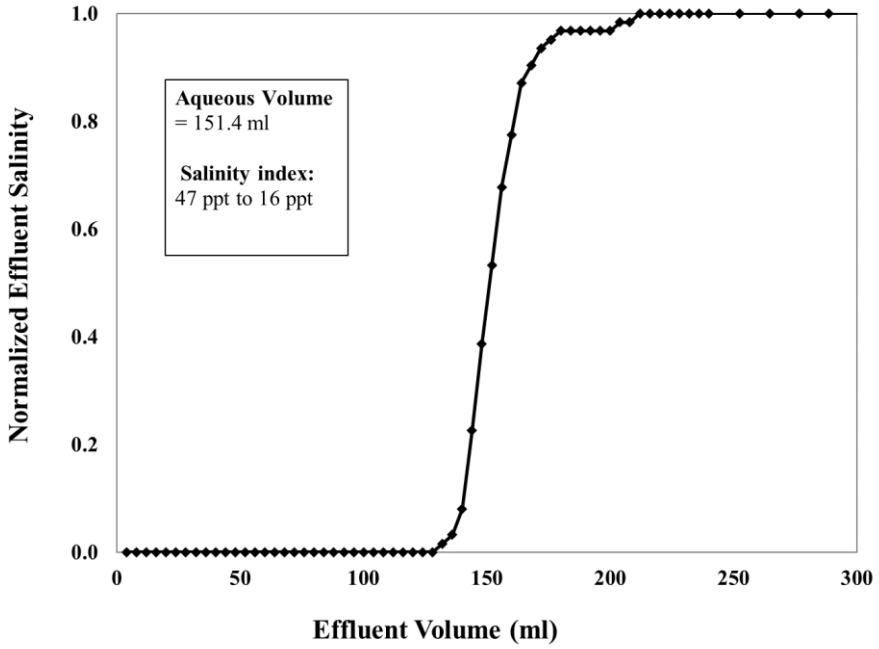

Figure 3.4: Typical tracer test result showing normalized effluent salinity during 2% KCl brine injection (displacing 6% KCl brine), from an initial salinity index of 46 parts per thousand (ppt) to a final salinity index of 15 ppt.

3.4 DETERMINING THE BRINE PERMEABILITY OF THE CORE

Brine permeability was measured before and after performing the tracer test by injecting brine at flow rates from 2 ml/min to 12 ml/min. The brine permeability was calculated using Darcy's law:

$$k = \frac{245 q \mu L}{\Delta P A} \tag{3.8}$$

Where k is the permeability in mD, q is the flow rate in ml/min, μ is the fluid viscosity in cP, L is the core length in cm, ΔP is the pressure drop in psi, A is the cross-sectional area in cm^2, and 245 is the conversion factor. The brine permeability reported in this research

is the average of the values using 2% and 6% KCl brine. Pressure drop data for one of the experiments is shown in Figure 3.5. The average brine permeability for the 7 coreflood experiments using Bentheimer sandstone is 1440 mD (minimum 1280 mD, and maximum 1600 mD).

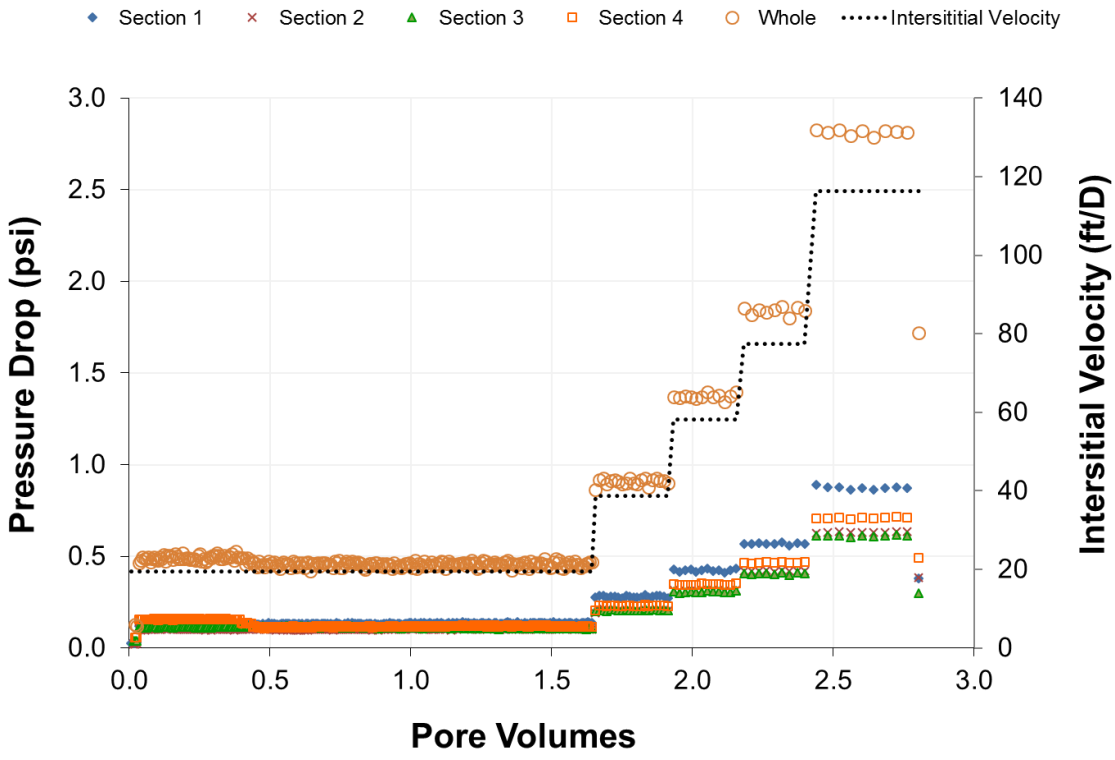

Figure 3.5: An example of pressure drop data during tracer test and permeability measurement

3.5 REDUCING THE CORE

The cores used in this research contained oxidized iron minerals whereas most reservoirs are in a highly-reduced state. Ferric ions can crosslink HPAM polymers to form microgels, increase the retention of the polymer, prevent good polymer transport and

degrade the polymer in the presence of oxygen. Therefore, it is a good practice to reduce the cores before injecting polymer solutions.

The following materials were used for the reduction step: deionized water, sodium chloride (NaCl), sodium bicarbonate ($NaHCO_3$), sodium dithionite ($Na_2S_2O_4$), tetra-sodium EDTA (EDTA-Na^{4+}), 0.45μm Millipore filter paper, mineral oil, and Iron Test Strips. Core reduction is conducted to remove amorphous oxidized iron from the core. In this research, the procedure explained by Lee (2015) was followed to reduce the core.

The core was flooded with an aqueous solution of 4% $NaHCO_3$, 1% EDTA-Na^{4+}, and 1% $Na_2S_2O_4$ at 23 ℃ and 0.5 ml/min (4.74 ft/D) to reduce the core and to remove amorphous oxidized iron from the core. Flooding was continued until the steady state iron concentration reached 3 ppm. Iron concentrations of the effluents were measured by using MQuant Iron Test Strips (0, 3, 10, 25, 50, 100, 250, 500 mg/l Fe^{2+}). Next, injected an aqueous solution of 4% $NaHCO_3$ and 1% $Na_2S_2O_4$ at 23 ℃ and 0.5 ml/min (4.74 ft/D) flow rate until the effluent iron concentration was steady-state at about 0.3 ppm measured by using Insta-Test Analytic Iron test strips (0, 0.3, 0.5, 1.3, 5 mg/l Fe^{2+}). Oxidation potential reductions (ORP), Iron Concentration, and pH of the effluent were measured and plotted against the pore volumes injected.

Typical ORP (R.mV) and iron concentration (ppm) data are shown in Figure 3.6 and typical pH and iron concentration (ppm) data are shown in Figure 3.7.

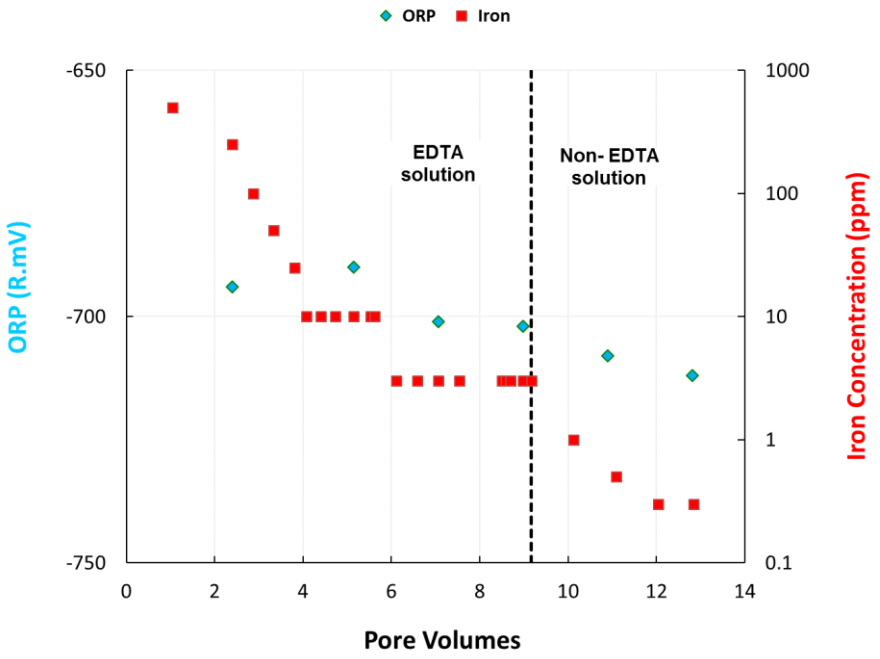

Figure 3.6: Typical ORP (R.mV) and iron concentration (ppm) data

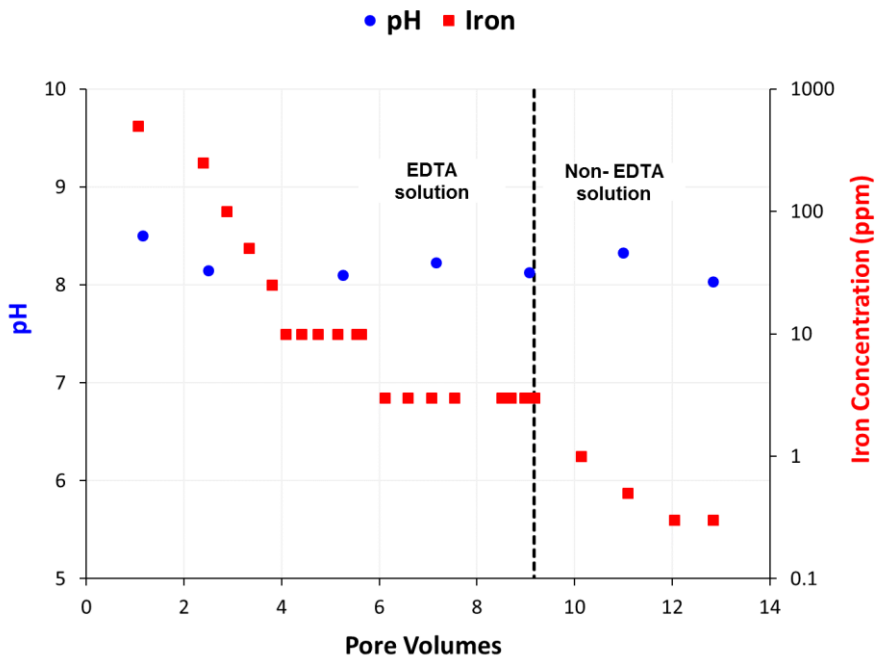

Figure 3.7: Typical pH and iron concentration (ppm) data

3.6 OIL FLOOD

Next the core was flooded with filtered crude oil at a constant pressure of ~80 psi by using air as the displacing fluid and then aged for 2 days at 23 °C. A viscous oil with a viscosity of ~125 cP was used for 6 coreflood experiments, while a light oil with a viscosity of 10 cP was used for 2 coreflood experiments.

The oil has an original viscosity of 160 cp, but is diluted with decalin to reduce its viscosity to the desired value of ~125 cp. 300 ml of the crude oil is filtered through 1.2 μm mixed cellulose ester membrane filter paper under 20 psi of air pressure. Filter paper is replaced when observing decline in the filtration rate. The viscosity of the oil was measured both after dilution and after the filtration.

Oil flooding continues until a steady state pressure drop is observed, and the oil cut is more than 99%. Generally, 1.5 PV of injected oil is needed to reach the desired oil cut. The oil is collected in 100 ml burettes and its volume is recorded manually. By using the volume versus time measurements, the flow rate during the oil flood is calculated. A typical plot of the flow rate during the oil flood is show in Figure 3.8. The pressure drop of the whole core is recorded from the beginning of the oil flood. However, it is recommended to record the pressure drops of section 1-4 after reaching steady state pressure for the whole core to prevent disturbance of the oil into the tubing connected to the transducer. A typical plot of the pressure drop and interstitial velocity during the oil flood is shown in Figure 3.9. **Interstitial velocity** (frontal velocity) is defined as the volumetric flow rate divided by the product of porosity and the cross-sectional area of flow (Eq. 3.8). **Darcy velocity** (superficial velocity) is defined as the ratio of the volumetric flow rate to the cross-sectional area of flow.

$$v = \frac{u}{\phi} = \frac{q}{A\phi} \tag{3.9}$$

Where v is interstitial velocity in ft/D, u is the darcy velocity, and ϕ is the porosity, q is volumetric flow rate, A is cross-sectional area of flow.

The core was initially saturated with brine, and the oil was injected to displace that water. Therefore, the volume of the produced brine equals to the volume of the oil remaining in the core.

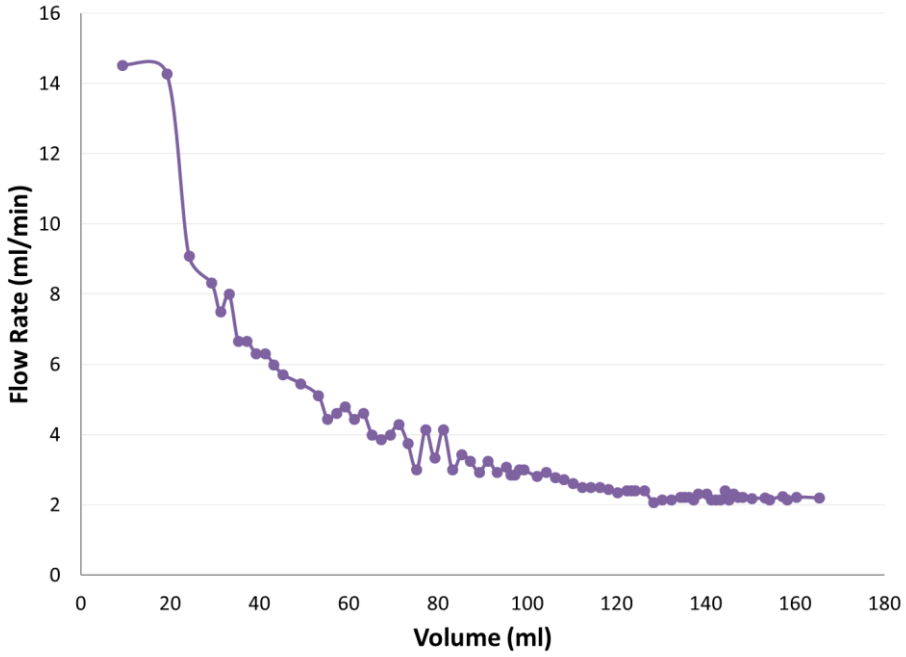

Figure 3.8: Typical plot of the flow rate during 137 cP crude oil flooding conducted at 85 psi constant pressure and 23 °C.

The initial oil saturation is calculated using equation 3.9:

$$S_{oi} = \frac{V_w}{PV} \tag{3.10}$$

Where S_{oi} is the initial oil saturation, V_w is the volume of the water produced in ml, and PV is the pore volume of the core in ml.

The residual water saturation is calculated as follows:

$$S_{wr} = 1 - S_{oi} \tag{3.11}$$

Where S_{wr} is the residual water saturation, and S_{oi} is the initial oil saturation.

The **effective oil permeability** is calculated from Darcy's law using the measured pressure drop and volumetric flow rate. The **end-point oil relative permeability** is the ratio of the effective oil permeability to the brine permeability.

$$k^{o}_{ro} = \frac{k_o}{k_{brine}} \tag{3.12}$$

Where k^{o}_{ro} is the end-point oil relative permeability, k_o is the effective oil permeability, k_{brine} is the brine permeability.

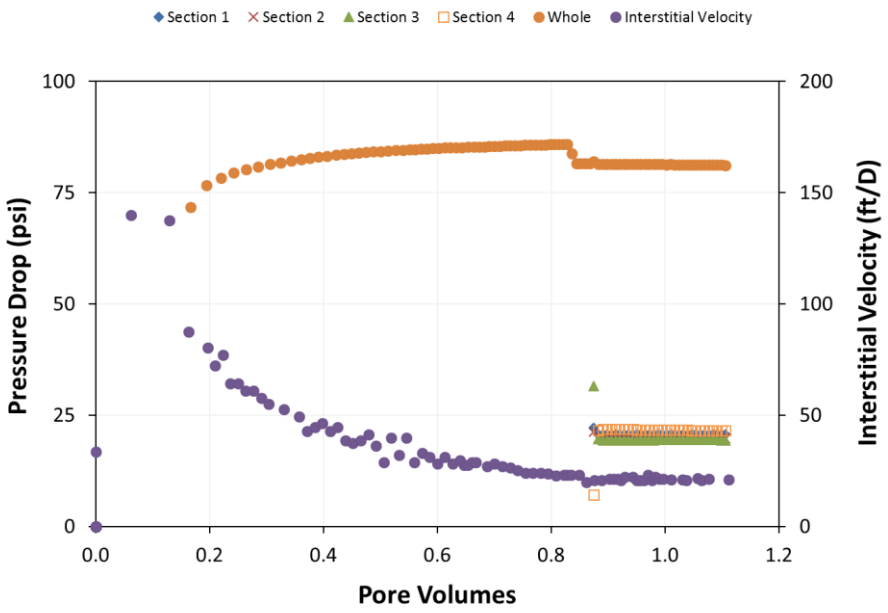

Figure 3.9: Typical plot of the pressure drop, and the interstitial velocity data during 137 cP crude oil flooding conducted at 85 psi constant pressure and 23 °C.

3.8 WATERFLOOD

After performing the oil flood and aging the core for 2 days at 23 °C, waterflood is performed by injecting filtered (0.45µm) 1000 ppm NaCl + 1000 ppm $Na_2S_2O_4$ brine at a constant flow rate of 0.5 ml/min (~5 ft/D) until steady state pressure is observed for all four sections and the oil cut is zero. **Oil cut** is defined as the ratio of the oil volume to the total volume in the effluent samples. Once steady state is reached, waterflood is continued for an additional 2 - 3 PVs. A typical pressure drop versus pore volumes plot for a waterflood is shown in Figure 3.10.

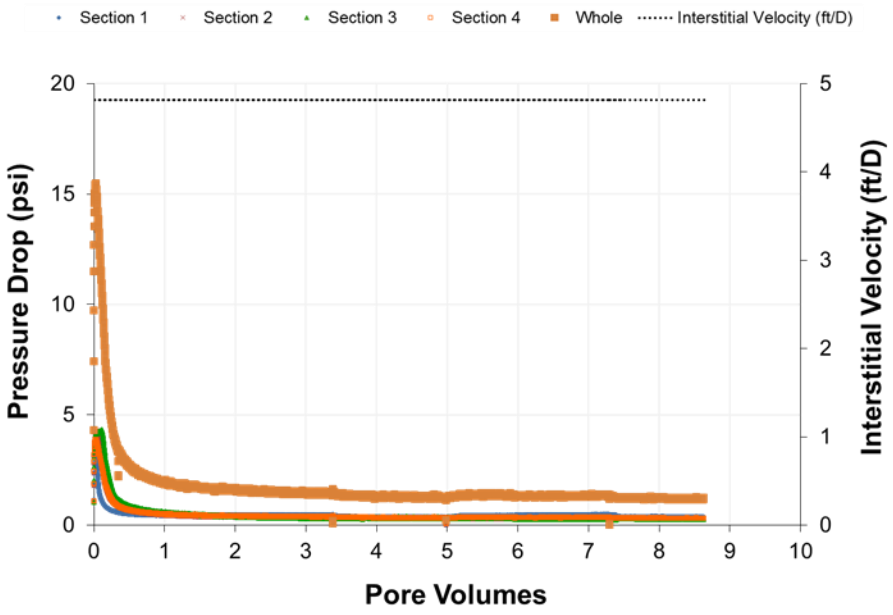

Figure 3.10: Typical pressure drop, and the interstitial velocity data during waterflooding at 23°C

Waterflood is performed to displace and produce the oil, and determine the oil saturation after waterflood. The oil saturation after waterflood is referred to here as remaining oil saturation and is not necessarily the residual oil saturation. The volume of

oil produced during the waterflood is measured and used to calculate the oil saturation at the end of the waterflood. For that purpose, a fractional retriever is used to collect effluents in 10 ml glass tubes to measure the oil recovery. Total volume and water volume of each effluent sample are read and recorded to calculate the produced oil. Produced oil in each sample is subtracted from oil volume in the core to determine the oil saturation change during waterflood.

The remaining oil saturation after waterflooding is calculated as follows:

$$S_{orw} = \frac{V_w - V_o}{PV} \tag{3.13}$$

Where S_{orw} is the remaining oil saturation after waterflood, V_w is the volume of the water produced with oil flood in ml, V_o is the volume of oil produced with waterflood in ml and PV is the pore volume of the core in ml.

The **effective water permeability** is calculated by using waterflood's effluent velocity and differential pressure drop at steady state by using Darcy's equation given in 3.7.

The end-point water relative permeability is the ratio of the effective water permeability to the brine permeability.

The end-point mobility ratio is calculated as following:

$$M_{ow} = \frac{k^o_{rw} / \mu_w}{k^o_{ro} / \mu_o} \tag{3.14}$$

Where M_{ow} is the end-point mobility ratio of waterflood, k^o_{rw} is the end-point water relative permeability in mD, k^o_{ro} is the end-point oil relative permeability in mD, μ_w is water viscosity in cP and μ_o is oil viscosity in cP. The end-point mobility ratio was typically around 15 in the experiments conducted in this work; this unfavorable mobility ratio

indicates viscous fingering and potentially unswept oil. For this reason, the remaining oil saturation was not assumed residual oil saturation.

3.9 GLYCERIN FLOOD

The waterflood is followed by a high-viscosity (~60 cP) inelastic glycerin flood to recover any bypassed oil. Unlike the waterflood, the glycerin flood has a favorable mobility ratio (less than 1.0); therefore, the oil saturation at the end of the glycerin flood is referred to herein as the residual oil saturation.

100% glycerin is diluted with the brine used in the waterflood (1000 ppm NaCl) to produce an 82 wt% glycerol/18 wt% brine solution. The glycerin solution is injected at a flow rate of ~0.210 ml/min (2 ft/D) until steady state for all of sections and zero oil cut is observed. The glycerin flood is generally continued for an additional ~1 PV. A typical pressure drop during the glycerin flood is shown in Figure 3.11. The volume of oil produced during the glycerin flood is measured and used to calculate the oil saturation at the end of glycerin flood. For that purpose, a fractional retriever is used to collect effluents in 10 ml glass tubes to measure the oil recovery. Total volume and water (or glycerin) volume of each effluent sample is read and recorded to calculate the produced oil. Produced oil in each sample is subtracted from oil volume in the core to determine the oil saturation change during the glycerin flood.

The glycerin solution is designed (ratio of glycerin to brine) to have a viscosity at least as high as the in-situ viscosity (at in-situ shear rate) of the polymer flood that followed in the next step of the experiment.

Glycerin solution is prepared by diluting pure glycerin inside 1000 ppm NaCl aqueous solution. By using the data in Segur and Oberstar (1951), glycerin wt% was plotted against viscosity for the temperatures 20 ℃ and 30 ℃. Then the values at 25 ℃ were

obtained by interpolating the values at 20 ℃ and 30 ℃ as shown in Figure 3.12. According to Figure 3.12, to obtain a viscosity of 60 cP or higher, at least 82 wt% of the glycerin needs to be mixed with brine. The viscosity of the glycerin solution was measured, and confirmed the estimated viscosities. Typical viscosity measurement result for 82 wt% glycerin is shown in Figure 3.13. After preparing the glycerin solution, it must be filtered through 90 mm diameter, 1.2 µm Millipore mixed cellulose ester membrane filter paper under 15 psi argon pressure into 250 mL graduated cylinder at 23 ℃ temperature.

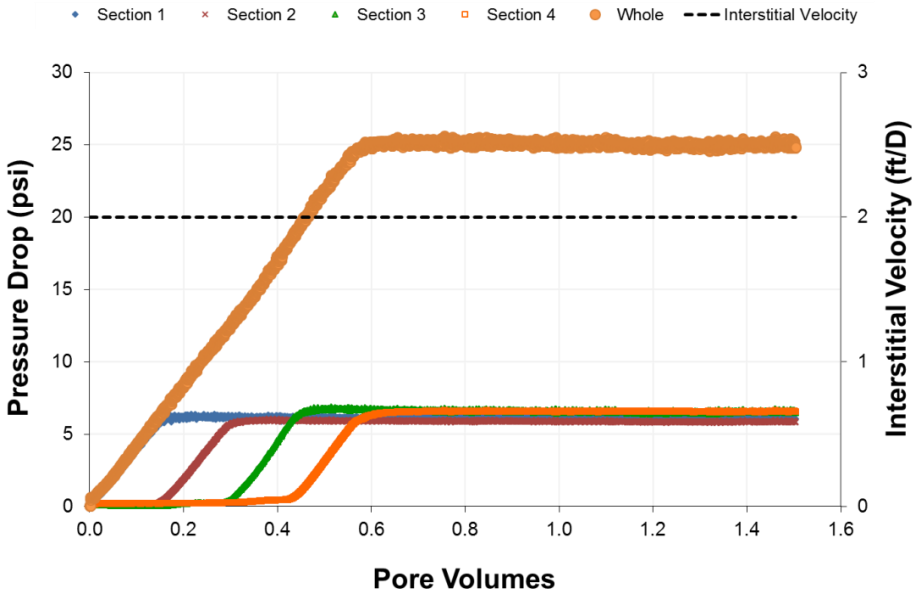

Figure 3.11: Typical pressure drop during a glycerin (60 cp) flood at 2 ft/D

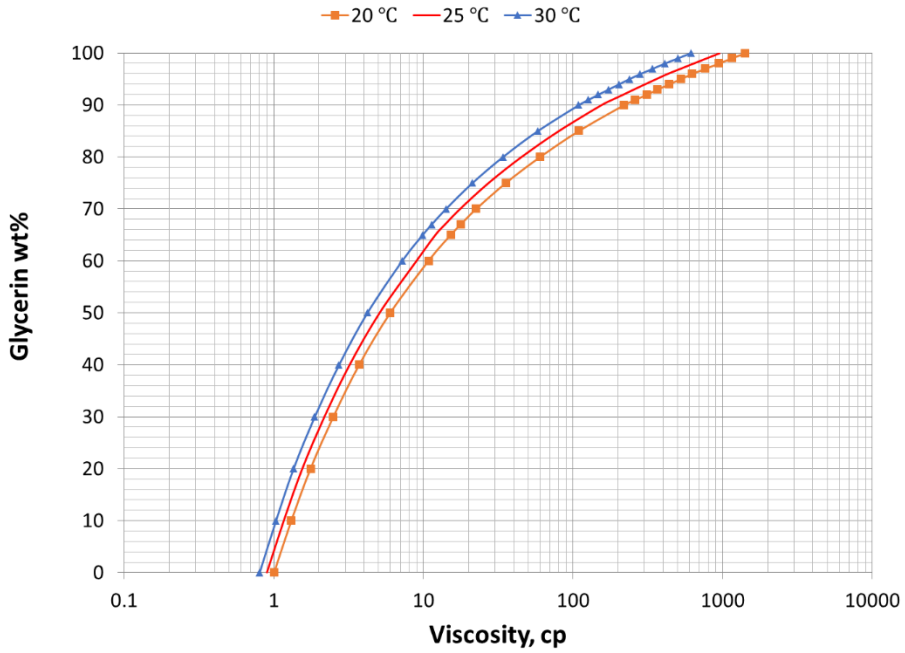

Figure 3.12: Viscosity of aqueous glycerin solutions, Glycerin wt% versus Viscosity (adapted from Segur and Oberstar (1951))

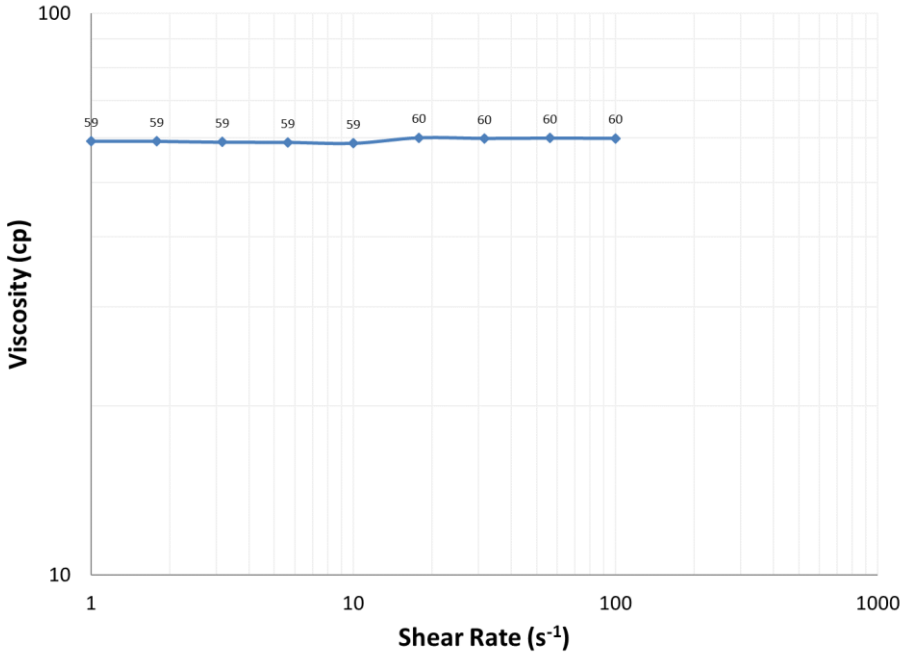

Figure 3.13: Typical viscosity measurement of 82 wt% glycerin in 12 wt% brine

The residual oil saturation after glycerin flood is calculated using equation 3.14:

$$S_{orgly} = S_{orw} - \frac{V_o}{PV} \tag{3.15}$$

Where S_{orgly} is the residual oil saturation after the glycerin flood, S_{orw} is the remaining oil saturation after the waterflood, and V_o is the volume of oil produced from the glycerin flood in ml.

The effective glycerin permeability is calculated by using the glycerin flood's effluent velocity and differential pressure drop at steady state along with the multiphase form of Darcy's law (Equation 3.7).

The end-point glycerin relative permeability is the ratio of the effective glycerin permeability to the brine permeability.

The end-point mobility ratio of glycerin flood is calculated as following:

$$M_{ogly} = \frac{k^o_{rgly} / \mu_{gly}}{k^o_{ro} / \mu_o} \tag{3.16}$$

Where M_{ogly} is the end-point mobility ratio of glycerin flood, k^o_{rgly} is the end-point glycerin relative permeability in mD, k^o_{ro} is the end-point oil relative permeability in mD, μ_{gly} is glycerin viscosity in cP, and μ_o is oil viscosity in cP. In this research, end-point mobility ratio of the glycerin flood was usually ~0.3 (favorable mobility ratio), suggesting no viscous fingering or unswept oil. Therefore, the oil saturation is residual oil saturation.

3.10 LOW-SALINITY, HIGH-VISCOELASTICITY POLYMER FLOOD

The glycerin flood is followed by a low-salinity, high-viscoelasticity polymer flood. 2000 ppm Flopaam™ (FP) 3630S polymer in 1000 ppm NaCl, 400 ppm NaHCO3 brine was injected at a constant flow rate of ~0.106 ml/min (1.0 ft/D) until steady state

pressure drop across all four sections of the core and zero oil cut was observed. The polymer flood was continued for an additional ~2 PV.

Typical pressure drop data versus PV during the low-salinity, high-viscoelasticity polymer flood are shown in Figure 3.14. Flopaam^{TM} 3630S was used for seven coreflood experiments, while Flopaam^{TM} 3330S was used for one coreflood experiment. High polymer concentration in low salinity brine was used so the relaxation time and thus the Deborah number would be as high. Deborah number used in this research is defined as the equivalent shear rate multiplied by the relaxation time as given in equation 2.4. The Deborah number for low-salinity polymer floods ranged from 30 to 300.

The volume of oil produced during low-salinity, high-viscoelasticity polymer flood was measured and used to calculate the oil saturation. Effluent samples were collected in 10 ml glass tubes using a fraction collector. Total volume and water (or polymer) volume of each effluent sample are read and recorded to calculate the produced oil. Produced oil in each sample is subtracted from oil volume in the core to determine the oil saturation change during low-salinity, high-viscoelasticity polymer flood. The viscosity of effluent samples was measured as soon as possible after the samples were produced.

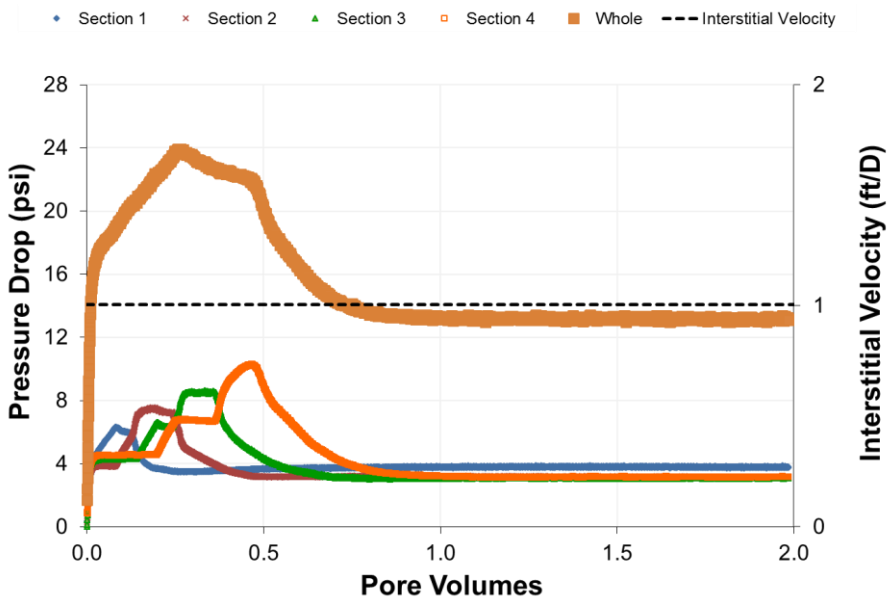

Figure 3.14: Typical pressure drop during 2000 ppm FP 3630S HPAM Polymer in 1000 ppm NaCl, 400 ppm NaHCO3 aqueous solution at 1 ft/D and 23 ℃

In this research, the standard protocol for polymer handling (Koh, 2015; Lee, 2015) was followed to prepare and filter the polymer stock solution, to dilute that stock solution, and finally to filter the diluted polymer solution. For the dilution process, after hydrating the diluted solution for16 hours, filtered the polymer solution through 90 mm diameter, 1.2 μm Millipore mixed cellulose ester membrane filter paper under 15 psi argon pressure into 250 mL graduated cylinder at 23 ℃ temperature. Filtration test is conducted to ensure that the polymer hydration was accomplished properly and the polymer solution is free of microgel. A polymer solution that passes the filtration test (filtration ratio less than 1.2) is then degassed with argon while stirring for 2 hours in a round bottom flask. Then the polymer solution is vacuum transferred into a polycarbonate injection column. A sample of the polymer solution is taken from the column to measure its relaxation time, viscosity,

pH and ORP. Relaxation time is determined by conducting a dynamic frequency sweep test, viscosity is measured by conducting steady rate sweep test, pH is measured by using pH meter, and ORP is measured by using ORP meter.

Residual oil saturation is calculated as follows:

$$S_{\text{orpLowSal}} = S_{\text{orgly}} - \frac{V_{\text{o}}}{PV} \tag{3.17}$$

Where $S_{\text{orpLowSal}}$ is the residual oil saturation after low-salinity, high-viscoelasticity polymer flood, S_{orgly} is the residual oil saturation after glycerin flood, V_{o} is the volume of oil produced with low-salinity, high-viscoelasticity polymer flood in ml and PV is the pore volume of the core in ml.

Effective permeability of low-salinity, high-viscoelasticity polymer is calculated from Darcy's law using the differential pressure drop data at steady state. .

End-point permeability of low-salinity, high-viscoelasticity polymer is the ratio of the effective low-salinity, high-viscoelasticity polymer permeability to the brine permeability.

End-point mobility ratio of low-salinity, high-viscoelasticity polymer is calculated as following:

$$M_{\text{opLowSal}} = \frac{k^{\text{o}}_{\text{rpLowSal}} / \mu_{\text{pLowSal}}}{k^{\text{o}}_{\text{ro}} / \mu_{\text{o}}} \tag{3.18}$$

Where M_{opLowSal} is the end-point mobility ratio of low-salinity, high-viscoelasticity polymer flood, $k^{\text{o}}_{\text{rpLowSal}}$ is the end-point relative permeability of low-salinity, high-viscoelasticity polymer in mD, k^{o}_{ro} is the end-point oil relative permeability in mD, μ_{pLowSal} is the viscosity of low-salinity, high-viscoelasticity polymer at equivalent shear rate in cP, and μ_{o} is oil viscosity in cP. In this research, end-point mobility ratio of low-salinity, high-viscoelasticity polymer flood was around 0.36 which is a favorable mobility ratio.

Capillary number of the whole core and for all four sections are calculated by using the maximum pressure drop reached.

3.11 HIGH-SALINITY, LOW-VISCOELASTICITY POLYMER FLOOD

The low-salinity, high-viscoelasticity polymer flood was followed by injection of a high-salinity, low-viscoelasticity polymer (e.g. 3548 ppm FP-3630S HPAM Polymer in 24030 ppm NaCl, 280 ppm NaHCO3 aqueous solution) with the same viscosity. The original purpose of this flood was a tracer test to determine the residual oil saturation and compare it with the value calculated from a material balance.

Polymer solution was injected at a constant flow rate of 0.106 ml/min (1.0 ft/D) until steady state for all four sections and zero oil cut is observed. Typical pressure drop versus pore volumes during high-salinity, low-viscoelasticity polymer flood is shown in Figure 3.15.

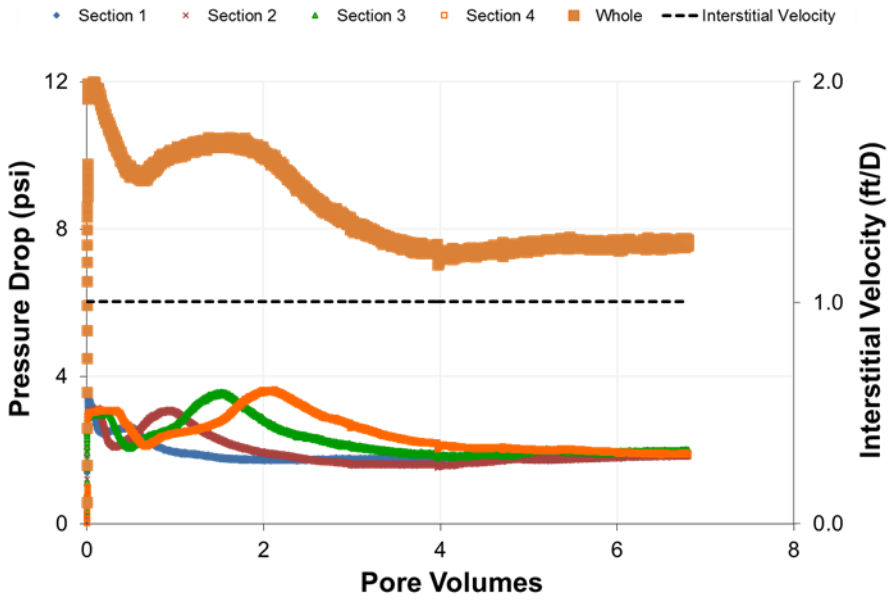

Figure 3.15: Typical pressure drop during 3548 ppm FP-3630S HPAM Polymer in 24030 ppm NaCl, 280 ppm NaHCO3 aqueous solution at 1 ft/D and 23 °C

The polymer concentration was chosen such that the in-situ viscosity was equal to that of the polymer in the previous flood. Concentration and salinity of the high-salinity, low-viscoelasticity polymer solution was estimated by using Carreau's model with the parameters determined by Yuan (2012). The same procedure as explained in section 3.10 was followed to prepare and filter the polymer solution. For the dilution process, after hydrating the diluted solution for 16 hours, filtered the polymer solution through 90 mm diameter, 1.2 μm Millipore mixed cellulose ester membrane filter paper under 15 psi argon pressure into 250 mL graduated cylinder at 23 ℃ temperature.

The original objective of injecting a second polymer solution was to perform a salinity tracer test to determine the residual oil saturation and compare it with the value from the material balance at the end of the preceding polymer flood. However, a significant volume of oil was unexpectedly produced during the tracer flood. Therefore, the objective of the research changed. First there was a need to find out if the surprising behavior could be reproduced. Then there was a need to understand why the residual oil saturation decreased to such a low value and how to optimize this very favorable behavior.

The volume of oil produced during the high-salinity, low-viscoelasticity polymer flood was measured and used to calculate the oil saturation at the end of high-salinity, low-viscoelasticity polymer flood using the same procedure as described above. The effective permeability and mobility ratio are also determined using the same procedures as described above.

3.12 FLUID PREPARATION EQUIPMENT

Mixing, filtration, degassing, and transferring to a column are the four main steps of the fluid preparation. In this section, the equipment used for fluid preparation is presented.

3.12.1 Mixing Equipment

The equipment used for preparing solutions included containers, jars, magnetic stirrer plates and magnetic stirrer bars. Polypropylene containers were used for storing brine and/or polymer solutions. Glass jars were used for storing glycerin. Magnetic stirrer plates and stirrer bars were used for mixing the fluids.

3.12.2 Filtration Equipment

Brine, oil, glycerin and polymer solutions were filtered before injecting into a core. For the brine filtration, a vacuum (or suction) filtration system is needed. The components of the vacuum filtration system are suction flask (conical flask), rubber disk, bucher funnel, filter paper, and vacuum pump.

For the polymer solutions, a filtration test is conducted to determine if the polymer has been adequately hydrated and is free of microgels or other aggregates that might plug the core. Filter Press Unit, filter bells, filter paper, inert gas such as argon or nitrogen, graduated cylinder, and a timer is needed for polymer filtration. The filtration bell is filled with polymer solution and then installed on the filter press unit. Inert gas pressure is set to 15 psig. Then. the polymer solution is filtered through 1.2 μm Millipore mixed cellulose ester membrane filter paper into 250 mL graduated cylinder, at 23 Celsius degree. The time is recorded in each 20 ml filtration of polymer solution until 200 ml filtration. It is important to record the times, at least, for 60 ml, 80 ml, 180 ml, and 200 mL of filtered polymer solution. Filtration ratio (FR) is calculated as follows:

$$FR = \frac{t_{200ml} - t_{180ml}}{t_{80ml} - t_{60ml}} \tag{3.19}$$

If the FR is less than 1.2, the polymer solution passes the filtration test and it is considered for rheological measurement and injection. After the test, the filter paper is inspected to see if any aggregates are present because of improper hydration or crosslinking (Koh, 2015; Lee, 2015).

3.12.3 Degassing Equipment

A cylinder tank containing inert gas such as argon and nitrogen, round-bottom flask, magnetic stir plate, magnetic stir bar, rubber stopper, and nylon tubing are needed for degassing the brine, glycerin, and polymer solutions. Figure 3.16 shows the degassing apparatus. One nylon tubing is placed in the polymer solution and another nylon tubing is placed above the polymer solution. Argon is introduced into the inlet tubing for degassing the polymer solution, and produced from the outlet tubing, while stirring the polymer solution for 2 hours.

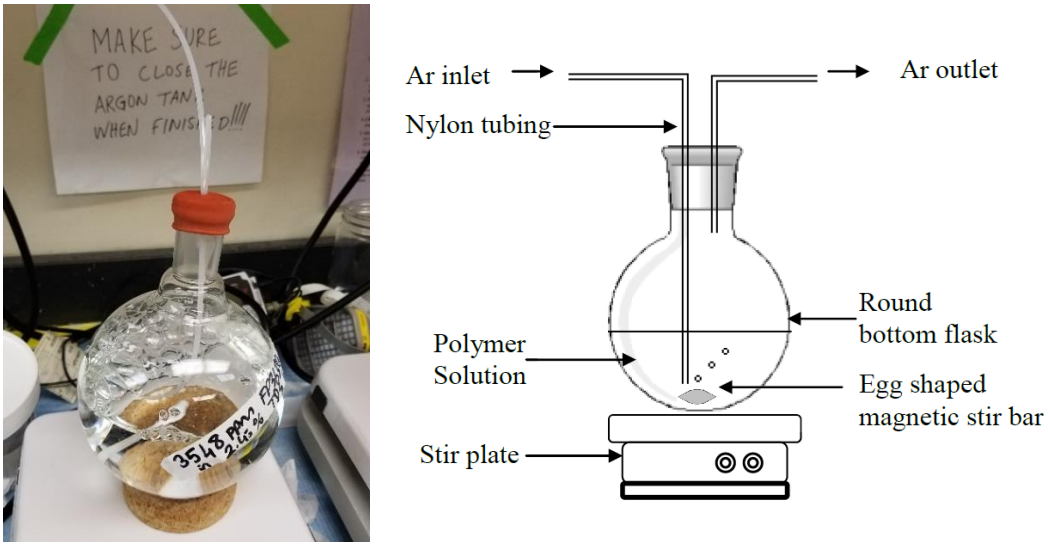

Figure 3.16: The apparatus used for polymer degassing (Koh, 2015), and an example picture of degassing

3.12.4 Equipment Used for Transferring the Fluid

A round bottom flask, nylon tubing, rubber stopper, vacuum pump, column (glass or polycarbonate), and vacuum pressure gauge are the equipment used for transferring the fluid to a column. Before transferring a fluid to a column, the column needs to be vacuumed, and then tested to see whether the column is holding the vacuuming pressure. This is done by turning off the valve which is connected to the vacuum pump, and checking the vacuum pressure gauge if the pressure is constant. If the pressure is not constant and increasing, then the column needs to be reinstalled and re-vacuumed. While transferring the fluid to the column, it is very important to make the connection between the fluid and the valve in a way that there is no leaking. Additionally, to prevent any air to move into the column, nylon tubing must be filled with the fluid by sucking the fluid by using a syringe before vacuum transferring the fluid into the column. Figure 3.17 shows a typical setup of transferring polymer solution to an injection column.

Figure 3.17: A typical setup of transferring polymer solution to an injection column

3.13 FLUID MEASUREMENT EQUIPMENT

In this section, the equipment for measuring mass, pH, iron concentration, oxidation reduction potential (ORP) and salinity is described.

3.13.1 Mass Measurement

A digital balance scale (Sartorius) with a 0-2 kg range and 0.01 g readability was used to measure the mass of solutions. A different balance scale (Ranger) with a 0-5 kg range and 0.0000 kg readability was used (Figure 3.18) to measure the mass of the core. Disposable weighing boats were used for the measurement of solids such as KCl, NaCl, $NaHCO_3$, EDTA-Na^{4+}, $Na_2S_2O_4$, and HPAM polymer.

Figure 3.18: Digital balance scales

3.13.2 Rheology

The Rheometer

TA instruments®' Advanced Rheometric Expansion System Low Shear-1 (ARES LS-1) equipment was used for rheological measurements. Dynamic, steady, and transient mechanical tests can be performed by the ARES rheometer (TA instrument, 2003). The Low Shear (LS) motor has dynamic and steady modes. In dynamic mode, strain and torque

are measured. In steady mode, rotational rate, sample torque, and normal force are measured.

In this study, dynamic strain sweep test (DSST), dynamic frequency sweep test (DFST), and steady rate sweep test (SRST) were conducted. For polymer rheology measurements, DSST, DFST, and SRST were conducted. On the other hand, for oil and glycerin rheology measurement only SRST was conducted.

Dynamic strain sweep test (DSST)

Dynamic strain sweep test (DSST) is performed to determine the linear viscoelasticity limits and the torque levels at a constant frequency and desired temperature. It can also be used to characterize the samples that exhibit extreme nonlinear behavior. DSST set-up screen is shown in Figure 3.19.

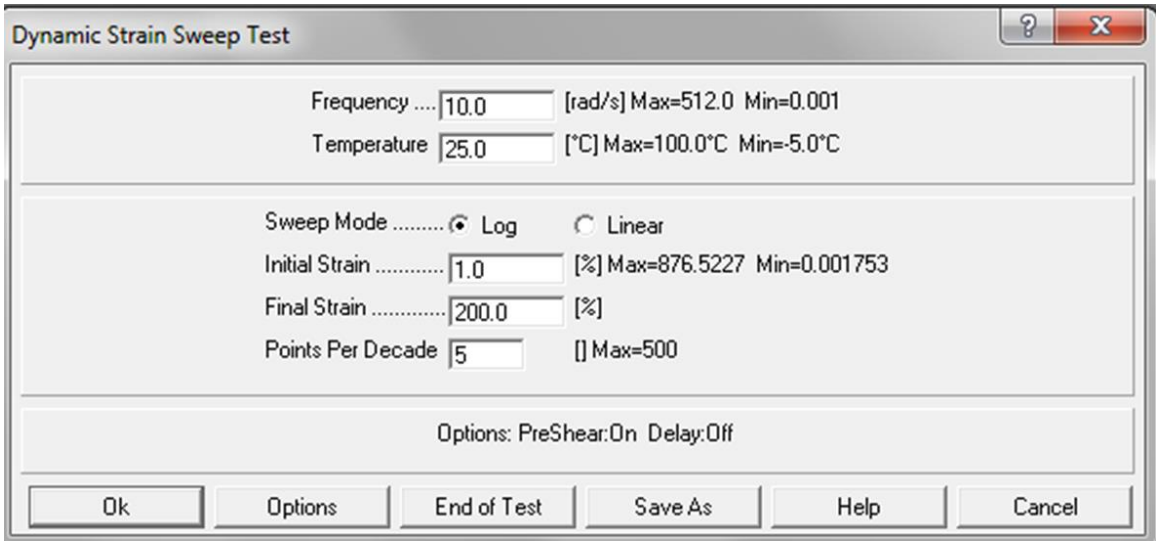

Figure 3.19: Dynamic strain sweep test (DSST) set-up screen

In this study DSST was performed at 10 rad/s frequency and 25 °C temperature from an initial strain of 1% to a final strain of 100% to obtain a strain value within the linear viscoelasticity range. The results of the DSST are presented on a plot of elastic modulus (G' [dyn/cm^2]),

viscous modulus (G" [dyn/cm^2]) and dynamic viscosity (η∗ [cP]) on vertical axis (y), and the strain (γ [%]) on horizontal axis (x). The elastic modulus (G') is defined as the ratio of the elastic stress to strain. The viscous modulus (G") is defined as the ratio of viscous stress to strain. An example of DSST is shown in Figure 3.20. The values of G', G", and η∗ are linear between ~5% and ~30% strain values, which shows the linear viscoelastic region of the sample. However, G' and η∗ tend to decrease for the strain values higher than 30%. For this example, to be in the linear viscoelastic region, any value of strain between 5% and 30% (i.e. 15%) can be used as an input for the proceeding dynamic frequency sweep test.

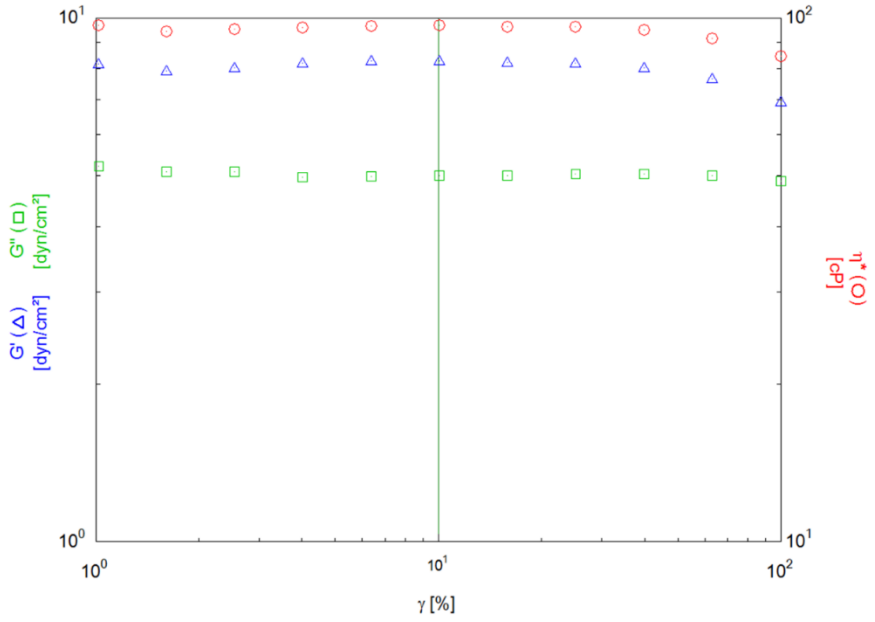

Figure 3.20: An example of dynamic strain sweep test (DSST) result for 2000 ppm FP-3630S HPAM Polymer in 1000 ppm NaCl + 400 ppm NaHCO3 aqueous solution at 23 ℃

Dynamic Frequency Sweep Test (DFST)

A dynamic frequency sweep test (DFST) is performed to analyze the frequency and time dependent behavior of the polymer solution samples at a desired temperature and a

constant strain. The strain value should be obtained from the linear viscoelastic region in the dynamic strain sweep test. The DFST set-up screen is shown in Figure 3.21.

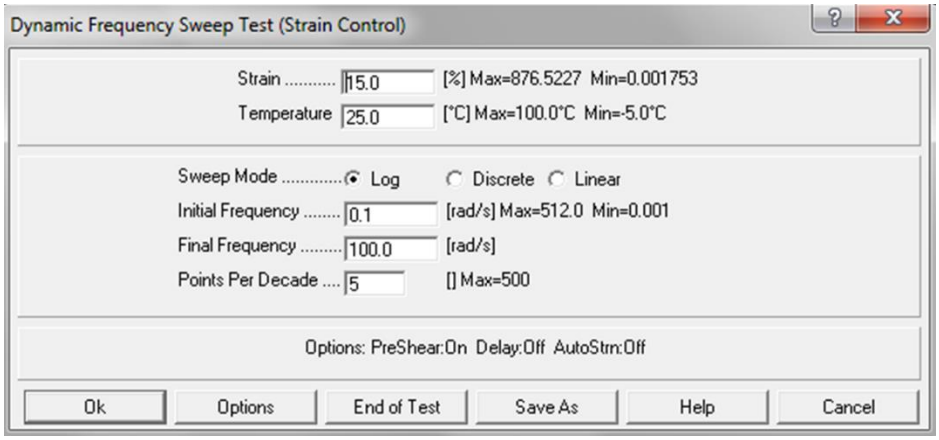

Figure 3.21: Dynamic frequency sweep test (DFST) set-up screen

The results of the DFST are presented in a plot of the dynamic properties of the fluid such as elastic modulus (G' [dyn/cm^2]) and viscous modulus (G" [dyn/cm^2]) on vertical axis (y), and the frequency (ω [rad/s]) on horizontal axis (x). In this study DFST was performed at a strain value between 10% and 20% strain, 25 ℃ temperature, from an initial frequency of 0.1 rad/s to a final frequency of 40 rad/s for high viscoelasticity polymer solution samples, and from 1 rad/s to 40 rad/s for low viscoelasticity polymer samples. If the intersection of G’ and G” curves (referred to herein as the G’/G” crossover point) was not observed, then the initial frequency was set to a lower value. In some cases, the initial frequency value was chosen as 40 rad/s and the final value was chosen as 0.01 rad/s.

An example of the DFST result for a low-salinity, high-viscoelasticity polymer solution is shown in Figure 3.22. Additionally, an example of the DFST result for high-salinity, low-viscoelasticity polymer solution is shown in Figure 3.23. The relaxation time

of the polymer solutions were estimated as the inverse of the frequency (ω) at which G' and G" intersect (cross-over point).

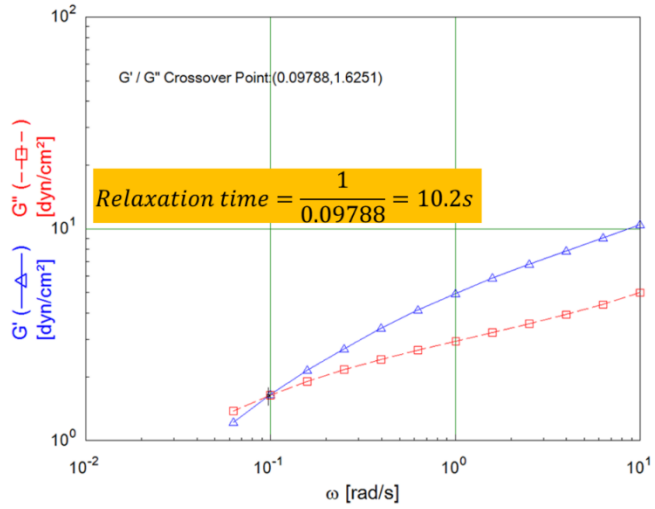

Figure 3.22: DFST result for 2000 ppm FP-3630S HPAM Polymer in 1000 ppm NaCl + 400 ppm NaHCO3 aqueous solution at 23 °C

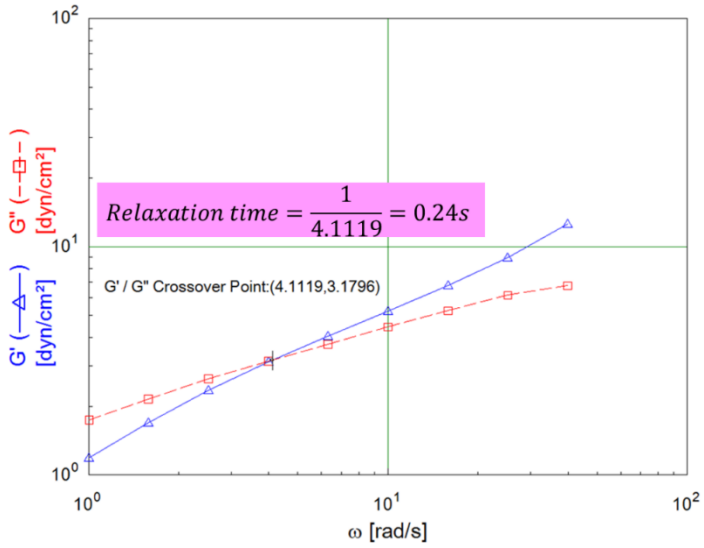

Figure 3.23: DFST result for 3548 ppm FP-3630S HPAM Polymer in 24030 ppm NaCl + 280 ppm NaHCO3 aqueous solution at 23 °C

Steady Rate Sweep Test (SRST)

A steady rate sweep test (SRST) provides the shear viscosity (μ) of the solution as a function of the shear rate ($\dot{\gamma}$) at a specified temperature. SRST set-up screen is shown in Figure 3.24.

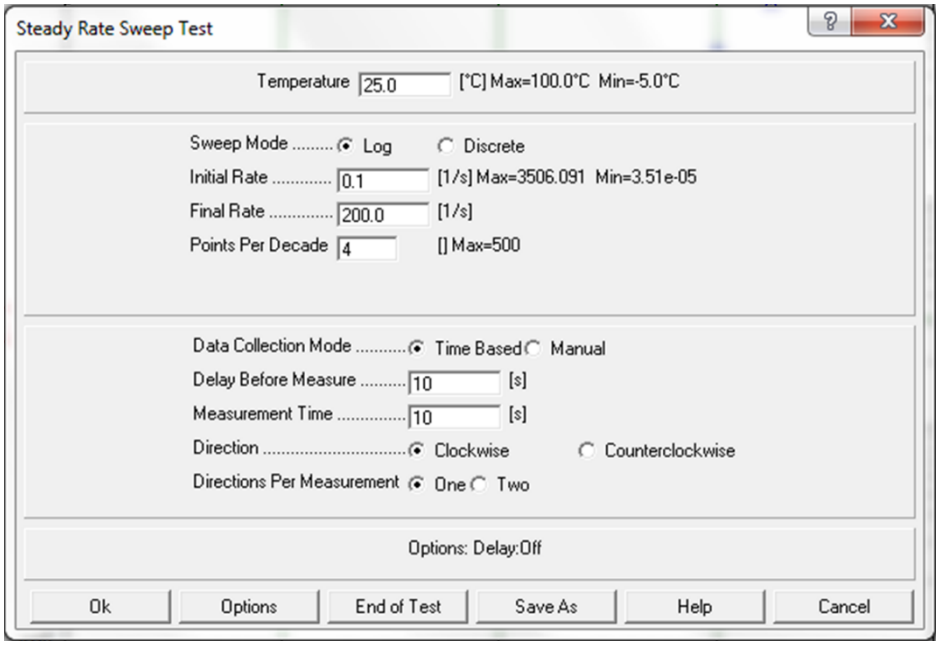

Figure 3.24: Steady rate sweep test (SRST) set-up screen

In this study, SRST was performed at 25 °C, from an initial rate of 0.1 s^{-1} to a final rate of 800 s^{-1}. An example of the SRST result for a polymer solution is shown in Figure 3.25. TA Orchestrator has a function (Curve Fit) which can be used to fit the data to a power-law model after choosing a set of viscosity data points from the shear thinning regime region of the data. For example, as shown in Figure 3.26 after choosing the viscosity data points from 0.6 s^{-1} to 100 s^{-1}, and fitting with Curve Fit function, the following result was obtained:

$$\mu = 536\dot{\gamma}^{-0.64}$$

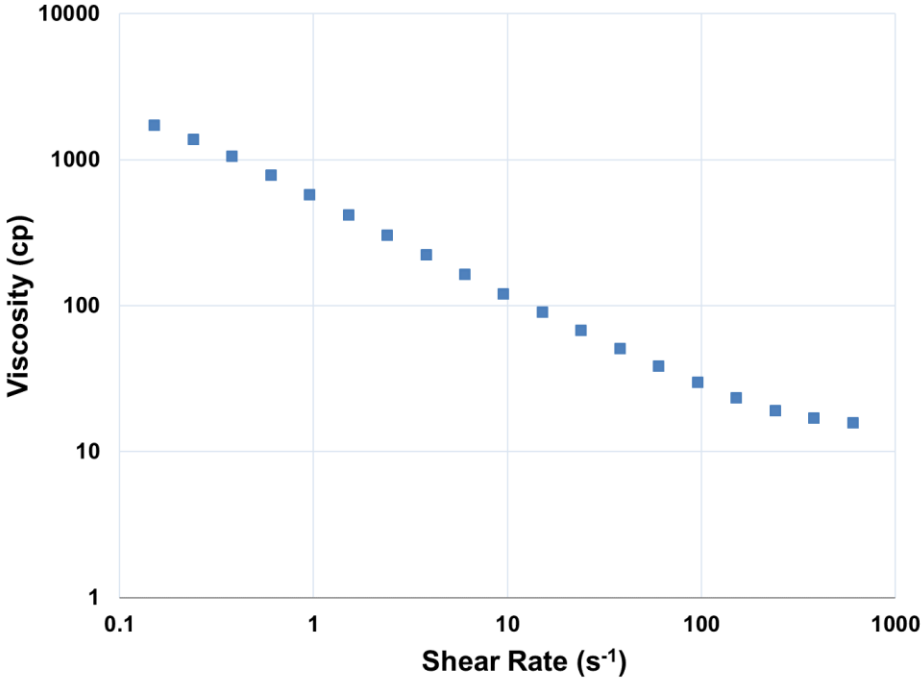

Figure 3.25: Steady rate sweep test (SRST) result for 2000 ppm FP-3630S HPAM Polymer in 1000 ppm NaCl + 400 ppm NaHCO3 aqueous solution at 23 °C

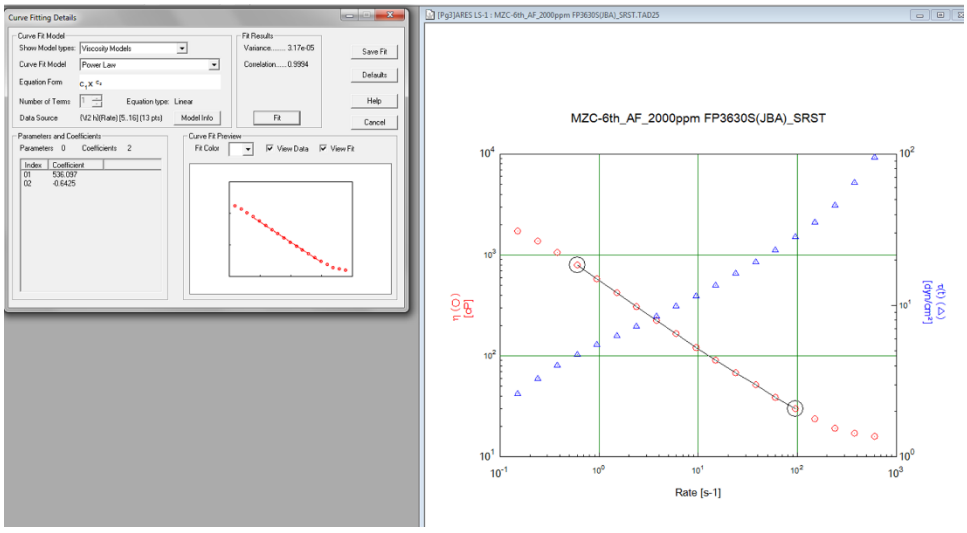

Figure 3.26: Example of curve fit function after steady rate sweep test (SRST) for 2000 ppm FP-3630S HPAM Polymer in 1000 ppm NaCl + 400 ppm NaHCO3 aqueous solution at 23 °C

3.13.3 Oxidation Reduction Potential (ORP) Measurement

In this study, the ORP was measured by using Oakton Waterproof ORPTestr® 10 (Figure 3.27) with a range of -999 to +1000 mV, a resolution of 1 mV, and an accuracy of ±2 mV.

Figure 3.27: Oakton Waterproof ORPTestr® 10

3.13.4 pH Measurement

In this study, pH was measured by using Thermo Scientific Orion 3 STAR Benchtop pH Meter (Figure 3.28). Range of pH meter is from -2 to 20, resolution is 0.001, and accuracy is ±0.002.

Figure 3.28: Thermo Scientific Orion 3 STAR Benchtop pH Meter

3.13.5 Salinity Measurement

A portable refractometer (Figure 3.29) was used for reading the refractive index (salinity index). The refractometer has dual scale which can measure salinity from 0 parts per thousand (‰=ppt) to 100 ppt. and specific gravity (d 20/20) from 1.000 to 1.070. When reading salinity index of the effluent samples, d 20/20 scale can be used with ‰ scale to read the salinity values more accurately.

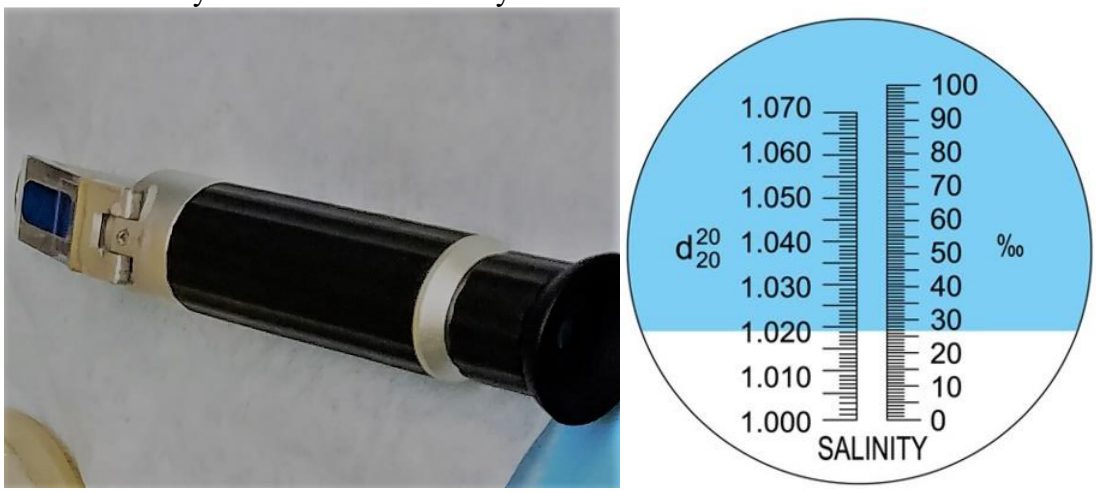

Figure 3.29: Portable refractometer and dual scale

3.14 FLUID FLOODING EQUIPMENT

3.14.1 Stainless Steel Cylinders

Stainless steel double ended 300 ml cylinders with Swagelok fittings (Figure 3.30) with a were used to inject oil up to 100 psi.

Figure 3.30: Stainless steel double ended cylinder

3.14.2 Glass columns

Kontes Chromaflex® glass columns (Figure 3.31) with a pressure rating of 50 psi were used for brine and polymer solution injection. There are numerous sizes and capacities of the glass columns available in the lab. In this study, columns which have 271 ml (4.8 cm diameter, 15 cm length) and 543 ml (4.8 cm diameter, 30 cm length) capacities were used. Columns are threaded, and they have polytetrafluoroethylene (PTFE)-shielded O-rings and end fittings.

Figure 3.31: Kontes Chromaflex® glass columns

Kontes Chromaflex® columns were used to contain fluids to be injected for core floods experiments. These columns were 0.5 to 2 feet in length and 2 inch in outer diameter. The end pieces include a Vitron O ring and washer to prevent leaking when hand tightened. These columns can withstand up to 50 psi, but usually, a maximum of 20 psi was used for additional safety precautions.

3.14.3 Pump

The pump used for injecting fluids at a desired flow rate into the core was a Teledyne Instrument Specialties Company (ISCO) 5000 syringe pump which is shown in Figure 3.32. The pump has a storage tank which has a capacity of ~507 ml for storing mineral oil which is used for displacing the fluids into the core. During the experiments, when the tank of mineral oil is emptied, the pump is refilled immediately with a flow rate of 200 ml/min. To confirm the injection flow rate displayed on the pump, the volume of the effluents within a certain time were checked regularly.

3.14.4 Pressure transducers and data acquisition recorder

The pressure tap on each section of the core is linked to a 0-35 psi differential pressure transducer, and inlet and outlet of the core is linked to a 0-300 psi differential pressure transducer. Additionally, inlet and outlet of the core are linked to two 0-150 psi absolute pressure transducers. The hydraulic connection between the pressure tap and the pressure transducer pressure drop of each section and the whole core to be measured and recorded by using National Instruments LabView™ data acquisition system software (Figure 3.32) on a lab computer.

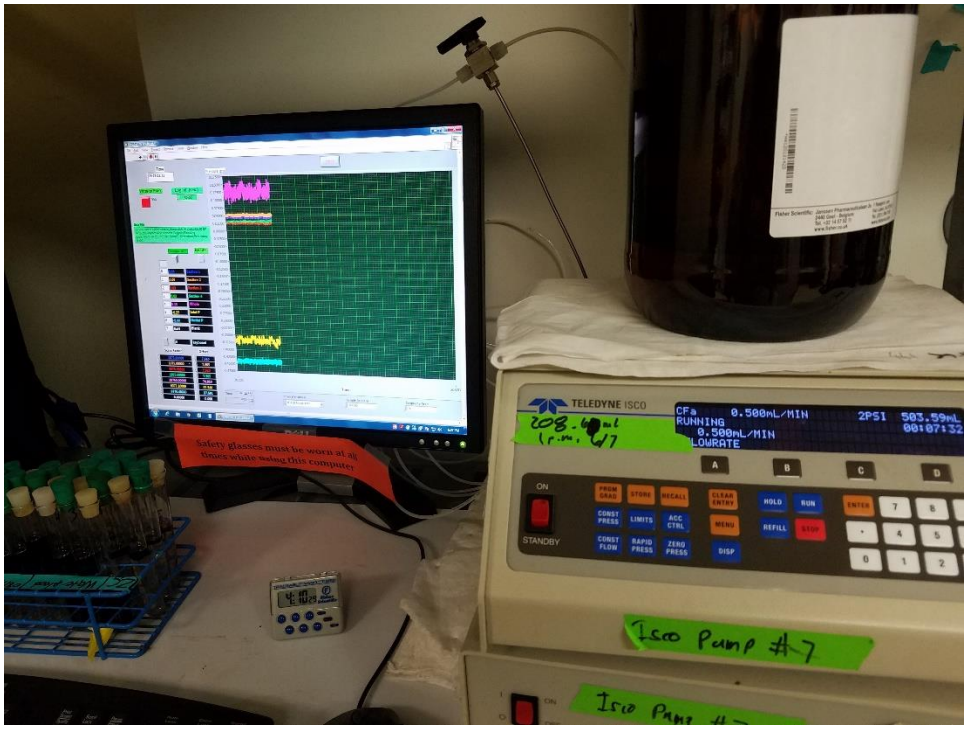

Figure 3.32: Teledyne ISCO 5000 syringe pump and LabView™ software

3.14.5 Fraction collector

The fraction collector used for collecting the effluent samples at desired time intervals was a Teledyne ISCO Retriever® 500. The modes used with this fraction collector

was 0.1 MIN, and MIN modes. 0.1 MIN mode helps to set the time interval for each tube with one decimal, while MIN mode is setting the time interval without a decimal. For example, to collect the effluent of polymer-flood which is injected with a flow rate of 0.106 ml/min in 9 ml tubes, the setting time needs to be 9/0.106=84.9 min, which can be set by using 0.1 MIN mode. Figure 3.33 shows a fraction collector equipped with glass tubes during a polymer flood.

Figure 3.33: Fraction collector

Chapter 4: Results and Analysis

In this chapter, results and analysis of eight coreflood experiments will be presented. The residual oil saturation was measured following the sequential injection of brine, glycerin, low-salinity polymer solution and high-salinity polymer solution. The first five experiments were conducted by the author of this thesis, Mehmet Zeki Erincik (MZE), and the other three experiments were conducted by another researcher, Pengpeng Qi (PPQ). The latter experiments are included in this thesis as evidence that the original experiments could be independently reproduced in another laboratory and to provide more complete data for understanding and interpreting the surprising results. Two different cores (Bentheimer and Berea), two different-viscosity crude oils (120 cP and 10 cP), and two different-molecular weight polymers (FP 3630S and FP 3330S) were used in those eight coreflood experiments. All percentage (%) values of the mixtures reported in this thesis are based on weight.

4.1 EXPERIMENT #1

The purpose of the coreflood experiment #1 was to measure the residual oil saturation in a Bentheimer sandstone core using Flopaam^{TM} 3630S polymer. The experiment was designed to have a very high Deborah number of 152. Table 4.1 summarizes the core and fluid properties of experiment #1.

4.1.1 Core Preparation, Saturating the Core, Salinity Tracer Test

A 1 ft long 2.016 in diameter, Bentheimer sandstone core was potted in epoxy to prepare for core flooding. The core passed the pressure test after conducting water leak test at 95 psi air pressure for 10 min. The core was vacuum saturated at 23 °C with 6% KCl aqueous solution. The volume of brine imbibed into the core was measured and used to calculate a pore volume of 146 ml (2 ml was subtracted from the reading to account for

Table 4.1: Core and fluid properties of experiment #1.

Experiment	**#1_Z4Z**
Coreflood name	MZE-1st
Rock type	Bentheimer Sandstone
Brine permeability (mD)	1341
Crude oil viscosity (cP)	124
Temperature (°C)	23
Porosity	0.22
Pore volume (ml)	139.5
Bulk volume (ml)	625
Dry core mass (g)	1247
Bulk density (g/cm^3)	2.0
Waterflood solution	1000 ppm NaCl + 1000 ppm $Na_2S_2O_4$ aqueous solution
Glycerin solution	81 wt% glycerol in in 1000 ppm NaCl + 400 ppm $NaHCO_3$ aqueous solution
Low-salinity polymer solution	2000 ppm FP-3630S HPAM polymer (#245 X) in 1000 ppm NaCl + 400 ppm $NaHCO_3$ aqueous solution; pH: 8.49, Salinity: 2.5 0%
High-salinity polymer solution	3800 ppm FP-3630S HPAM polymer (# 245X) in 20000 ppm NaCl + 300 ppm $NaHCO_3$ aqueous solution

fluid in the tubes). A pore volume of 147 ml was calculated based on the mass of the core before and after saturation. The same 6% KCl brine was vacuum transferred to an injection column and then injected into the core at 2 ml/min (20.7 ft/D) for 2 PV. A salinity tracer test was performed to measure the pore volume and heterogeneity of the core. 2% KCl brine was injected at 2 ml/min (20.7 ft/D) to displace the 6% KCl brine. The effluent samples were collected in volumes of 5 ml. During the salinity tracer test, salinities were

measured and plotted to determine the aqueous volume (pore volume) of 139.5 ml from the area above the normalized salinity versus effluent volume curve shown in Figure 4.1.

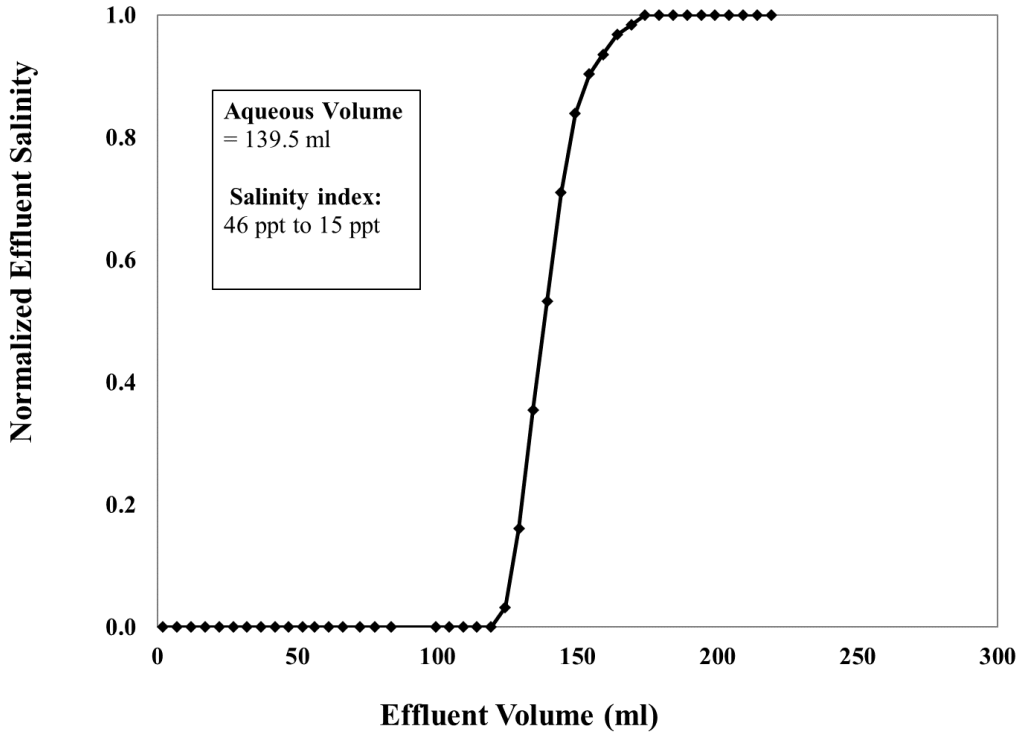

Figure 4.1: Normalized effluent salinity during 2% KCl brine injection for experiment #1, from a salinity index of 46 ppt to 15 ppt.

4.1.2 Core Reduction and Conditioning

The core was flooded at 23 °C with an aqueous solution of 40000 ppm $NaHCO_3$, 10000 ppm Na_4EDTA, and 10000 ppm $Na_2S_2O_4$ at 0.5 ml/min (5.2 ft/D) to reduce the core and to remove amorphous oxidized iron. The iron concentration was about 3 ppm at 6 PV. Flooding was continued until the iron concentration in the effluent decreased to 0.3 ppm, the ORP was -720 RmV and the pH was 8.8 (the pH of the injected solution was 8.7). The

flow rate was then varied from 2 ml/min (20 ft/D) to 8 ml/min (80 ft/D) to determine the brine permeability, which was found to be 1341 mD using equation 3.8 (Darcy's Law).

4.1.3 Oil Flood

Crude oil with a viscosity of 124 cp at 23 °C was filtered through 1.2 μm filter paper under 20 psi of air pressure. 300 ml of the crude oil was filtered in 5 hrs. (300 minutes). During filtration, the filter paper was replaced with new ones when a decline in the filtration rate was observed. In this experiment, crude oil was injected at a constant pressure of 50 psi and 23 °C. Oil flooding of this experiment (#1) was conducted at 50 psi, while all others (#2-#8) were conducted at ~80 psi. Oil flooding was continued until steady state pressure drop was observed and the oil cut exceeded 99%. A total of 1.4 PV of oil was injected. The flow rate at steady state was 1.6 ml/min (16.5 ft/D).

The initial oil saturation (S_{oi}) of 0.89 was determined by using the displaced water volume of 124 ml in equation 3.10. The residual water saturation (S_{wr}) was 0.11 using equation 3.11. The effective oil permeability at S_{wr} was determined 1481 md from Darcy's law using pressure drop and volumetric flow rate, and the end-point oil relative permeability (k^{o}_{ro}) was 1.1 for the whole core was calculated using equation 3.12. Steady-state pressure drop data, effective oil permeability, and end-point oil permeability data are presented in Table 4.2. The oil flow rate is shown in Figure 4.2. Pressure drop and the interstitial velocity data are shown in Figure 4.3. In this coreflood, the pressure drop data for all four sections were recorded from the beginning of the oil flood. The core was aged for 2 days at 23 °C after the oil flood.

Table 4.2: Steady-state pressure drop data, effective oil permeability, and end-point oil permeability from oil flood of experiment #1.

Oil Flooding	Whole	Section 1	Section 2	Section 3	Section 4
Pressure drop (psi)	49	12	11	11	14
Effective Oil Permeability (mD)	1481	1446	1679	1613	1254
k^{o}_{ro}	1.1	1.3	1.1	1.1	1.0

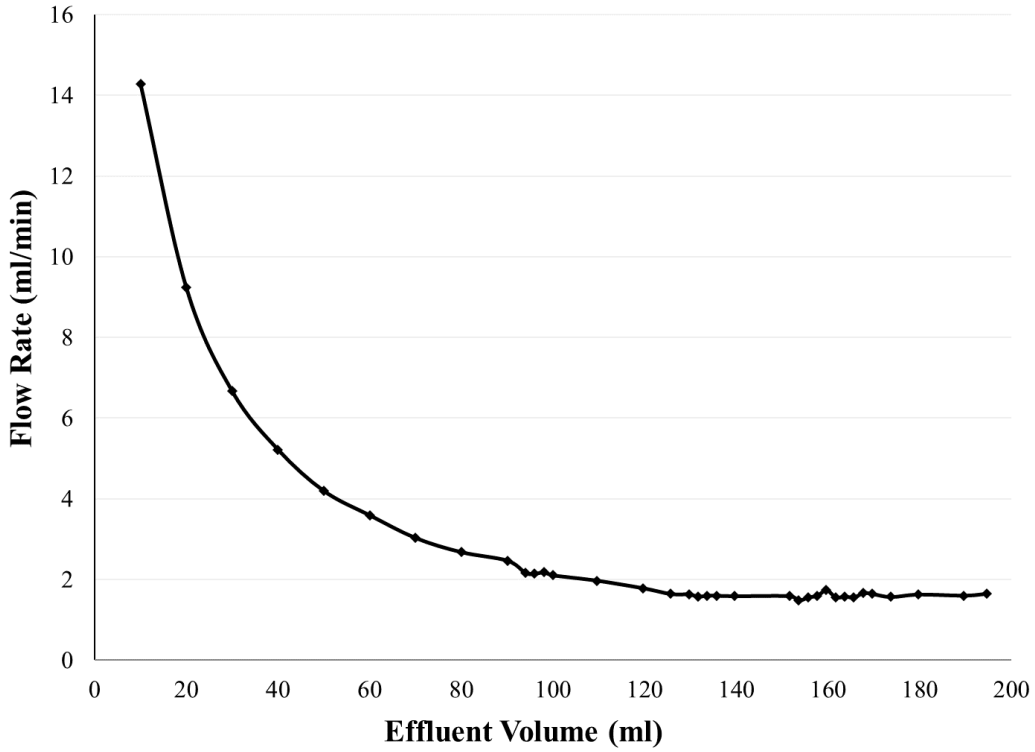

Figure 4.2: Flow rate during 124 cP crude oil flooding conducted at 50 psi constant pressure and 23 °C for experiment #1.

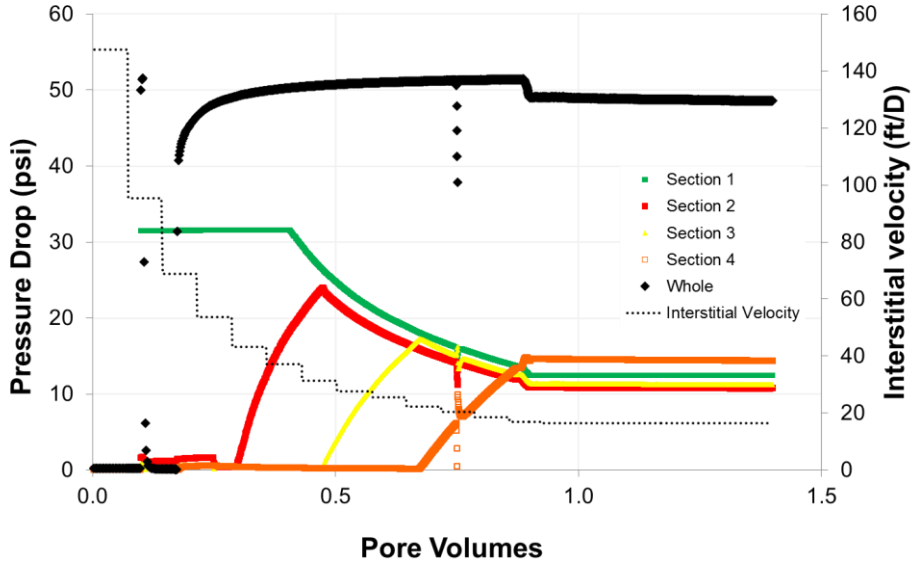

Figure 4.3: Pressure drop, and the interstitial velocity data during 124 cP crude oil flooding conducted at 50 psi constant pressure and 23 °C for experiment #1.

4.1.4 Waterflood

An aqueous solution of 1000 ppm NaCl and 1000 ppm $Na_2S_2O_4$ was injected at a constant flow rate of 1 ml/min (10.3 ft/D) until steady state pressure for all four sections and zero oil cut was observed. The pressure drop and the interstitial velocity data are shown in Figure 4.4. The capillary number was calculated as 5×10^{-5} using the maximum pressure gradient (26 psi/ft) and equation 2.3. The pressure drop reached steady state after 3 PV. Waterflooding continued for an additional 2 PV. The remaining oil saturation after the waterflood was 0.48 using equation 3.13. The effective water permeability was 133 mD using effluent velocity and differential pressure drop at steady state using Darcy's law, and the end-point water relative permeability was 0.10. The end-point mobility ratio was calculated as 12.5 using equation 3.14.

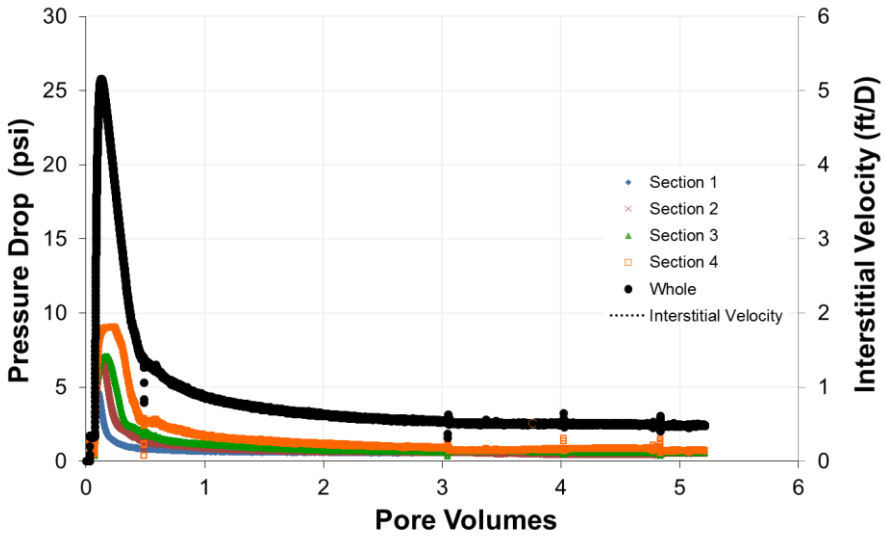

Figure 4.4: Pressure drop, and the interstitial velocity data during waterflooding at 23°C for experiment #1.

4.1.5 Glycerin Flood

An aqueous solution of 81 wt% glycerin and 19 wt% brine (1000 ppm NaCl, 400 ppm $NaHCO_3$) with a viscosity of 56 cP (measured with rheometer) was injected at a flow rate of 0.2 ml/min (2.1 ft/D) until steady state pressure drop for all four sections and an oil cut of 0.06% was observed. The results here and elsewhere in this thesis are referred to as glycerin data even though the solution is a mixture of glycerin and brine. The maximum oil cut was 28%. The pressure drop data and the interstitial velocity are shown in Figure 4.5. Steady state pressure drop was observed after 0.7 PV, but the flood continued until 1.8 PV. The residual oil saturation was reduced from 0.48 following the waterflood to 0.45 following the glycerin flood using equation 3.15. The effective permeability was 178 mD

using Darcy's law and the end-point glycerin relative permeability was 0.13. The end-point mobility ratio was calculated as 0.27 using equation 3.16.

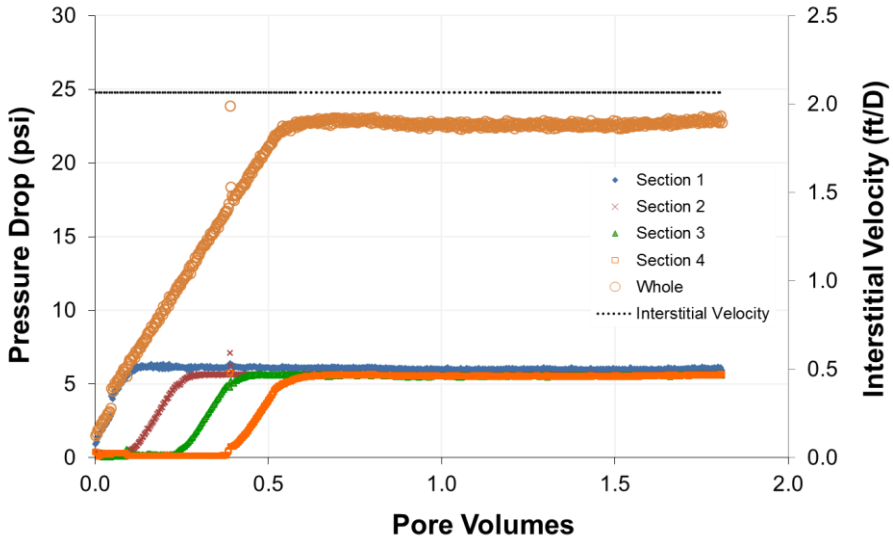

Figure 4.5: Pressure drop data and the interstitial velocity during glycerin flooding at 23 °C for experiment #1.

4.1.6 Low-Salinity Polymer Flood

A high molecular weight polymer (2000 ppm FP 3630S #245X) was prepared in a low-salinity brine (1000 ppm NaCl and 400 ppm $NaHCO_3$) to obtain a polymer solution with a high relaxation time. After hydrating 16 hours, the solution was filtered under 15 psi Argon pressure at 23 °C using a 1.2 µm Millipore mixed cellulose ester membrane filter paper. The filtration ratio was 1.02. The polymer solution was bubbled with argon while stirring for 2 hours in a round bottom flask and then vacuum-transferred to an injection column. $Na_2S_2O_4$ was not added to the polymer solution since in

a previous solution the viscosity decreased 14% and the relaxation time decreased 50% after adding $Na_2S_2O_4$.

A sample of the polymer solution was taken from the column to measure its rheology, pH, salinity and ORP. The pH was 8.5, the salinity index was 2.5 and the ORP was -20 mv. A relaxation time of 3.17 s was determined from the G', G" crossover point using the dynamic frequency sweep test (DFST) shown in Figure 4.6. The steady rate sweep test (SRST) data in the power-law viscosity region of shear thinning as shown in Figure 4.7 were fit to obtain a power-law equation of μ=454 $\dot{\gamma}^{(-0.61)}$. A power-law model was used for convenience.

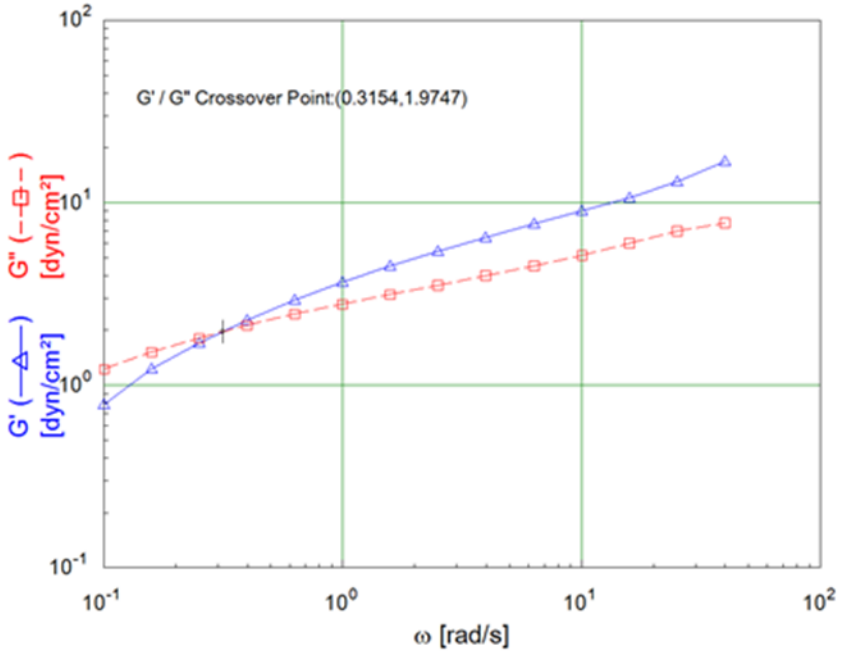

Figure 4.6: DFST result for 2000 ppm FP-3630S HPAM polymer in 1000 ppm NaCl + 400 ppm NaHCO3 aqueous solution at 23 °C for experiment #1.

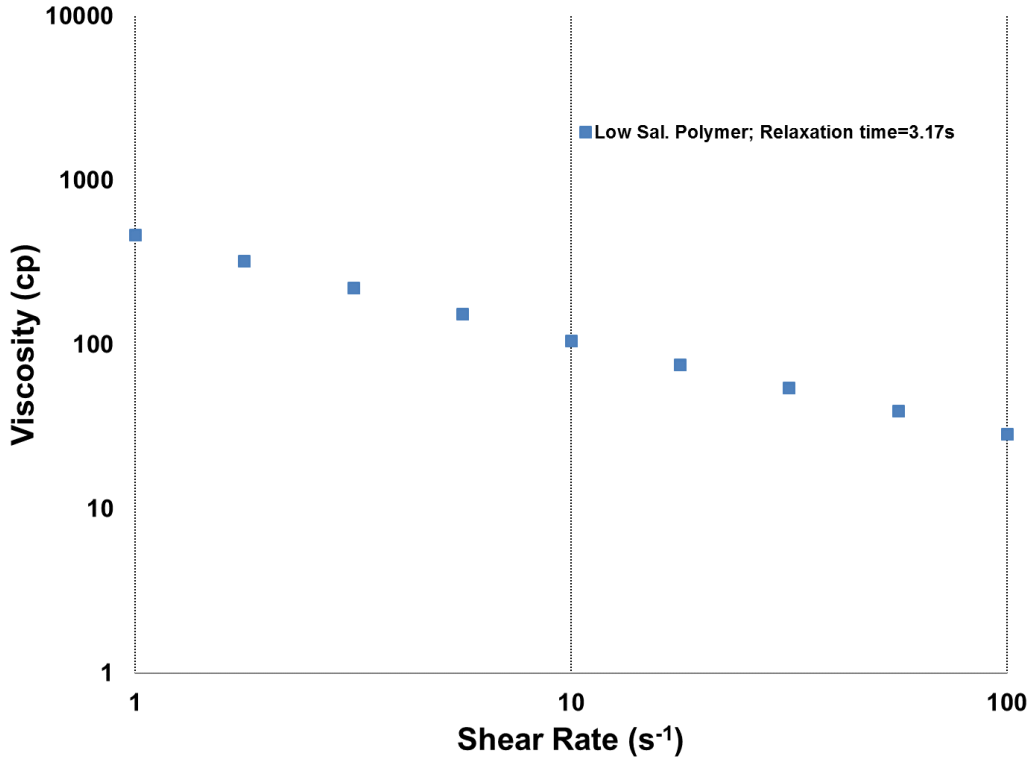

Figure 4.7: SRST result for 2000 ppm FP-3630S HPAM polymer in 1000 ppm NaCl and 400 ppm NaHCO3 aqueous solution at 23 °C for experiment #1.

This low-salinity polymer solution was injected at a constant flow rate of 0.194 ml/min (2 ft/D) until steady state pressure drop for all four sections and zero oil cut was observed. Pressure drop data and the interstitial velocity are shown in Figure 4.8. The injection continued for an additional 1.1 PV at 4 ft/D and 8 ft/D to determine the shear correction factor C. No oil recovery was observed during this time.

The residual oil saturation following low-salinity polymer flood decreased to 0.29 using equation 3.17, a 16% reduction in oil saturation compared to the glycerin flood. Cumulative oil recovery at the end of the polymer flood was 67% of the OOIP. The effective permeability for the polymer flood was 164 mD at 2 ft/D, 133 mD at 4 ft/D and 103 mD at 8 ft/D calculated from Darcy's law using the differential pressure drop data at

steady state. The end-point relative permeability was 0.12 at 2 ft/D, 0.1 at 4 ft/D and 0.08 at 8 ft/D, determined from dividing the effective permeability by the brine permeability. The end-point mobility ratio was calculated to be 0.37 at 2 ft/D, 0.45 at 8 ft/D, and 0.53 at 8 ft/D using equation 3.18. The maximum capillary number, using equation 2.3, was calculated to be 8.3×10^{-5} for the whole core using the maximum pressure gradient (48 psi/ft) reached during the 8 ft/D polymer flood. The capillary number was calculated to be 2.8×10^{-5} for the 2 ft/D polymer flood (maximum pressure was 16 psi), 4.5×10^{-5} for the 4 ft/D polymer flood (maximum pressure 26 psi), and 7.6×10^{-5} for the 8 ft/D polymer flood (maximum pressure was 44 psi). All maximum capillary numbers are below the critical capillary number (1×10^{-4} for Bentheimer sandstone). Equivalent shear rate was calculated as 48 s^{-1} using equation 2.6 and Deborah number (N_{De}) was calculated as 152.2 using equation 2.5.

The steady state pressure data for each section of the core as well as the entire core were used to calculate the apparent viscosity for the polymer at each flow rate using Darcy's law. A shear correction factor of $C = 4 \pm 0.2$ was determined from a best fit of the apparent viscosities to the viscosities measured in the rheometer as shown in Figure 4.9. The viscosity and pH of the effluent were measured as soon as possible after the samples were produced. Effluent pH and normalized effluent polymer viscosity data are shown in Figure 4.10. Viscosity versus shear rate is shown in Figure 4.11.

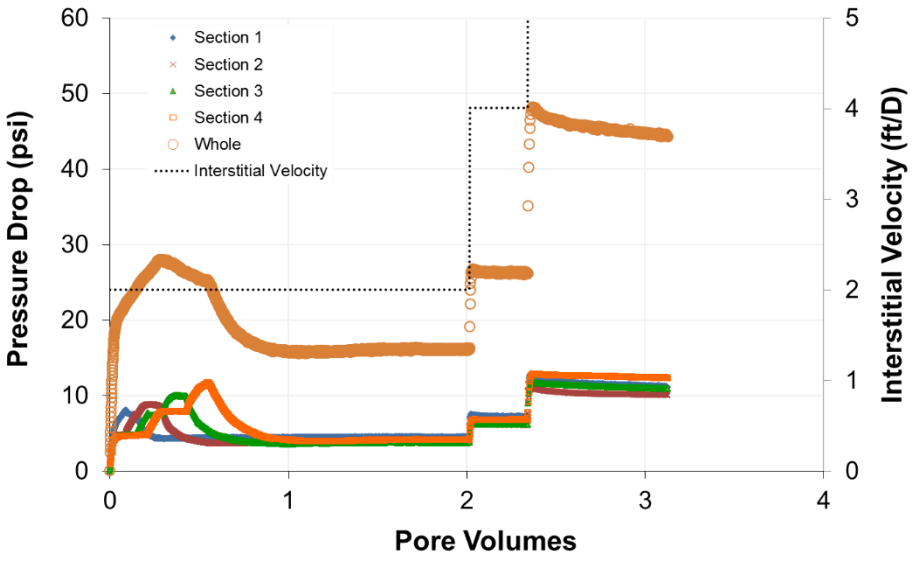

Figure 4.8: Pressure drop data, and the interstitial velocity during 2000 ppm FP-3630S HPAM Polymer in 1000 ppm NaCl + 400 ppm $NaHCO_3$ aqueous solution flood at 23 °C for experiment #1.

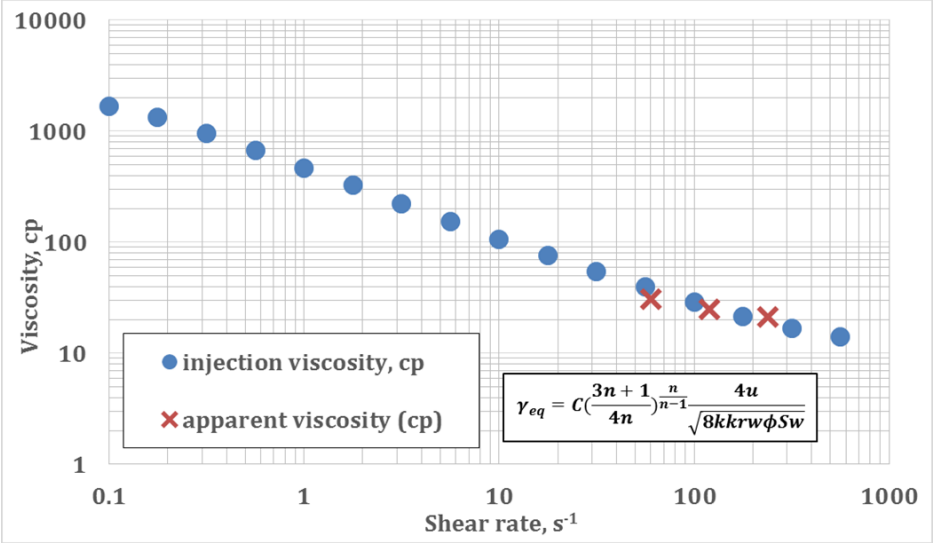

Figure 4.9: Injection and apparent viscosity comparison by using C=4 for Bentheimer sandstone core for experiment #1 at 23 °C.

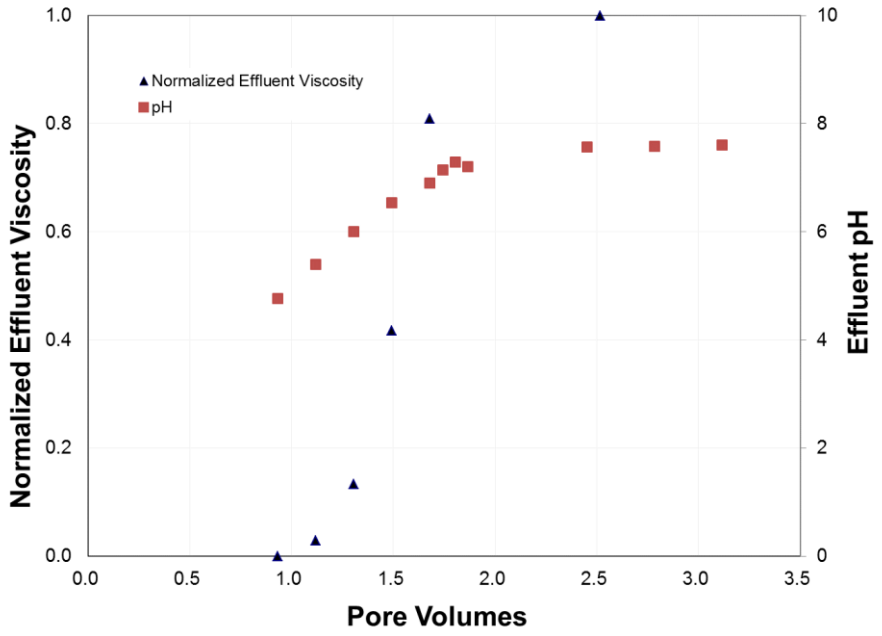

Figure 4.10: Effluent pH and normalized effluent viscosity at 23 °C for experiment #1.

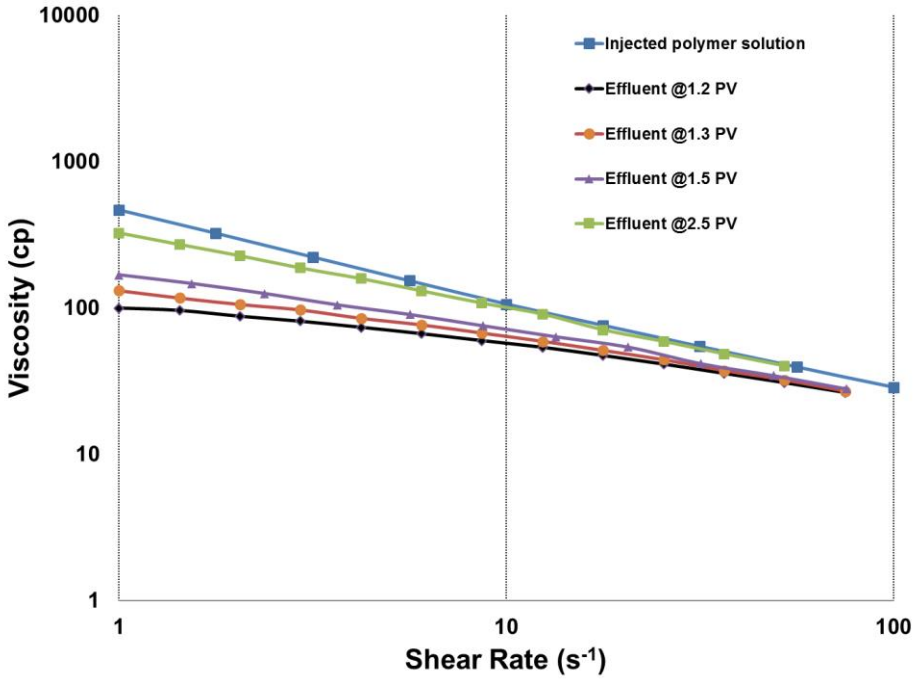

Figure 4.11: Viscosity comparison of the injected polymer solution and the effluents at 23 °C for experiment #1.

4.1.7 High-Salinity Polymer Flood

Tracer tests can be used as an independent measurement of residual oil saturation that can be compared with the value determined from a material balance using produced oil and water volumes. A polymer solution with a higher salinity was injected as a convenient conservative tracer test. The target viscosity of the polymer solution used for the tracer test was the same as the first polymer flood to avoid an unstable displacement.

A 3800 ppm FP 3630S polymer in 26400 ppm NaCl, 300 ppm $NaHCO_3$ brine was prepared for the tracer test. After hydrating 18 hours, the polymer solution was filtered through 90 mm diameter, 1.2 μm Millipore mixed cellulose ester membrane filter paper under 15 psi Argon pressure into 250 ml graduated cylinder at 23 °C. The filtration ratio was 1.01. The polymer solution was bubbled with argon while stirring for 2 hours in a round bottom flask and then vacuum-transferred to an injection column. A sample of the polymer solution was taken from the column to measure its rheology. The dynamic frequency sweep test (DFST) data are shown in Figure 4.12. The relaxation time was estimated to be 0.19 s using the G' and G" crossover point. The steady rate sweep test (SRST) data are shown in Figure 4.13. The data was fit to a power-law model with the equation $\mu=508 \times \dot{\gamma}^{(-0.50)}$

This high-salinity polymer solution was injected at a constant flow rate of 0.388 ml/min (4 ft/D) to displace the low-salinity polymer solution. Pressure drop data and the interstitial velocity are shown in Figure 4.14. The effluent samples were collected in volumes of 5 ml. During the salinity tracer test, salinities were measured and plotted. An aqueous volume of 107.3 ml was determined from the area above the normalized salinity curve shown in Figure 4.15. The normalized salinity, oil cut and oil saturation data are shown in Figure 4.16 and it shows that the oil recovery is observed after the salinity is reaching the injection salinity value.

Unexpectedly oil production was observed starting at 1.1 PV. A total of 9.95 ml of additional oil was recovered. The maximum oil cut was 11.8% as shown in Figure 4.18. The flood was continued for an additional 0.8 PV. At the end of the polymer flood, the oil cut was 7.8%, suggesting additional oil could be recovered. However, the injection was stopped because no more polymer solution was left. The cumulative oil recovery at the end of the flood was 75% of the OOIP.

The final oil saturation based on the tracer data was 0.23 (1-107.3/139.5) and 0.22 based on the material balance. At the end of the low-salinity polymer flood, the effective permeability was calculated as 367 mD using the data and Darcy's law, the end-point relative permeability was calculated as 0.27 using the ratio of the effective permeability to the brine permeability, the end-point mobility ratio was calculated as 0.67 using the end-point relative permeability in equation 3.18, and the maximum capillary number was calculated as 4.5×10^{-5} for the whole core using the maximum pressure gradient of 26 psi/ft and equation 2.3. The maximum capillary number was below the critical capillary number (1×10^{-4} for Bentheimer sandstone). Equivalent shear rate was calculated as 85 s^{-1} using equation 2.6 and Deborah number (N_{De}) was calculated as 16.5 using equation 2.5.

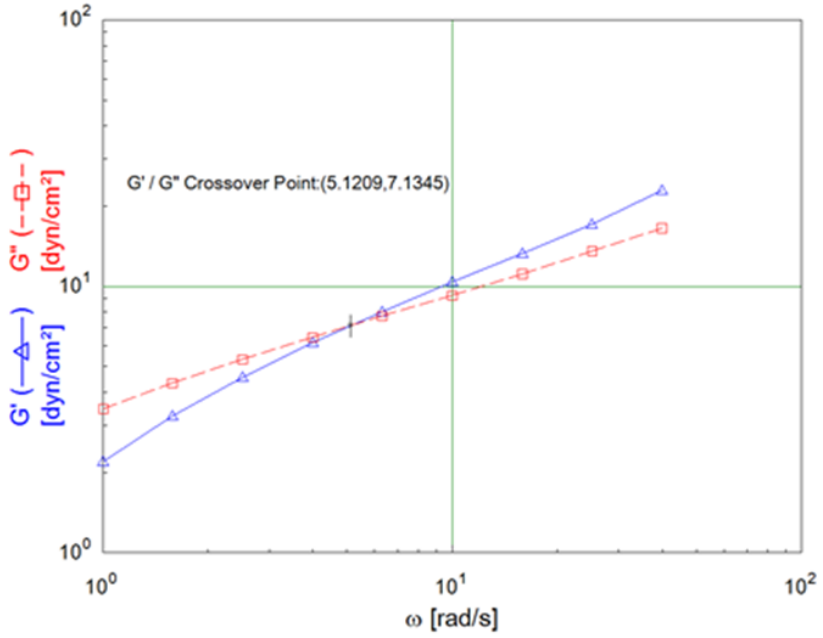

Figure 4.12: DFST result for 3800 ppm FP-3630S HPAM polymer in 26400 ppm NaCl, 300 ppm $NaHCO_3$ aqueous solution at 23 °C for experiment #1.

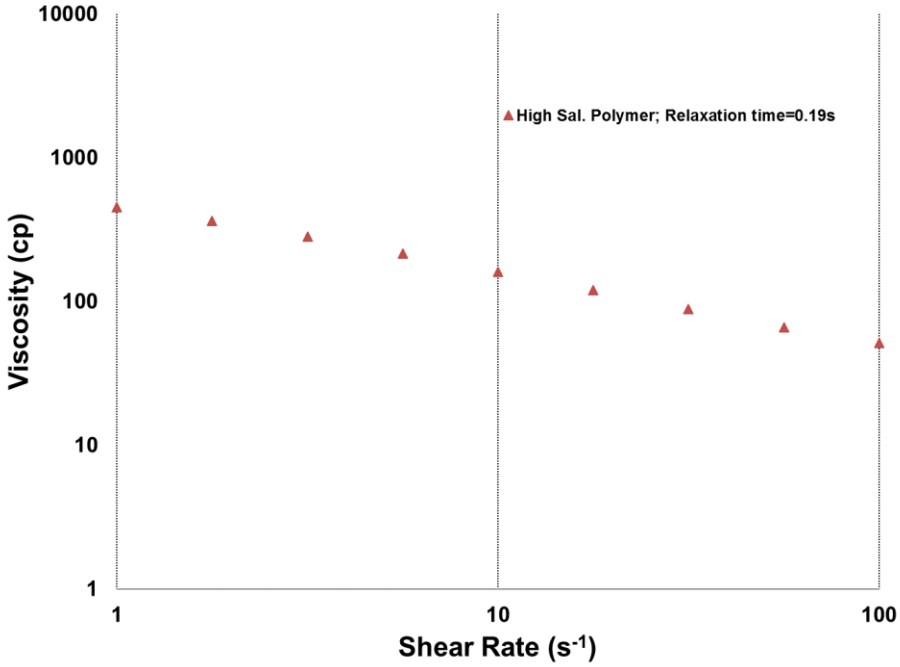

Figure 4.13: SRST result for 3800 ppm FP-3630S HPAM polymer in 26400 ppm NaCl, 300 ppm $NaHCO_3$ aqueous solution at 23 °C for experiment #1.

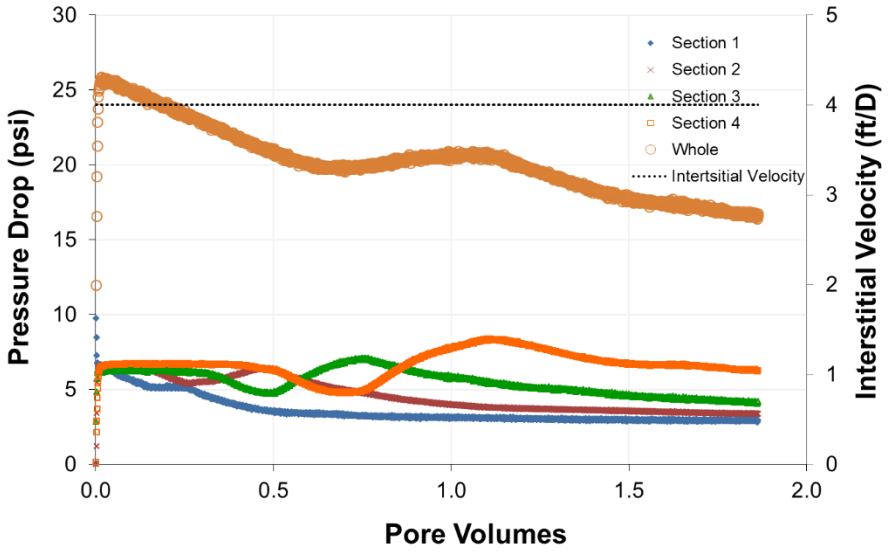

Figure 4.14: Pressure drop data and the interstitial velocity during high-salinity polymer flood at 23 °C for experiment #1.

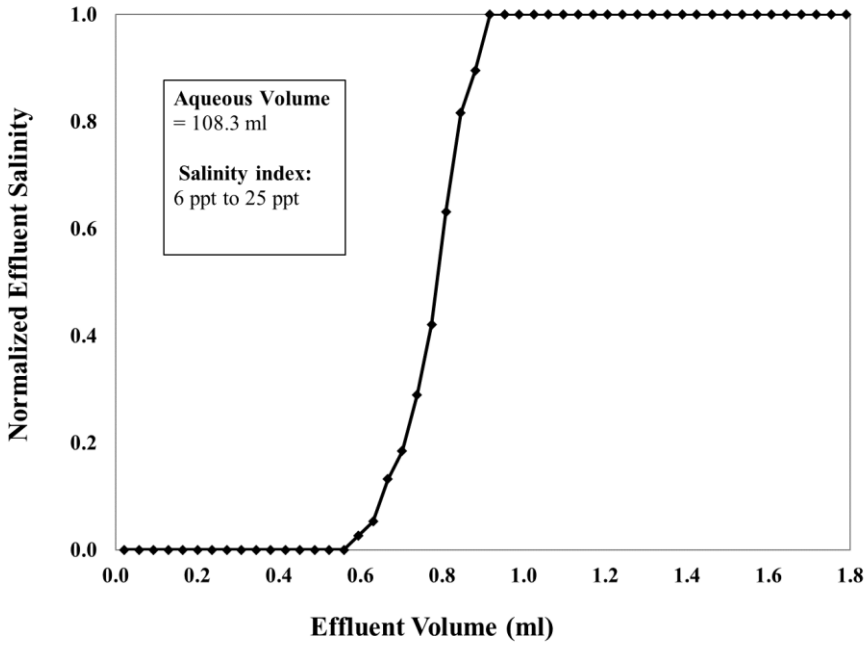

Figure 4.15: Normalized effluent salinity during high-salinity polymer flood for experiment #1.

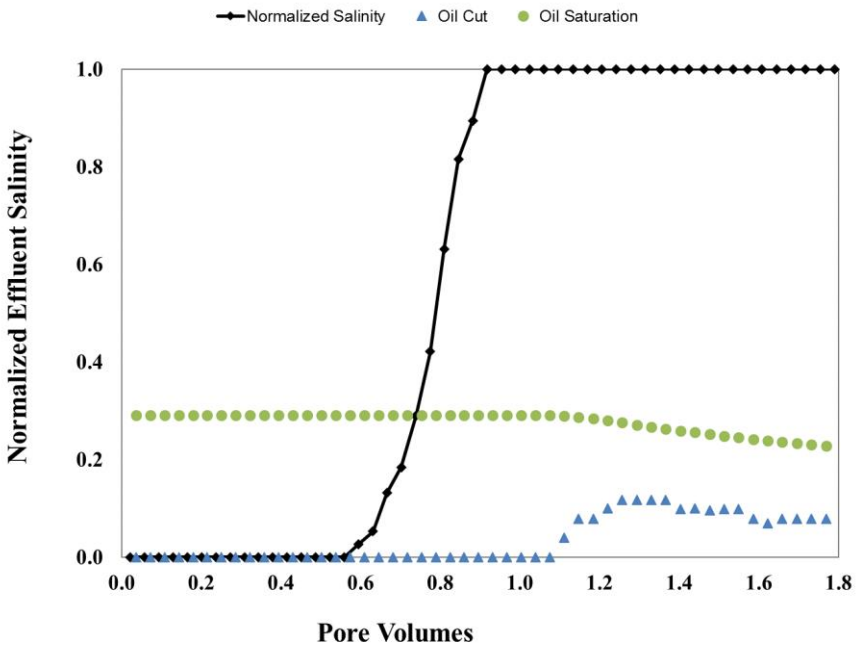

Figure 4.16: Normalized effluent salinity, oil cut and oil saturation during the high-salinity polymer flood for experiment #1

4.1.8 Oil Saturation, Oil Cut, and Pressure Drop

Oil saturation data for all floods performed during experiment #1 are shown in Figure 4.17. Oil cut for both low-salinity and high-salinity polymer floods are shown in Figure 4.18. Pressure drop data are shown in Figure 4.19.

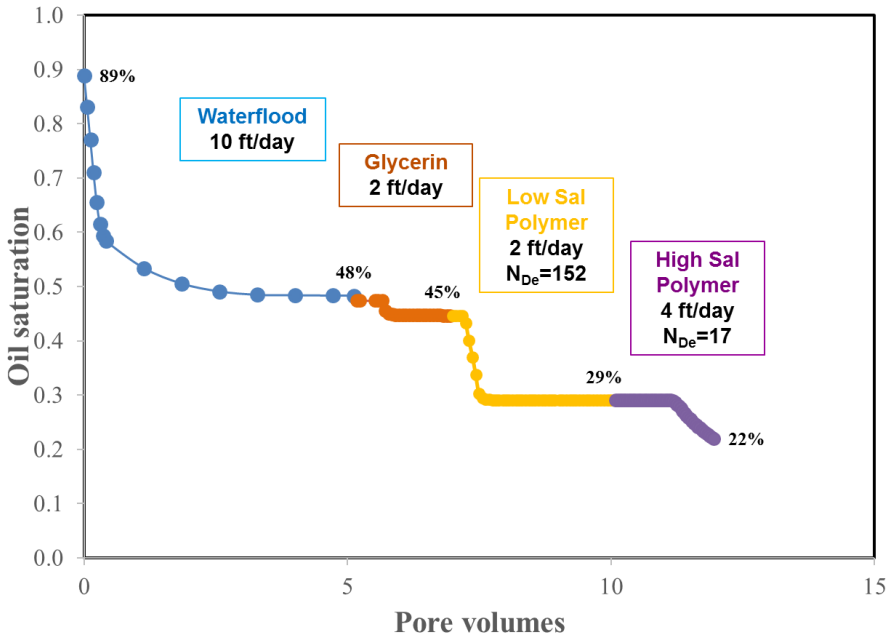

Figure 4.17: Oil saturation for experiment #1.

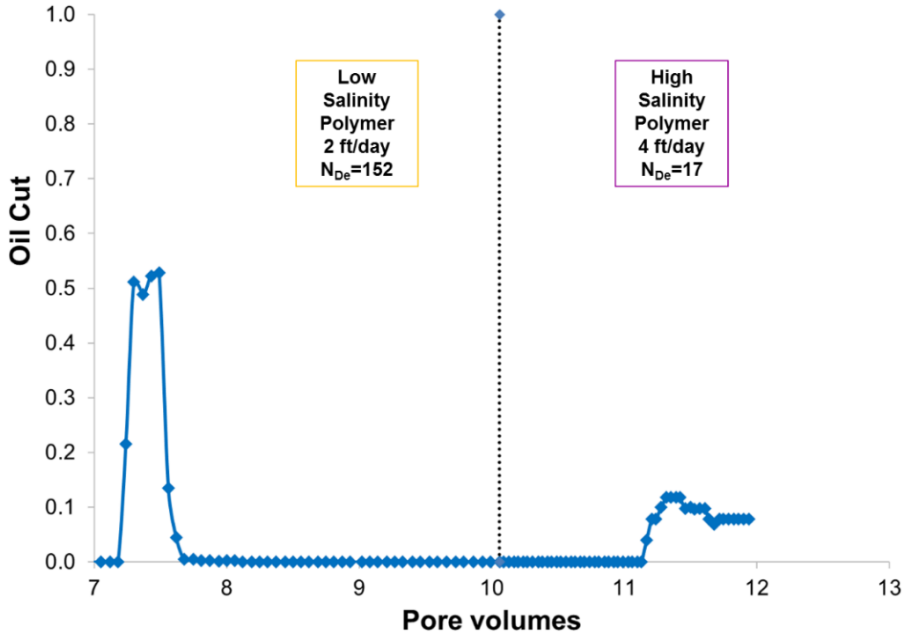

Figure 4.18: Oil cut versus pore volumes injected for both the low-salinity and high-salinity polymer floods for experiment #1.

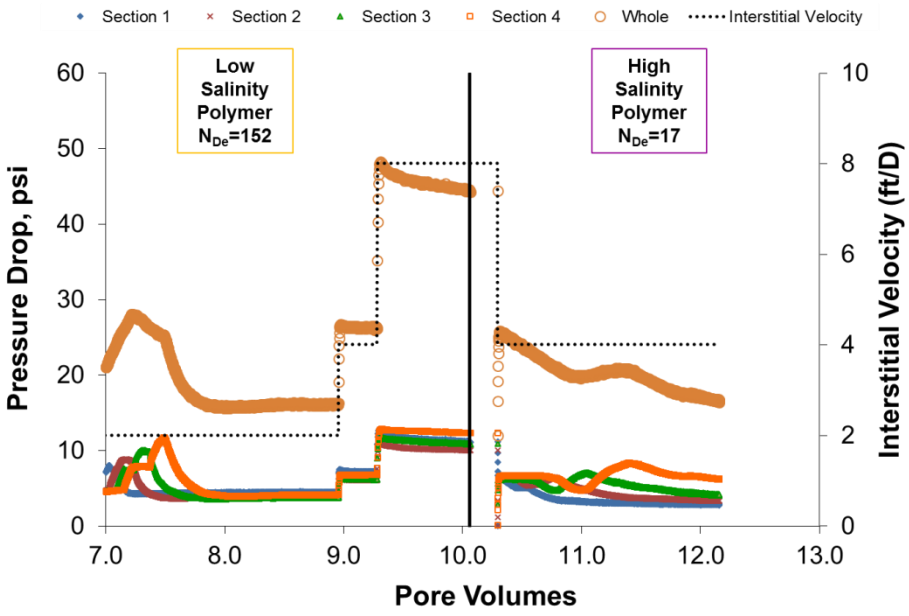

Figure 4.19: Pressure drop for both low-salinity and high-salinity polymer floods for experiment #1.

4.2 EXPERIMENT #2

Experiment #2 was a repeat of Experiment #1 to determine if the same unexpected reduction in residual oil saturation would be observed when high-salinity polymer was injected following low-salinity polymer. Table 4.3 summarizes the core and fluid properties of experiment #2.

Table 4.3: Core and fluid properties of experiment #2.

Experiment	**#2_Z4Z**
Coreflood name	MZE-2nd
Rock type	Bentheimer Sandstone
Brine permeability (mD)	1483
Crude oil viscosity (cP)	126
Temperature (°C)	23
Porosity	0.24
Pore volume (ml)	152.6
Bulk volume (ml)	625
Dry core mass (g)	1267
Bulk density (g/cm^3)	2.0
Waterflood solution	1000 ppm NaCl + 1000 ppm $Na_2S_2O_4$ aqueous solution
Glycerin solution	80 wt% glycerol in in 1000 ppm NaCl aqueous solution
Low-salinity polymer solution	2000 ppm FP-3630S HPAM polymer (#245 X) in 1000 ppm NaCl + 400 ppm $NaHCO_3$ aqueous solution; pH: 8.71, Salinity: 3 0%; FR: 1.05
High-salinity polymer solution	3400 ppm FP-3630S HPAM polymer (# 245X) in 26366 ppm NaCl + 272ppm $NaHCO_3$ aqueous solution; FR: 1.075

4.2.1 Core Preparation, Saturating the Core, and Salinity Tracer Test

A 1 ft long 2.016 in diameter, Bentheimer sandstone core was potted in epoxy to prepare for core flooding. The core passed the pressure test after conducting water leak test at 95 psi air pressure for 10 min. The core was vacuum saturated at 23 °C with 6% KCl aqueous solution. The volume of brine imbibed into the core was measured and used to calculate a pore volume of 149 ml (2 ml was subtracted from the reading to account for fluid in the tubes). A pore volume of 148.4 ml was calculated based on the mass of the core before and after saturation. The same 6% KCl brine was vacuum transferred to an injection column and then injected at varying flow rates from 1 ml/min (9.4 ft/D) to 12 ml/min (112.6 ft/D) to determine the brine permeability, which was found to be 1482 mD using Darcy's Law given in equation 3.7. Injection continued for 1.8 PV.

A salinity tracer test was performed to measure the pore volume and heterogeneity of the core. 2% KCl brine was injected at 2 ml/min (18.8 ft/D) to displace the 6% KCl brine. The effluent samples were collected in volumes of 4 ml. During the salinity tracer test, salinities were measured and plotted to determine the aqueous volume (pore volume) of 152.6 ml from the area above the normalized salinity versus effluent volume curve shown in Figure 4.20.

After the salinity tracer test, the same 2% KCl brine was injected at varying flow rates from 2 ml/min (18.8 ft/D) to 12 ml/min (112.6 ft/D) to determine the permeability, which was calculated as 1485 mD using the data and Darcy's law. The average brine permeability of both 6% KCl and 2% KCl flood was calculated as 1483.5 mD.

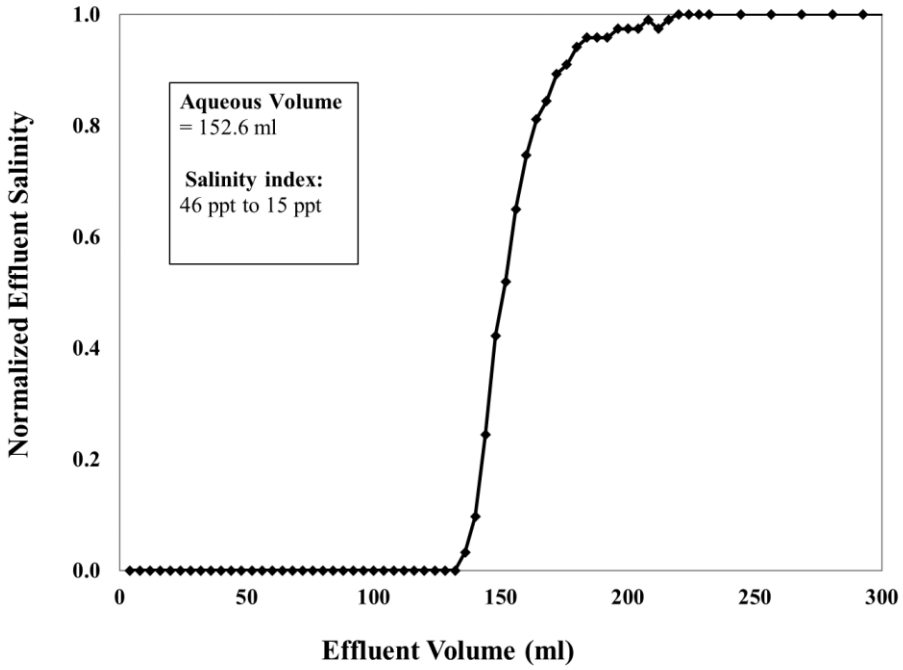

Figure 4.20: Normalized effluent salinity during 2% KCl brine injection for experiment #2, from a salinity index of 46 ppt to 15 ppt.

4.2.2 Core Reduction and Conditioning

The core was flooded at 23 °C with an aqueous solution of 40000 ppm $NaHCO_3$, 10000 ppm Na_4EDTA, and 10000 ppm $Na_2S_2O_4$ at 0.5 ml/min (4.7 ft/D) to reduce the core and to remove amorphous oxidized iron. The iron concentration was about 3 ppm at 6.1 PV. Flooding was continued until the iron concentration in the effluent decreased to 0.3 ppm, the ORP was -710 RmV and the pH was 8.5 (the pH of the injected solution was 8.7). Injection was continued until 10 PV injected. ORP (R.mV) and iron concentration of the effluents are shown in Figure 4.21, and pH and iron concentration of the effluents are shown in Figure 4.22.

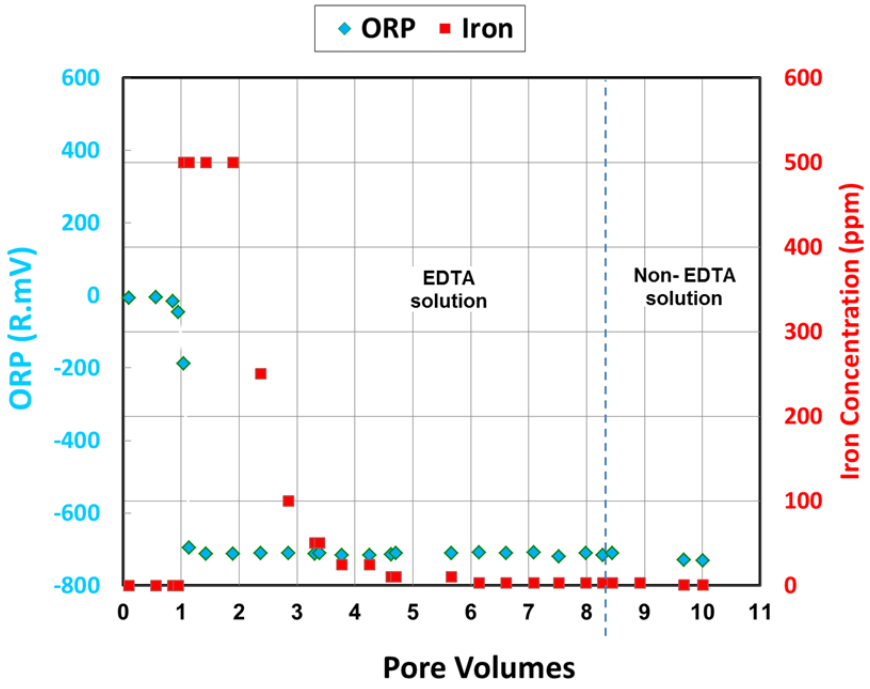

Figure 4.21: ORP (R.mV) and Iron Concentration (ppm) of the effluents.

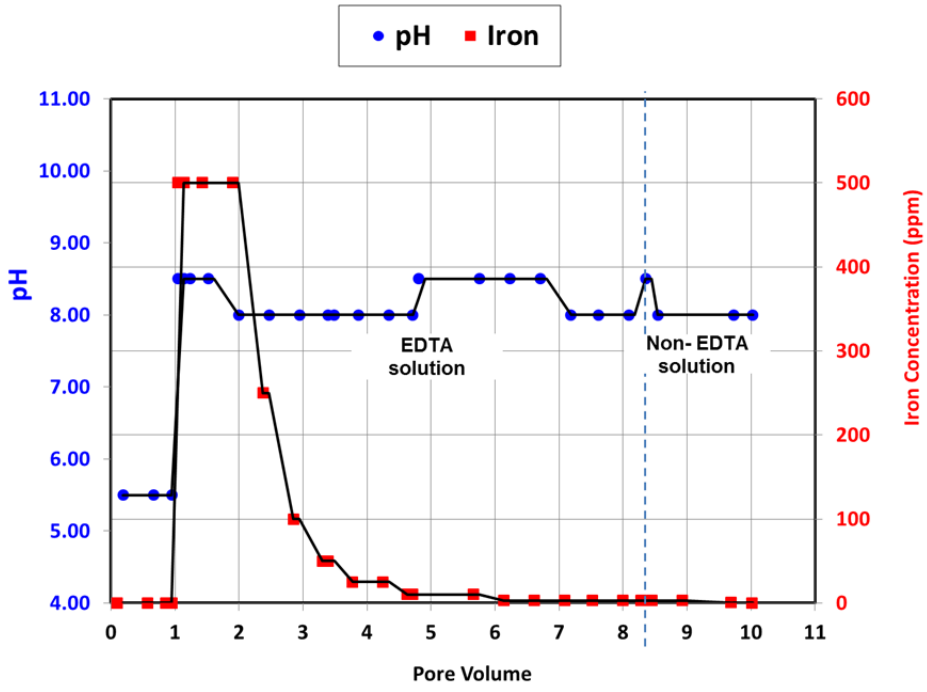

Figure 4.22: pH and Iron concentration (ppm) of the effluents.

4.2.3 Oil Flood

Crude oil with a viscosity of 126 cp at 23 °C was filtered through 1.2 μm filter paper under 20 psi of air pressure. 300 ml of the crude oil was filtered. During filtration, the filter paper was replaced with new ones when a decline in the filtration rate was observed. In this experiment, crude oil was injected at a constant pressure of 85 psi and 23 °C. Oil flooding was continued until steady state pressure drop was observed and the oil cut exceeded 99%. A total of 0.94 PV of oil was injected. The flow rate at steady state was 2 ml/min (18.8 ft/D).

The initial oil saturation (S_{oi}) of 0.84 was determined by using the displaced water volume of 128 ml in equation 3.10. The residual water saturation (S_{wr}) was 0.16 using equation 3.11. The effective oil permeability at S_{wr} was determined 1129 md from Darcy's law using pressure drop and volumetric flow rate, and the end-point oil relative permeability (k^{o}_{ro}) was calculated as 0.74 for the whole core using equation 3.12. Steady-state pressure drop data, effective oil permeability, and end-point oil permeability data are presented in Table 4.4. The oil flow rate is shown in Figure 4.23. Pressure drop and the interstitial velocity data are shown in Figure 4.24. In this coreflood, the pressure drop data for all four sections were recorded from the beginning of the oil flood. The core was aged for 2 days at 23 °C after the oil flood.

Table 4.4: Steady-state pressure drop data, effective oil permeability, and end-point oil permeability from oil flooding for experiment #2.

Oil flood	**Whole**	**Section 1**	**Section 2**	**Section 3**	**Section 4**
Pressure drop (psi)	80	21	18	20	21
Effective oil permeability (mD)	1129	1093	1226	1128	1072
$\boldsymbol{k^{o}_{ro}}$	0.76	0.85	0.74	0.76	0.74

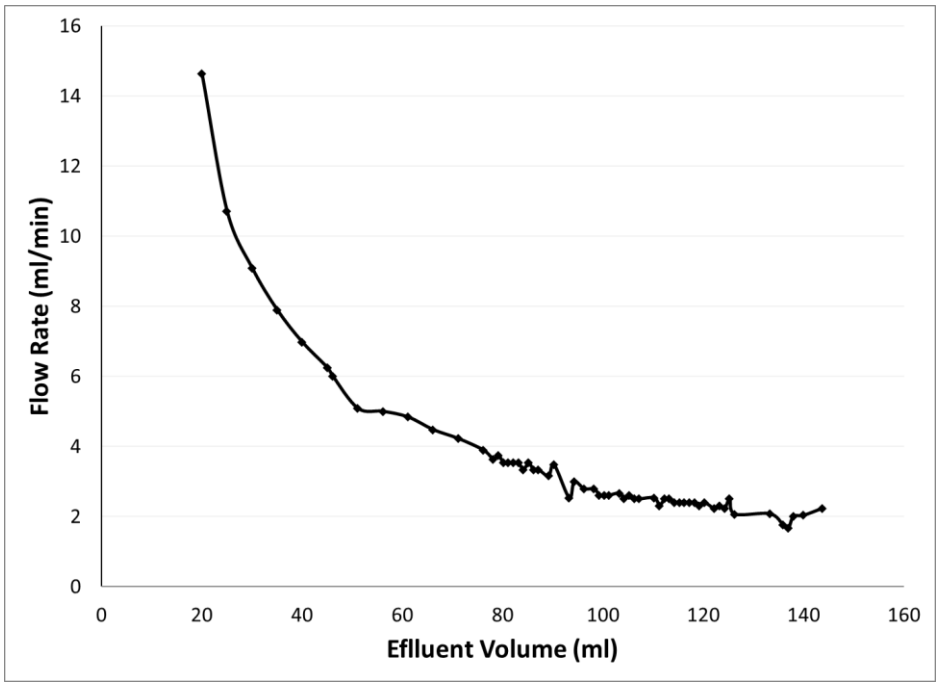

Figure 4.23: Flow rate during 126 cP crude oil flooding conducted at 85 psi constant pressure and 23 ℃ temperature for experiment #2.

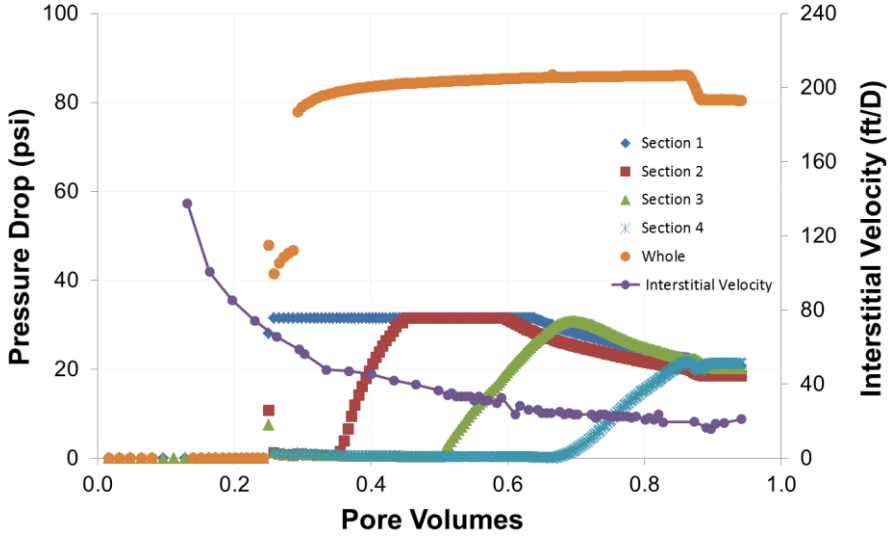

Figure 4.24: Pressure drop and the interstitial velocity data during 126 cP crude oil flooding conducted at 85 psi constant pressure and 23 °C for experiment #2.

4.2.4 Waterflood

An aqueous solution of 1000 ppm NaCl and 1000 ppm $Na_2S_2O_4$ was injected at a constant flow rate of 0.5 ml/min (4.7 ft/D) until steady state pressure for all four sections and zero oil cut was observed. The pressure drop and the interstitial velocity data are shown in Figure 4.25. The capillary number was calculated as 3.5×10^{-5} using the maximum pressure gradient (16.4 psi/ft) and equation 2.3. The pressure drop reached steady state after 3 PV. Waterflooding continued for an additional 2 PV. The remaining oil saturation after the waterflood was 0.395 using equation 3.13. The effective water permeability was calculated as 140 md using the data and Darcy's law, and the end-point water relative permeability was 0.09. The end-point mobility ratio was calculated as 16.7 using equation 3.14.

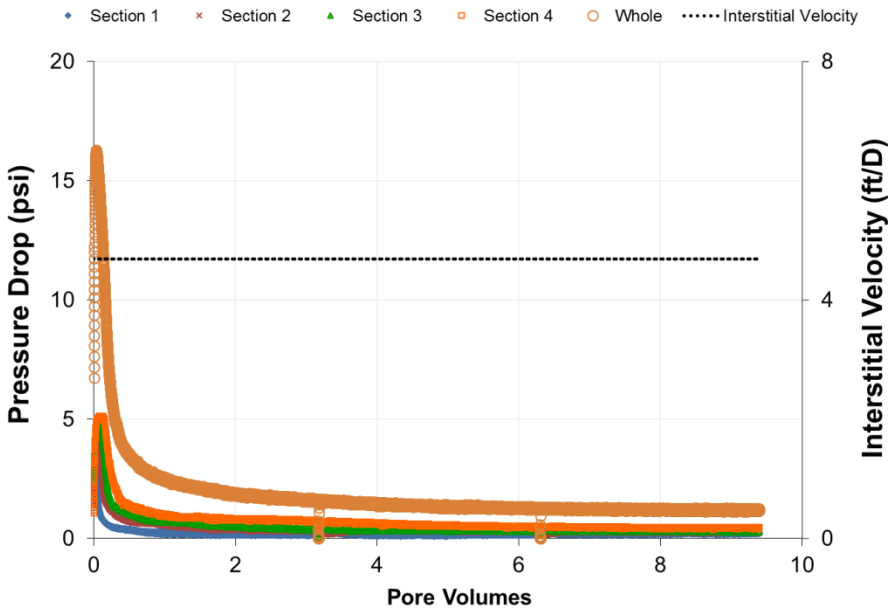

Figure 4.25: Pressure drop and the interstitial velocity data during waterflooding at 23°C for experiment #2.

A 2nd salinity tracer test was performed as an independent measurement of residual oil saturation to compare with the remaining oil saturation value obtained from material balance using produced oil and water volumes. An aqueous solution of 30000 ppm NaCl and 1000 ppm $Na_2S_2O_4$ was injected at 2 ml/min (18.77 ft/day) to displace the aqueous solution of 1000 ppm NaCl and 1000 ppm $Na_2S_2O_4$ brine. The effluent samples were collected in volumes of 5 ml. During the salinity tracer test, salinities were measured and plotted to determine the aqueous volume of 86.3 ml from the area above the normalized effluent salinity vs. effluent volume curve shown in Figure 4.26. After performing the tracer test, an aqueous solution of 1000 ppm NaCl and 1000 ppm $Na_2S_2O_4$ was injected at 2 ml/min (18.77 ft/day) to displace the solution of 30000 ppm NaCl and 1000 ppm $Na_2S_2O_4$ brine for 1 PV. By using the aqueous volume determined from salinity tracer test, the oil saturation after waterflood was obtained as 0.43 (1-86.3/152.6) while the material balance had given 0.40. The relative error is 7%. Material balance values were reported for comparison purposes in this research.

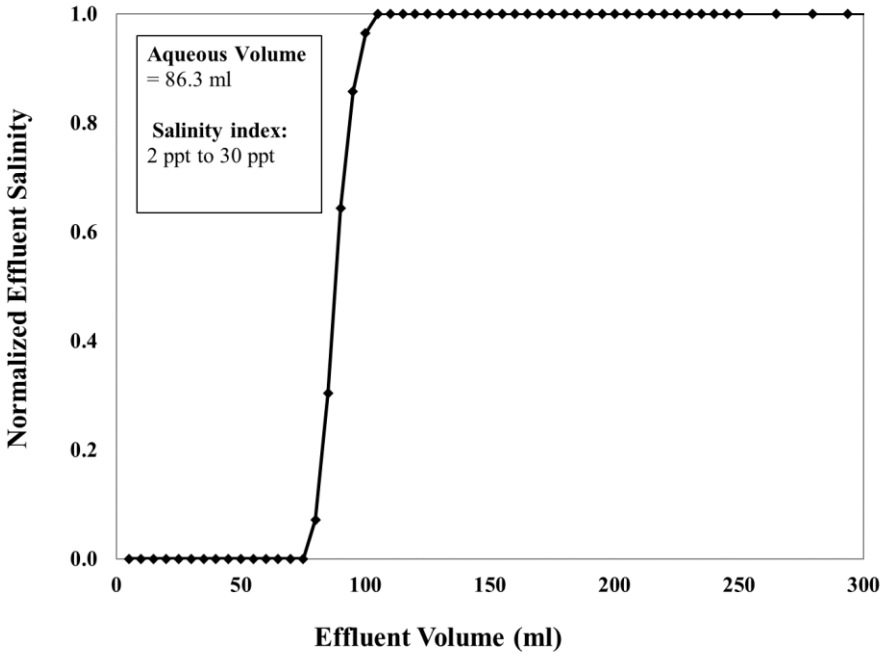

Figure 4.26: Normalized effluent salinity during 2nd salinity tracer test for experiment #2, from a salinity index of 2 ppt to 30 ppt.

4.2.5 Glycerin Flood

An aqueous solution of 80 wt% glycerin and 20 wt% brine (1000 ppm NaCl, 400 ppm $NaHCO_3$) with a viscosity of 46 cP (measured with rheometer) was injected at a flow rate of 0.2 ml/min (2.1 ft/D) until steady state pressure drop for all four sections and an oil cut of 0.04% was observed. The maximum oil cut was 7.6%. The pressure drop data and the interstitial velocity are shown in Figure 4.27. Steady state pressure drop was observed after 0.7 PV, but the flood continued until 1.5 PV. The residual oil saturation was reduced from 0.40 following the waterflood to 0.38 following the glycerin flood using equation 3.15. The effective permeability was 141 mD using Darcy's law and the end-point glycerin

relative permeability was 0.1. The end-point mobility ratio was calculated as 0.4 using equation 3.16.

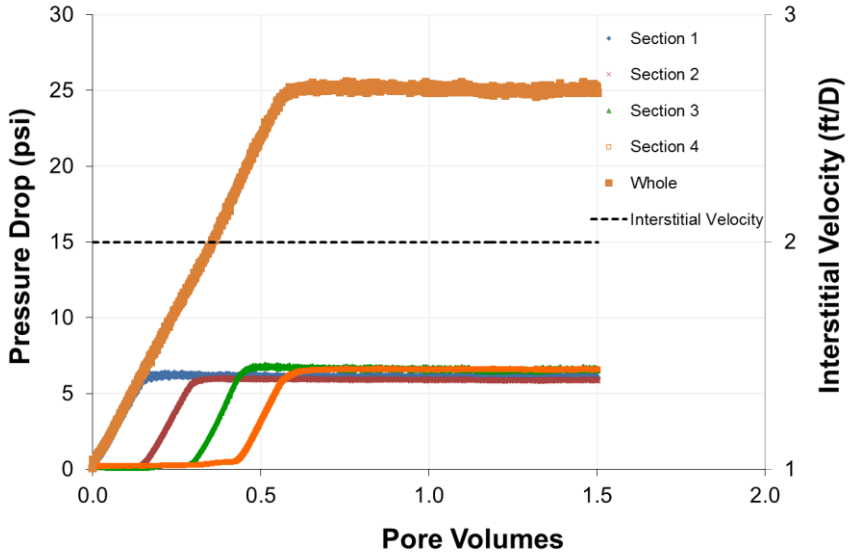

Figure 4.27: Pressure drop data, and the interstitial velocity during glycerin flooding at 23 °C for experiment #2.

4.2.6 Low-salinity Polymer Flood

A high molecular weight polymer (2000 ppm FP 3630S #245X) was prepared in a low-salinity brine (1000 ppm NaCl and 400 ppm $NaHCO_3$) to obtain a polymer solution with a high relaxation time. After hydrating 24 hours, the solution was filtered under 15 psi Argon pressure at 23 °C using a 1.2 µm Millipore mixed cellulose ester membrane filter paper. The filtration ratio was 1.05. The polymer solution was

bubbled with argon while stirring for 2 hours in a round bottom flask and then vacuum-transferred to an injection column.

A sample of the polymer solution was taken from the column to measure its rheology and pH, salinity. The pH was 8.7 and the salinity index was 3 ppt. A relaxation time of 1.9 s was determined from the G', G" crossover point using the dynamic frequency sweep test (DFST) shown in Figure 4.28. The steady rate sweep test (SRST) data in the power-law viscosity region of shear thinning as shown in Figure 4.29 were fit to obtain a power-law equation of μ=411 $\dot{\gamma}^{(-0.60)}$.

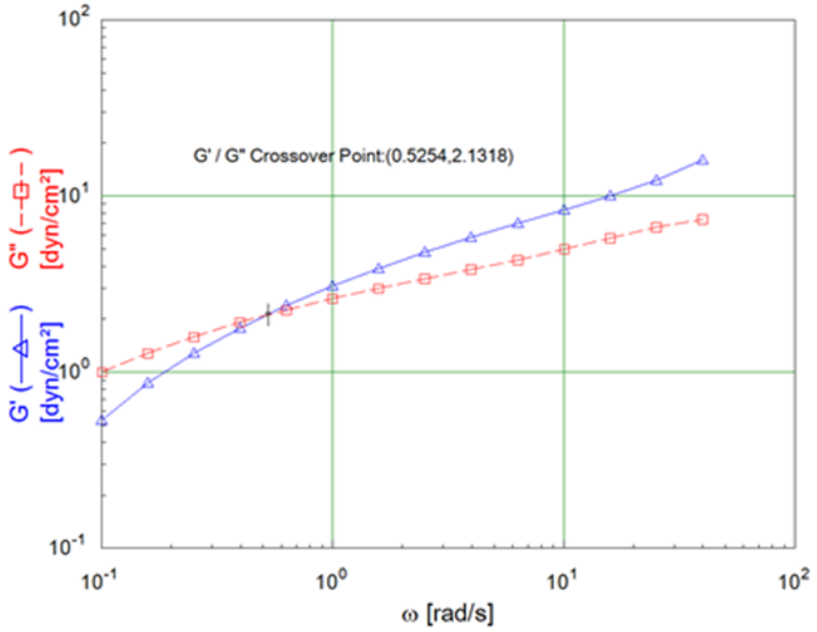

Figure 4.28: DFST result for 2000 ppm FP-3630S HPAM polymer in 1000 ppm NaCl + 400 ppm NaHCO3 aqueous solution at 23 °C for experiment #2.

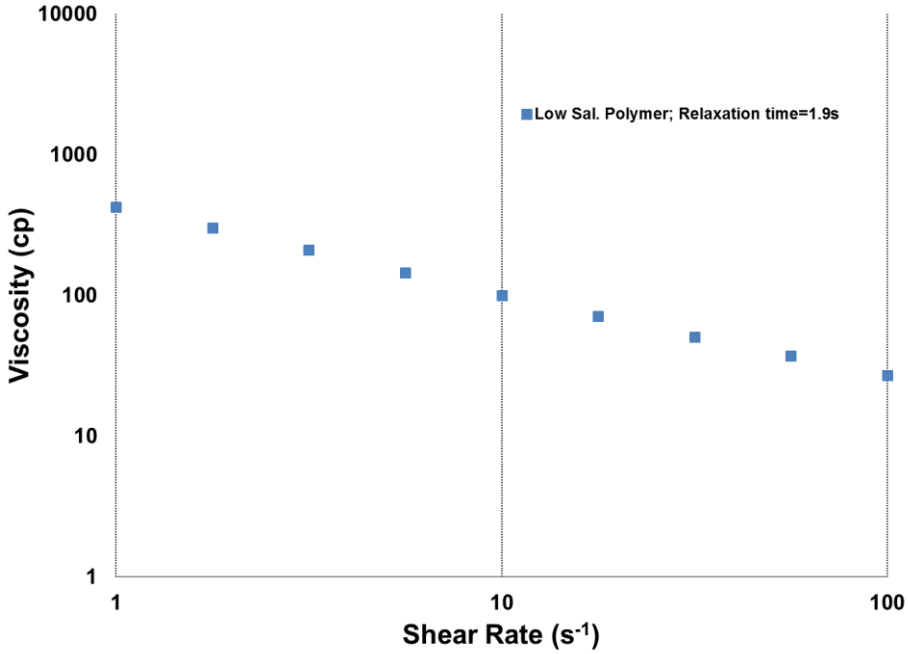

Figure 4.29: SRST result for 2000 ppm FP-3630S HPAM polymer in 1000 ppm NaCl + 400 ppm NaHCO3 aqueous solution at 23 °C for experiment #2.

This low-salinity polymer solution was injected at a constant flow rate of 0.213 ml/min (2 ft/D) until steady state pressure drop for all four sections and zero oil cut was observed. Pressure drop data and the interstitial velocity are shown in Figure 4.30.

The residual oil saturation following low-salinity polymer flood decreased to 0.29 using equation 3.17, a 9% reduction in oil saturation compared to the glycerin flood. Cumulative oil recovery at the end of the polymer flood was 65% of the OOIP. The effective permeability for the polymer flood was 158 mD at 2 ft/D calculated from Darcy's law using the differential pressure drop data at steady state. The end-point relative permeability was 0.11 at 2 ft/D determined from dividing the effective permeability by the brine permeability. The end-point mobility ratio was calculated to be 0.5 at 2 ft/D using equation 3.18. The maximum capillary number was calculated as 5.6×10^{-5} for the whole core using the maximum pressure gradient of 29 psi/ft and equation 2.3. Maximum

capillary number is below the critical capillary number (1×10^{-4} for Bentheimer sandstone). Equivalent shear rate was calculated as 52.6 s^{-1} using equation 2.6 and Deborah number (N_{De}) was calculated as 100.1 using equation 2.5.

The viscosities of the effluent samples were measured as soon as possible after the samples were produced. A comparison of the viscosities of injected polymer solution and the effluent samples retrieved at different pore volumes are shown in Figure 4.31.

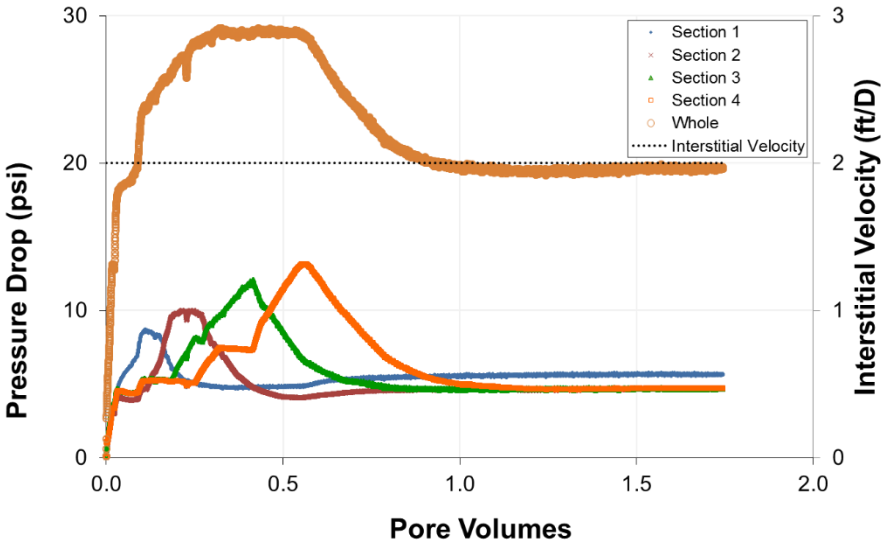

Figure 4.30: Pressure drop data, and the interstitial velocity during 2000 ppm FP-3630S HPAM polymer in 1000 ppm NaCl + 400 ppm NaHCO3 aqueous solution flood at 23 °C for experiment #2.

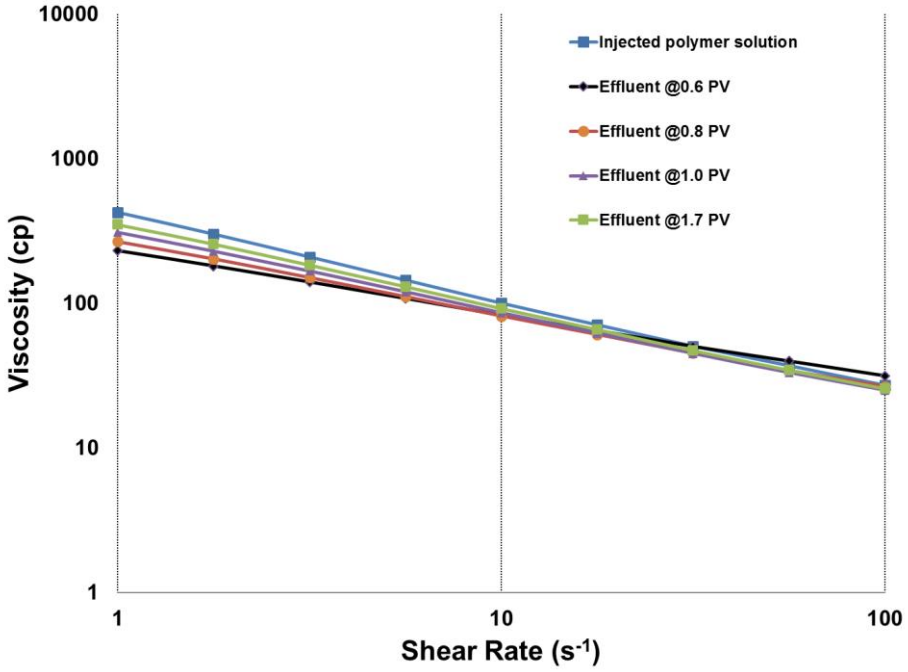

Figure 4.31: Viscosity comparison of the injected polymer solution and the effluents at 23 °C for experiment #2.

4.2.7 High-Salinity Polymer Flood

A 3400 ppm FP 3630S polymer in 26400 ppm NaCl, 300 ppm $NaHCO_3$ brine was prepared for the tracer test. After hydrating 18 hours, the polymer solution was filtered through 90 mm diameter, 1.2 μm Millipore mixed cellulose ester membrane filter paper under 15 psi Argon pressure into 250 ml graduated cylinder at 23 °C. The filtration ratio was 1.07. The polymer solution was bubbled with argon while stirring for 2 hours in a round bottom flask and then vacuum-transferred to an injection column. A sample of the polymer solution was taken from the column to measure its rheology. The dynamic frequency sweep test (DFST) data are shown in Figure 4.32a. The relaxation time was estimated as 0.12 s using the G' and G" crossover point. It is significantly less than the 1.9s

for the polymer solution injected into the core in the previous step. Figure 4.32b compares the results of the SRST for this polymer (3400 ppm FP-3630S HPAM polymer in 26400 ppm NaCl, 300 ppm $NaHCO_3$) and the polymer (2000 ppm FP-3630S HPAM polymer in 1000 ppm NaCl + 400 ppm $NaHCO_3$) in the preceding flood. The viscosities are similar, but the high salinity polymer in slightly less viscous than the low salinity one. The data was fit to a power-law model with the equation $\mu=205 \times \dot{\gamma}^{(-0.46)}$.

This high-salinity polymer solution was injected at a constant flow rate of 0.426 ml/min (4 ft/D) to displace the low-salinity polymer solution. Pressure drop data and the interstitial velocity are shown in Figure 4.33. The effluent samples were collected in volumes of 4 ml. During the salinity tracer test, salinities were measured and plotted. An aqueous volume of 98.9 ml was determined from the area above the normalized salinity curve shown in Figure 4.34. The normalized salinity, oil cut and oil saturation data are shown in Figure 4.35, and it shows that the oil recovery is observed after the salinity is reaching the injection salinity value.

Oil production was observed starting at 0.92 PV. A total of 32.1 ml of additional oil was recovered. The maximum oil cut was 15% as shown in figure 4.35. The flood continued 6.8 PV total. The residual oil saturation after this polymer flood was 0.08, a 21% reduction in oil saturation (0.29) from the preceding polymer flood. The cumulative oil recovery at the end of the flood was 90% of the OOIP.

The final oil saturation based on the tracer data was compared to the oil saturation following the low-salinity polymer flood, as the oil recovery was after the salinity tracer test was finished. The final oil saturation based on the tracer data was 0.36 (1-98.9/152.6) and 0.29 based on the material balance.

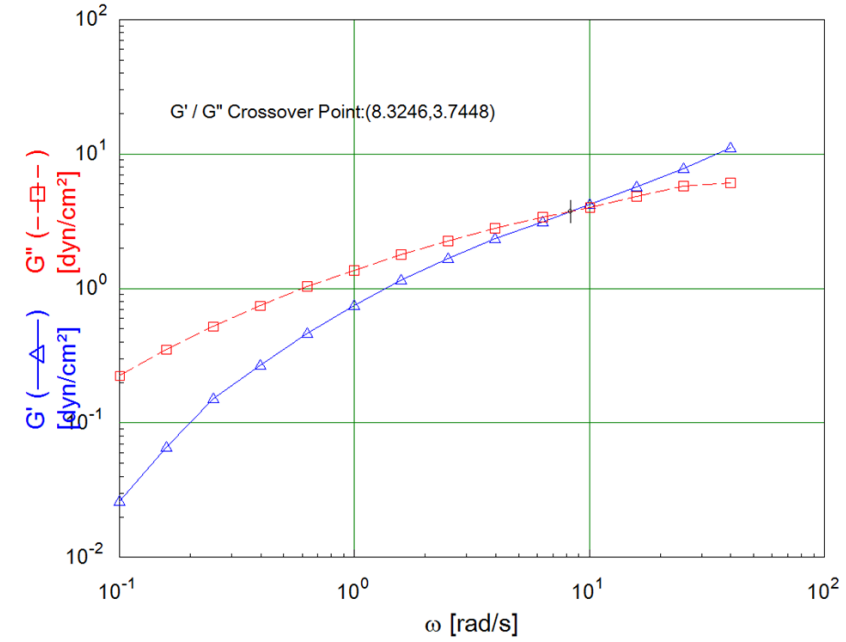

Figure 4.32a: DFST result for 3400 ppm FP-3630S HPAM polymer in 26400 ppm NaCl, 300 ppm $NaHCO_3$ aqueous solution at 23 °C for experiment #2.

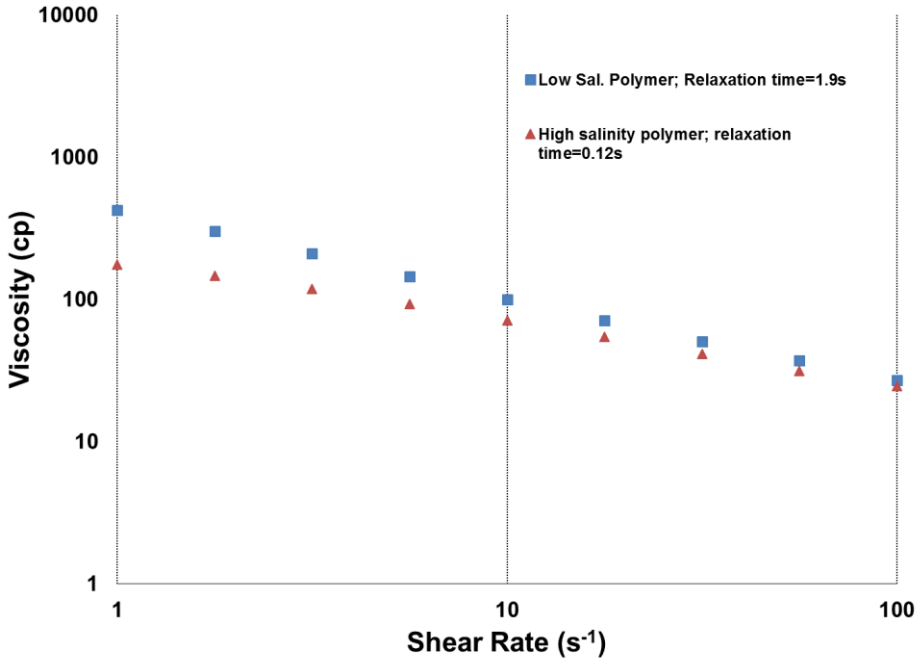

Figure 4.32b: SRST result for high-salinity polymer solution compared to the low-salinity polymer solution at 23 °C for experiment #2.

At the end of the low-salinity polymer flood, the effective permeability was calculated as 350 mD using the data and Darcy's law, the end-point relative permeability was calculated as 0.24 using the ratio of the effective permeability to the brine permeability, the end-point mobility ratio was calculated as 1.6 using the end-point relative permeability and equation 3.18, and the maximum capillary number was calculated as 5.8×10^{-5} for the whole core using the maximum pressure gradient of 30.6 psi/ft in equation 2.3. Equivalent shear rate was calculated as 92 s^{-1} using equation 2.6 and Deborah number (N_{De}) was calculated as 11 using equation 2.5.

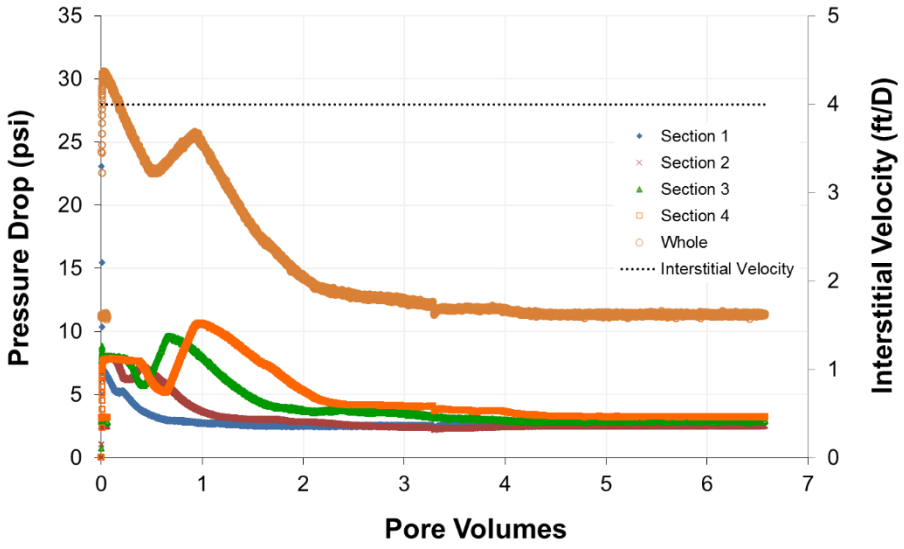

Figure 4.33: Pressure drop data, and the interstitial velocity during high-salinity polymer flood at 23 °C for experiment #2.

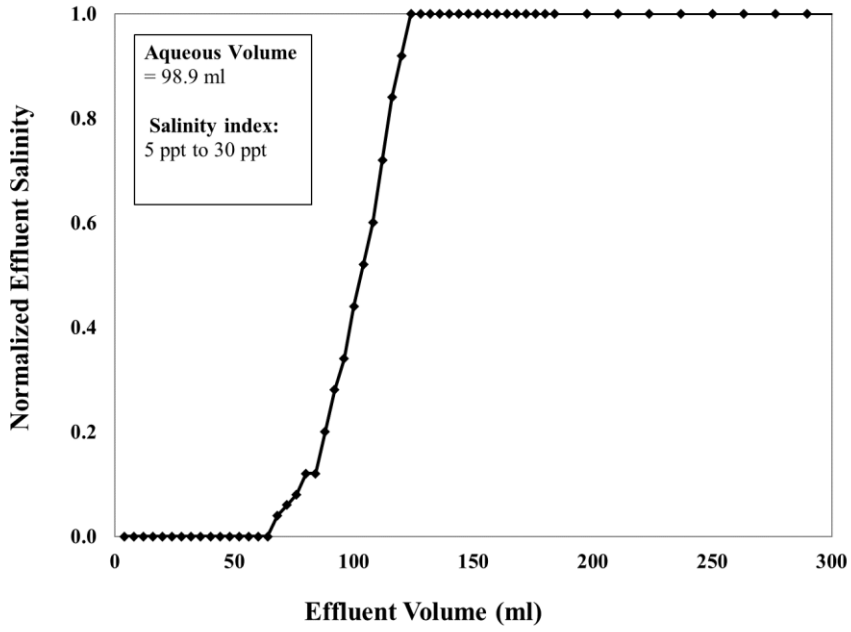

Figure 4.34: Normalized effluent salinity during high-salinity polymer flood for experiment #2, from a salinity index of 5 ppt to 30 ppt.

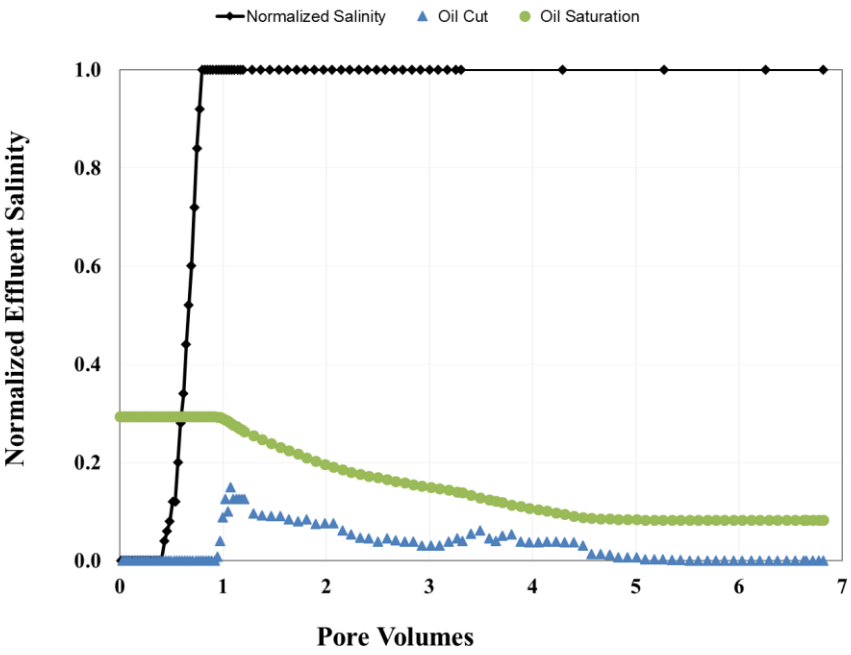

Figure 4.35: Normalized effluent salinity, oil cut, and oil saturation during high-salinity polymer flood for experiment #2.

4.2.8 Oil Saturation, Oil Cut, and Pressure Drop

Oil saturation data for all floods performed during experiment #2 are shown in Figure 4.36. Oil cut for both low-salinity and high-salinity polymer floods are shown in Figure 4.37. Pressure drop data are shown in Figure 4.38.

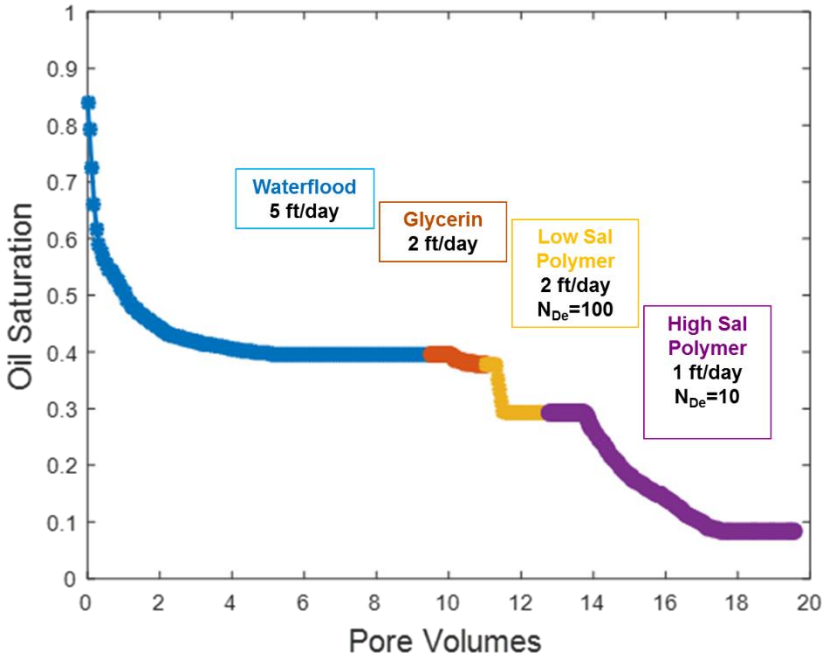

Figure 4.36: Oil saturation versus pore volumes for experiment #2.

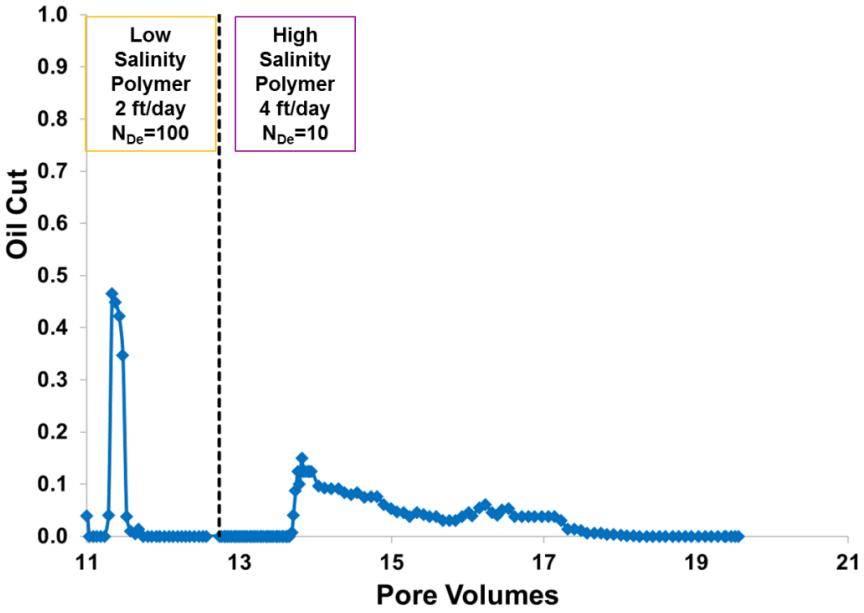

Figure 4.37: Oil cut versus pore volumes for both low-salinity and high-salinity polymer floods for experiment #2.

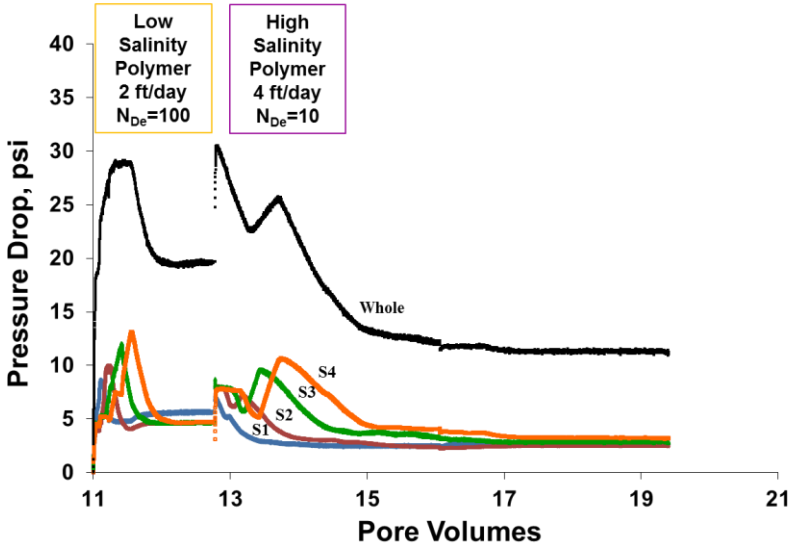

Figure 4.38: Pressure drop for both low-salinity and high-salinity polymer floods for experiment #2.

4.3 EXPERIMENT #3

The purpose of the coreflood experiment #3 was to determine the effect of using a high-salinity polymer flood after a low-salinity, high elasticity polymer flood on residual oil saturation. The unusual recovery during second polymer injection in experiment #1 and experiment #2 motivated more experiments. In this experiment, a lower interstitial velocity (e.g. 1 ft/D) was used to reduce the capillary number. Experiment #3 was similar in most aspects to experiment #1 and #2, except the interstitial velocity was decreased to 1 ft/D. Table 4.5 summarizes the core and fluid properties of experiment #3.

4.3.1 Core Preparation, Saturating the Core, Salinity Tracer Test

A 1 ft long 2.157 in diameter, Bentheimer sandstone core was potted in epoxy to prepare for core flooding. The core passed the pressure test after conducting water leak test at 95 psi air pressure for 10 min. The core was vacuum saturated at 23 °C with 6% KCl aqueous solution. The volume of brine imbibed into the core was measured and used to calculate a pore volume of 148 ml (2 ml was subtracted from the reading to account for fluid in the tubes). A pore volume of 147.7 ml was calculated based on the mass of the core before and after saturation. The same 6% KCl brine was vacuum transferred to an injection column and then injected at varying flow rates from 1 ml/min (9.5 ft/D) to 12 ml/min (113.7 ft/D) to determine the brine permeability, which was found to be 1475 mD using Darcy's Law given in equation 3.7. Injection continued for 12 PV.

A salinity tracer test was performed to measure the pore volume and heterogeneity of the core. 2% KCl brine was injected at 2 ml/min (18.9 ft/D) to displace the 6% KCl brine. The effluent samples were collected in volumes of 4 ml. During the salinity tracer test, salinities were measured and plotted to determine the aqueous volume (pore volume) of 151.4 ml from the area above the normalized salinity versus effluent volume curve shown in Figure 4.39.

Table 4.5: Core and fluid properties of experiment #3.

Experiment	**#3_Z4Z**
Coreflood name	MZE-3rd
Rock type	Bentheimer Sandstone
Brine permeability (mD)	1480
Crude oil viscosity (cP)	114
Temperature (°C)	23
Porosity	0.25
Pore volume (ml)	151.4
Bulk volume (ml)	616
Dry core mass (g)	1230
Bulk density (g/cm^3)	2.0
Waterflood solution	1000 ppm NaCl + 1000 ppm $Na_2S_2O_4$ aqueous solution
Glycerin solution	82 wt% glycerol in in 1000 ppm NaCl aqueous solution
Low-salinity polymer solution	2000 ppm FP-3630S HPAM polymer (#245 X) in 1000 ppm NaCl + 400 ppm $NaHCO_3$ aqueous solution; FR: 1.0
High-salinity polymer solution	3548 ppm FP-3630S HPAM polymer (# 245X) in 24030 ppm NaCl + 280 ppm $NaHCO_3$ aqueous solution; Salinity: 28 o%; FR: 1.1

After the salinity tracer test, the same 2% KCl brine was injected at varying flow rates from 2 ml/min (18.9 ft/D) to 12 ml/min (113.7 ft/D) to determine the permeability, which was calculated as 1482 mD using the data and Darcy's law. The average brine permeability of both 6% KCl and 2% KCl flood was calculated as 1480 mD.

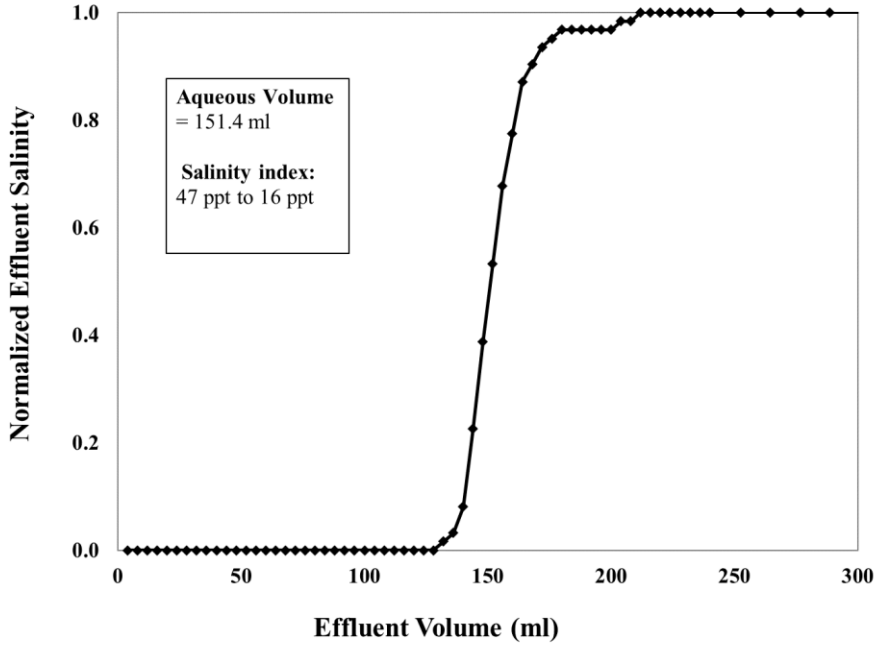

Figure 4.39: Normalized effluent salinity during 2% KCl brine injection for experiment #3, from a salinity index of 47 ppt to 16 ppt.

4.3.2 Core Reduction and Conditioning

The core was flooded at 23 °C with an aqueous solution of 40000 ppm $NaHCO_3$, 10000 ppm Na_4EDTA, and 10000 ppm $Na_2S_2O_4$ at 0.5 ml/min (4.7 ft/D) to reduce the core and to remove amorphous oxidized iron. The iron concentration was about 3 ppm at 6 PV. Flooding was continued until the iron concentration in the effluent decreased to 0.3 ppm, the ORP was -750 RmV and the pH was 8. Injection was continued until 12.8 PV injected. ORP (R.mV) and iron concentration of the effluents are shown in Figure 4.40, and pH and iron concentration of the effluents are shown in Figure 4.41.

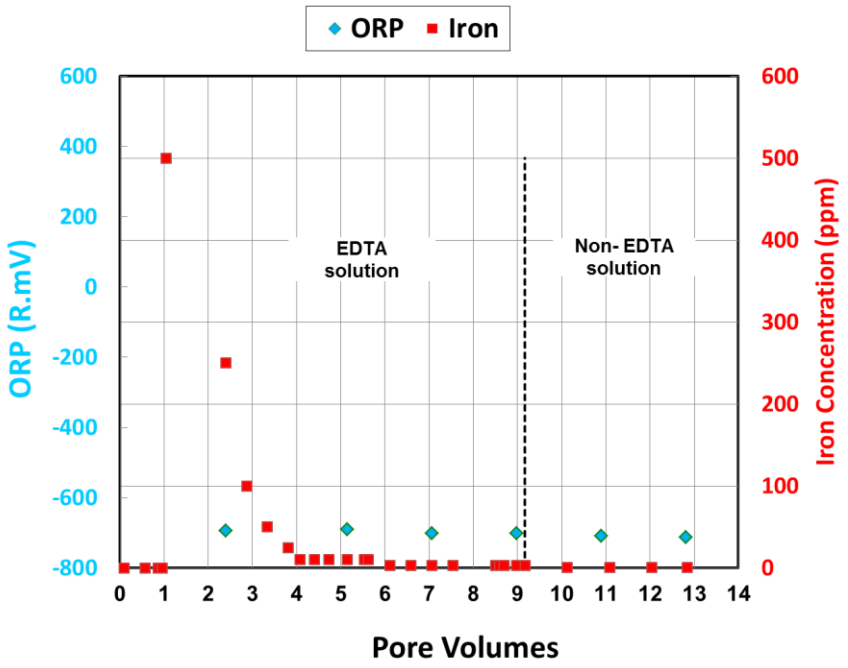

Figure 4.40: ORP (R.mV) and Iron Concentration (ppm) of the effluents.

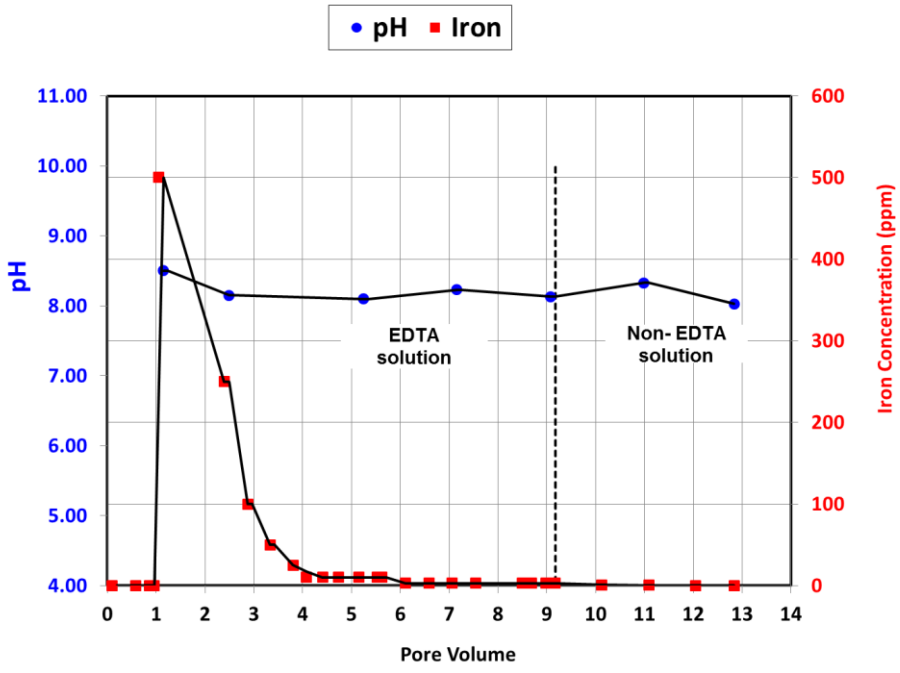

Figure 4.41: pH and Iron Concentration (ppm) of the effluents.

4.3.3 Oil Flood

Crude oil with a viscosity of 114 cp at 23 °C was filtered through 1.2 μm filter paper under 20 psi of air pressure. 300 ml of the crude oil was filtered. During filtration, the filter paper was replaced with new ones when a decline in the filtration rate was observed. Crude oil was injected at a constant pressure of 85 psi and 23 °C. Oil flooding was continued until steady state pressure drop was observed and the oil cut exceeded 99%. A total of 1.3 PV of oil was injected. The flow rate at steady state was 2.4 ml/min (22.7 ft/D).

The initial oil saturation (S_{oi}) of 0.82 was determined by using the displaced water volume of 123.4 ml in equation 3.10. The residual water saturation (S_{wr}) was 0.18 using equation 3.11. The effective oil permeability at S_{wr} was determined 1245 md from Darcy's law using pressure drop and volumetric flow rate, and the end-point oil relative permeability (k^o_{ro}) was calculated as 0.84 for the whole core using equation 3.12. Steady-state pressure drop data, effective oil permeability, and end-point oil permeability data are presented in Table 4.6. The oil flow rate is shown in Figure 4.42. Pressure drop and the interstitial velocity data are shown in Figure 4.43. The core was aged for 2 days at 23 °C after the oil flood.

Table 4.6: Steady-state pressure drop data, effective oil permeability, and end-point oil permeability from oil flooding for experiment #3.

Oil flood	**Whole**	**Section 1**	**Section 2**	**Section 3**	**Section 4**
Pressure drop (psi)	81	21	19	20	21
Effective oil permeability (mD)	1245	1216	1308	1251	1201
k^o_{ro}	0.84	1.03	0.81	0.76	0.82

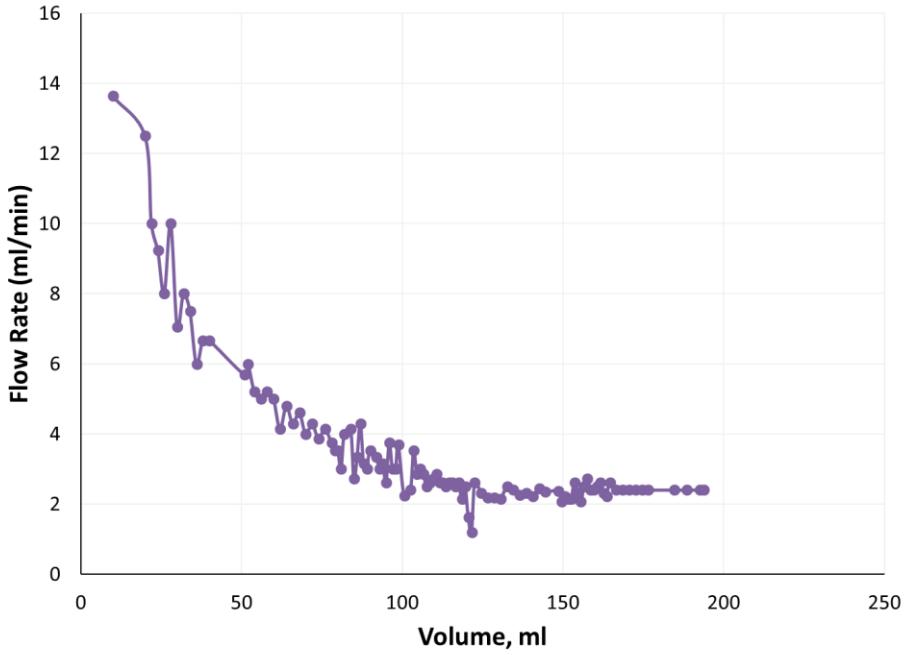

Figure 4.42: Flow rate during 114 cP crude oil flooding conducted at 85 psi constant pressure and 23 °C temperature for experiment #3.

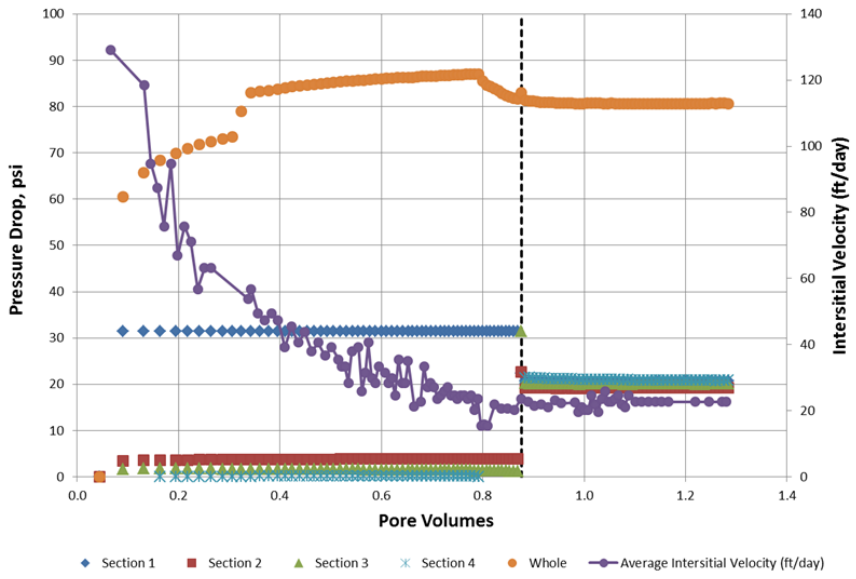

Figure 4.43: Pressure drop, and the interstitial velocity data during 114 cP crude oil flooding conducted at 85 psi constant pressure and 23 °C for experiment #3.

4.3.4 Waterflood

An aqueous solution of 1000 ppm NaCl and 1000 ppm $Na_2S_2O_4$ was injected at a constant flow rate of 0.5 ml/min (4.7 ft/D) until steady state pressure for all four sections and zero oil cut was observed. The pressure drop and the interstitial velocity data are shown in Figure 4.44. The capillary number was calculated as 3.3×10^{-5} using the maximum pressure gradient and equation 2.3. The pressure drop reached steady state after 4 PV. Waterflooding continued for an additional 5 PV. The remaining oil saturation after the waterflood was 0.45 using equation 3.13. The effective water permeability was calculated as 130 md using the data and Darcy's law, and the end-point water relative permeability was 0.09. The end-point mobility ratio was calculated as 12.8 using equation 3.14.

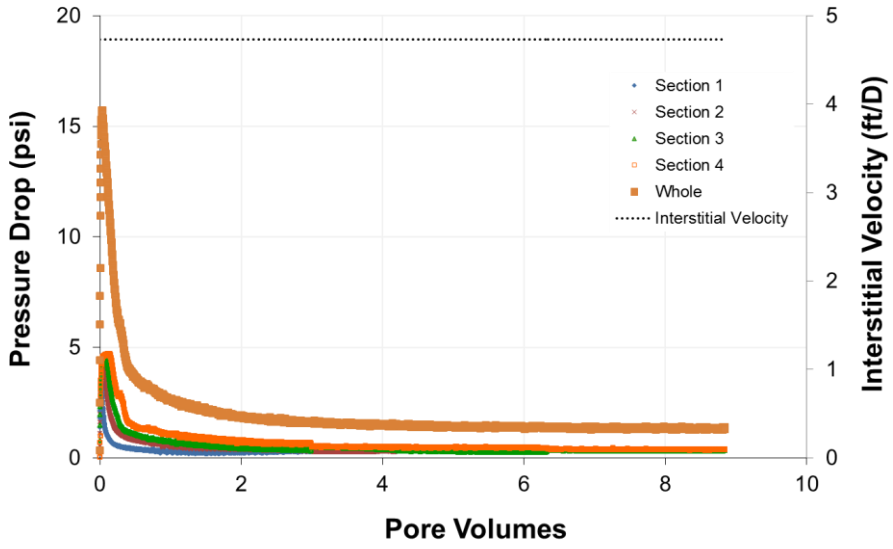

Figure 4.44: Pressure drop, and the interstitial velocity data during waterflooding at 23°C for experiment #3.

A 2nd salinity tracer test was performed as an independent measurement of residual oil saturation to compare with the remaining oil saturation value obtained from material balance using produced oil and water volumes. An aqueous solution of 30000 ppm NaCl and 1000 ppm $Na_2S_2O_4$ was injected at 2 ml/min (18.8 ft/day) to displace the aqueous solution of 1000 ppm NaCl and 1000 ppm $Na_2S_2O_4$ brine. The effluent samples were collected in volumes of 4 ml. During the salinity tracer test, salinities were measured and plotted to determine the aqueous volume of 84.7 ml from the area above the normalized effluent salinity vs. effluent volume curve shown in Figure 4.45. After performing the tracer test, an aqueous solution of 1000 ppm NaCl and 1000 ppm $Na_2S_2O_4$ was injected at 2 ml/min (18.8 ft/day) to displace the solution of 30000 ppm NaCl and 1000 ppm $Na_2S_2O_4$ brine for 1 PV. By using the aqueous volume determined from salinity tracer test, the oil saturation after waterflood was obtained as 0.44 (1-84.7/151.4) while the material balance had given 0.45. The relative error is 2%.

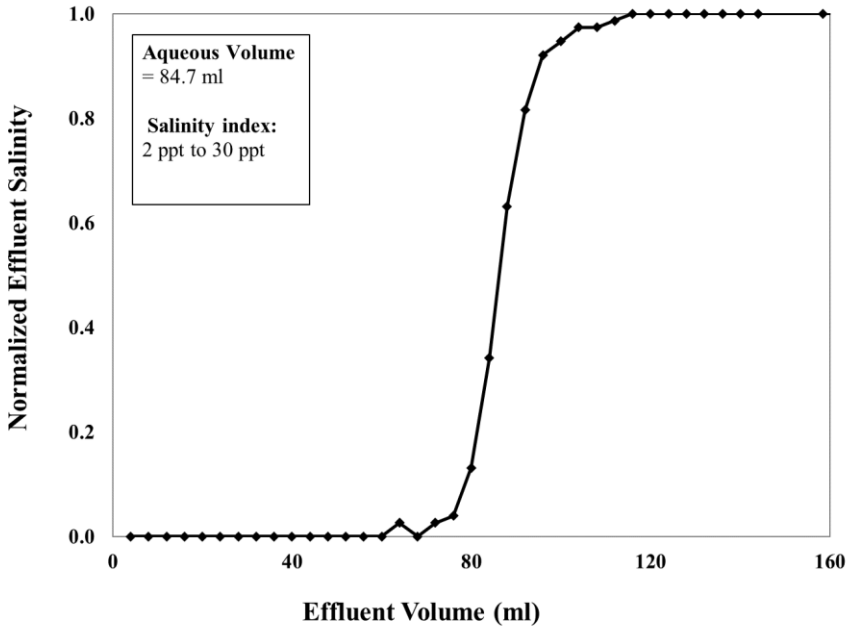

Figure 4.45: Normalized effluent salinity of 2nd salinity tracer test, from a salinity index of 2 ppt to 30 ppt.

4.3.5 Glycerin Flood

An aqueous solution of 82 wt% glycerin and 18 wt% brine (1000 ppm NaCl) with a viscosity of 57 cP (measured with rheometer) was injected at a flow rate of 0.211 ml/min (2 ft/D) until steady state pressure drop for all four sections and zero oil cut was observed. The maximum oil cut was 14.4%. The pressure drop data and the interstitial velocity are shown in Figure 4.46. It was assumed (based on figure 4.46) that the pressure drop reached steady state around 0.6 PV, but the flood continued until 1.9 PV. The residual oil saturation was reduced from 0.45 following the waterflood to 0.43 following the glycerin flood using equation 3.15. The effective permeability was 132 mD using Darcy's law and the end-point glycerin relative permeability was 0.09. The end-point mobility ratio was calculated as 0.2 using equation 3.16.

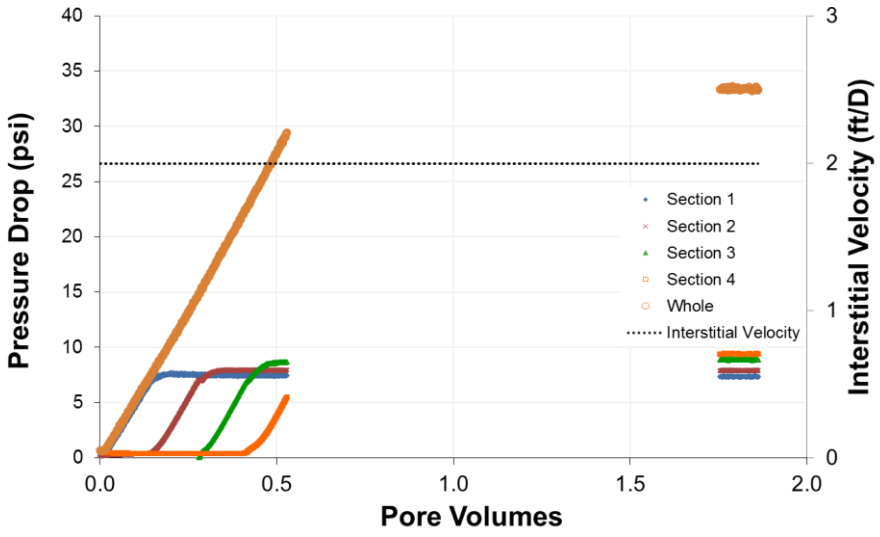

Figure 4.46: Pressure drop data, and the interstitial velocity during glycerin flooding at 23 °C for experiment #3.

4.3.6 Low-salinity Polymer Flood

A high molecular weight polymer (2000 ppm FP 3630S #245X) was prepared in a low-salinity brine (1000 ppm NaCl and 400 ppm $NaHCO_3$) to obtain a polymer solution with a high relaxation time. After hydrating 16 hours, the solution was filtered under 15 psi Argon pressure at 23 °C using a 1.2 μm Millipore mixed cellulose ester membrane filter paper. The filtration ratio was 1.0. The polymer solution was bubbled with argon while stirring for 2 hours in a round bottom flask and then vacuum- transferred to an injection column.

A sample of the polymer solution was taken from the column to measure its rheology and pH, salinity. The pH was 8.5 and the salinity index was 5 ppt. A relaxation time of 1.2 s was determined from the G', G" crossover point using the dynamic frequency sweep test (DFST) shown in Figure 4.47. The steady rate sweep test (SRST) data in the power-law viscosity region of shear thinning as shown in Figure 4.51 were fit to obtain a power-law equation of μ=366 $\dot{\gamma}^{(-0.57)}$.

This low-salinity polymer solution was injected at a constant flow rate of 0.106 ml/min (1 ft/D) until steady state pressure drop for all four sections and zero oil cut was observed. Pressure drop data and the interstitial velocity are shown in Figure 4.48.

The residual oil saturation following low-salinity polymer flood decreased to 0.31 using equation 3.17, an 11% reduction in oil saturation compared to the glycerin flood. Cumulative oil recovery at the end of the polymer flood was 61% of the OOIP. The effective permeability for the polymer flood was 169 mD at 1 ft/D calculated from Darcy's law using the differential pressure drop data at steady state. The end-point relative permeability was 0.114 at 1 ft/D determined from dividing the effective permeability by the brine permeability. The end-point mobility ratio was calculated to be 0.3 at 1 ft/D using equation 3.18. The maximum capillary number was calculated as 4.6×10^{-5} for the whole

core using the maximum pressure gradient of 24 psi/ft and equation 2.3. Maximum capillary number is below the critical capillary number (1×10^{-4} for Bentheimer sandstone). Equivalent shear rate was calculated as 26.9 s^{-1} using equation 2.6 and Deborah number (N_{De}) was calculated as 32.3 using equation 2.5.

The viscosities of the effluent samples were measured as soon as possible after the samples were produced. A comparison of the viscosities of injected polymer solution and the effluent samples retrieved at different pore volumes are shown in Figure 4.49.

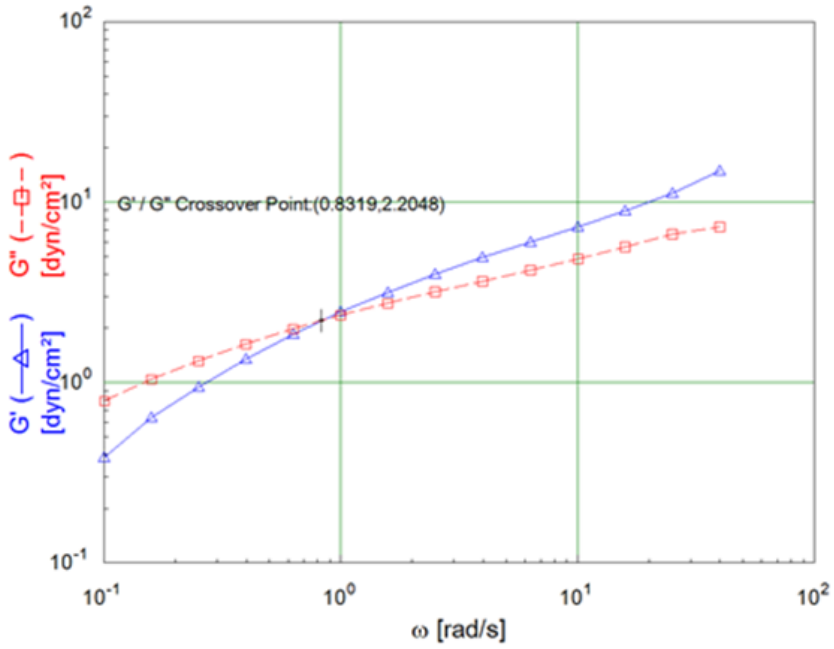

Figure 4.47: DFST result for 2000 ppm FP-3630S HPAM polymer in 1000 ppm NaCl + 400 ppm NaHCO3 aqueous solution at 23 °C for experiment #3.

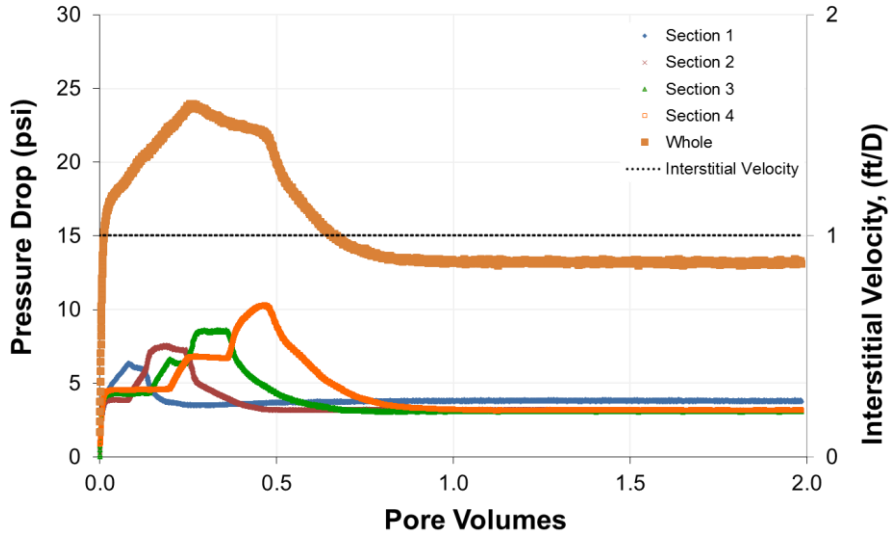

Figure 4.48: Pressure drop data, and the interstitial velocity during low-salinity polymer flood at 23 °C for experiment #3.

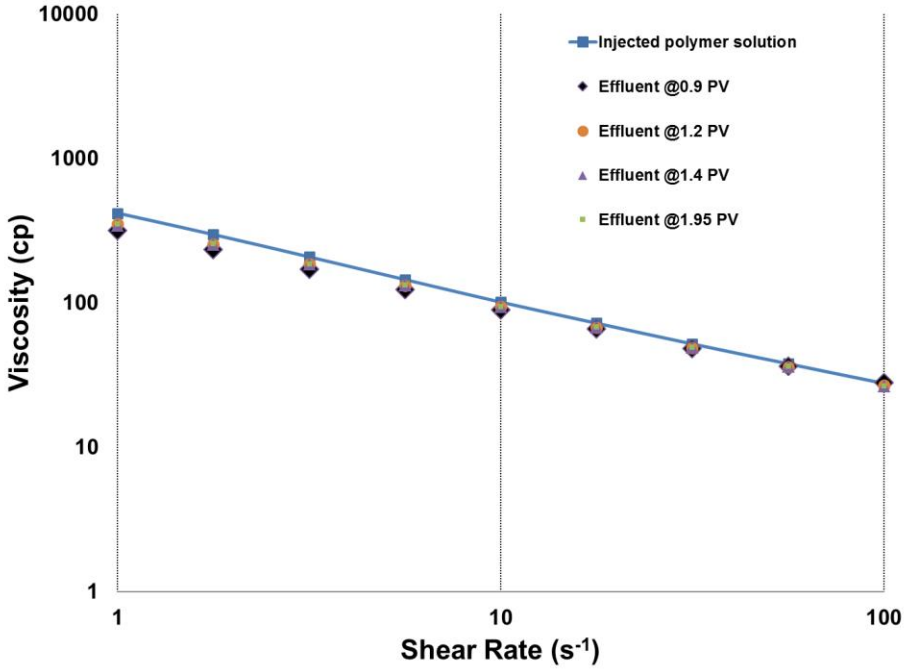

Figure 4.49: Viscosity comparison of the injected low-salinity polymer solution and the effluents at 23 °C for experiment #3.

4.3.7 High-Salinity Polymer Flood

A 3548 ppm FP 3630S polymer in 24000 ppm NaCl, 300 ppm $NaHCO_3$ brine was prepared for the tracer test. After hydrating 19.5 hours, the polymer solution was filtered through 90 mm diameter, 1.2 μm Millipore mixed cellulose ester membrane filter paper under 15 psi Argon pressure into 250 ml graduated cylinder at 23 °C. The filtration ratio was 1.1. The polymer solution was bubbled with argon while stirring for 2 hours in a round bottom flask and then vacuum-transferred to an injection column. A sample of the polymer solution was taken from the column to measure its rheology. The dynamic frequency sweep test (DFST) data are shown in Figure 4.50. The relaxation time was estimated as 0.24 s using the G' and G" crossover point. It is significantly less than the 1.2s for the polymer solution injected into the core in the previous step. Figure 4.51 compares the results of the SRST for this high-salinity polymer (3548 ppm FP-3630S HPAM polymer in 24000 ppm NaCl, 300 ppm $NaHCO_3$) and the low-salinity polymer (2000 ppm FP-3630S HPAM polymer in 1000 ppm NaCl + 400 ppm $NaHCO_3$) in the preceding flood. The viscosities are similar, but the high salinity polymer in slightly less viscous than the low salinity one. The data high salinity polymer was fit to a power-law model with the equation $\mu=250 \times \dot{\gamma}^{(-0.49)}$.

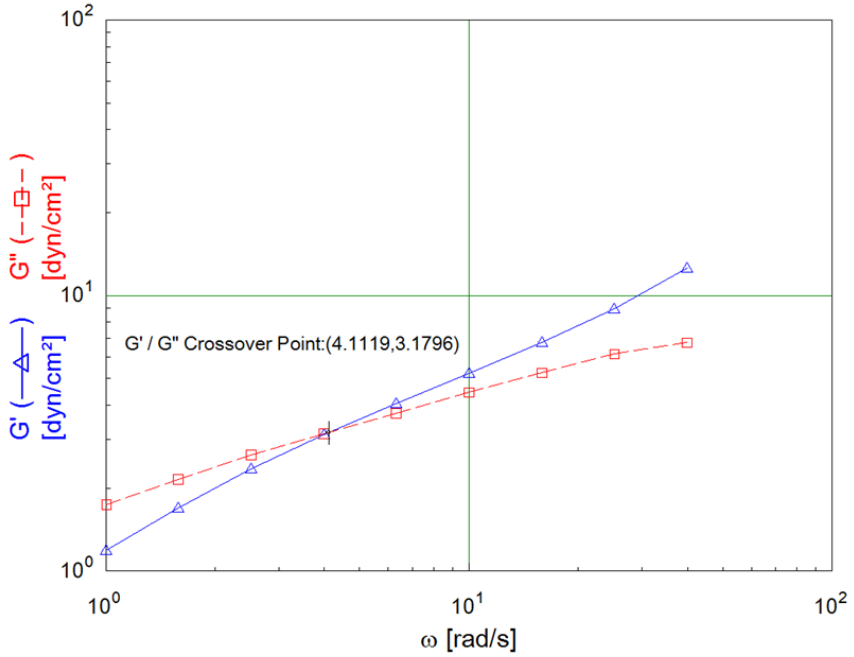

Figure 4.50: DFST result for 3548 ppm FP-3630S HPAM polymer in 24000 ppm NaCl, 300 ppm $NaHCO_3$ aqueous solution at 23 °C for experiment #3.

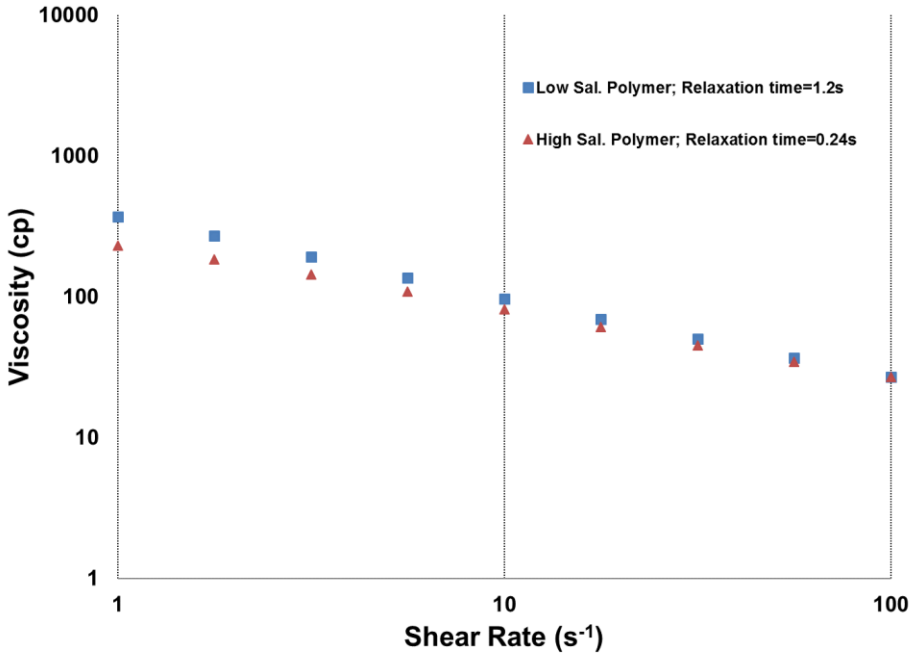

Figure 4.51: SRST result for high-salinity polymer compared to the low-salinity polymer solution at 23 °C for experiment #3.

This high-salinity polymer solution was injected at a constant flow rate of 0.106 ml/min (1 ft/D) to displace the low-salinity polymer solution. Pressure drop data and the interstitial velocity are shown in Figure 4.52. The effluent samples were collected in volumes of 4 ml. During the salinity tracer test, salinities were measured and plotted. An aqueous volume of 104.9 ml was determined from the area above the normalized salinity curve shown in Figure 4.53. The normalized salinity, oil cut and oil saturation data are shown in Figure 4.54, and it shows that the oil recovery is observed after the salinity is reaching the injection salinity value.

Oil production was observed starting at 1.17 PV. A total of 18.5 ml of additional oil was recovered. The maximum oil cut was 4.5% as shown in figure 4.54. The flood continued 6.8 PV total. The residual oil saturation after this polymer flood was 0.24, a 7% reduction in oil saturation (0.31) from the preceding polymer flood. The cumulative oil recovery at the end of the flood was 71% of the OOIP.

The final oil saturation based on the tracer data was compared to the oil saturation following the low-salinity polymer flood, as the oil recovery was after the salinity tracer test was finished. The final oil saturation based on the tracer data was 0.306 (1-105.1/151.4) and 0.31 based on the material balance.

At the end of the low-salinity polymer flood, the effective permeability was calculated as 265 mD using the data and Darcy's law, the end-point relative permeability was calculated as 0.18 using the ratio of the effective permeability to the brine permeability, the end-point mobility ratio was calculated as 0.5 using the end-point relative permeability and equation 3.18, and the maximum capillary number was calculated as 2.4×10^{-5} for the whole core using the maximum pressure gradient of 12.4 psi/ft in equation 2.3. Equivalent shear rate was calculated as 25.1 s^{-1} using equation 2.6 and Deborah number (N_{De}) was calculated as 6.1 using equation 2.5.

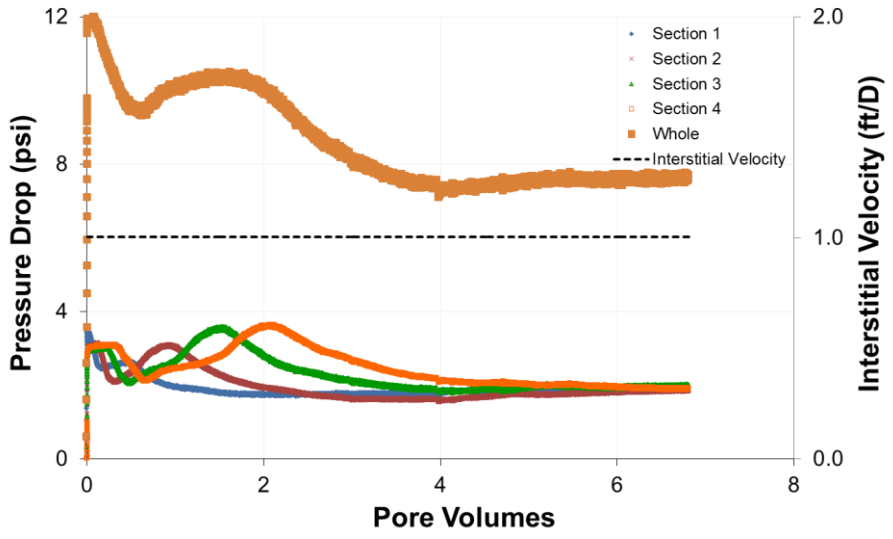

Figure 4.52: Pressure drop data and the interstitial velocity during high-salinity polymer flood at 23 °C for experiment #3.

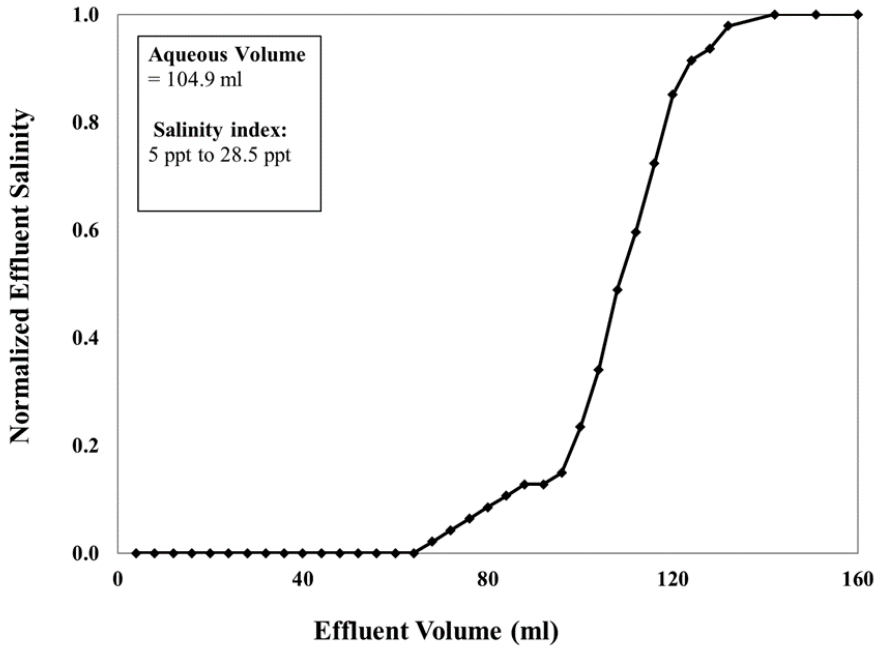

Figure 4.53: Normalized effluent salinity during high-salinity polymer flood for experiment #3, from a salinity index of 5 ppt to 28.5 ppt.

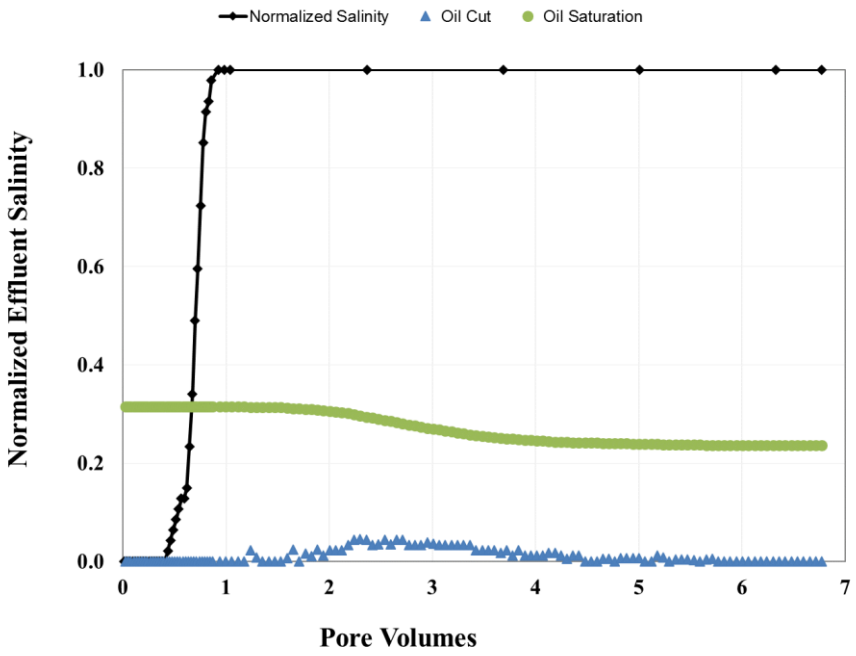

Figure 4.54: Normalized effluent salinity, oil cut, and oil saturation during high-salinity polymer flood for experiment #3.

4.3.8 Oil Saturation, Cumulative Oil Recovered, and Oil Cut

Oil saturation versus pore volumes injected for all floods performed in experiment #3 are shown in Figure 4.55. Oil cut versus pore volumes for both low-salinity and high-salinity polymer floods are shown in Figure 4.56. Pressure drop data for both low-salinity and high-salinity polymer floods are shown in Figure 4.57.

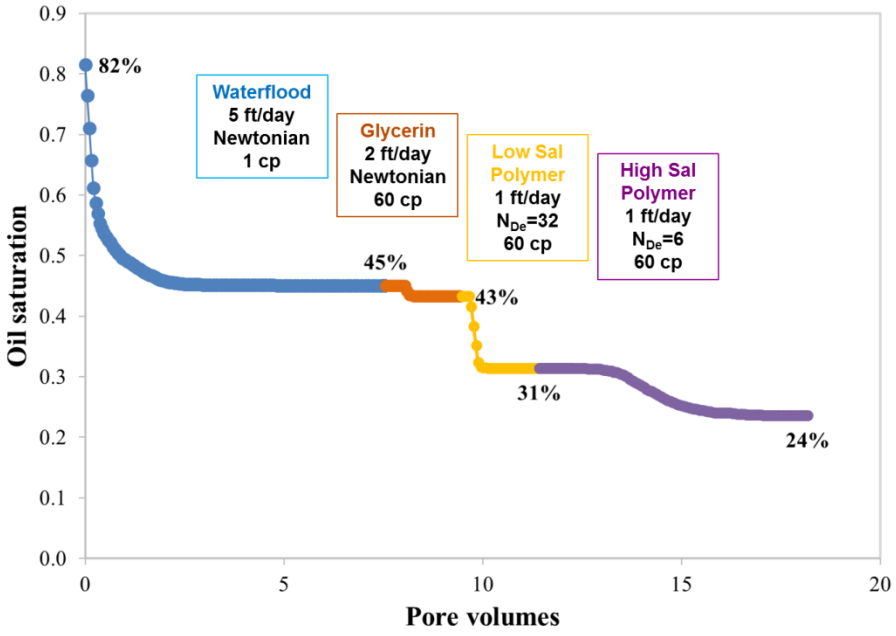

Figure 4.55: Oil saturation versus pore volumes for experiment #3.

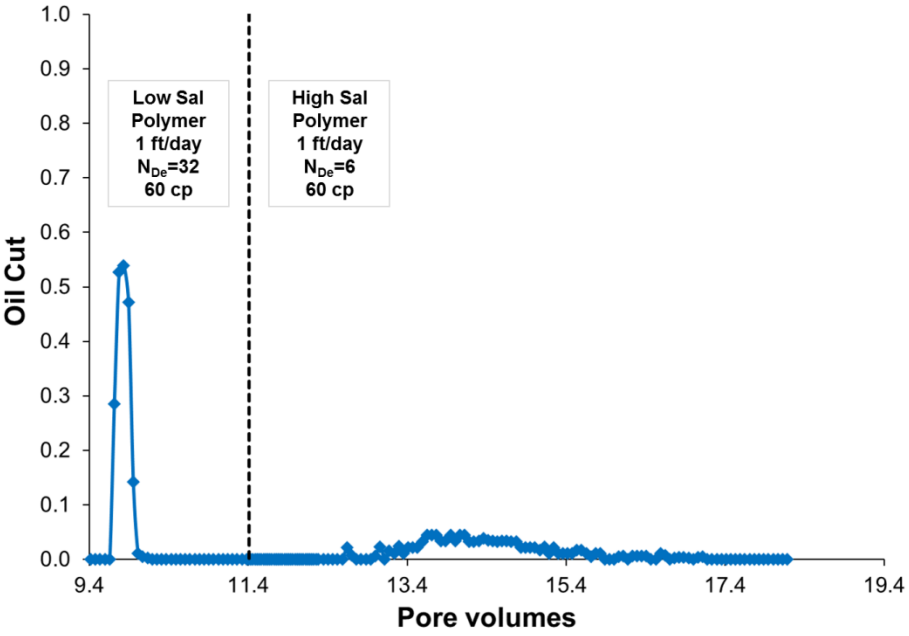

Figure 4.56: Oil cut versus pore volumes for both low-salinity and high-salinity polymer floods for experiment #3.

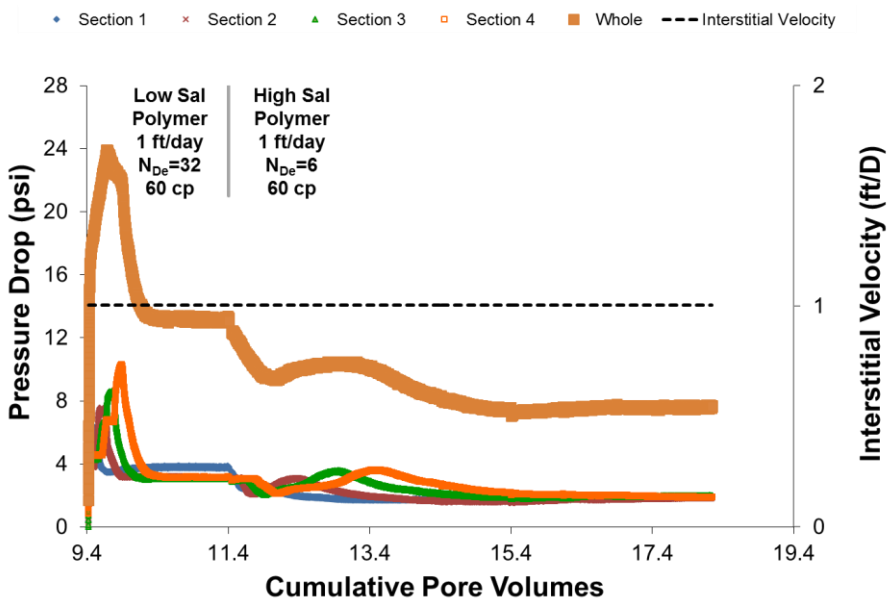

Figure 4.57: Pressure drop for both low-salinity and high-salinity polymer floods for experiment #3.

4.4 EXPERIMENT #4

The purpose of coreflood experiment #4 was to determine the effect of using a high-salinity polymer flood after a low-salinity, high elasticity polymer flood on residual oil saturation. In experiment #4, low-salinity and high-salinity polymers were alternated after 0.5 PV injection of each polymer to determine the effect of alternating salinity and to understand the mechanism. Table 4.7 summarizes the core and fluid properties of experiment #4.

Table 4.7: Core and fluid properties of experiment #4.

Experiment	**#4_Z4Z**
Coreflood name	MZE-4th
Rock type	Bentheimer Sandstone
Brine permeability (mD)	1604
Crude oil viscosity (cP)	129
Temperature (°C)	23
Porosity	0.24
Pore volume (ml)	148.0
Bulk volume (ml)	620
Dry core mass (g)	1249
Bulk density (g/cm^3)	2.0
Waterflood solution	1000 ppm NaCl + 1000 ppm $Na_2S_2O_4$ aqueous solution
Glycerin solution	82 wt% glycerol in 1000 ppm NaCl aqueous solution
Low-salinity polymer solution	2000 ppm FP-3630S HPAM polymer (#JBA 2114/4-6) in 1000 ppm NaCl + 400 ppm $NaHCO_3$ aqueous solution; pH: 8.2, Salinity: 2 o%; FR: 1.1
High-salinity polymer solution	3547 ppm FP-3630S HPAM polymer (#JBA 2114/4-6) in 24030 ppm NaCl + 280 ppm $NaHCO_3$ aqueous solution; pH: 8.47, Salinity: 27 o%; FR: 1.02

4.4.1 Core Preparation, Saturating the Core, Salinity Tracer Test

A 1 ft long 2.157 in diameter, Bentheimer sandstone core was potted in epoxy to prepare for core flooding. The core passed the pressure test after conducting a water leak test at 95 psi air pressure for 10 min. The core was vacuum saturated at 23 °C with 6% KCl aqueous solution. The volume of brine imbibed into the core was measured and used to calculate a pore volume of 148 ml (2 ml was subtracted from the reading to account for

fluid in the tubes). A pore volume of 147.5 ml was calculated based on the mass of the core before and after saturation. The same 6% KCl brine was vacuum transferred to an injection column, and then injected into the core at increasing flow rates; from 1 ml/min (9.7 ft/D) to 12 ml/min (116.1 ft/D) to determine the permeability which was calculated as 1592 using Darcy's Law given in equation 3.7. The injection continued for 1.7 PV.

A salinity tracer test was performed to measure the pore volume and heterogeneity of the core. 2% KCl brine was injected at 2 ml/min (19.3 ft/D) to displace the 6 % KCl brine. The effluent samples were collected in volumes of 4 ml. During the salinity tracer test, salinities were measured and plotted to determine the aqueous volume (pore volume) of 148 ml from the area above the normalized salinity versus effluent volume curve shown in Figure 4.58. After the salinity tracer test, the same 2% KCl brine was injected at flow rates, increasing from 2 ml/min (19.3 ft/D) to 12 ml/min (116.1 ft/D) to determine the permeability, which was found to be 1616 mD using the data and Darcy's law. The average brine permeability of both the 6% KCl and 2% KCl flood was calculated as 1604 mD.

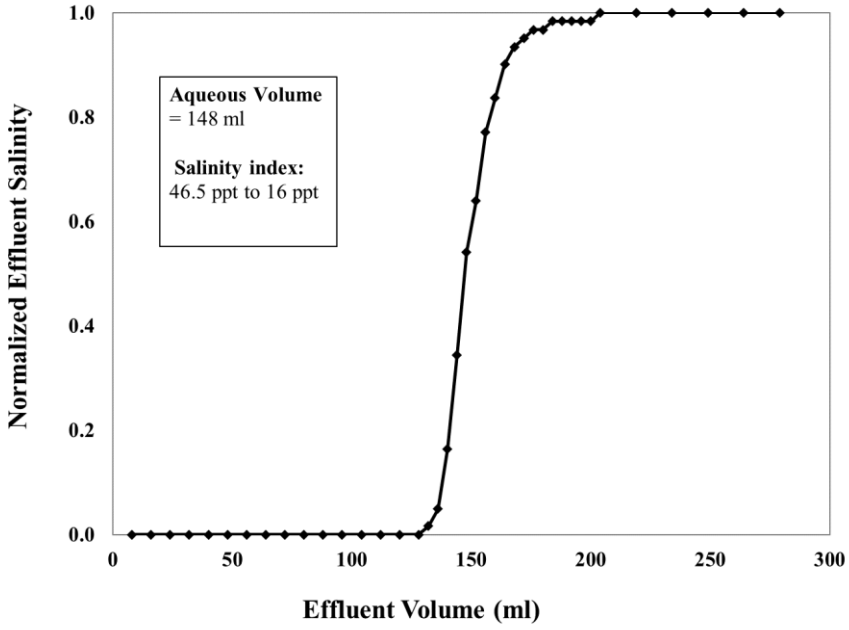

Figure 4.58: Normalized effluent salinity during 2% KCl brine injection for experiment #4, from a salinity index of 46.5 ppt to 16 ppt.

4.4.2 Core Reduction and Conditioning

The core was flooded at 23 °C with an aqueous solution of 40000 ppm $NaHCO_3$, 10000 ppm Na_4EDTA, and 10000 ppm $Na_2S_2O_4$ at 0.5 ml/min (4.8 ft/D) to reduce the core and to remove amorphous oxidized iron. The iron concentration was about 3 ppm at 5.4 PV. Flooding was continued until the iron concentration in the effluent decreased to 0.3 ppm, the ORP was -740 RmV and the pH was 8. Injection was continued until 13.2 PV injected. ORP (R.mV) and iron concentration of the effluents are shown in Figure 4.59, and pH and iron concentration of the effluents are shown in Figure 4.60.

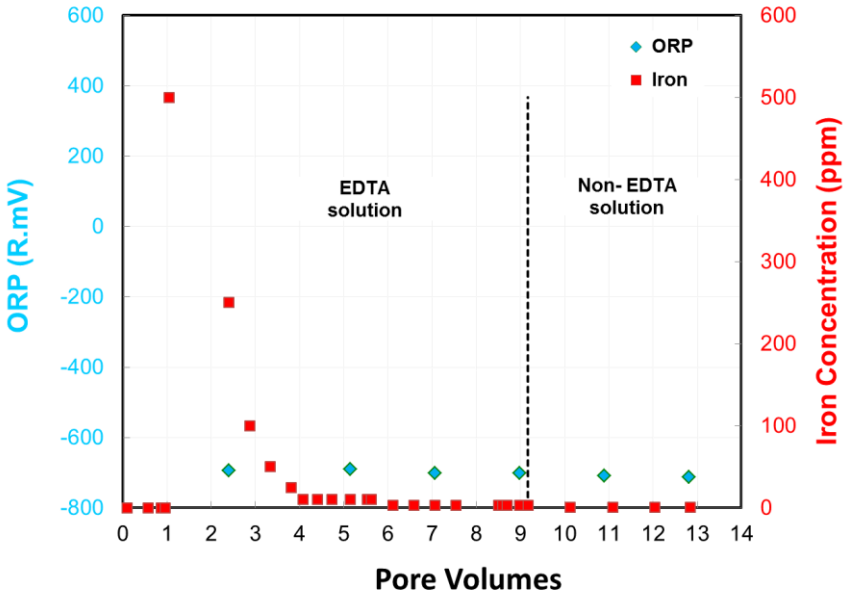

Figure 4.59: ORP (R.mV) and iron concentration (ppm) of the effluents.

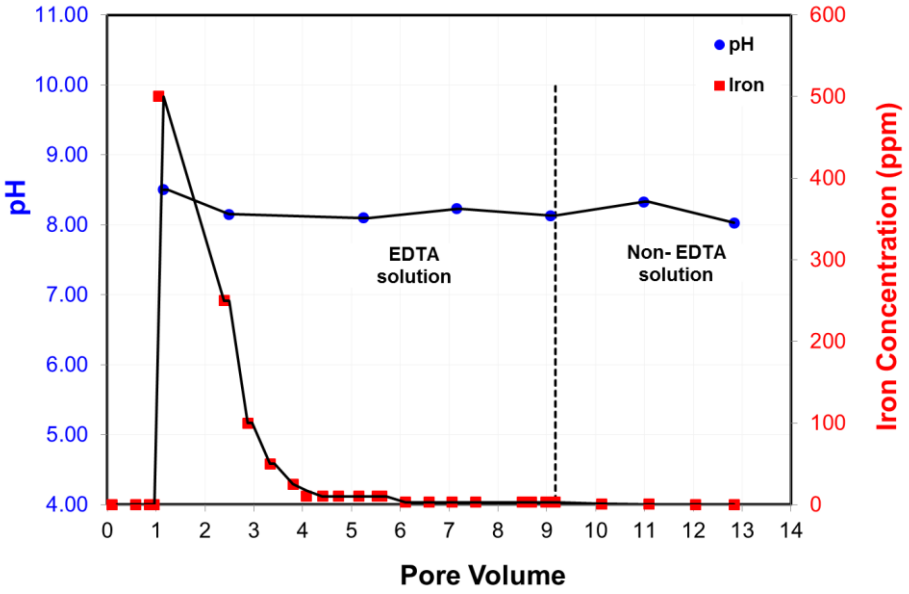

Figure 4.60: pH and iron concentration (ppm) of the effluents.

4.4.3 Oil Flood

Crude oil with a viscosity of 129 cp at 23 °C was filtered through 1.2 μm filter paper under 20 psi of air pressure. 300 ml of the crude oil was filtered. During filtration, the filter paper was replaced with new ones when a decline in the filtration rate was observed. Crude oil was injected at a constant pressure of 85 psi and 23 °C. Oil flooding was continued until steady state pressure drop was observed and the oil cut exceeded 99%. A total of 1.44 PV of oil was injected. The flow rate at steady state was 2 ml/min (18.8 ft/D).

The initial oil saturation (S_{oi}) of 0.89 was determined by using the displaced water volume of 132 ml in equation 3.10. The residual water saturation (S_{wr}) was 0.11 using equation 3.11. The effective oil permeability at S_{wr} was determined 954 md from Darcy's law using pressure drop and volumetric flow rate, and the end-point oil relative permeability (k^o_{ro}) was calculated as 0.6 for the whole core using equation 3.12. Steady-state pressure drop data, effective oil permeability, and end-point oil permeability data are presented in Table 4.8. Pressure drop data are shown in Figure 4.61. The core was aged for 2 days at 23 °C after the oil flood.

Table 4.8: Steady-state pressure drop data, effective oil permeability, and end-point oil permeability from oil flooding for experiment #4.

Oil flood	**Whole**	**Section 1**	**Section 2**	**Section 3**	**Section 4**
Pressure drop (psi)	81	21	19	20	21
Effective oil permeability (mD)	1245	1216	1308	1251	1201
k^o_{ro}	0.84	1.03	0.81	0.76	0.82

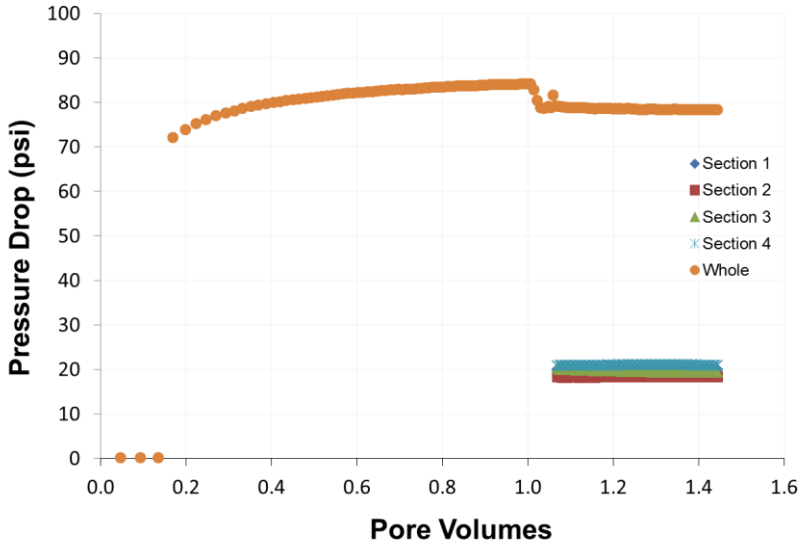

Figure 4.61: Pressure drop and the interstitial velocity data during 129 cP crude oil flood conducted at 85 psi constant pressure and 23 °C for experiment #4.

4.4.4 Waterflood

An aqueous solution of 1000 ppm NaCl and 1000 ppm $Na_2S_2O_4$ was injected at a constant flow rate of 0.5 ml/min (4.8 ft/D) until steady state pressure for all four sections and zero oil cut was observed. The pressure drop and the interstitial velocity data are shown in Figure 4.62. The capillary number was calculated as 5.2×10^{-5} using the maximum pressure gradient (22.3 psi/ft) and equation 2.3. The pressure drop reached steady state after 3 PV. Waterflooding continued for an additional 6.2 PV. The remaining oil saturation after the waterflood was 0.463 using equation 3.13. The effective water permeability was calculated as 122 md using the data and Darcy's law, and the end-point water relative permeability was 0.08. The end-point mobility ratio was calculated as 17.6 using equation 3.14.

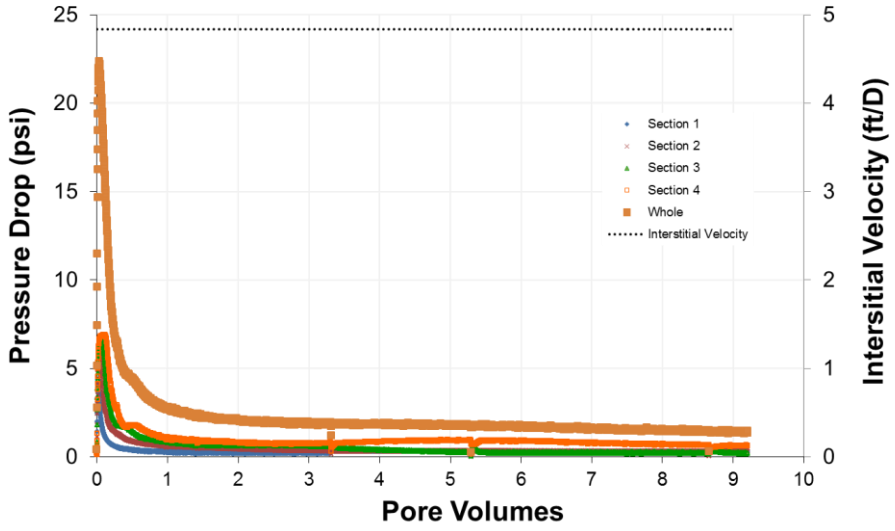

Figure 4.62: Pressure drop and the interstitial velocity data during waterflooding at 23°C for experiment #4.

A 2nd salinity tracer test was performed as an independent measurement of residual oil saturation to compare with the remaining oil saturation value obtained from material balance using produced oil and water volumes. An aqueous solution of 30000 ppm NaCl and 1000 ppm $Na_2S_2O_4$ was injected at 2 ml/min (19.4 ft/day) to displace the aqueous solution of 1000 ppm NaCl and 1000 ppm $Na_2S_2O_4$ brine. The effluent samples were collected in volumes of 4 ml. During the salinity tracer test, salinities were measured and plotted to determine the aqueous volume of 79.7 ml from the area above the normalized effluent salinity vs. effluent volume curve shown in Figure 4.63. After performing the tracer test, an aqueous solution of 1000 ppm NaCl and 1000 ppm $Na_2S_2O_4$ was injected at 2 ml/min (18.4 ft/day) to displace the solution of 30000 ppm NaCl and 1000 ppm $Na_2S_2O_4$ brine for 1 PV. By using the aqueous volume determined from salinity tracer test, the oil

saturation after waterflood was obtained as 0.461 (1-79.7/148) while the material balance had given 0.463. The relative error is 0.4%.

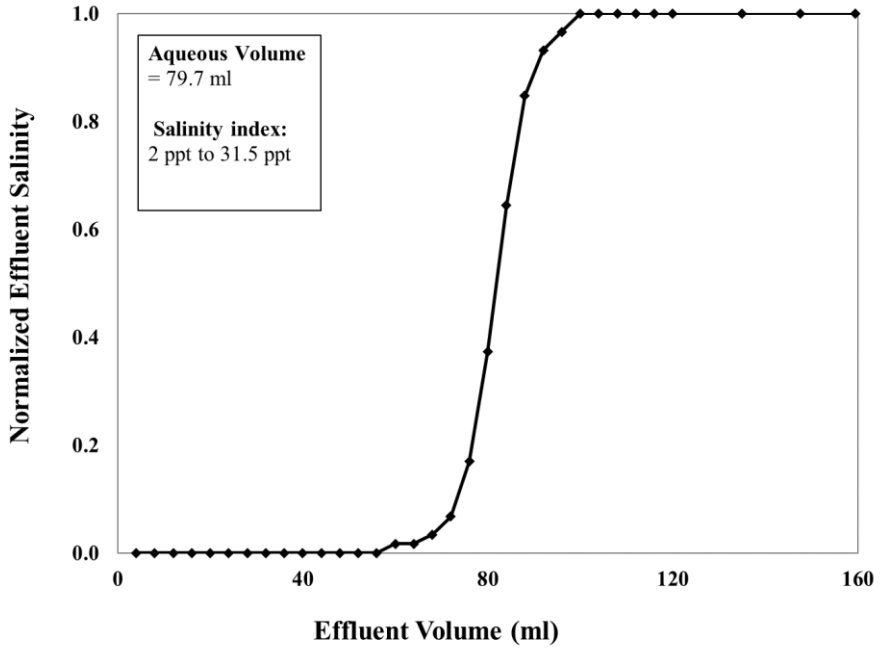

Figure 4.63: Normalized effluent salinity during 2nd salinity tracer test for experiment #4, from a salinity index of 2 ppt to 31.5 ppt.

4.4.5 Glycerin Flood

An aqueous solution of 82 wt% glycerin and 18 wt% brine (1000 ppm NaCl) with a viscosity of 60 cP (measured with rheometer) was injected at a flow rate of 0.207 ml/min (2 ft/D) until steady state pressure drop for all four sections and zero oil cut was observed. The maximum oil cut was 28.4%. The pressure drop data and the interstitial velocity are shown in Figure 4.64. Pressure drop reached steady state after 0.62 PV injection, but the flood continued until 1.6 PV. The residual oil saturation was reduced from 0.463 following the waterflood to 0.436 following the glycerin flood using equation 3.15. The effective permeability was 153 mD using Darcy's law and the end-point glycerin relative

permeability was 0.1. The end-point mobility ratio was calculated as 0.34 using equation 3.16.

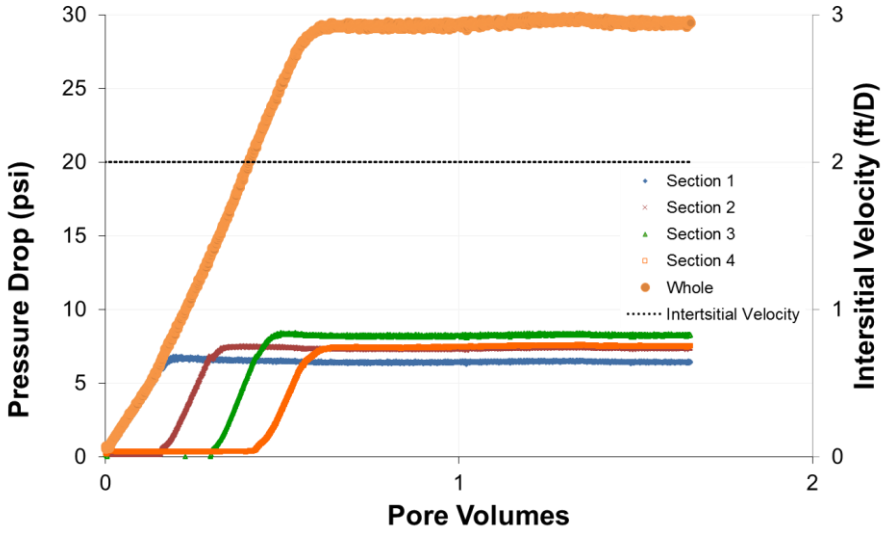

Figure 4.64: Pressure drop data, and the interstitial velocity during glycerin flooding at 23 °C for experiment #4.

4.4.6 Low-salinity Polymer Properties

A high molecular weight polymer (2000 ppm FP 3630S #JBA 2114/4-6) was prepared in a low-salinity brine (1000 ppm NaCl and 400 ppm $NaHCO_3$) to obtain a polymer solution with a high relaxation time. After hydrating 16 hours, the solution was filtered under 15 psi Argon pressure at 23 °C using a 1.2 µm Millipore mixed cellulose ester membrane filter paper. The filtration ratio was 1.1. The polymer solution was bubbled with argon while stirring for 2 hours in a round bottom flask and then vacuum- transferred to an injection column.

A sample of the polymer solution was taken from the column to measure its rheology, pH, and salinity. The pH was 8.2 and the salinity index was 2 ppt. A relaxation time of 9.3 s was determined from the G', G" crossover point using the dynamic frequency sweep test (DFST) shown in Figure 4.65. The steady rate sweep test (SRST) data of low-salinity polymer in the power-law viscosity region of shear thinning as shown in Figure 4.67 were fit to obtain a power-law equation of $\mu=507 \times \dot{\gamma}^{(-0.63)}$.

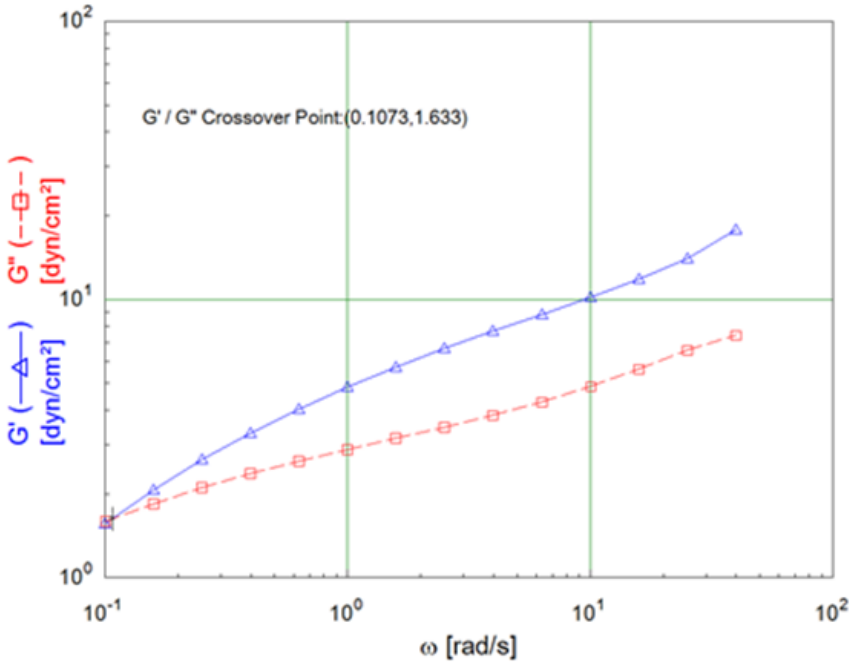

Figure 4.65: DFST result for 2000 ppm FP-3630S HPAM polymer in 1000 ppm NaCl + 400 ppm $NaHCO_3$ aqueous solution at 23 °C for experiment #4.

4.4.7 High-Salinity Polymer Properties

A 3547 ppm FP 3630S polymer (#JBA 2114/4-6) in 24000 ppm NaCl, 300 ppm $NaHCO_3$ brine was prepared for the tracer test. Note that this is a new lot of FP 3630S. After hydrating 16 hours, the polymer solution was filtered through 90 mm diameter, 1.2

μm Millipore mixed cellulose ester membrane filter paper under 15 psi Argon pressure into 250 ml graduated cylinder at 23 °C. The filtration ratio was 1.02. The polymer solution was bubbled with argon while stirring for 2 hours in a round bottom flask and then vacuum-transferred to an injection column.

A sample of the polymer solution was taken from the column to measure its rheology, pH, and salinity. The pH was 8.5 and the salinity index was 27 ppt. The dynamic frequency sweep test (DFST) data are shown in Figure 4.66. The relaxation time was estimated as 1.03 s using the G' and G" crossover point. It is much less than the 9.3 s for the polymer solution injected into the core in the previous step. Figure 4.67 compares the results of the SRST for this high-salinity polymer (3547 ppm FP-3630S HPAM polymer in 24000 ppm NaCl, 300 ppm $NaHCO_3$) and the low-salinity polymer (2000 ppm FP-3630S HPAM polymer in 1000 ppm NaCl + 400 ppm $NaHCO_3$) in the preceding flood. The viscosities are similar, but the high salinity polymer in slightly less viscous than the low salinity one. The steady rate sweep test (SRST) data of high-salinity polymer in the power-law viscosity region of shear thinning as shown in Figure 4.67 were fit to obtain a power-law equation of $\mu=342 \times \dot{\gamma}^{(-0.54)}$.

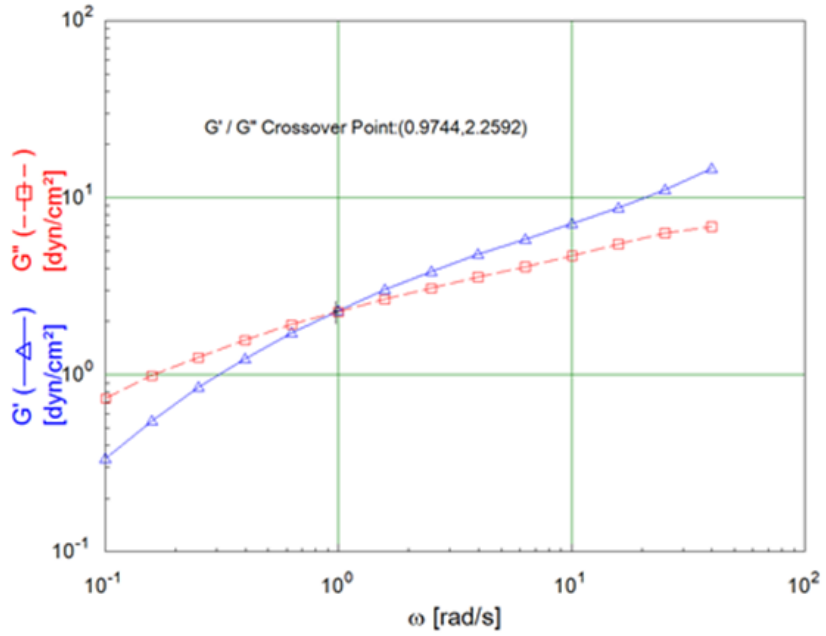

Figure 4.66: (DFST) result of the high-salinity polymer (# JBA 2114/4-6) in 24000 ppm NaCl, 300 ppm $NaHCO_3$ aqueous solution at 23 °C for experiment #4.

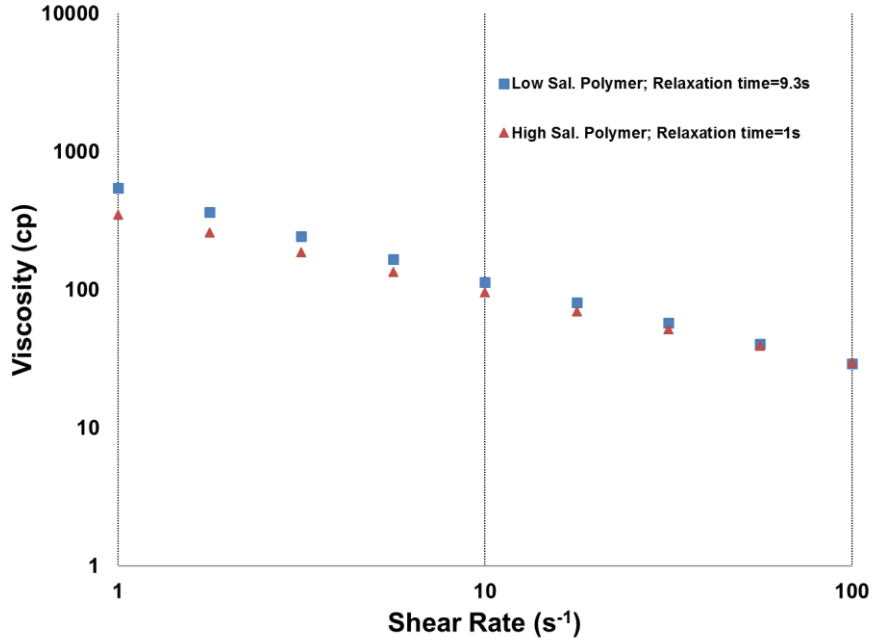

Figure 4.67: SRST result for high-salinity polymer compared to the low-salinity polymer solution at 23 °C for experiment #4.

4.4.8 Alternating Polymer Floods

The properties of both the low-salinity and high-salinity polymer solutions were presented in the previous section. Low-salinity polymer was 2000 ppm FP-3630S HPAM polymer (#JBA 2114/4-6) in 1000 ppm NaCl + 400 ppm $NaHCO_3$ aqueous solution, and high-salinity polymer was 3548 ppm FP-3630S HPAM polymer (#JBA 2114/4-6) in 24030 ppm NaCl + 280 ppm $NaHCO_3$ aqueous solution. After preparation of both polymer solutions and transferring to the injection columns, those columns were connected with 3-way valves so that there wouldn't be any stoppage when alternating between those two polymer injections.

Polymers were injected at a constant flow rate of 0.103 ml/min (1.0 ft/day) 0.5 PV, with the low-salinity polymer solution first (following the glycerin flood). The polymers' injections were alternated for between the two salinities for a total of 8 PV each.

After 8.0 PV, the alternating polymer injections continued for an additional 3.6 PV but for a longer time (1 PV). The final flood was only 0.6 PV.

Results are shown in figure 4.72. Oil recovery started after 0.24 PV injection of the low-salinity polymer and oil cut increased as high as 44% during the first 0.5 PV injection. Oil recovery was ceased once high-salinity polymer injection was started at 0.5 PV. Oil recovery was observed again between 2.15 PV and 3 PV of low-salinity and then high-salinity polymer injections (max oil cut was 2.2% and reduction in residual oil saturation was 0.6%). Then, oil recovery ceased between 3 PV and 3.6 PV. Figures 4.71 through 4.73 show that oil cut was inconsistent until the end of the core flood.

Table 4.9 summarizes the oil saturation reduction, and maximum oil cut for alternating polymer injection intervals in terms of PV and cumulative PV.

Table 4.9: Oil saturation reduction for alternating polymer injection intervals.

Polymer	Starting PV	Cum PV	Oil Saturation at the end	ΔS_{or}	Max Oil Cut
			0.436		
Low-Sal	0.00	10.98	0.342	10.0%	44.3%
High-Sal	0.48	11.46	0.336	0.5%	9.6%
Low-Sal	1.00	11.98	0.336	0.0%	0.0%
High-Sal	1.54	12.52	0.336	0.0%	0.0%
Low-Sal	2.09	13.06	0.334	0.3%	2.2%
High-Sal	2.63	13.61	0.331	0.3%	2.2%
Low-Sal	3.17	14.15	0.330	0.1%	1.1%
High-Sal	3.71	14.69	0.316	1.4%	6.6%
Low-Sal	4.26	15.24	0.312	0.5%	3.3%
High-Sal	4.81	15.79	0.301	1.0%	4.4%
Low-Sal	5.35	16.33	0.300	0.2%	0.4%
High-Sal	6.12	17.10	0.299	0.1%	0.4%
Low-Sal	6.49	17.47	0.295	0.4%	0.8%
High-Sal	6.98	17.96	0.285	0.9%	1.8%
Low-Sal	7.49	18.47	0.277	0.8%	0.7%
High-Sal	8.65	19.63	0.275	0.2%	0.6%
Low-Sal	9.95	20.93	0.258	1.7%	7.6%
High-Sal	10.90	21.88	0.246	1.3%	6.3%

For low-salinity polymer flood, based on the maximum pressure gradient reached at 1 ft/D, 24 psi, maximum capillary number was calculated as 5×10^{-5} for the whole core. For high-salinity polymer flood, based on the maximum pressure gradient reached at 1 ft/D, 15 psi, maximum capillary number was calculated as 3×10^{-5} for the whole core. Pressure drop data for both the low-salinity and high-salinity polymer floods are shown in Figure 4.68. Capillary number data for both low-salinity and high-salinity polymer floods are shown in Figure 4.69.

For low-salinity polymer flood; equivalent shear rate was calculated as 27.3 s^{-1} using equation 2.6 and Deborah number (N_{De}) was calculated as 254.4 using equation 2.5. For high-salinity polymer flood; equivalent shear rate was calculated as 26.8 s^{-1} using equation 2.6 and Deborah number (N_{De}) was calculated as 27.6 using equation 2.5. Note that this polymer was a new lot of FP 3630S (#JBA 2114/4-6), and it showed higher relaxation times, therefore higher Deborah numbers were obtained.

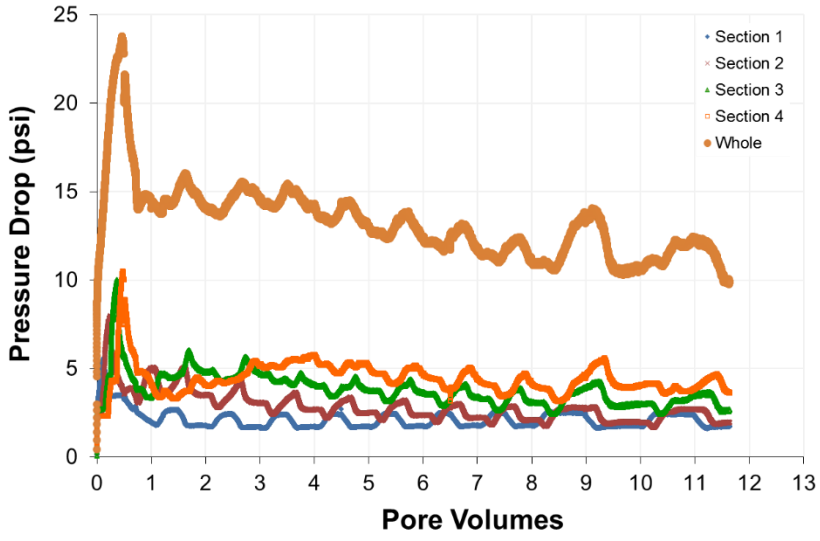

Figure 4.68: Pressure drop for both low-salinity and high-salinity polymer floods for experiment #4.

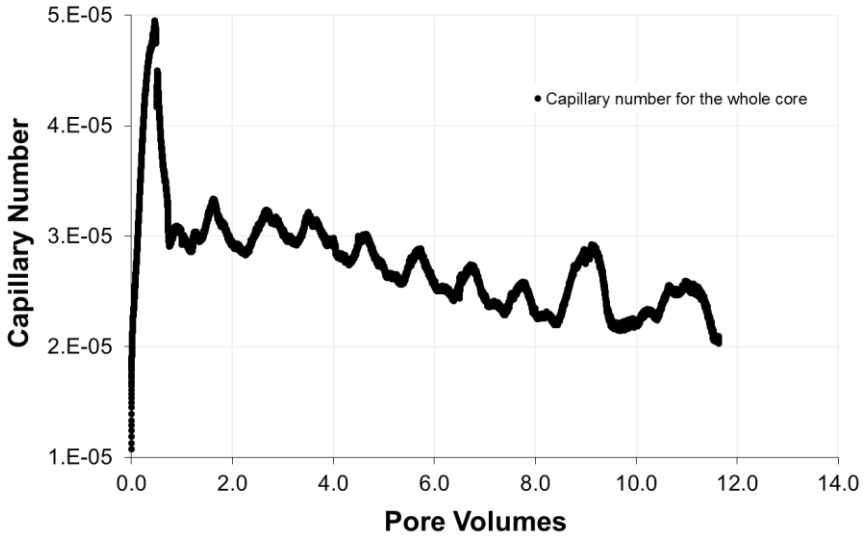

Figure 4.69: Capillary number for both low-salinity and high-salinity polymer floods for experiment #4.

The effluents of the high-salinity polymer injection hat occurred in the interval 9.1 and 10.3 PV were used as a salinity tracer test to compare the oil saturation obtained from material balance. The effluent samples were collected in volumes of 9 ml. During the test, salinities were measured and plotted. 107.2 ml was obtained from the area above the normalized salinity versus effluent volume curve. Normalized salinity versus effluent volume of the polymer tracer test is shown in Figure 4.70. The oil saturation calculated from the results of the tracer test was 27.6% (=1-107.2/148) while the oil saturation after tracer test was 27.5% according to the material balance. Relative error is 0.4%.

Normalized salinity, oil cut, and oil saturation versus pore volumes for all the alternating polymer floods is shown in Figure 4.71.

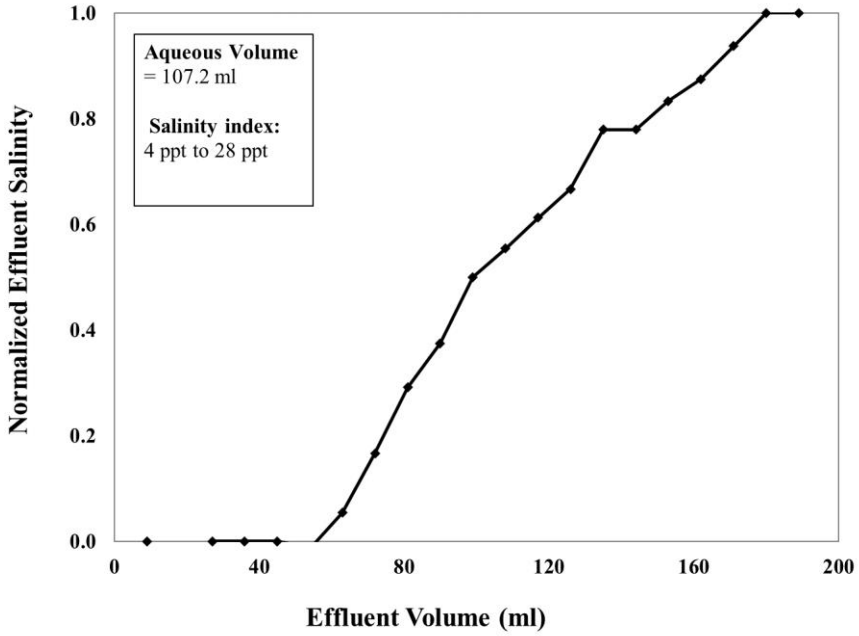

Figure 4.70: Normalized effluent salinity during high-salinity polymer injection between 9.1 and 10.3 PV for experiment #4, from a salinity index of 4 ppt to 28 ppt.

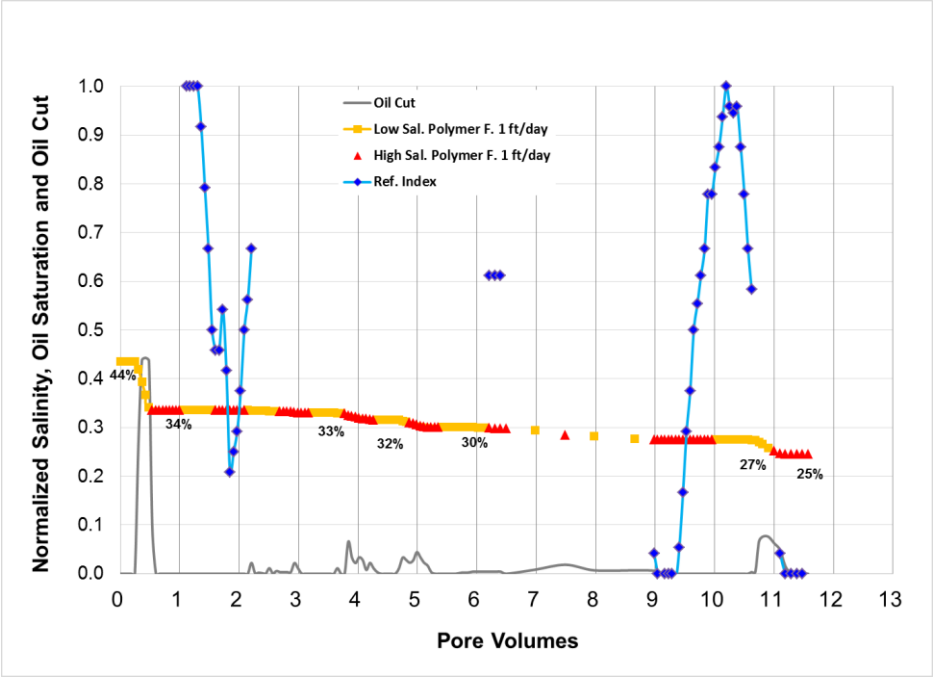

Figure 4.71: Normalized effluent salinity, oil cut, and oil saturation during alternating polymer floods for experiment #4.

4.4.9 Oil Saturation, Oil Cut, and Cumulative Oil Recovered

Oil saturation versus pore volumes for all floods performed in experiment #4 are shown in Figure 4.72. Oil saturation, cumulative oil recovered, and oil cut data are shown in Figure 4.73.

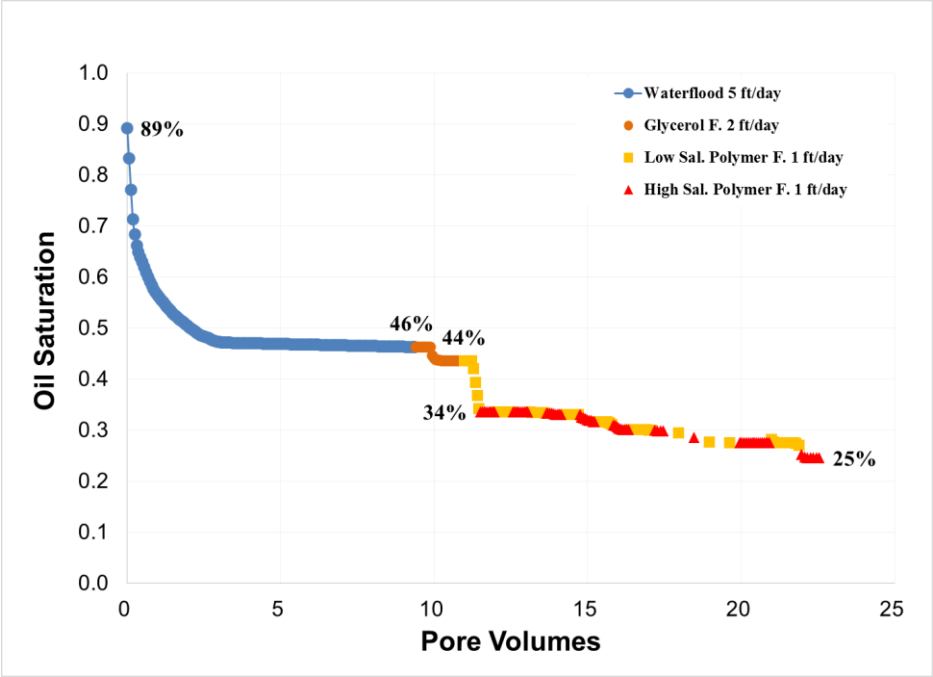

Figure 4.72: Oil saturation versus pore volumes for experiment #4.

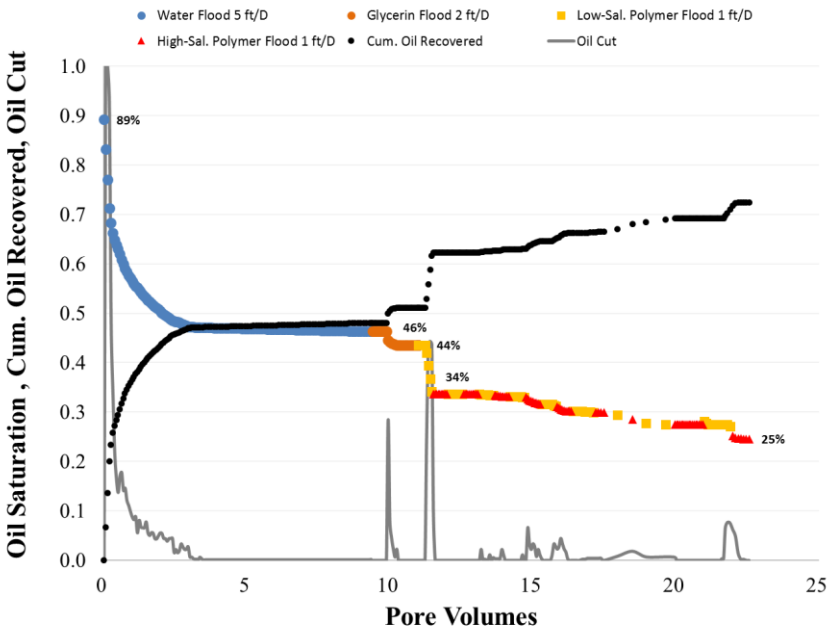

Figure 4.73: Oil saturation, cumulative oil recovered, and oil cut for experiment #4.

4.5 EXPERIMENT #5

The purpose of the coreflood experiment #5 was to determine the effect of using a high-salinity polymer flood after a low-salinity, high elasticity polymer flood on residual oil saturation. Experiment #5 was conducted like experiment #4, except the injection of the low-salinity and high-salinity polymers were alternated at larger PV (e.g. 1 PV of low-salinity polymer and 2 PV of high-salinity polymer). Table 4.10 summarizes the core and fluid properties of experiment #5.

4.5.1 Core Preparation and Saturating the Core

A 1 ft long 2.02 in diameter, Bentheimer sandstone core was potted in epoxy to prepare for core flooding. The core passed the pressure test after conducting a water leak test at 95 psi air pressure for 10 min. The core was vacuum saturated at 25 °C with 8% NaCl aqueous solution. However, air was mistakenly vacuumed into the core while

saturating the core. A pore volume of 134.2 ml was calculated based on the mass of the core before and after saturation.

Table 4.10: Core and fluid properties of experiment #5.

Experiment	**#5_Z4Z**
Coreflood name	MZE-5th
Rock type	Bentheimer Sandstone
Brine permeability (mD)	1453
Crude oil viscosity (cP)	137
Temperature (℃)	23
Porosity	0.24
Pore volume (ml)	148.7
Bulk volume (ml)	615
Dry core mass (g)	1228
Bulk density (g/cm^3)	2.0
Waterflood solution	1000 ppm NaCl + 400ppm $NaHCO_3$ + 1000 ppm $Na_2S_2O_4$ aqueous solution
Glycerin solution	82% glycerol in 1000 ppm NaCl + 400 ppm $NaHCO_3$ aq. solution
Low-salinity polymer solution	2000 ppm FP-3630S HPAM polymer (#JBA 2114/4-6) in 1000 ppm NaCl + 400 ppm $NaHCO_3$ aqueous solution; pH: 7.8, Salinity: 2.7 o%; FR: 1.1
High-salinity polymer solution	3547 ppm FP-3630S HPAM polymer (#JBA 2114/4-6) in 24030 ppm NaCl + 280 ppm $NaHCO_3$ aqueous solution; pH: 7.92; Salinity: 26.7 o%; FR: 1.12

4.5.2 Core Reduction and Conditioning, Salinity Tracer Test

The core was flooded at 23 °C with 40000 ppm $NaHCO_3$, 10000 ppm Na_4EDTA, and 10000 ppm $Na_2S_2O_4$ aqueous solution (reduction-1 fluid) at 0.5 ml/min (4.84 ft/D) to reduce the core and to remove amorphous oxidized iron from the core. Effluent iron concentration reached a steady state of about 3 ppm by 9.8 PV injection. Flooding was continued until 10.2 PV injected.

Permeability was obtained as 925 mD during reduction-1 fluid injection. Since the PV (134.2 ml) and the permeability (925 mD) were not in the expected range, and the pressure during higher interstitial velocities were not constant, it was assumed that a significant volume of air remained inside the core. To displace the air from the core, a back-pressure regulator (BPR) was used while injecting non-EDTA solution (reduction-2).

An aqueous solution of 40000 ppm $NaHCO_3$ and 10000 ppm $Na_2S_2O_4$ was injected at 23 °C and 0.5 ml/min (4.8 ft/D) flow rate until the effluent iron concentration was steady-state at about 0.3 ppm. To displace the air from the core, a back-pressure regulator (BPR) was used and set to 50 psi. Injection continued until 13.2 PV were injected. ORP, and iron concentration of the effluents are shown in Figure 4.74; pH and iron concentration of the effluents are shown in Figure 4.75. After displacing the air, a pore volume of 148.4 ml was calculated by the mass method.

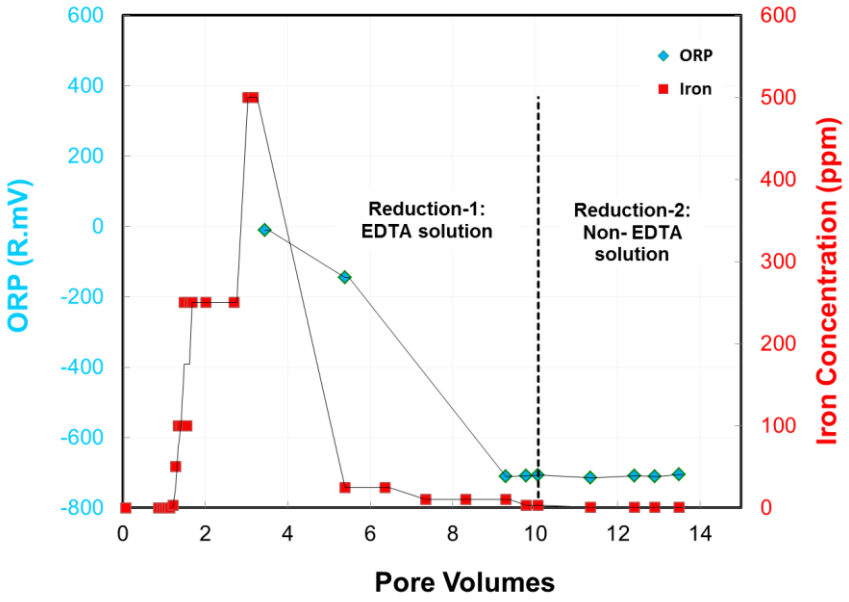

Figure 4.74: ORP (R.mV) and iron concentration (ppm) of the effluents.

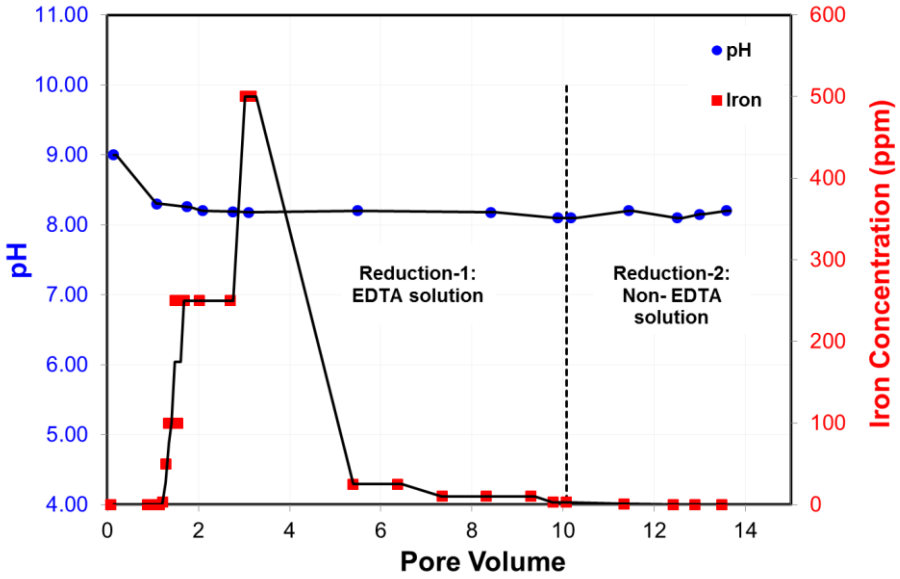

Figure 4.75: pH and iron concentration (ppm) of the effluents.

A salinity tracer test was performed to measure the pore volume and heterogeneity of the core. 0.1% NaCl brine was injected at 2 ml/min (19.3 ft/D) to displace the 4% $NaHCO_3$ and 1% $Na_2S_2O_4$ brine. The effluent samples were collected in volumes of 8 ml, and then 4 ml. During the salinity tracer test, salinities were measured and plotted to determine the aqueous volume (pore volume) of 148.7 ml from the area above the normalized salinity versus effluent volume curve shown in Figure 4.76.

After the salinity tracer test, the same 0.1% NaCl brine was injected at flow rates increasing from 2 ml/min (19.3 ft/D) to 8 ml/min (77.1 ft/D) to determine the permeability, which was found to be 1453 mD.

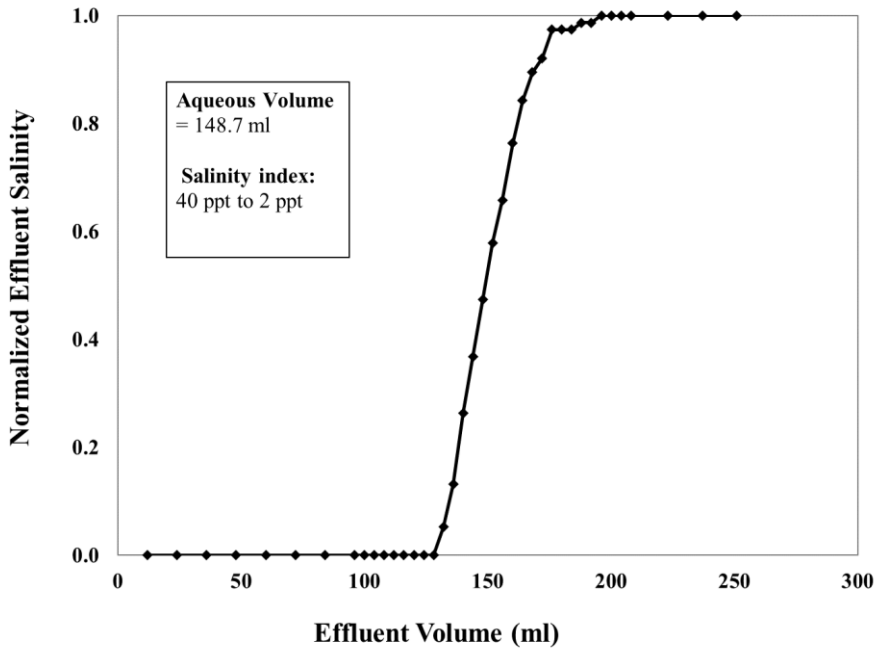

Figure 4.76: Normalized effluent salinity during 0.1% NaCl brine injection for experiment #5, from a salinity index of 40 ppt to a 2 ppt.

4.5.3 Oil Flood

Crude oil with a viscosity of 137 cP at 23 °C was filtered through 1.2 μm filter paper under 20 psi of air pressure. Crude oil was injected at a constant pressure of 85 psi and 23 °C. Oil flooding was continued until steady state pressure drop was observed, and the oil cut exceeded 99%. 1.11 PV of the oil was injected. The flow rate at steady state was 2 ml/min (18.8 ft/D).

The initial oil saturation (S_{oi}) of 0.84 was determined by using the displaced water volume of 125.3 ml in equation 3.10. The residual water saturation (S_{wr}) was 0.16 using equation 3.11. The effective oil permeability at S_{wr} was determined 1360 md from Darcy's law using pressure drop and volumetric flow rate, and the end-point oil relative permeability (k^o_{ro}) was calculated as 0.94 for the whole core using equation 3.12. Steady-state pressure drop data, effective oil permeability, and end-point oil permeability data are presented in Table 4.11. Flow rate during oil flood is shown in Figure 4.77. Pressure drop, and the interstitial velocity data are shown in Figure 4.78. The core was aged for 2 days at 23 °C after the oil flood.

Table 4.11: Steady-state pressure drop data, effective oil permeability, and end-point oil permeability from oil flooding for experiment #5.

Oil flood	**Whole**	**Section 1**	**Section 2**	**Section 3**	**Section 4**
Pressure drop (psi)	81	21	20	19	22
Effective oil permeability (mD)	1360	1335	1396	1425	1280
$\boldsymbol{k^o_{ro}}$	0.9	1.2	0.9	0.8	0.8

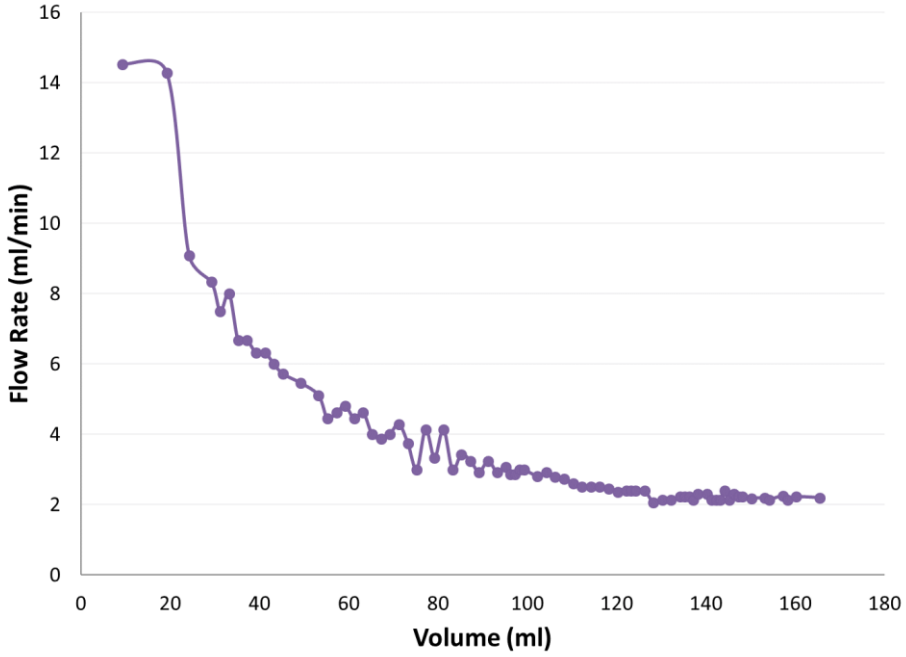

Figure 4.77: Flow rate during 137 cP crude oil flooding conducted at 85 psi constant pressure and 23 °C temperature for experiment #5.

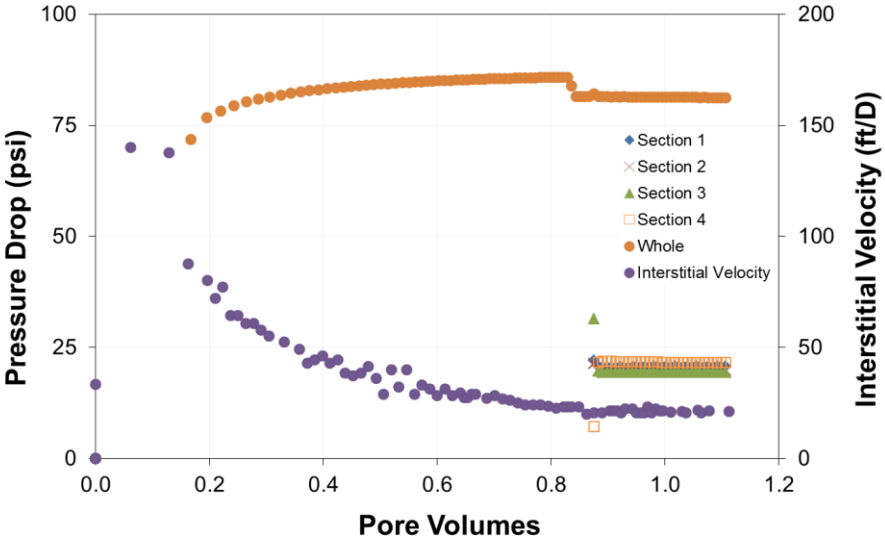

Figure 4.78: Pressure drop, and the interstitial velocity data during 137 cP crude oil flooding conducted at 85 psi constant pressure and 23 °C for experiment #5.

4.5.4 Waterflood

An aqueous solution of 1000 ppm NaCl and 1000 ppm $Na_2S_2O_4$ was injected at a constant flow rate of 0.5 ml/min (4.8 ft/D) until steady state pressure for all four sections and zero oil cut was observed. The pressure drop and the interstitial velocity data are shown in Figure 4.79. The capillary number was calculated as 3.2×10^{-5} using the maximum pressure gradient (15.5 psi/ft) and equation 2.3. The pressure drop reached steady state after 3 PV. Waterflooding continued for an additional 8.7 PV. The remaining oil saturation after the waterflood was 0.439 using equation 3.13. The effective water permeability was calculated as 144 md using the data and Darcy's law, and the end-point water relative permeability was 0.1. The end-point mobility ratio was calculated as 17.6 using equation 3.14.

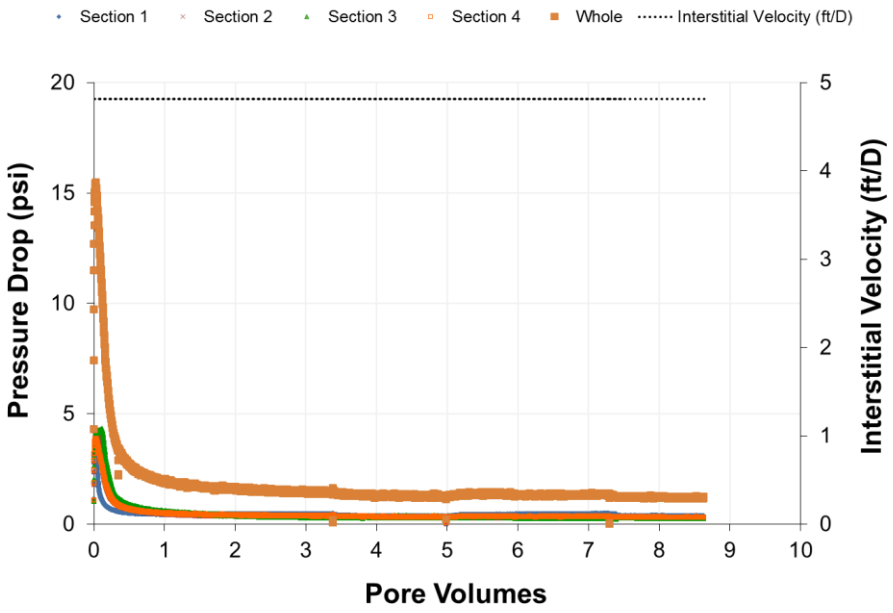

Figure 4.79: Pressure drop and the interstitial velocity data during waterflooding at 23°C for experiment #5.

A 2nd salinity tracer test was performed as an independent measurement of residual oil saturation to compare with the remaining oil saturation value obtained from material balance using produced oil and water volumes. An aqueous solution of 30000 ppm NaCl and 1000 ppm $Na_2S_2O_4$ was injected at 2 ml/min (19.3 ft/day) to displace the aqueous solution of 1000 ppm NaCl and 1000 ppm $Na_2S_2O_4$ brine. The effluent samples were collected in volumes of 8 ml. During the salinity tracer test, salinities were measured and plotted to determine the aqueous volume of 83.4 ml from the area above the normalized effluent salinity vs. effluent volume curve shown in Figure 4.80. After performing the tracer test, an aqueous solution of 1000 ppm NaCl and 1000 ppm $Na_2S_2O_4$ was injected at 2 ml/min (18.35 ft/day) to displace the solution of 30000 ppm NaCl and 1000 ppm $Na_2S_2O_4$ brine for 1 PV. By using the aqueous volume determined from salinity tracer test, the oil saturation after waterflood was obtained as 0.44 (1-83.4/148.7) while the material balance was also giving 0.44.

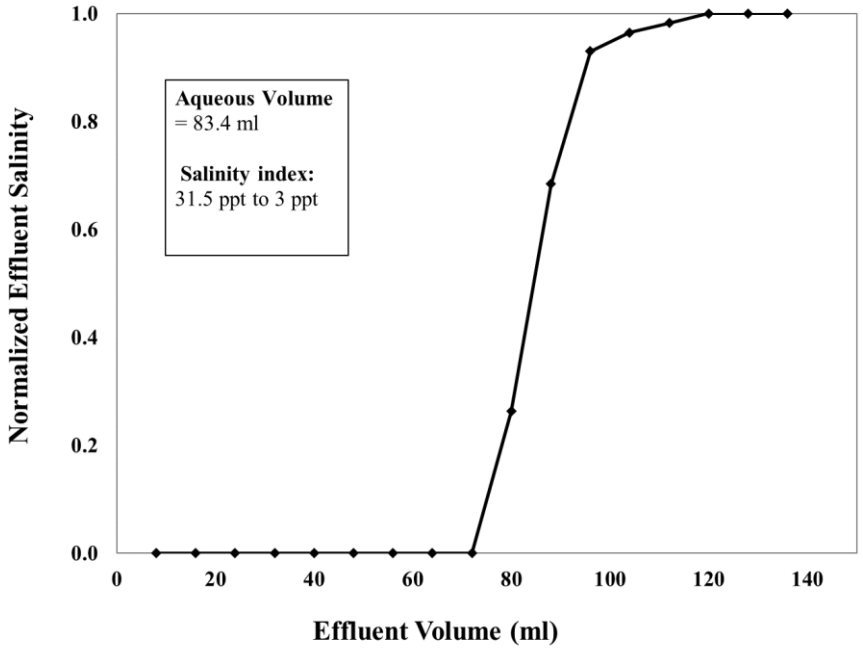

Figure 4.80: Normalized effluent salinity during 2nd salinity tracer test for experiment #5, from a salinity index of 31.5 ppt to 3 ppt.

4.5.5 Glycerin Flood

An aqueous solution of 82 wt% glycerin and 18 wt% brine (1000 ppm NaCl) with a viscosity of 57 cP (measured with rheometer) was injected at a flow rate of 0.208 ml/min (2 ft/D) until steady state pressure drop for all four sections and zero oil cut was observed. The maximum oil cut was 17.8%. The pressure drop data and the interstitial velocity are shown in Figure 4.81. Pressure drop reached steady state after 0.66 PV injection, but the flood continued until 1.8 PV. The residual oil saturation was reduced from 0.439 following the waterflood to 0.406 following the glycerin flood using equation 3.15. The effective permeability was 169 mD using Darcy's law and the end-point glycerin relative permeability was 0.12. The end-point mobility ratio was calculated as 0.33 using equation 3.16.

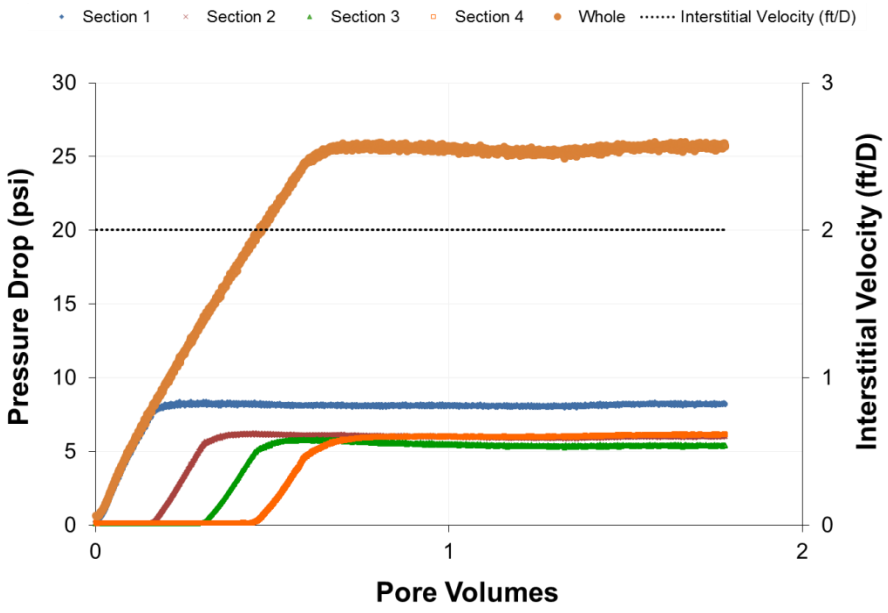

Figure 4.81: Pressure drop data, and the interstitial velocity during glycerin flooding at 23 °C for experiment #5.

4.5.6 Low-salinity Polymer Properties

A high molecular weight polymer (2000 ppm FP 3630S #JBA 2114/4-6) was prepared in a low-salinity brine (1000 ppm NaCl and 400 ppm $NaHCO_3$) to obtain a polymer solution with a high relaxation time. After hydrating 16 hours, the solution was filtered under 15 psi Argon pressure at 23 °C using a 1.2 µm Millipore mixed cellulose ester membrane filter paper. The filtration ratio was 1.1. The polymer solution was bubbled with argon while stirring for 2 hours in a round bottom flask and then vacuum- transferred to an injection column.

A sample of the polymer solution was taken from the column to measure its rheology, pH, and salinity. The pH was 7.8 and the salinity index was 2.7 ppt. A relaxation time of 10.2 s was determined from the G', G" crossover point using the dynamic frequency sweep test (DFST) shown in Figure 4.82. The steady rate sweep test (SRST) data of low-

salinity polymer in the power-law viscosity region of shear thinning as shown in Figure 4.84 were fit to obtain a power-law equation of μ=536 × $\dot{\gamma}^{(-0.64)}$.

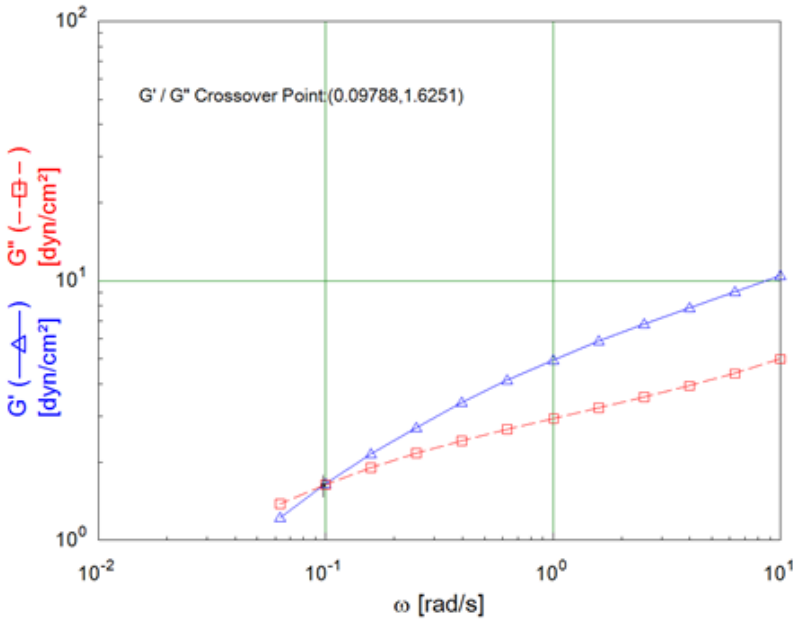

Figure 4.82: DFST result for 2000 ppm FP-3630S HPAM polymer in 1000 ppm NaCl + 400 ppm $NaHCO_3$ aqueous solution at 23 °C for experiment #5.

4.5.7 High-salinity Polymer Properties

A 3547 ppm FP 3630S polymer (#JBA 2114/4-6) in 24000 ppm NaCl, 300 ppm $NaHCO_3$ brine was prepared for the tracer test. Note that this is a new lot of FP 3630S. After hydrating 16 hours, the polymer solution was filtered through 90 mm diameter, 1.2 μm Millipore mixed cellulose ester membrane filter paper under 15 psi Argon pressure into 250 ml graduated cylinder at 23 °C. The filtration ratio was 1.12. The polymer solution was bubbled with argon while stirring for 2 hours in a round bottom flask and then vacuum-transferred to an injection column.

A sample of the polymer solution was taken from the column to measure its rheology, pH, and salinity. The pH was 7.9 and the salinity index was 27 ppt. The dynamic frequency sweep test (DFST) data are shown in Figure 4.83. The relaxation time was estimated as 0.45 s using the G' and G" crossover point. It is much less than the 10.2 s for the polymer solution injected into the core in the previous step. Figure 4.84 compares the results of the SRST for this high-salinity polymer (3547 ppm FP-3630S HPAM polymer in 24000 ppm NaCl, 300 ppm $NaHCO_3$) and the low-salinity polymer (2000 ppm FP-3630S HPAM polymer in 1000 ppm NaCl + 400 ppm $NaHCO_3$) in the preceding flood. The viscosities are similar, but the high salinity polymer in slightly less viscous than the low salinity one. The steady rate sweep test (SRST) data of high-salinity polymer in the power-law viscosity region of shear thinning as shown in Figure 4.84 were fit to obtain a power-law equation of $\mu=349. \times \dot{\gamma}^{(-0.53)}$.

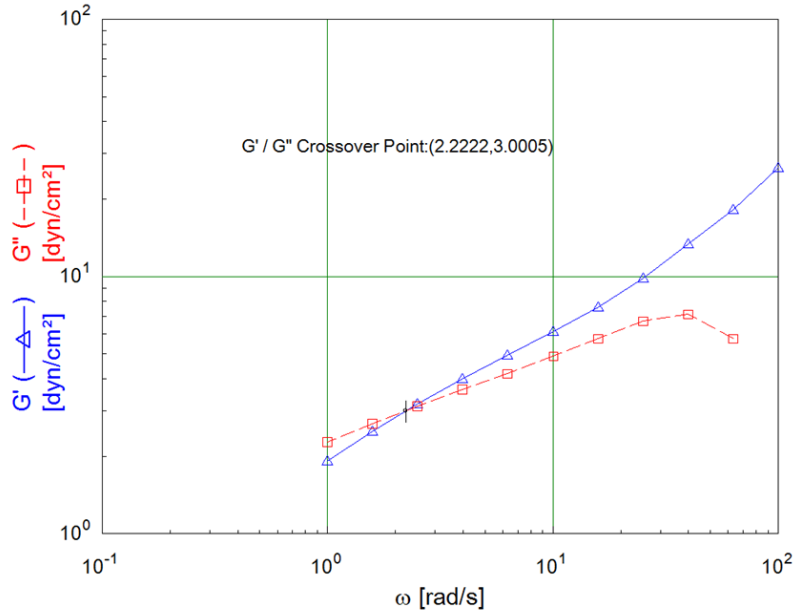

Figure 4.83: DFST result of the 3547 ppm FP-3630S HPAM polymer (# JBA 2114/4-6) in 24000 ppm NaCl, 300 ppm $NaHCO_3$ aqueous solution at 23 °C for experiment #5.

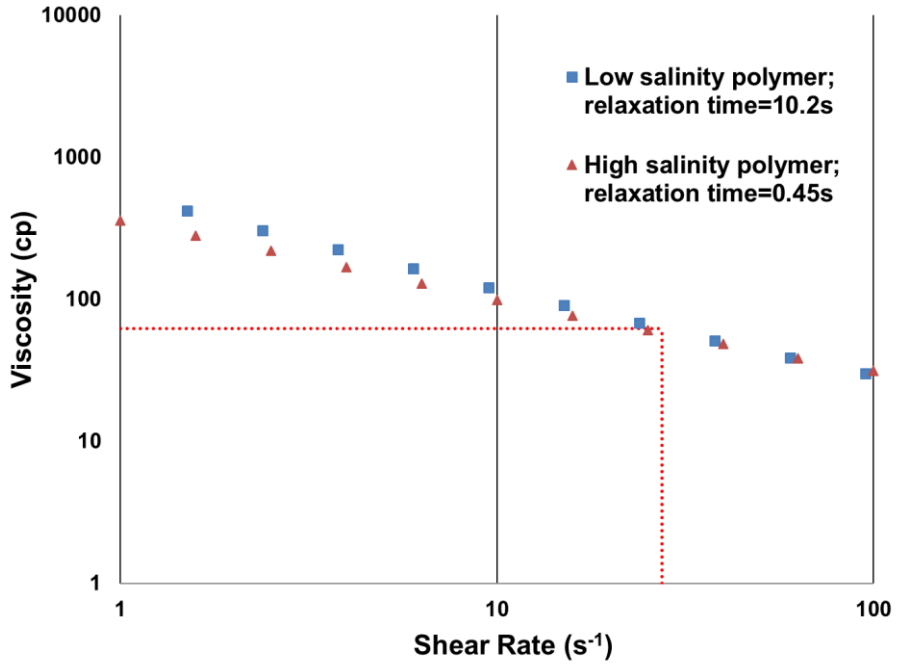

Figure 4.84: SRST result for 3547 ppm FP-3630S HPAM polymer in 24000 ppm NaCl, 300 ppm NaHCO3 aqueous solution compared with 2000 ppm FP-3630S HPAM polymer in 1000 ppm NaCl + 400 ppm $NaHCO_3$ aqueous solution at 23 °C for experiment #5.

4.5.8 Alternating Polymer Floods

The properties of both the low-salinity and high-salinity polymer solutions were presented in the previous section. Low-salinity polymer was 2000 ppm FP-3630S HPAM polymer (#JBA 2114/4-6) in 1000 ppm NaCl + 400 ppm $NaHCO_3$ aqueous solution, and high-salinity polymer was 3548 ppm FP-3630S HPAM polymer (#JBA 2114/4-6) in 24030 ppm NaCl + 280 ppm $NaHCO_3$ aqueous solution. After preparation of both polymer solutions and transferring to the injection columns, those columns were connected with 3-

way valves so that there wouldn't be any stoppage when alternating between those two polymer injections.

Polymer flooding using the two polymers (referred to as low-salinity and high-salinity, respectively) was performed as follows:

a) 0-1 PV (10.4-11.4 cumulative PV); injected low-salinity polymer for 1 PV; 0.104 ml/min (1 ft/day). Oil recovery started after 0.24 PV injection of the low-salinity polymer and the maximum oil cut was 48% during the first 1 PV injection. Oil recovery ceased after 0.84 PV of polymer injection. Oil saturation decreased from 40.6% to 28.4%.

b) 1-3 PV; injected high-salinity polymer for 2 PV; 0.104 ml/min (1 ft/day); no oil was recovered

c) 3-4 PV; injected Low-salinity polymer for 1 PV; 0.104 ml/min (1 ft/day); no was oil recovered

d) 4-6 PV; injected High-salinity polymer for 2 PV; 0.104 ml/min (1 ft/day); no oil was recovered

e) 6-8 PV; injected Low-salinity polymer for 2 PV; 0.104 ml/min (1 ft/day); very little amount of oil recovered. Maximum oil cut was 0.3%. Oil saturation decreased from 28.4% to 28.2%.

f) 8-8.14 PV; continued injection of low-salinity polymer for 0.14 PV; 0.01 ml/min (0.1 ft/day); no oil recovered

g) 8.14 – 8.4 PV; continued injecting low-salinity polymer for 0.26 PV; 0.005 ml/min (0.05 ft/day); no oil was recovered

h) No injection for 16 days

i) 8.4 – 11.5 PV (18.8 – 21.9 cumulative PV); started injecting a new batch of high-salinity polymer for 3.1 PV; 0.104 ml/min (1 ft/day); Oil recovery started

after 1 PV injection of the high-salinity polymer and oil cut increased as high as 4.3%. Oil saturation decreased from 28.2% to 21.3%.

j) 11.5– 12 PV (21.9 – 22.4 cumulative PV); continued injecting high-salinity polymer for 0.5 PV; 0.052 ml/min (0.5 ft/day); oil recovery continued. Oil saturation decreased from 28.2% to 20.6%.

k) 12– 13.5 PV (22.4 – 23.9 cumulative PV); injected low-salinity polymer for 1.5 PV; 0.104 ml/min (1 ft/day); oil recovery continued. Oil saturation decreased from 20.6% to 16.3%.

l) 13.5– 14.7 PV; injected high-salinity polymer for 1.2 PV with the purpose of salinity tracer test; 0.104 ml/min (1 ft/day); very little amount of oil recovered; Oil recovery started after 1.05 PV injection of the high-salinity polymer; max oil cut 0.15%. Oil saturation decreased from 16.31% to 16.29%.

m) 14.7– 15.2PV; continued injecting high-salinity polymer for 0.5 PV; 0.052 ml/min (0.5 ft/day); Oil saturation decreased from 16.29% to 16.24%.

n) 15.2– 16.9 PV (25.6 – 27.3 cumulative PV); injected low-salinity polymer for 1.7 PV for a salinity tracer test; 0.104 ml/min (1 ft/day); very little amount of oil was recovered; maximum oil cut 3.08%. Oil saturation decreased from 16.24% to 15.95%.

In terms of cumulative PV, the polymer injection started at 10.4 cumulative PV and finished at 27.3 PV.

Low-salinity and high-salinity polymers were alternated five times as follows:

- First: 1 PV low-salinity polymer (oil recovered), 2 PV high-salinity polymer (no oil recovery),

- Second: 1 PV low-salinity polymer (no oil recovery), 2 PV high-salinity polymer (no oil recovery),
- Third: 2.4 PV low-salinity polymer (no oil recovery), 3.4 PV high-salinity polymer (oil recovered),
- Fourth: 1.5 PV low-salinity polymer (oil recovered), 1.7 PV high-salinity polymer (no oil recovery),
- Fifth: 1.7 PV low-salinity polymer (no oil recovery)

For the first cycle of the alternating; for low-salinity polymer flood, based on the maximum pressure gradient reached at 1 ft/D, 24.3 psi, maximum capillary number was calculated as 4.6 × 10-5 for the whole core, and for high-salinity polymer flood, based on the maximum pressure gradient reached at 1 ft/D, 18.5 psi, maximum capillary number was calculated as 3.5 × 10-5 for the whole core.

Pressure drop data during alternating polymer floods are shown in Figure 4.85. As it can be seen from the graph at 1 PV injection, when switched from low-salinity polymer to high-salinity polymer, the pressure was not at steady state (it was decreasing), although the oil cut was zero. This suggests that oil may have been mobile in the core even if not produced. Similarly, at 3 PV injection, when switched from low-salinity polymer to high-salinity polymer, the pressure was not at steady state (increasing). On the other hand, the pressure gradient of the low-salinity polymer flood was at steady state before injecting the third high-salinity polymer, and we recovered oil during that third high-salinity polymer injection. As stated above, during the third alternating flowing was observed: 2.4 PV low-salinity polymer (no oil recovery) and 3.4 PV high-salinity polymer (oil recovered).

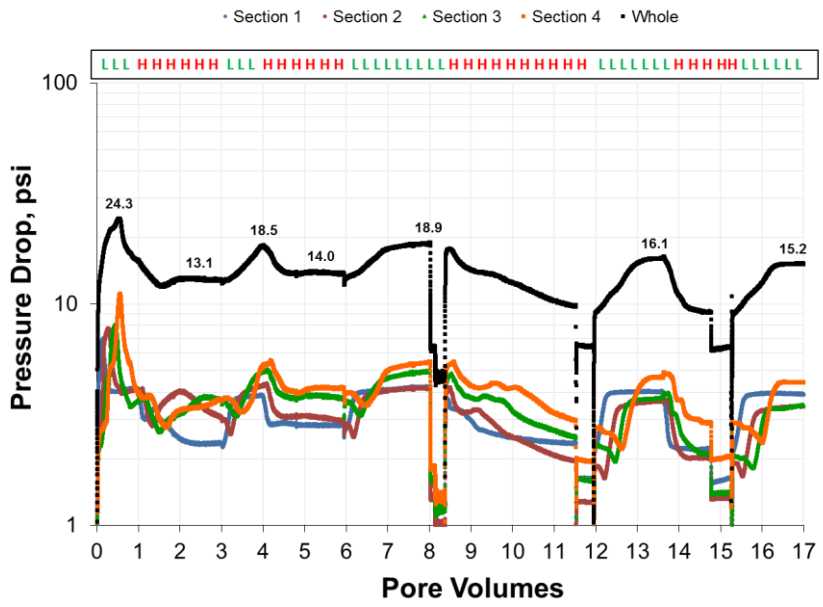

Figure 4.85: Pressure drop data during alternating polymer floods for experiment #5.

Capillary number data during alternating polymer floods are shown in Figure 4.86.

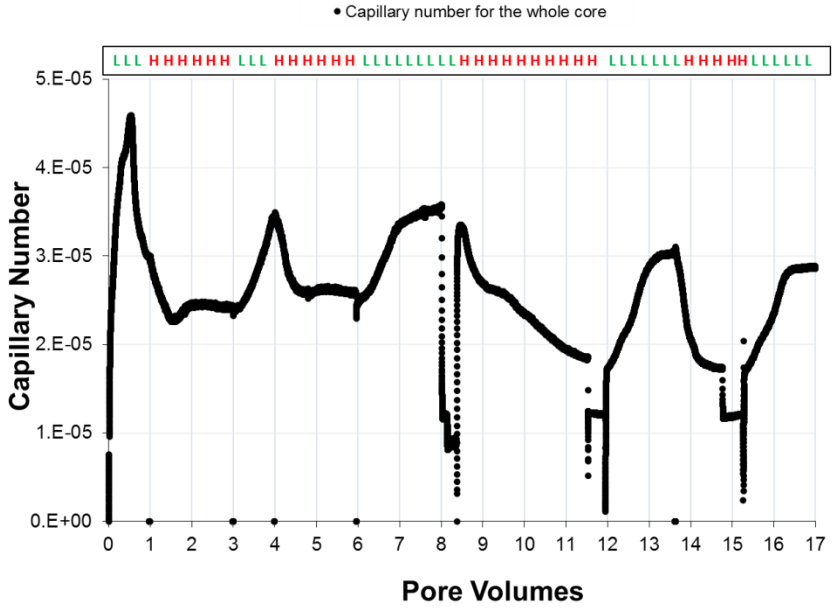

Figure 4.86: Capillary number data during alternating polymer floods for experiment #5.

The effluents of the high-salinity polymer injection between 13.5 and 15.2 PV were used as a salinity tracer test to compare the oil saturation obtained from material balance. The effluent samples were collected in volumes of 13 ml. During the test, salinities were measured and plotted. 128.3 ml was obtained from the area above the normalized salinity versus effluent volume curve. Normalized salinity versus effluent volume of the polymer tracer test is shown in Figure 4.87. Tracer test gives an oil saturation of 13.7% (=1-128.3/148.7) while the oil saturation after tracer test was 16.24 % according to the material balance. There is a 2.51% difference between two of the results.

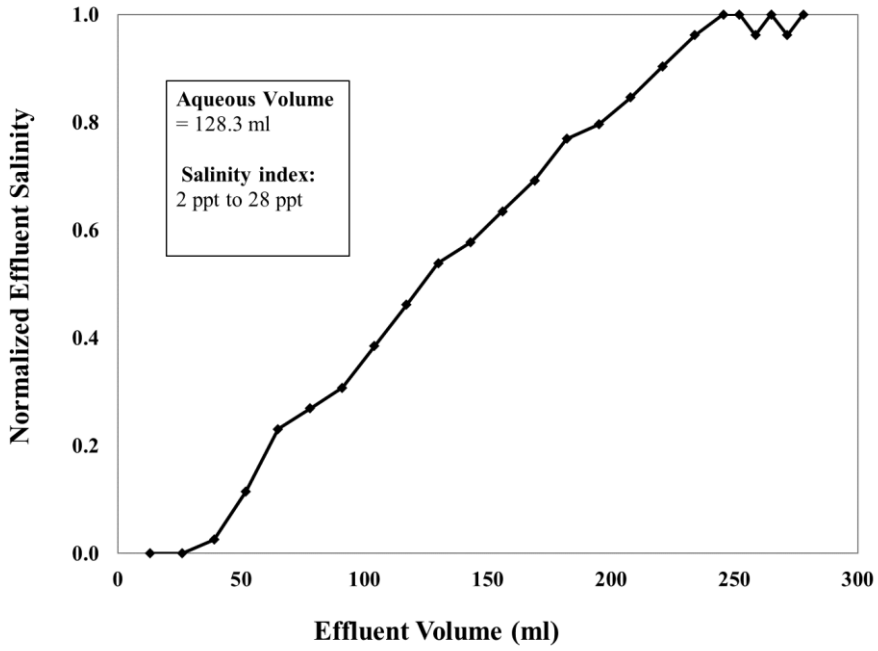

Figure 4.87: Normalized salinity versus effluent volume of the polymer salinity tracer test, from a salinity index of 2 ppt to 28 ppt.

The effluents of the low-salinity polymer injection that occurred in the interval15.2 PV and 16.9 PV were used as a salinity tracer test to compare the oil saturation obtained from material balance. The effluent samples were collected in volumes of 6.5 ml. During

the test, salinities were measured and plotted. 125.4 ml was obtained from the area above the normalized salinity vs. effluent volume curve. Normalized salinity vs effluent volume of the polymer tracer test is shown in Figure 4.88. The oil saturation determined from the tracer test was 15.7 % (=1-125.4/148.7) while the oil saturation after tracer test was 15.95 % according to the material balance. The relative error is 1.6%.

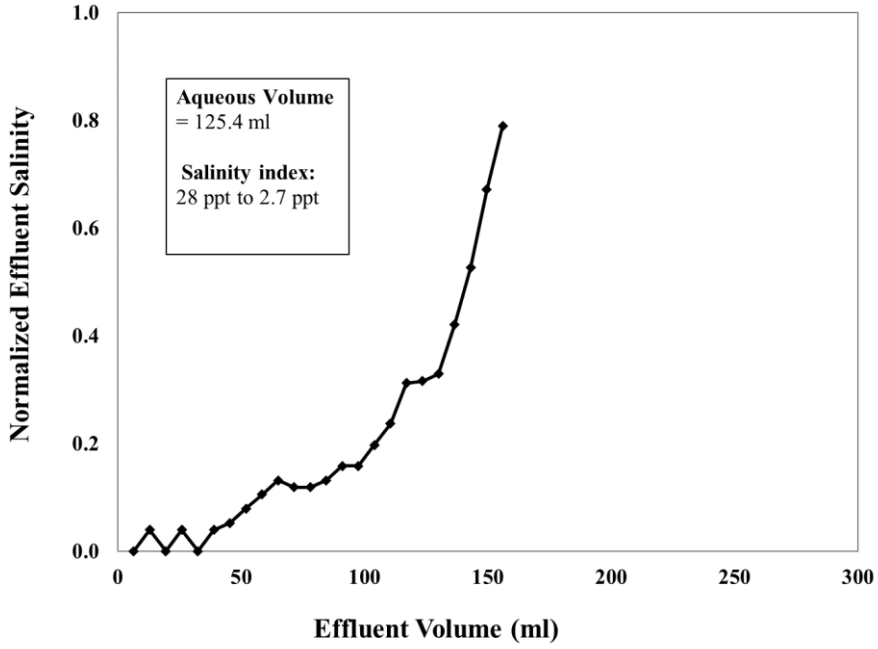

Figure 4.88: Normalized salinity versus effluent volume of the polymer salinity tracer test, from a salinity index of 28 ppt to 2.7 ppt.

4.5.9 Oil Saturation, Oil Cut, and Pressure Drop

Oil saturation versus pore volumes for all floods performed in experiment #5 are shown in Figure 4.89. Oil saturation, cumulative oil recovered, and oil cut data are shown in Figure 4.90.

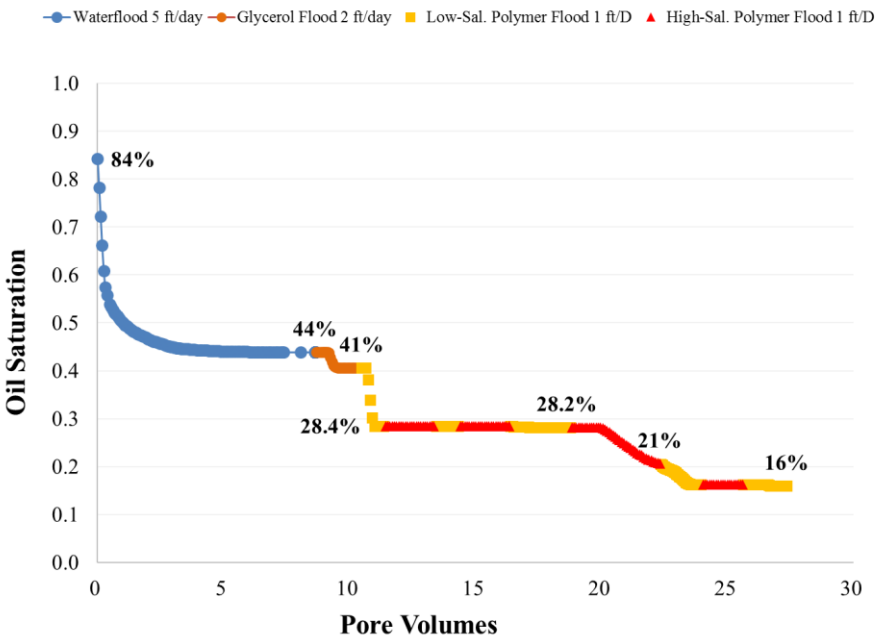

Figure 4.89: Oil saturation versus pore volumes for experiment #5.

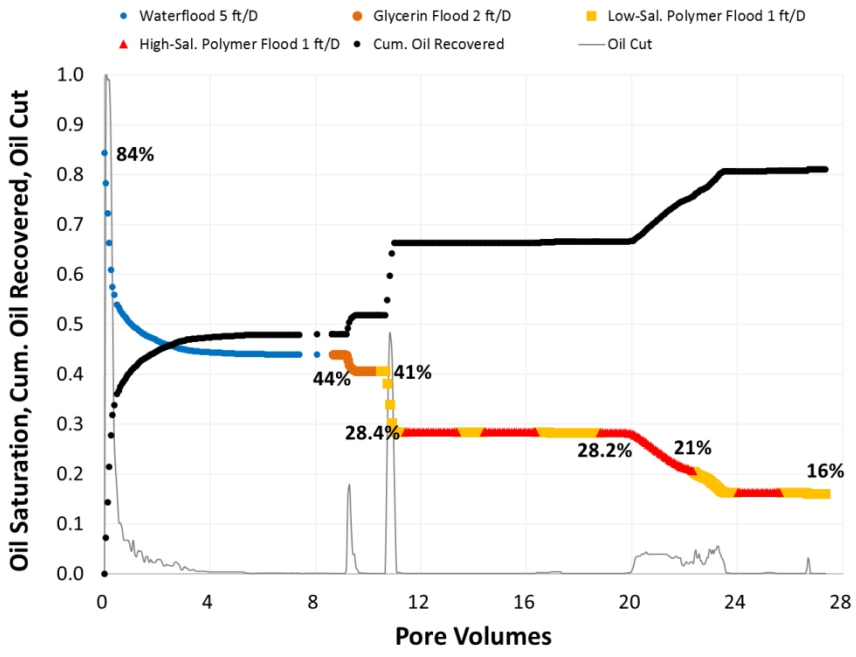

Figure 4.90: Oil saturation, cumulative oil recovered, and oil cut for experiment #5.

4.6 EXPERIMENT #6

Experiment #6 was conducted by another researcher (Pengpeng Qi) in a different laboratory (also at UT-Austin) to confirm the new discovery of using high-salinity polymer flood after a low-salinity, high elasticity polymer flood. Experiment #6 was a repeat of experiment #3. Table 4.12 summarizes the core and fluid properties of experiment #6.

Table 4.12: Core and fluid properties of experiment #6.

Experiment	**#6**
Coreflood name	PPQ-1st
Rock type	Bentheimer Sandstone
Brine permeability (mD)	1277
Crude oil viscosity (cP)	128
Temperature (℃)	23
Porosity	0.24
Pore volume (ml)	147.5
Bulk volume (ml)	608
Dry core mass (g)	1215
Bulk density (g/cm^3)	2.0
Waterflood solution	1000 ppm NaCl + 1000 ppm $Na_2S_2O_4$ aqueous solution
Glycerin solution	82 wt% glycerol in in 1000 ppm NaCl aqueous solution
Low-salinity polymer solution	2000 ppm FP-3630S HPAM polymer (#JBA 2128/4-6) in 1000 ppm NaCl + 400 ppm $NaHCO_3$ aqueous solution
High-salinity polymer solution	3548 ppm FP-3630S HPAM polymer (# 245X) in 24030 ppm NaCl + 280 ppm $NaHCO_3$ aqueous solution

4.6.1 Core Preparation, Saturating the Core, Salinity Tracer Test

A 1 ft long 1.966 in diameter, Bentheimer sandstone core was potted in epoxy to prepare for core flooding. The core passed the pressure test after conducting water leak test at 95 psi air pressure for 10 min. The core was vacuum saturated at 23 °C with 6% KCl aqueous solution. The volume of brine imbibed into the core was measured and used to calculate a pore volume of 147 ml (2 ml was subtracted from the reading to account for fluid in the tubes). The same 6% KCl brine was vacuum transferred to an injection column and then injected at varying flow rates from 3 ml/min (29.4 ft/D) to 10 ml/min (98.1 ft/D) to determine the brine permeability, which was found to be 1277 mD using Darcy's Law given in equation 3.7.

A salinity tracer test was performed to measure the pore volume and heterogeneity of the core. 2% KCl brine was injected at 2 ml/min (19.6 ft/D) to displace the 6% KCl brine. The effluent samples were collected in volumes of 7.5 ml. During the salinity tracer test, salinities were measured and plotted to determine the aqueous volume (pore volume) of 147.5 ml from the area above the normalized salinity versus effluent volume curve shown in Figure 4.91.

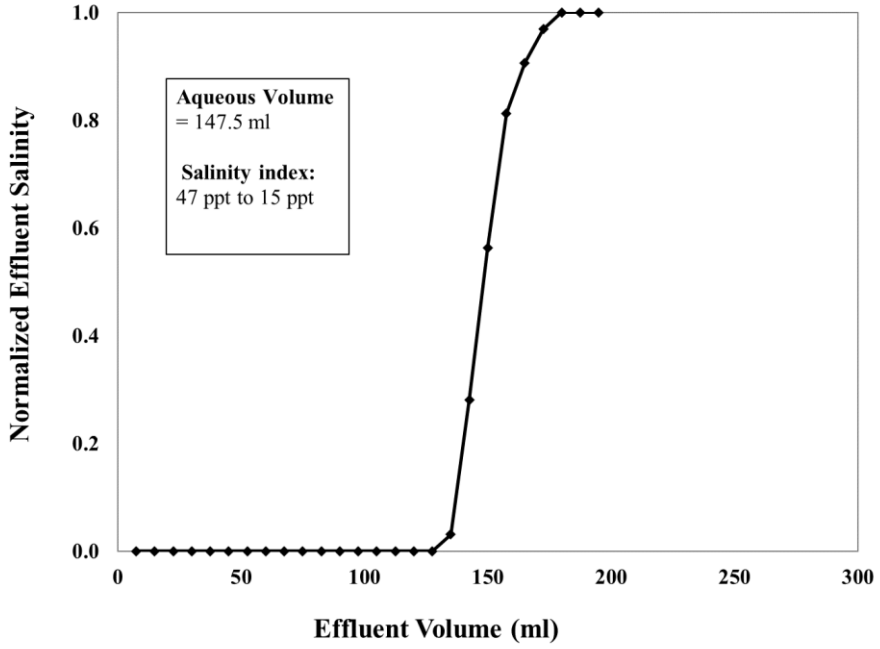

Figure 4.91: Normalized effluent salinity during the 2% KCl brine injection for experiment #6, from a salinity index of 47 ppt to15 ppt.

4.6.2 Core Reduction and Conditioning

The core was flooded at 23 °C with an aqueous solution of 40000 ppm $NaHCO_3$, 10000 ppm Na_4EDTA, and 10000 ppm $Na_2S_2O_4$ at 0.5 ml/min (4.9 ft/D) to reduce the core and to remove amorphous oxidized iron. Flooding was continued until the iron concentration in the effluent decreased to 0.3 ppm. After the reduction, same reduction brine was injected at different flow rates from 3 ml/min (29.4 ft/D) to 20 ml/min (196.1 ft/D) to determine the permeability. The average brine permeability was obtained as 1277 mD.

4.6.3 Oil Flood

Crude oil with a viscosity of 128 cp at 23 °C was filtered through 1.2 μm filter paper under 20 psi of air pressure. Crude oil was injected at a constant pressure of 80 psi and 23 °C. Oil flooding was continued until steady state pressure drop was observed and

the oil cut exceeded 99%. A total of 1.3 PV of oil was injected. The flow rate at steady state was 1.2 ml/min (11.8 ft/D).

The initial oil saturation (S_{oi}) of 0.87 was determined using equation 3.10. The residual water saturation (S_{wr}) was 0.13 using equation 3.11. The effective oil permeability at S_{wr} was determined 767 md from Darcy's law using pressure drop and volumetric flow rate, and the end-point oil relative permeability (k^{o}_{ro}) was calculated as 0.60 for the whole core using equation 3.12.

4.6.4 Waterflood

An aqueous solution of 1000 ppm NaCl and 1000 ppm $Na_2S_2O_4$ was injected at a constant flow rate of 0.204 ml/min (2 ft/D) until steady state pressure for all four sections and zero oil cut was observed. The capillary number was calculated as 2.9×10^{-5} using the maximum pressure gradient and equation 2.3. The pressure drop reached steady state after 4 PV. Waterflooding continued for an additional 2.8 PV. The remaining oil saturation after the waterflood was 0.43 using equation 3.13. The effective water permeability was calculated as 391 md using the data and Darcy's law, and the end-point water relative permeability was 0.03. The end-point mobility ratio was calculated as 7.2 using equation 3.14.

A 2nd salinity tracer test was performed as an independent measurement of residual oil saturation to compare with the remaining oil saturation value obtained from material balance using produced oil and water volumes. An aqueous solution of 30000 ppm NaCl and 1000 ppm $Na_2S_2O_4$ was injected at 2 ml/min (19.6 ft/day) to displace the aqueous solution of 1000 ppm NaCl and 1000 ppm $Na_2S_2O_4$ brine. The effluent samples were collected in volumes of 4 ml. During the salinity tracer test, salinities were measured and

plotted to determine the aqueous volume of 82.6ml from the area above the normalized effluent salinity vs. effluent volume curve. After performing the tracer test, an aqueous solution of 1000 ppm NaCl and 1000 ppm $Na_2S_2O_4$ was injected at 2 ml/min (19.6 ft/day) to displace the solution of 30000 ppm NaCl and 1000 ppm $Na_2S_2O_4$ brine for 1 PV. By using the aqueous volume determined from salinity tracer test, the oil saturation after waterflood was obtained as 0.44 (1-82.6/147.5) while the material balance had given 0.43. The relative error is 2%.

4.6.5 Glycerin Flood

An aqueous solution of 82 wt% glycerin and 18 wt% brine (1000 ppm NaCl) with a viscosity of 60 cP (measured with rheometer) was injected at a flow rate of 0.204 ml/min (2 ft/D) until steady state pressure drop for all four sections and zero oil cut was observed. The maximum oil cut was 52%. The pressure drop data and the interstitial velocity are shown in Figure 4.92. The pressure drop reached steady state around 0.53 PV, but the flood continued until 1.45 PV. The residual oil saturation was reduced from 0.43 following the waterflood to 0.36 following the glycerin flood using equation 3.15. The effective permeability was 137 mD using Darcy's law and the end-point glycerin relative permeability was 0.11. The end-point mobility ratio was calculated as 0.4 using equation 3.16.

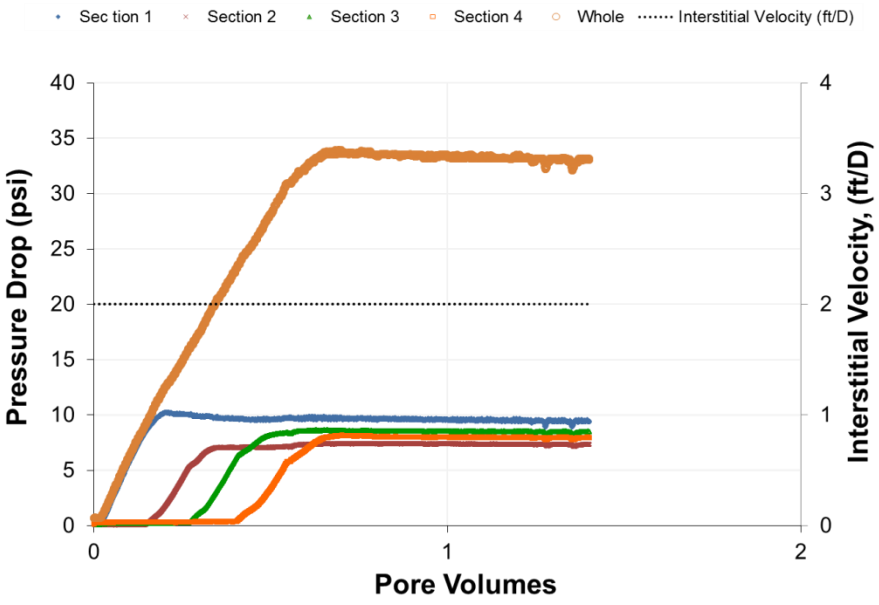

Figure 4.92: Pressure drop data and the interstitial velocity during glycerin flooding at 23 °C for experiment #6.

4.6.6 Low-salinity Polymer Flood

A high molecular weight polymer (2000 ppm FP 3630S #JBA 2114/4-6) was prepared in a low-salinity brine (1000 ppm NaCl and 400 ppm $NaHCO_3$) to obtain a polymer solution with a high relaxation time. After hydrating 16 hours, the solution was filtered under 15 psi Argon pressure at 23 °C using a 1.2 µm Millipore mixed cellulose ester membrane filter paper. The filtration ratio was 1.1. The polymer solution was bubbled with argon while stirring for 2 hours in a round bottom flask and then vacuum- transferred to an injection column.

A sample of the polymer solution was taken from the column to measure its rheology and pH, salinity. A relaxation time of 6.8 s was determined. This low-salinity

polymer solution was injected at a constant flow rate of 0.102 ml/min (1 ft/D) until steady state pressure drop for all four sections and zero oil cut was observed.

This low-salinity polymer solution (2000 ppm FP-3630S HPAM polymer (# 245X) in 1000 ppm NaCl and 400 ppm $NaHCO_3$ aqueous solution) was injected into the core at a constant flow rate of 0.102 ml/min (1 ft/D) until steady state for all four sections and zero oil cut was observed. Oil recovery was observed after 0.28 PV injection of the polymer solution. Oil cut was increased as high as 55%. Polymer flooding continued for 1.6 PV. Residual oil saturation after the low-salinity, high elasticity polymer flood was 0.22, a 14% reduction in oil saturation from the glycerin flood. Cumulative oil recovery at the end of the flood was calculated as 61% of OOIP.

- The effective polymer permeability was calculated as 169 mD for 1 ft/D polymer flood.
- The end-point polymer relative permeability was calculated as 0.12 for 1 ft/D polymer flood.
- The end-point mobility ratio was calculated as 0.4 for 1 ft/D polymer flood.
- The maximum capillary number was calculated as 4.6×10^{-5} for the whole core Based on the maximum pressure gradient reached at 1 ft/D polymer flood, 28 psi/ft,
- The capillary number was calculated as 2.5×10^{-5} based on the steady state pressure gradient (15 psi/ft)

4.6.7 High-Salinity, Low Elasticity Polymer Flood

An aqueous solution of 3548 ppm FP-3630S HPAM polymer (#245 X) in 24000 ppm NaCl, 300 ppm $NaHCO_3$ was prepared. The relaxation time was calculated was estimated as 1.3 s, which was significantly less than the relaxation time of 6.8s of the low-salinity polymer in the preceding flood.

This high-salinity polymer solution (3548 ppm FP-3630S HPAM polymer (#245 X) in 24000 ppm NaCl, 300 ppm $NaHCO_3$ aqueous solution) was injected at a constant flow rate of 0.102 ml/min (1 ft/D) until steady state for all four sections and zero oil cut was observed. Oil recovery was observed after 0.95 PV injection of this high-salinity polymer solution. 22 ml of oil was recovered. Maximum oil cut was 18%. The high-salinity polymer flood continued for 4.4 PV. Residual oil saturation after the high-salinity polymer flood was 0.07, and additional 15% reduction in oil saturation. The effective polymer permeability was calculated as 281 mD. The end-point polymer relative permeability was calculated as 0.22. The end-point mobility ratio was calculated as 0.8. The maximum capillary number was calculated as 2.4×10^{-5} for the whole core, based on the maximum pressure gradient, 14.8 psi/ft

4.6.8 Oil Saturation, Oil Cut, and Pressure Drop

Oil saturation data for all floods performed in experiment #6 are shown in Figure 4.93. Oil cut data for the glycerin flood, low-salinity, and high-salinity polymer floods are shown in Figure 4.94. Pressure drop data for glycerin flood, low-salinity, and high-salinity polymer floods are shown in Figure 4.95.

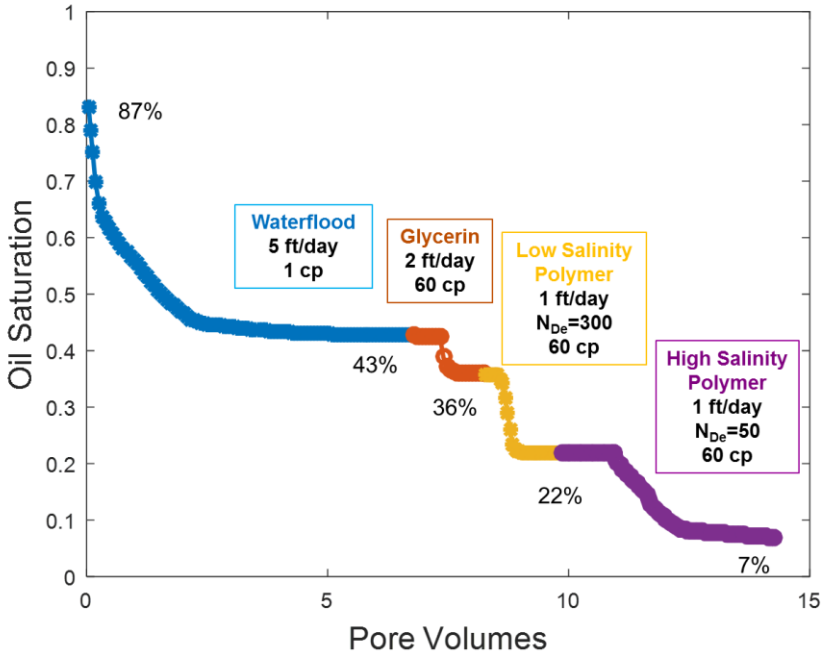

Figure 4.93: Oil saturation versus pore volumes for experiment #6.

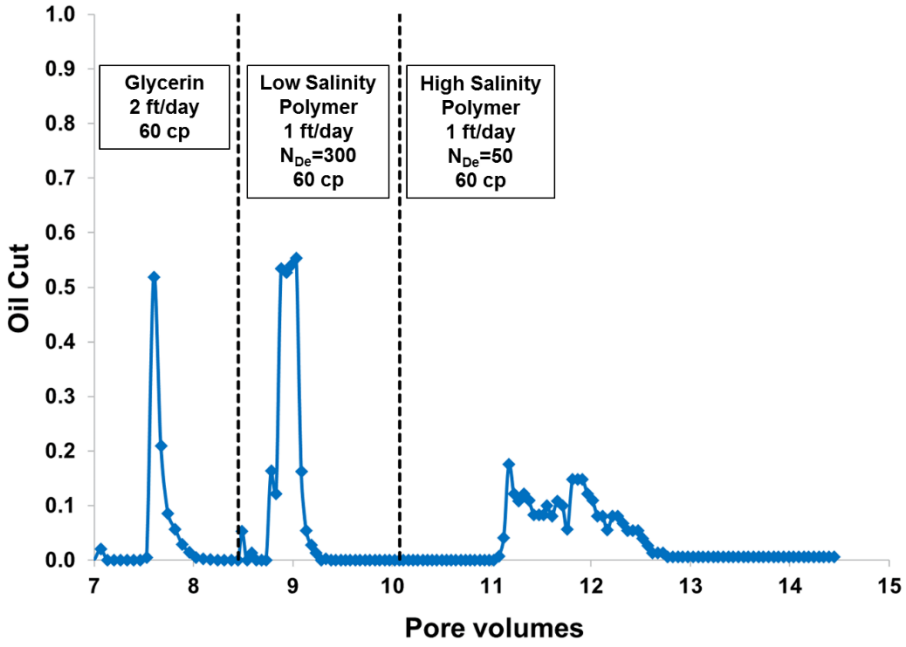

Figure 4.94: Oil cut data for the glycerin flood, low-salinity, and high-salinity polymer floods for experiment #6.

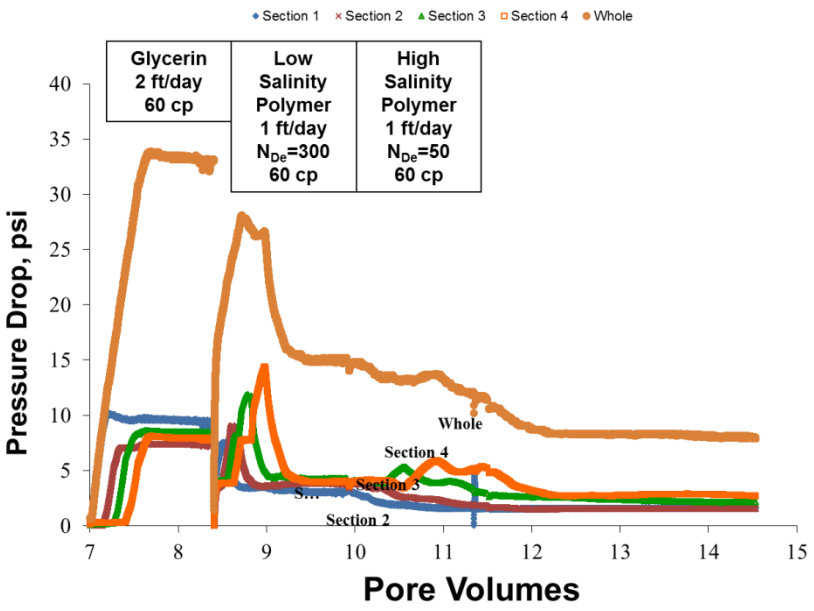

Figure 4.95: Pressure data for glycerin flood, low-salinity, and high-salinity polymer floods for experiment #6.

4.7 EXPERIMENT #7

Experiment #7 was also conducted by Pengpeng Qi. Unlike all previous experiments, the oil used had a relatively low viscosity (10 cP viscosity) Table 4.13 summarizes the core and fluid properties of experiment #7.

Table 4.13: Core and fluid properties of experiment #7.

Experiment	**#7**
Coreflood name	PPQ-2nd
Porous medium	Bentheimer Sandstone
Brine permeability (mD)	1448
Crude oil viscosity (cP)	10
Temperature (℃)	23
Porosity	0.25
Pore volume (ml)	148
Bulk volume (ml)	584
Dry core mass (g)	1167
Bulk density (g/cm^3)	2.0
Waterflood solution	1000 ppm NaCl + 400 ppm $NaHCO_3$ + 400ppm $Na_2S_2O_4$ aqueous solution
Glycerin solution	No glycerin flood
Low-salinity polymer solution	1500 ppm FP-3630S HPAM polymer (#JBA 2114/4-6) in 1000 ppm NaCl + 400 ppm $NaHCO_3$ aqueous solution; pH:8.2
High-salinity polymer solution	Not reported

4.7.1 Core Preparation, Saturating the Core, Salinity Tracer Test

A 30.3 cm long, 4.96 cm diameter, Bentheimer sandstone core was potted in epoxy to prepare for core flooding. The core was vacuum saturated at 23 °C with 6% KCl aqueous

solution. The volume of brine imbibed into the core was measured and used to calculate a pore volume of 148 ml (subtracted 2 ml from reading to account for fluid in the tubes

The same 6% KCl brine was vacuum transferred to an injection column, and then injected into the core at different flow rates from 3 ml/min (29.4 ft/D) to 10 ml/min (98.1 ft/D) to determine the permeability which was calculated as 1448 mD using the data and Darcy's law.

A salinity tracer test was performed to measure the pore volume and heterogeneity of the core. 2% KCl brine was injected at 2 ml/min (19.3 ft/D) to displace the 6% KCl brine. The effluent samples were collected in volumes of 7.5 ml. During the salinity tracer test, salinities were measured and plotted to determine the aqueous volume (pore volume) of 148 ml from the area above the normalized salinity versus effluent volume curve shown in Figure 4.96.

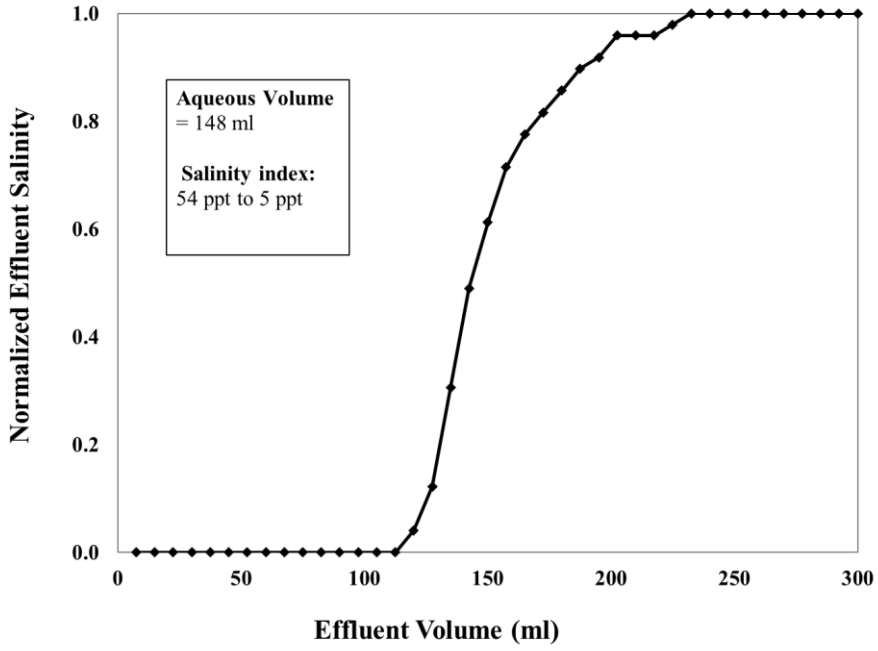

Figure 4.96: Normalized effluent salinity during 2% KCl brine injection for experiment #7, from a salinity index of 54 ppt to 5 ppt.

4.7.2 Core Reduction and Conditioning

An aqueous solution of 40000 ppm $NaHCO_3$, 10000 ppm Na_4EDTA, and 10000 ppm $Na_2S_2O_4$ was prepared and used to flood the core at 23 °C at 0.5 ml/min (4.8 ft/D) to reduce the core and to remove amorphous oxidized iron from the core until the iron concentration was about 3 ppm.

An aqueous solution of 40000 ppm $NaHCO_3$ and 10000 ppm $Na_2S_2O_4$ was then injected at 23 °C and 0.5 ml/min (4.8 ft/D) flow rate until the effluent iron concentration was steady-state at about 0.3 ppm. After the reduction, the same brine was injected at flow rates increasing from 3 ml/min (29.4 ft/D) to 20 ml/min (196.1 ft/D) to determine the permeability. The average brine permeability was calculated as1448 mD.

4.7.3 Oil Flood

Crude oil with a viscosity of 9.6 cP at 25 °C was filtered through 1.2 μm filter paper under 20 psi of air pressure. Crude oil was injected at a constant pressure of 30 psi and 25 °C. Oil flooding was continued until steady state pressure drop was observed and the oil cut exceeded 99%. The flow rate at steady state was 4.8 ml/min (46.4 ft/D).

- The initial oil saturation (S_{oi}) was calculated as 0.73 and residual water saturation (S_{wr}) was calculated as 0.27.
- The effective oil permeability was calculated as 602 mD. The end-point oil relative permeability (k^{o}_{ro}) was calculated as 0.42 for the whole core.

After performing oil flood, the core was aged for 2 days at 25 °C.

4.7.4 Waterflood

An aqueous solution of 1000 ppm NaCl, 1000 ppm $Na_2S_2O_4$ was injected at a constant flow rate of 0.103 ml/min (1 ft/D) until steady state pressure for all four sections and zero oil cut was observed. The capillary number was calculated as 1.3×10^{-6} by using the maximum pressure gradient reached. 3.5 PV of brine was injected to reach steady state and residual oil, which was0.383. Importantly, it is believed that this saturation was residual saturation, because the oil had a low viscosity (10 cP) and the calculated mobility ratio was less than 1.0 (calculated as 0.99). Therefore, no glycerin flood was conducted.

- The effective water permeability was calculated as 157 mD.
- The end-point water relative permeability was calculated as 0.11.

4.7.6 Low-Salinity, High Elasticity Polymer Flood

A high molecular weight polymer (FP 3630S) was prepared in a low-salinity brine (1500 ppm FP-3630S HPAM polymer in 1000 ppm NaCl and 400 ppm $NaHCO_3$ aqueous solution) to obtain a polymer solution with a high relaxation time.

- The relaxation time was estimated to be 11.8 s.

This low-salinity, high elasticity polymer solution was injected into the core at a constant flow rate of 0.103 ml/min (1 ft/D) until steady state for all four sections and zero oil cut was observed. Oil recovery was observed after 0.47 PV injection of the polymer solution. The maximum oil cut was 27%. Polymer flooding continued for 2.3 PV. The residual oil saturation after the low-salinity, high elasticity polymer flood was 0.336 which shows 4.7% reduction in oil saturation from the waterflood.

- The maximum capillary number was calculated as 6.9×10^{-5} for the whole core, based on the maximum pressure gradient reached at 1 ft/D polymer flood, 36.9 psi,

4.7.7 High-salinity Polymer Flood

The high-salinity polymer solution was injected at a constant flow rate of 0.103 ml/min (1 ft/D) until steady state for all four sections and zero oil cut was observed. Oil recovery was observed after 0.25 PV injection of high-salinity the polymer solution. 10.3 ml of oil was recovered. Maximum oil was 13%. The high-salinity polymer flood continued for 2 PV. The residual oil saturation after the high-salinity polymer flood was 0.267, a 7% reduction in oil saturation from the waterflood.

4.7.8 Oil Saturation, Cumulative Oil Recovered, and Oil Cut

Oil saturation data for all floods performed in experiment #7 are shown in Figure 4.97. Oil cut data for low-salinity and high-salinity polymer floods are shown in Figure 4.98. Pressure drop data for low-salinity and high-salinity polymer floods are shown in Figure 4.99.

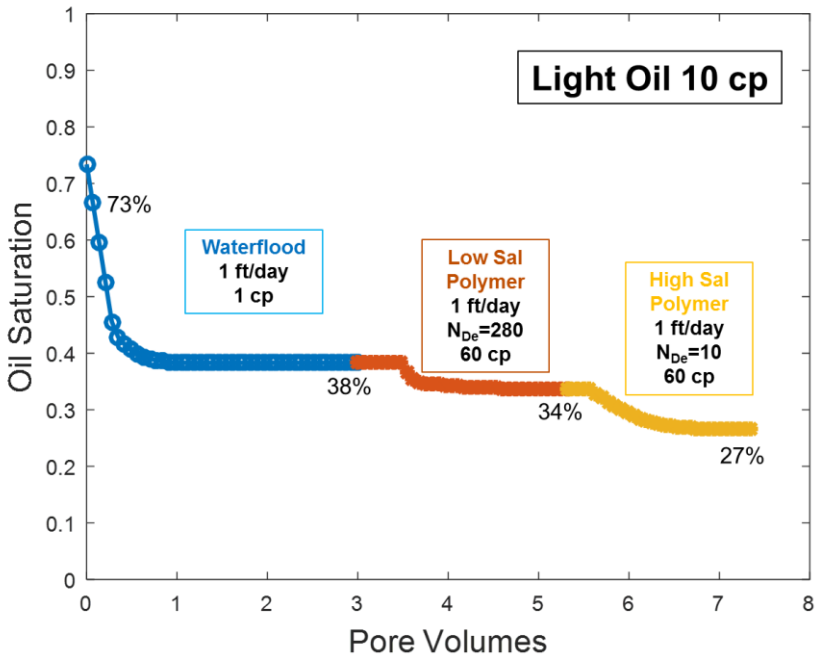

Figure 4.97: Oil saturation versus pore volumes for experiment #7.

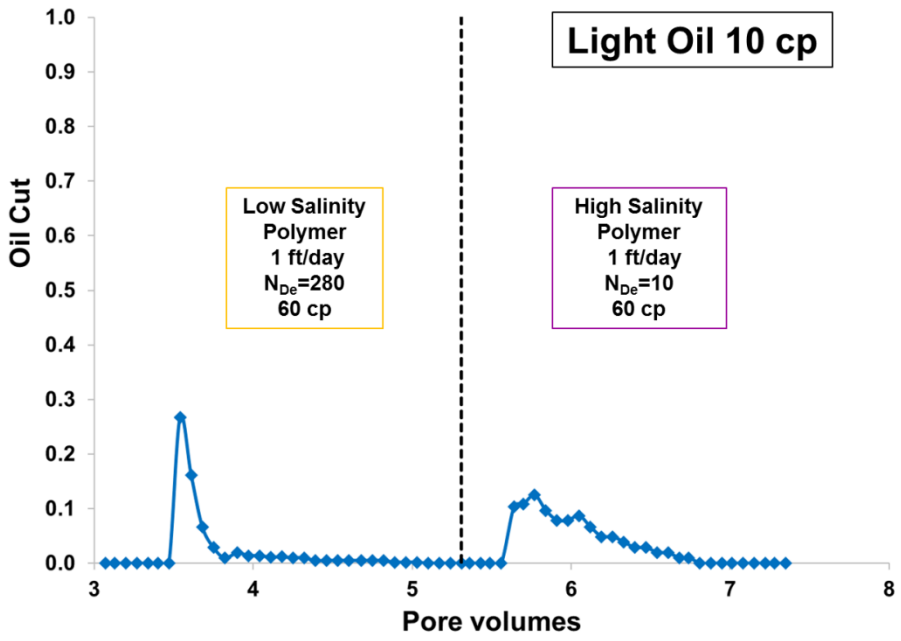

Figure 4.98: Oil cut data for low-salinity, and high-salinity polymer floods for experiment #7.

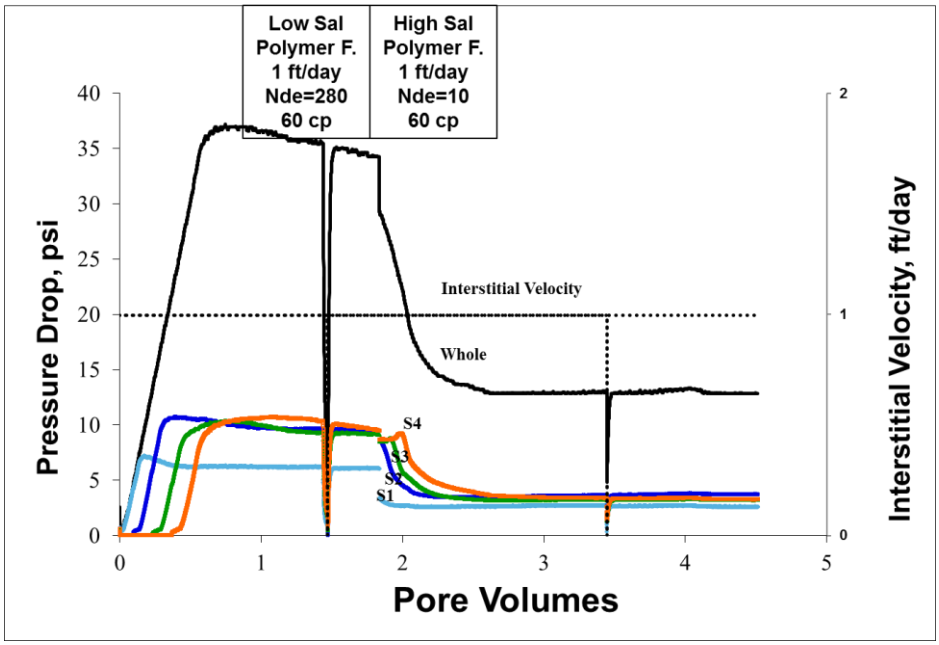

Figure 4.99: Pressure data for glycerin flood, low-salinity, and high-salinity polymer floods for experiment #7.

4.8 EXPERIMENT #8

Experiment #8 was also conducted Pengpeng Qi Unlike experiments #1-7, experiment #8 was performed in a different rock type (Berea sandstone) and a different (lower molecular weight) polymer was used (FP-3330). Like experiment #7, a light oil (10 cP viscosity) was used. Table 4.14 summarizes the core and fluid properties of experiment #8.

Table 4.14: Core and fluid properties of experiment #8.

Experiment	**#8**
Coreflood name	PPQ-3rd
Rock type	Berea Sandstone
Brine permeability (mD)	140
Crude oil viscosity (cP)	10
Temperature (°C)	23
Porosity	0.24
Pore volume (ml)	116.0
Bulk volume (ml)	485
Waterflood solution	1000 ppm NaCl + 400 ppm NaHCO3 + 400ppm Na2S2O4 aqueous solution
Glycerin solution	No glycerin flood
Low-salinity polymer solution	1500 ppm FP-3330S HPAM Polymer in 3000 ppm NaCl + 2000 ppm Na2CO3 aqueous solution
High-salinity polymer solution	2800 ppm FP-3330S HPAM Polymer in 20000 ppm NaCl + 10000 ppm Na2CO3 aqueous solution

Experiment #8 was conducted as follows with the procedures described in Chapter 3 and in experiments 1-7:

1. The core was reduced and conditioned.
2. The brine permeability was measured as 140 mD.
3. The pore volume was measured as 116 ml. Porosity was 0.24.
4. A light oil with a viscosity of 10 cP was injected. The initial oil saturation was determined as 0.61 form oil flooding.
5. The core was aged for 2 days at 25 ℃.
6. A waterflood was performed at 5 ft/D. The residual oil saturation after the waterflood was 0.32. The maximum capillary number was calculated as 2.8×10^{-6} for the whole core, based on the maximum pressure gradient reached at 1 ft/D polymer flood, 14 psi/ft.
7. No glycerin flood was performed in this experiment because the oil had a low viscosity and a favorable mobility ratio existed between water and oil. The oil saturation was believed to be residual saturation.
8. An aqueous solution with low molecular weight polymer (FP 3330S) was prepared in a low-salinity brine (1500 ppm FP3330S polymer in 3000 ppm NaCl and 2000 Na_2CO_3 aqueous solution). The lower-molecular weight polymer was used because of filtration concerns in the low permeability (140 md) Berea core. The polymer solution was injected at 1 ft/D. The Deborah number (N_{De}) was calculated as 3.0. The apparent viscosity at equivalent shear rate 48.4 s^{-1} was 18 cP. Injection of the low-salinity polymer reduced the residual oil saturation to 0.27, a 5% reduction in residual oil saturation. The maximum capillary number was calculated as 1.2×10^{-5} for the whole core based on the maximum pressure gradient reached at 1 ft/D polymer flood, 66 psi/ft.
9. Another aqueous solution of low molecular weight polymer (FP 3330S) was prepared, but in a high-salinity brine (2800 ppm FP3330S in 20000 ppm NaCl and 10000 ppm Na_2CO_3 aqueous solution) was prepared. The polymer solution was injected at 1 ft/D.

The Deborah number (N_{De}) was calculated as 2.0 The apparent viscosity at the equivalent shear rate was 18 cP. Injection of high-salinity polymer solution, reduced the residual oil saturation to 0.24, an additional 3% reduction in the residual oil saturation. The maximum capillary number was calculated as 8.5×10^{-6} for the whole core, based on the maximum pressure gradient reached at 1 ft/D polymer flood, 47 psi/ft.

In all, an 8% reduction in oil saturation from the two polymer floods (compared to the waterflood) was observed in the Berea core using a light (10 cp) oil. The oil saturation data for all floods performed in experiment #8 are shown in Figure 4.100. Oil cut data for low-salinity and high-salinity polymer floods are shown in Figure 4.101.

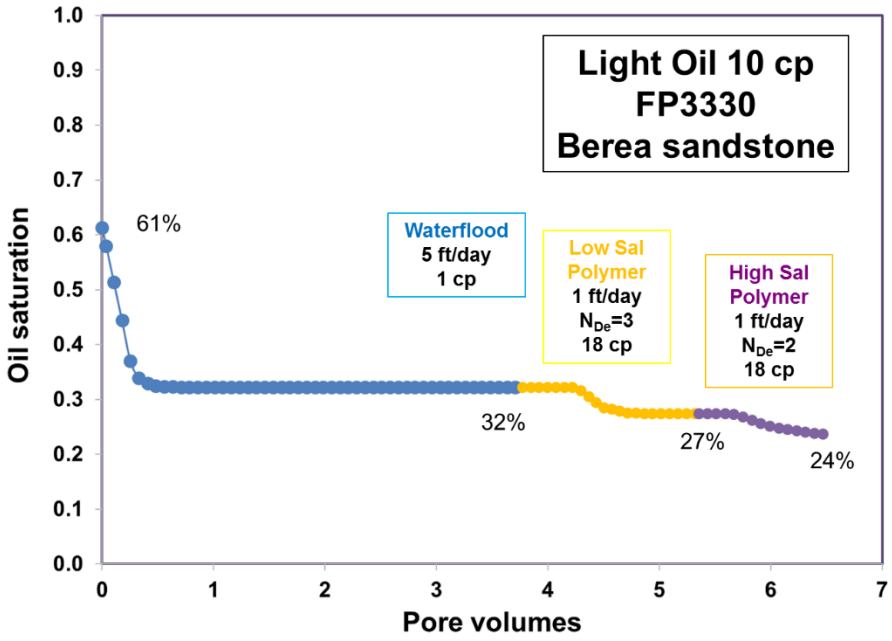

Figure 4.100: Oil saturation versus pore volumes for experiment #8.

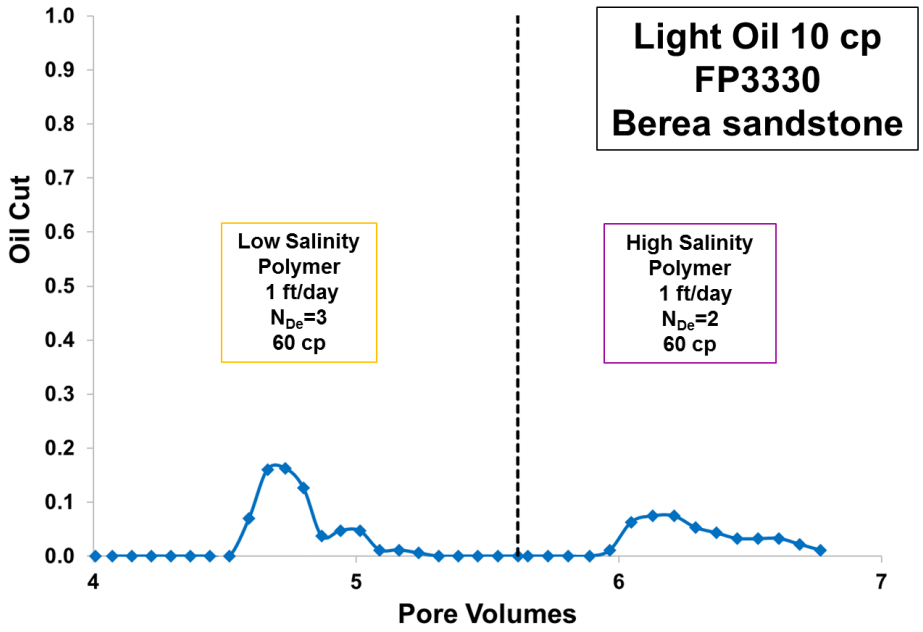

Figure 4.101: Oil cut data for low-salinity, and high-salinity polymer floods for experiment #8.

4.9 ANALYSIS OF THE EXPERIMENTS

A summary of the results all eight experiments is shown in Table 4.15. In experiments 1-6, viscous (~30 cp) glycerin was used to produce any unswept, remaining (viscous, ~120 cP) oil from the waterflood; usually a 2-4% reduction in oil saturation was observed. In experiments 7 and 8, a light (10 cp) oil was used and no glycerin was injected because of the favorable mobility ratio of the waterflood. All eight experiments were believed to be at residual saturation, prior to the injection of polymer. The average residual oil saturation was 0.41 excluding the Berea coreflood experiment, and 0.40 including Berea coreflood experiment.

Table 4.15: Summary of the residual oil saturation results of all eight coreflood experiments in this thesis

Exp #	Oil (cP)	S_{or} water	S_{or} glycerin	N_{De-1}	S_{or} low-sal polymer	N_{De-2}	S_{or} high-sal polymer
1	120	0.48	0.45	152	0.29	17	0.22
2	120	0.39	0.38	100	0.29	11	0.08
3	120	0.45	0.43	32	0.32	6	0.22
4	120	0.46	0.44	254	0.34	28	0.25
5	120	0.44	0.41	280	0.28	11	0.16
6	120	0.43	0.36	302	0.22	53	0.07
7	10	0.38	-	280	0.34	10	0.27
8	10	0.32	-	3	0.27	2	0.24
Average		**0.42**	**0.40**		**0.30**		**0.19**
			ΔS_{or}		**10%**	**+**	**11%**

The original objective of this work was to investigate the effect of viscoelastic polymers on residual oil saturation, particularly by using high dimensionless Deborah numbers (by hydrolysis, low salinities, high velocities, or a combination of these variables). The results of our experiments were consistent with similar studies (e.g. Qi et al., 2017) that viscoelastic polymers do reduce the residual oil saturation beyond that of inelastic fluids (e.g. water or glycerin). These polymers were also of low salinity (1400 ppm TDS brine) and it is well established that low salinity, aqueous solutions can also reduce residual saturation.

The average reduction in saturation from the first (low salinity, high elasticity) polymer flood was 11% for the 7 experiments in Bentheimer cores. The high recovery is

attributed the very high Deborah numbers (30-300), and, to a lesser extent the low-salinity. All experiments were performed at capillary numbers below the critical number (~ 5E-5) of Bentheimer and the capillary number was less than or equal to the capillary number of the preceding glycerin flood (for experiments 1-6). The apparent viscosity of the polymer was also less than the glycerin viscosity in these experiments. Capillary end effects were also small. There was a correlation between the residual saturation (with considerable scatter) after polymer flood and Deborah number which is also consistent with the finding so Qi et al. (2017).

In all eight experiments, a second polymer flood was conducted with the same polymer (HPAM 3630S, except in experiment #8) as the first polymer flood. The original purpose was to conduct a salinity tracer test for material balance purposes. The second polymer flood always had a higher salinity (24300 ppm TDS brine) than the first flood. The polymer concentration was also increased (~3500 ppm) so that apparent viscosity of both polymer floods was nearly equal. The high salinity resulted in a low polymer relaxation time, and therefore much lower N_{De} than the first polymer flood in the coreflood.

A significant quantity oil was unexpectedly recovered from the second polymer flood in experiment #1 and all subsequent experiments. The average reduction in oil saturation was an additional 12%; the total average reduction from polymer floods was 24% from the water/glycerin residual saturation. While there are published studies of low salinity and/or high elasticity polymers reducing residual saturation, the recovery from the high salinity and low elasticity polymers has not been observed to the author's knowledge. The high recovery cannot be explained improved sweep, capillary desaturation, or capillary-end effects because the variables were controlled and maintained less than or equal to the first polymer flood. Importantly, the effect was observed for two rock types (Bentheimer and Berea) and two oils (heavy, 120 cp oil and light, 10 cp, oil).

Oil breakthrough for the second, high-salinity polymer flood usually required more volumes (~1 PV) than the first, low-salinity polymer flood (< 0.5 PV). Also, the second flood usually had a lower maximum oil cut (~0.15 versus 0.5) and longer duration (2-4 PV versus <0.5 PV). These observations may provide insight into the mechanism for recovery.

Many of the experiments were performed to better understand the recovery mechanism from the second polymer flood and to optimize the process. In experiment #4, additional recovery was observed when additional (beyond the first two) polymer floods were performed by alternating between the low-salinity and high-salinity polymers. Some success was found, with diminishing returns, using this approach and injecting at least 1 PV of polymer before changing the polymer injection. After several polymer floods, no additional recovery was found by alternating the injected polymers.

In experiment #5 it was observed that the second (high-salinity) polymer did not recover a significant amount of oil when steady-state in pressure was not reached for the first polymer flood. It is therefore recommended to inject at least 1.0 PV, reach steady state in pressure and zero oil cut before changing polymer fluids. Another important observation from experiment #5 was that although several (5) alternating cycles and 20 total pore volumes injected of polymer (and no oil observed), a high salinity polymer flood reduced the residual saturation from 28% to 21% and then a low salinity polymer flood further reduced it to its final value of 16%. It should be noted that these high recoveries came after a long delay (16 days) in the experiment where the core flood was inactive.

The experiment (#8) in the Berea core was promising as it was the only experiment in a rock type other than Bentheimer. Both the low and high polymer floods recovered oil (5% and 3%, respectively) after waterflood. Unfortunately, the low permeability (140 mD) of the Berea core restricted the use of a high molecular weight polymer and HOAM 3330S was used. The low molecular weight resulted in relatively low relaxation times and

Deborah numbers (~2-3). Additional experiments are recommended in Berea using polymers with higher elasticity. It is possible to inject HPAM 3630S in Berea cores with higher permeability (> 400 mD).

Chapter 5: Conclusions and Future Work

5.1 CONCLUSIONS

Eight coreflood experiments were conducted to investigate the effect of aqueous hydrolyzed polyacrylamide (HPAM) polymer solutions on residual oil saturation in sandstone cores. Seven of the experiments were conducted in high-permeability (~1500 mD) Bentheimer sandstones, six of the cores were saturated with a viscous oil (~120 cp), and one core was saturated with a light (10 cp) oil. The eighth experiment was performed in a Berea sandstone core using the light oil. Experiments #6 to 8 were done by Pengpeng Qi. These experiments are included in this thesis to provide more complete and convincing results.

All experiments were first saturated with brine, flooded with oil to reach initial oil saturation, and then waterflooded with brine to zero oil cut. For experiments with viscous oil, a viscous glycerin solution was injected after the waterflood until the oil cut was zero. FP 3630S polymer was used in the seven Bentheimer coreflood experiments and FP 3330S polymer was used in the Berea coreflood experiment. The polymer solutions in low salinity brine had a high relaxation time. Additional hydrolysis of the polymers was done to further increase the relaxation time. The coreflood experiments were designed to maximize the effect of viscoelasticity on the residual oil saturation by flooding the cores at a high Deborah number, N_{De}, which ranged from 30-300.

The low-salinity polymer floods were followed by a second polymer flood with a similar viscosity, but higher salinity (viscosity was controlled by increasing polymer concentration). The higher salinity resulted in a much lower polymer relaxation time than the first polymer in low salinity brine, and therefore a lower N_{De} for the coreflood. Two of the experiments included additional polymer floods by alternating between the low and high salinity polymer solutions.

The original objective of this work was to investigate the effect of polymer elasticity (measured by the dimensionless Deborah number, N_{De}) on residual oil saturation. The polymer flooding experiments were designed to keep the capillary number less than the capillary number of the preceding glycerin floods as well as less than the critical capillary number to avoid a reduction in the residual oil saturation caused by a high capillary number. Early in this experimental study, a surprising and remarkable discovery was made that completely changed the direction of the research. The residual oil saturation following the high-salinity polymer floods was reduced to remarkably low values.

All eight experiments showed that the low-salinity polymer floods with high Deborah numbers resulted in additional oil recovery. The average reduction in oil saturation was ~10% for the seven Bentheimer corefloods, including the one with light oil (4%). There was a (weak) correlation indicating lower residual oil saturations with increasing N_{De} consistent with the observations by Qi et al. (2017).

The most surprising observation and discovery was that the residual oil saturation decreased between 4 and 21% with an average reduction of 11% when high-salinity polymer solution was injected following the low-salinity polymer flood with the same viscosity and at the same or similar flow rates. The total reduction in residual oil saturation from both polymer floods was 21% below the residual oil saturation of the glycerin floods with the same viscosity. The lowest residual oil saturation in these experiments was only 7%. This is a truly remarkable result considering the interfacial tension between the polymer solution and oil is about the same as between water and oil.

The results were unexpected for the particular experimental conditions of this study. Although both low-salinity brine and viscoelastic polymer solutions have been reported to reduce residual oil saturation, a high-salinity polymer solution with less elasticity would not be expected to reduce the residual oil saturation and such unexpected

behavior has not been previously reported. The viscosity of the second polymer solution was the same (or slightly less) than the preceding polymer flood, the capillary number was equal to or less than the first polymer flood and the N_{De} was lower than the first polymer flood. Moreover, the reduction in residual oil saturation was not likely due to capillary desaturation because the capillary number (of 5×10^{-5}) was carefully controlled below the critical capillary number (1×10^{-4} for Bentheimer sandstone). The pressure data also confirms that the pressure gradients (and therefore capillary numbers) for the second polymer flood were smaller than the first polymer flood, which was smaller than the glycerin flood. Furthermore, the Bentheimer cores used in this study were nearly homogeneous and many pore volumes of water, glycerin and the first low-salinity polymer solution were injected until zero oil cut was observed after each fluid injection. Therefore, the volumetric sweep efficiency of these cores should have been almost 100% and high sweep efficiency is consistent with the observations reported by Qi et al. (2017) for very similar experiments done in a CT scanner.

The first low-salinity polymer flood started producing oil at ~0.3 PV, had a maximum oil cut near 50%, and continued at decreasing oil cuts for ~0.5 PV. However, the second high-salinity polymer flood did not start producing oil until ~1 PV, had a much smaller maximum oil cut (~10-15%), and continued producing oil for several pore volumes. This delayed oil bank is very unusual and difficult to explain based on conventional fluid flow theory.

Two coreflood experiments in Bentheimer sandstone with viscous oil were continued beyond the two polymer floods by alternating more low and high salinity polymer floods. Continued alternating low and high salinity polymer floods were less effective with diminishing returns. An experiment was done by starting the high-salinity polymer flood after 1 PV of low-salinity polymer flooding, but this was mostly

unsuccessful. However, after several polymer floods and leaving the core shut in for 16 days, significant oil production was observed.

5.2 FUTURE WORK

The observations of oil recovery after the second, high-salinity polymer flood with a low relaxation time were unexpected and largely remain unexplained. The first polymer flood appears to be necessary for the second polymer flood to be successful, but it is unknown if the change of salinity, polymer elasticity, or some other variable or combination of variables is needed to induce additional oil production. Additional coreflood experiments are needed to understand the mechanism and how to optimize it. Specifically, a few of the many types of experiments that are needed include:

1. Although the pressure gradients were controlled to maintain capillary numbers below the critical capillary number and the velocity of the polymer floods was low, the pressure gradients were high compared to typical field values. Therefore, coreflood experiments should be performed at much lower pressure gradients (e.g. 1 psi/ft) and correspondingly lower capillary numbers, but it is challenging to do so while maintaining a high N_{De}. High permeability cores, high molecular weight polymers, and changes in the polymer structure may be helpful in addressing both issues. Additional hydrolysis has already been shown to increase the relaxation time of HPAM.
2. Experiments should be done using CT imaging to visualize the changes in oil saturation during both low and high salinity polymer floods.
3. All experiments except one were conducted in Bentheimer cores. Bentheimer sandstone was chosen due to its relatively high homogeneity and high permeability. However, future experiments should be done in different rock

types (both sandstones and carbonates) with a wide range of rock properties. One experimental challenge is that it is difficult to simultaneously obtain high N_{De} and low N_c in a low permeability coreflood.

4. More experiments should be done to both make the process more realistic and practical for field applications e.g. by injecting fewer pore volumes of each polymer solution, lower polymer concentrations, lower pressure gradients, or some combination of these variables.
5. Experiments should be done where the first polymer flood is followed by a second polymer flood in the same salinity brine but with a lower elasticity. For example, this could be done by using a polymer such as xanthan gum or scleroglucan.
6. Experiments should be done to optimize the salinity of the first and second polymer floods. The brine composition should also be varied including changes in hardness.
7. Additional measurements are needed to understand the mechanisms e.g. wettability measurements before and after the polymer floods in low and high salinity brines.

References

Abrams, A. (1975). The Influence of Fluid Viscosity, Interfacial Tension, and Flow Velocity on Residual Oil Saturation Left by Waterflood. *SPE J.* **15**: 437-447. SPE-5050-PA. https://doi.org/10.2118/5050-PA.

Afsharpoor, A., & Balhoff, M. (2013). Static and Dynamic CFD Modeling of Viscoelastic Polymer: Trapped Oil Displacement and Deformation at the Pore-Level. Society of Petroleum Engineers. https://doi.org/10.2118/166114-MS.

Brownell, L., and Katz, D. (1947). Flow of Fluids through Porous Media - Part II Simultaneous Flow of Two Homogeneous Phases. *Chemical Engineering Process* **43**: 601-612.

Cannella, W. J., Huh, C., & Seright, R. S. (1988). Prediction of Xanthan Rheology in Porous Media. Society of Petroleum Engineers. https://doi.org/10.2118/18089-MS.

Chatzis, I., Morrow, N. R., & Lim, H. T. (1983). Magnitude and Detailed Structure of Residual Oil Saturation. Society of Petroleum Engineers. https://doi.org/10.2118/10681-PA.

Delshad, M. (1990). Trapping of Micellar Fluids in Berea Sandstone. PhD Dissertation. The University of Texas at Austin.

Delshad, M., Kim, D. H., Magbagbeola, O. A., Huh, C., Pope, G. A., & Tarahhom, F. (2008). Mechanistic Interpretation and Utilization of Viscoelastic Behavior of Polymer Solutions for Improved Polymer-Flood Efficiency. Society of Petroleum Engineers. https://doi.org/10.2118/113620-MS.

Durst, F., Haas, R. and Kaczmar, B. U. (1981), Flows of Dilute Hydrolyzed Polyacrylamide Solutions in Porous Media Under Various Solvent Conditions. J. Appl. Polym. Sci., 26: 3125–3149. https://doi.org/10.1002/app.1981.070260926.

Ehrenfried, D. H. (2013). Impact of Viscoelastic Polymer flooding on Residual Oil Saturation in Sandstones. MS Thesis. University of Texas at Austin.

Fortenberry, R. P. (2013). Experimental Demonstration and Improvement of Chemical EOR Techniques in Heavy Oils. MS Thesis. The University of Texas at Austin.

Green, D., and Willhite, P. (1998). Enhanced Oil Recovery. Richardson, TX: SPE Textbook Series Volume 6.

Haas, R., and Durst, F. (1982). Viscoelastic Flow of Dilute Polymer Solutions in Regularly Packed Beds, Rheologica Acta, 21, 566-571. https://doi.org/10.1007/BF01534349.

Hirasaki, G. J., & Pope, G. A. (1974). Analysis of Factors Influencing Mobility and Adsorption in the Flow of Polymer Solution Through Porous Media. Society of Petroleum Engineers. https://doi.org/10.2118/4026-PA.

Huh, C., & Pope, G. A. (2008). Residual Oil Saturation from Polymer Floods: Laboratory Measurements and Theoretical Interpretation. Society of Petroleum Engineers. https://doi.org/10.2118/113417-MS.

Jiang, H., Wu, W., Wang, D., Zeng, Y., Zhao, S., & Nie, J. (2008). The Effect of Elasticity on Displacement Efficiency in the Lab and Results of High-Concentration Polymer

Flooding in the Field. Society of Petroleum Engineers. https://doi.org/10.2118/115315-MS.
Jones, D., Walters, K., Williams, P., (1987). On the Extensional Viscosity of Mobile Polymer Solutions. Rheologica Acta 30.
Kamath, J., Meyer, R. F., & Nakagawa, F. M. (2001). Understanding Waterflood Residual Oil Saturation of Four Carbonate Rock Types. Society of Petroleum Engineers. https://doi.org/10.2118/71505-MS
Kim, D. H., Lee, S., Ahn, C. H., Huh, C., & Pope, G. A. (2010). Development of a Viscoelastic Property Database for EOR Polymers. Society of Petroleum Engineers. https://doi.org/10.2118/129971-MS.
Koh, H. (2015). Experimental Investigation of the Effect of Polymers on Residual Oil Saturation. PhD Dissertation. The University of Texas at Austin.
Koh, H., Lee, V. B., & Pope, G. A. (2016). Experimental Investigation of the Effect of Polymers on Residual Oil Saturation. Society of Petroleum Engineers. https://doi.org/10.2118/179683-MS.
Koval, E. J. (1963). A Method for Predicting the Performance of Unstable Miscible Displacement in Heterogeneous Media. Trans Soc Petrol Eng AIME. 228:145-154
Lake, L.W., Johns, R.T., Rossen, W.R., Pope, G.A., (2014). *Fundamentals of Enhanced Oil Recovery*. Society of Petroleum Engineers, Richardson, TX, ISBN: 9781613993286.
Lee, V. B. (2015). The Development and Evaluation of Polymers for Enhanced Oil Recovery. MS Thesis. The University of Texas at Austin.
Levitt, D., & Pope, G. A. (2008). Selection and Screening of Polymers for Enhanced-Oil Recovery. Society of Petroleum Engineers. https://doi.org/10.2118/113845-MS.
Lindey, J. R., (2001). EOR Process Drawings, National Energy Technology Laboratory, U.S. Department of Energy, retrieved on April 19, 2017 from https://www.netl.doe.gov/research/oil-and-gas/enhanced-oil-recovery/eor-process-drawings.
Masuda, Y., Tang, K.-C., Miyazawa, M., & Tanaka, S. (1992). 1D Simulation of Polymer Flooding Including the Viscoelastic Effect of Polymer Solution. Society of Petroleum Engineers. https://doi.org/10.2118/19499-PA.
Metzner, A., White, J., Denn, M., (1966). Constitutive equations for viscoelastic fluids for short deformation periods and for rapidly changing flows: significance of the Deborah number. AIChE J. 12, 863–866
Moore, T. F., and Slobod, R. L. (1956). Displacement of Oil by Water Effect of Wettability, Rate, and Viscosity on Recovery. SPE Journal Article 000502.
Moradi-Araghi, A., & Doe, P. H. (1987). Hydrolysis and Precipitation of Polyacrylamides in Hard Brines at Elevated Temperatures. Society of Petroleum Engineers. https://doi.org/10.2118/13033-PA.
Morrow, N., & Buckley, J. (2011). Improved Oil Recovery by Low-Salinity Waterflooding. Society of Petroleum Engineers. https://doi.org/10.2118/129421-JPT.

Pope, G. A. (2015). Polymer Flooding Overview_EOR-II, unpublished course notes. The University of Texas at Austin.

Pope, G. A. (1980). The Application of Fractional Flow Theory to Enhanced Oil Recovery, Society of Petroleum Engineers Journal, p191-205, SPE 7660-PA.

Pope, G. A., Wu, W., Narayanaswamy, G., Delshad, M., Sharma, M. M., & Wang, P. (2000). Modeling Relative Permeability Effects in Gas-Condensate Reservoirs With a New Trapping Model. Society of Petroleum Engineers. https://doi.org/10.2118/62497-PA.

Pye, D. J. (1964). Improved Secondary Recovery by Control of Water Mobility. Society of Petroleum Engineers. https://doi.org/10.2118/845-PA.

Qi, P., Ehrenfried, D. H., Koh, H., & Balhoff, M. T. (2017). Reduction of Residual Oil Saturation in Sandstone Cores by Use of Viscoelastic Polymers. Society of Petroleum Engineers. https://doi.org/10.2118/179689-PA.

Rajapaksha, S., Britton, C., McNeil, R. I., Kim, D. H., Unomah, M., Kulawardana, E., Pope, G. A. (2014). Restoration of Reservoir Cores to Reservoir Condition before Chemical Flooding Tests. In SPE Improved Oil Recovery Symposium. Society of Petroleum Engineers. doi:10.2118/169887-MS

Rouse, P. E. (1953). A Theory of the Linear Viscoelastic Properties of Dilute Solutions of Coiling Polymers. The Journal of Chemical Physics 21, 1272. https://doi.org/10.1063/1.1699180.

Ryles, R. G. (1988). Chemical Stability Limits of Water-Soluble Polymers Used in Oil Recovery Processes. Society of Petroleum Engineers. https://doi.org/10.2118/13585-PA.

Schiessel, H., Metzler, R., Blumen, A. et al. (1995). Generalized Viscoelastic Models: their fractional equations with solutions. Journal of Physics A: Mathematical and General, Volume 28, Number 23.

Segur, J. B. and Oberstar, H. E. (1951). Viscosity of Glycerol and Its Aqueous Solutions. Industrial&Engineering Chemistry. pp 2117-2120. https://doi.org/10.1021/ie50501a040

Sheng, J. (2010). *Modern Chemical Enhanced Oil Recovery: Theory and Practice*. Gulf Professional Publishing.

SNF. (2012). Enhancing Polymer Flooding Performance brochure, retrieved on April 1st, 2017, from http://www.snf.us/wp-content/uploads/2014/08/EOR-Oil-30-Years-of-EOR.pdf

Sorbie, K.S. (1991). *Polymer-Improved Oil Recovery*. Glasgow and London: Blackie and Son Ltd. CRC Press, Inc.

Stegemeier, G. (1977). Mechanisms of Entrapment and Mobilization of Oil in Porous Media. *Improved Oil Recovery by Surfactant and Polymer Flooding* D. O. Shah and R. S. Schecter (eds.). pp. 55-89. New York, NY: Academic Press.

TA Instruments, (2003). ARES Rheometer - Rheometrics Series User Manual, PN 902-30026 Rev D: Waters LLC, New Castle, DE

Taber, J. (1969). Dynamic and Static Forces Required to Remove a Discontinuous Oil Phase from Porous Media Containing Both Oil and Water. SPE Journal, March, 3-12.

Unomah, M. O. (2013). Chemical Enhanced Oil Recovery Utilized Alternative Alkalis. MS Thesis. The University of Texas at Austin.

Urbissinova, T., Trivedi, J. J., & Kuru, E. (2010). Effect of Elasticity during Viscoelastic Polymer Flooding - A Possible Mechanism of Increasing the Sweep Efficiency. Society of Petroleum Engineers. https://doi.org/10.2118/133471-MS.

Vermolen, E. C. M., van Haasterecht, M. J. T., & Masalmeh, S. K. (2014). A Systematic Study of the Polymer Visco-Elastic Effect on Residual Oil Saturation by Core Flooding. Society of Petroleum Engineers. https://doi.org/10.2118/169681-MS.

Volpert, E., Selb, J., & Candau, F. (1998). Associating Behavior of Polyacrylamide Hydrophobically modified with Dihexylacrylamide. Polymer, 39, 1025-1033.

Wang, D., Cheng, J., Yang, Q., Wenchao, G., Qun, L., & Chen, F. (2000). Viscous-Elastic Polymer Can Increase Microscale Displacement Efficiency in Cores. Society of Petroleum Engineers. https://doi.org/10.2118/63227-MS.

Wang, D., Xia, H., Liu, Z., & Yang, Q. (2001). Study of the Mechanism of Polymer Solution With Visco-Elastic Behavior Increasing Microscopic Oil Displacement Efficiency and the Forming of Steady "Oil Thread" Flow Channels. Society of Petroleum Engineers. https://doi.org/10.2118/68723-MS.

Wreath, D. (1989). A Study of Polymer Flooding and Residual Oil Saturation, University of Texas at Austin, MS Thesis.

Wu, W., Wang, D., & Jiang, H. (2007). Effect of the Visco-elasticity of Displacing Fluids on the Relationship of Capillary Number and Displacement Efficiency in Weak Oil-Wet Cores. Society of Petroleum Engineers. https://doi.org/10.2118/109228-MS.

Xia, H., Wang, D., Wang, G., Ma, W., Deng, H. W., & Liu, J. (2008). Mechanism of the Effect of Micro-Forces on Residual Oil in Chemical Flooding. Society of Petroleum Engineers. https://doi.org/10.2118/114335-MS.

Xia, H., Wang, D., Wu, J., and Kong, F. (2004). Elasticity of HPAM Solutions Increases Displacement Efficiency under Mixed Wettability Conditions. SPE 88456. https://doi.org/10.2118/88456-MS.

Yin, H., Wang, D., & Zhong, H. (2006). Study on Flow Behavoirs of Viscoelastic Polymer Solution in Micropore With Dead End. Society of Petroleum Engineers. https://doi.org/10.2118/101950-MS.

Yuan, C. (2012). Commercial Scale Simulations of Surfactant/Polymer Flooding. The University of Texas at Austin, PhD Dissertation